Copyright Warning & Restrictions

The copyright law of the United States (Title 17, United States Code) governs the making of photocopies or other reproductions of copyrighted material.

Under certain conditions specified in the law, libraries and archives are authorized to furnish a photocopy or other reproduction. One of these specified conditions is that the photocopy or reproduction is not to be "used for any purpose other than private study, scholarship, or research." If a, user makes a request for, or later uses, a photocopy or reproduction for purposes in excess of "fair use" that user may be liable for copyright infringement,

This institution reserves the right to refuse to accept a copying order if, in its judgment, fulfillment of the order would involve violation of copyright law.

Please Note: The author retains the copyright while the New Jersey Institute of Technology reserves the right to distribute this thesis or dissertation

Printing note: If you do not wish to print this page, then select "Pages from: first page # to: last page #" on the print dialog screen

ABSTRACT

CO_2 REDUCTION OVER NOBLE METAL/CARBON NANOTUBE CATALYST

by
Yuan Zhu

Carbon nanotube-based Pt/Pd and Ru catalysts, independently synthesized by a microwave reaction technique, show good catalytic activity for CO_2 reduction in the contexts of dry reforming (DR) of methane ($CH_4 + CO_2 \rightarrow 2CO + 2H_2$) and reverse water gas shift (RWGS) ($H_2 + CO_2 \rightarrow CO + H_2O$). Reaction temperatures range from 773 to 973 K, with system pressure at 30 psig. The feed molar ratios CH_4/CO_2 and CO_2/H_2 are varied from 0.5 to 2.0. Reactant conversions in DR and RWGS are strongly influenced by temperature and feed molar ratio, but insignificantly affected by flow rate.

Based on data from an integral packed bed reactor, a simple power law model of CO_2 conversion indicates global reaction rates of DR and RWGS showing first order dependencies on each reactant. Linear Arrhenius plots of the global rate constants are also obtained. More robust semi-global 3-reaction models are developed based on regressions of experimental gas species concentration data. They adequately simulate observed species concentrations. Detailed catalytic chemistry simulations were made using a literature Ni-based catalyst mechanism. Adequate results were obtained for the Pt/Pd and Ru carbon nanotube catalysts used for DR. However, generally poor simulation results for the RWGS using Pt/Pd strongly suggest the limits of using the Ni mechanism within this context.

CO_2 REDUCTION OVER NOBLE METAL/CARBON NANOTUBE CATALYST

by
Yuan Zhu

A Dissertation
Submitted to the Faculty of
New Jersey Institute of Technology
in Partial Fulfillment of the Requirements for the Degree of
Doctor of Philosophy in Chemical Engineering

Otto H. York Department of Chemical, Biological and Pharmaceutical Engineering

December 2017

.

APPROVAL PAGE

CO_2 REDUCTION OVER NOBLE METAL/CARBON NANOTUBE CATALYST

Yuan Zhu

Dr. Robert B. Barat, Dissertation Advisor Professor of Chemical Engineering, NJIT	Date
Dr. Somenath Mitra, Dissertation Co-Advisor Distinguished Professor of Chemistry, NJIT	Date
Dr. Edward L. Dreyzin, Committee Member Distinguished Professor of Chemical Engineering, NJIT	Date
Dr. Xianqin Wang, Committee Member Associate Professor of Chemical Engineering, NJIT	Date
Dr. Lucas Dorazio, Committee Member Team Leader, Refinery catalyst at BASF, Iselin, NJ	Date

BIOGRAPHICAL SKETCH

Author: Yuan Zhu

Degree: Doctor of Philosophy

Date: December 2017

Undergraduate and Graduate Education:

- Doctor of Philosophy in Chemical Engineering,
  New Jersey Institute of Technology, Newark, NJ, 2017

- Master of Science in Chemical Engineering,
  New Jersey Institute of Technology, Newark, NJ, 2013

- Bachelor of Science in Chemical Engineering,
  China University of Petroleum, Qingdao, P. R. China, 2010

Major: Chemical Engineering

Presentations and Publications:

Yuan Zhu and Robert B. Barat. (2014). Partial Oxidation of Methane over a Ruthenium Phthalocyanine Catalyst. *Chemical Engineering Science.* 116, 71-76.

Yuan Zhu, Nadia Al-ebbinni, Richard Henney, Chen Yi, and Robert B. Barat. (2017). Extension to Multiple Temperatures of a Three-Reaction Global Kinetic Model for Methane Dehydroaromatization. *Chemical Engineering Science.* In press.

Yuan Zhu and Robert B. Barat, "Partial Oxidation of Methane over a Ruthenium Phthalocyanine Catalyst," The Catalysis Society of Metropolitan New York, Princeton, NJ. March 2013.

Yuan Zhu and Robert B. Barat, "Dry Reforming of Methane over Pt/Pd-Carbon Nanotube Catalyst," The Catalysis Society of Metropolitan New York, New Brunswick, NJ. March 2016.

谨以此博士论文，献给我亲爱的父亲、母亲

To my beloved parents, for their love, support, and encouragement

ACKNOWLEDGMENT

I would like to show my great heartfelt appreciation to Prof. Robert B. Barat, who not only served as my research supervisor, providing valuable resources and amazing academic guidance, and showing me the superb research methods, guidance, but also building up my confidence by his trust and encouragement. I am also fully grateful to his care on my daily life. It is my huge honor to get acquainted and serve with such a brilliant grandmaster.

Special gratitude to Prof. Somenath Mitra, Prof. Edward L. Dreyzin, Prof. Xianqin Wang and Dr. Lucas Dorazio for serving as my committee members and their brilliant advice.

I also appreciate Dr. Larisa Krishtopa and Dr. Jeong Seop Shim of the NJIT Materials Characterization Lab for their help.

The catalyst in this research was provided by the Chemistry Department of NJIT. I also wish to thank Prof. Somenath Mitra's group for their support and contribution.

Finally, I give my most sincere gratitude to my beloved parents. Their concern, love, support, selfless, encouragement, and sacrifice made me keep moving forward.

TABLE OF CONTENTS

TABLE OF CONTENTS
(Continued)

Chapter **Page**

TABLE OF CONTENTS
(Continued)

Chapter **Page**

TABLE OF CONTENTS
(Continued)

Chapter **Page**

TABLE OF CONTENTS
(Continued)

TABLE OF CONTENTS
(Continued)

Chapter **Page**

TABLE OF CONTENTS
(Continued)

TABLE OF CONTENTS
(Continued)

Chapter **Page**

TABLE OF CONTENTS
(Continued)

Chapter **Page**

TABLE OF CONTENTS
(Continued)

Chapter **Page**

LIST OF TABLES

LISTS OF TABLES
(Continued)

LIST OF FIGURES

LISTS OF FIGURES
(Continued)

Figure **Page**

LISTS OF FIGURES
(Continued)

Figure **Page**

LISTS OF FIGURES
(Continued)

Figure **Page**

LISTS OF FIGURES
(Continued)

Figure **Page**

LISTS OF FIGURES
(Continued)

Figure **Page**

LISTS OF FIGURES
(Continued)

LISTS OF FIGURES
(Continued)

Figure **Page**

CHAPTER 1

INTRODUCTION

1.1 CO_2 Reduction Processes

Carbon dioxide (CO_2), resulting from combustion of fossil fuel, is the chief greenhouse gas in the atmosphere (Daza, 2016). The global CO_2 atmospheric concentration recently reached the 400 ppm threshold, putting the world at 1.5℃ above the average temperature prior to the industrial revolution (Alaba, 2017). In 2013, 32.19 gigatons (Gt) of CO_2 were emitted to the atmosphere, and emissions are expected to increase to 45 Gt/year by 2040 (Daza, 2016). Moreover, CO_2 absorption will lower the pH of the oceans. By 2030, the acidification of the Southern Ocean will likely have real consequences on organisms that could potentially affect the food web of the area (Hauri, 2016). The rapidly increasing atmospheric CO_2 concentration and the threat it poses upon the environment has led to increased efforts to reduce or minimize CO_2 atmospheric emissions.

1.2 Methane Dry Reforming

Catalytic methane (CH_4) dry reforming (DR), which is also known as CO_2 reforming of CH_4, converts CH_4 and CO_2 into the synthesis gas (CO and H_2) product. (Usman, 2015) The overall DR reaction is (Khavarian, 2016):

$$CH_4 + CO_2 \rightarrow 2CO + 2H_2 \quad \Delta H_{298K} = 247.3 kJ/mol \tag{1.1}$$

The DR reaction is usually accompanied by several side reactions, including CH_4 decomposition (MD) (2), Boudouard (3), reverse water gas shift (RWGS) (4), and steam reforming (5) (Khavarian, 2016):

$$CH_4 \rightarrow C + 2H_2 \quad \Delta H_{298K} = 86.3kJ/mol \tag{1.2}$$

$$2CO \rightarrow C + CO_2 \quad \Delta H_{298K} = -159.9kJ/mol \tag{1.3}$$

$$CO_2 + H_2 \rightarrow H_2O + CO \quad \Delta H_{298K} = 41kJ/mol \tag{1.4}$$

$$H_2O + CH_4 \rightarrow CO + 3H_2 \quad \Delta H_{298K} = 206.2kJ/mol \tag{1.5}$$

1.2.1 Why Methane Dry Reforming

Methane DR is not only an efficient CO_2 reduction process, but is also a promising way for nature gas (mostly CH_4) utilization (Qu, 2008). Nature gas reservoirs are large and widespread throughout the world. The estimated reserves at the end of 2006 are approximately 6300 trillion cubic feet, which make natural gas a promising alternative energy source to petroleum (Alvarez-Galvan, 2011). However, for the lack of a cost-effective technology for CH_4 conversion and liquefaction, as much as 20% of the natural gas is often flared – an economic waste that also adds to greenhouse gas emissions. Due to the rapid development of fuel cells, the need for a cheap and constant hydrogen (H_2) supply is growing. Such conditions motivated us to focus on CH_4 DR, as a potentially effective method to simultaneously remove these two greenhouse gases in one overall chemical reaction while generating H_2 and CO, which would be beneficial for both energy supplies and the environment (Usman, 2015), (Ma, 2013), (Qu, 2008). The synthesis gas [carbon monoxide (CO) and H_2] product is also a crucial intermediate resource for production of hydrogen, ammonia, methanol, and especially synthetic

petroleum for use as fuels or lubricants via the Fischer–Tropsch process (Wu, 2015), (Drif, 2015).

1.2.2 Catalysts

Dry reforming requires a heterogeneous catalyst. Typical DR catalysts are supported on alumina (Al_2O_3), silica (SiO_2), magnesia (MgO), titania (Ti_2O_2), and zirconia (ZrO_2) (Usman, 2015), (Zhang, 2015), (Yamagishi, 2006), and active sites can be classified into two groups. The first group is supported base-metal catalysts, including iron (Fe), cobalt (Co), and nickel (Ni) (Usman, 2015), (Zhang, 2015). The Ni is widely researched because of its considerable activity and relatively low cost. But the Ni catalyst particularly suffers the main shortcomings of DR catalysts. First, Ni has a higher sintering tendency at common DR reaction temperatures (600-900 ^oC). Second, the Ni catalyst has a relative weak coking resistance (Usman, 2015), (Zhang, 2015).

The second group consists of supported noble metal catalysts, most commonly rhodium (Rh), ruthenium (Ru), platinum (Pt), pladium (Pd), and iridium (Ir) (Usman, 2015), (Yamagishi, 2006), (Tomishige, 2004). Although their cost is relatively high, noble metal catalysts typically have superior coking resistance, higher stability (i.e., less sintering), and better activity especially for higher temperature applications.

To enhance DR catalyst performance, selected promoters such as magnesium (Mg), manganese (Mn), potassium (K), and calcium (Ca) are introduced into catalyst (Khajenoori, 2015). Another promotor is ceria (CeO_2) (Ay, 2015). Due to its redox property, CeO_2 has an “oxygen storage capacity” that makes it a local sources or sinks for oxygen involved in reactions taking place on its surface. The CeO_2 could enhance coking resistance.

Although CH_4 DR has already been widely researched, due to its potential advantages, there is still much of attention focused on this area now. Moral et al. (2017) studied DR over Rh based catalyst using different supports (Al_2O_3, SiO_2, and CeO_2) at 973 K and the inlet CH_4 flow rate was 30 litters /(gram of catalyst hour), Their observed CH_4 conversion was as high as 52%, essentially the equilibrium conversion. Their product ratio H_2/CO was 1.0. Moral et al. concluded the activity of Rh based catalyst in DR as Rh/Al_2O_3 > Rh/SiO_2 > Rh/CeO_2. Garcí a-Diéguez et al. (2010) studied Pt/Al_2O_3 and Pt-Ni/Al_2O_3 for CH_4 DR at 673-973K. Their observed CH_4 and CO_4 conversions were ranged of 5-70%. Their H_2 /CO ratio reached 0.7. They also found the activity of Pt-Ni/Al_2O_3 is higher than that of Pt/Al_2O_3 at the same experimental conditions. Whang et al. (2017) applied Ru/ZrO_2-SiO_2 catalyst in DR, and observed that both of CH_4 and CO_2 conversions were over 60% with a stable catalytic activity. Their H_2/CO was 0.84. Abdullah et al. (2017) summarized the activity of Ni based catalyst could be represented as Ni/La_2O_3-ZrO_2 > Ni/ZrO_2 > $Ni/MgO·Al_2O_3$ > Ni/TiO_2 > Ni/MgO > Ni/Al_2O_3 > Ni/SiO_2.

1.3 Reverse Water Gas Shift

Reverse water gas shift (RWGS), the reverse process of water gas shift, convert CO_2 and H_2 into CO and water (H_2O vapor). The reaction is shown as: (Oshima, 2014)

$$H_2 + CO_2 \rightarrow CO + H_2O \quad \Delta H_{298K} = 42.1 \text{ kJ/mol} \tag{1.6}$$

The RWGS reaction is thermodynamically favorable at high temperature because of its endothermic nature (Galván, 2016), (Yang, 2017), as shown in equation (6). Additional side reactions, however, include the methanation (7) and Sabatier reaction (8),

would occur under similar reaction conditions, making it difficult to achieve high selectivity of product CO (Daza, 2016), (Yang, 2017).

$$3H_2 + CO \rightarrow CH_4 + H_2O \quad \Delta H_{298K} = -206.5 \text{ kJ/mol} \tag{1.7}$$

$$4H_2 + CO_2 \rightarrow CH_4 + 2H_2O \quad \Delta H_{298K} = -165.0 \text{ kJ/mol} \tag{1.8}$$

1.3.1 Why Reverse Water Gas Shift

The necessity of CO_2 reduction was discussed in Section 1.1. Meanwhile however, we should also recognize CO_2 as an abundant and inexpensive carbon resource for the chemical industry (Yang, 2017). Technologies are currently under research to transform CO_2 to chemicals of wide use include synthesis of polymers, oxalates, formates, dimethyl ether, ethylene and propylene (Ishito, 2016). But, even if all the methanol (CH_3OH) and chemicals (made from oil) consumed globally were synthesized from CO_2, emissions would not decrease by more than 3.8% (Daza, 2016), respectively. Therefore, we would like to focus on converting CO_2 into fuels, which needs concentrated CO_2 to produce chemicals of significantly high demand. The technologies with the highest readiness for converting CO_2 to synthetic fuels or their precursors (i.e., H_2 and/or CO) are: CH_4 DR, RWGS and direct hydrogenation of CO_2 (Daza, 2016). The products of CO_2 hydrogenation are mainly CH_4 and CH_3OH (Saeidi, 2014). But CO, the product of DR and RWGS could be the feed stock for variety of processes, especially for Fischer-Tropsch syntheses with H_2 to produce liquid fuel (Chen, 2017).

1.3.2 Catalysts and Recent Research Progress (Literature)

The metal catalysts of RWGS consist primarily of copper (Cu), Pt, and Rh immobilized on a variety of supports. The use of Cu for RWGS has two major advantages. First, it has

been shown to perform RWGS at low temperatures (~ 438 K) (Rodriguez, 2013), (Chen, 2003); second, little or no CH_4 is formed as a side product (Taheri, 2015). But without H_2, CO_2 dissociation is highly unfavorable on clean Cu surfaces (Liu, 2012), which directly translates to the need of high H_2/CO_2 feed ratios to achieve high CO_2 conversions. Chen et al (2010). have studied RWGS on Cu nanoparticles supported on Al_2O_3 and SiO_2. They concluded that the RWGS mechanism goes through a formate intermediate, the CO_2 and CO adsorption sites for the forward and reverse mechanisms are independent. Gines et al. (1997) observed that high Cu dispersion was a characteristic of the catalyst with highest activity on a $Cu/ZnO/Al_2O_3$ system.

Platinum-based catalyst shows RWGS activity even at low temperatures (373 to 573 K) (Sato, 1984). The CO_2 is converted to CO on the interface between Pt and CeO_2 after H_2 pre-treatment, but CO formation was not observed on CeO_2 or Pt alone (Sato, 1984). Tibiletti et al. (2004) researched RWGS studies on Pt/CeO_2, finding that the most reactive surface intermediates were carbonates and carbonyls under steady state conditions. The effect of adsorbed reactants and products has also been investigated in Pt systems. Jacobs et al. (2005) studied the effect of H_2O and H_2 adsorption on Pt/CeO_2 during RWGS and observed different spectator species formed under different conditions, suggesting that the forward and backwards water gas shift (WGS) mechanisms could be different. It was found that Pt/SiO_2 systems achieved higher conversion than Cu/SiO_2 at 773 K (Chen, 2006), but poisoning of Pt by CO has been observed in 2% Pt/ CeO_2 (Goguet, 2004).

Rhodium is widely used in homogeneous CO_2 hydrogenation, mostly in amine solutions (Jessop, 2004). However, for Rh deposited on different supports (MgO, Nb_2O_5,

ZrO_2 and TiO_2), the combined selectivity towards CH_4 and CH_3OH added to more than 80% at temperatures between 373 and 573 K and H_2/CO_2 =3 feed ratios (Inoue, 1989). Matsubu et al. (2015) found that the selectivity of CO over CH_4 on Rh/TiO_2 increased with lower Rh loadings at 473 K and lower H_2/CO_2 feed ratio. As a promoter, lithium (Li) was added to an Rh Y-zeolite (Li/RhY) (Bando, 1998) catalyst and the selectivity towards CO (vs. CH_4) was found to increase from 0.3% to 86.6% as Li/Rh atomic ratios increased from 0 to 10/1, but the CO_2 conversion was decreased by half with Li addition.

1.4 Carbon Nanotube-Supported Metal Catalyst

Catalyst development is the core of the research on DR and RWGS. It is desirable to achieve high CH_4 and CO_2 conversions together with high selectivities to target products at lower temperatures. Especially, a lower carbon deposit tendency (coking) is desperately desired. Because of its special structure and properties, in this project, we apply carbon nanotube (CNT) supported metal catalyst in DR and RWGS.

1.4.1 CNT Structure and Properties

A CNT, shown as Figure 1.1 (right), is a tube-shaped material, made of carbon atoms. The CNTs are one-dimensional (1D) cylindrical structures consisting of wrapped single or multi-layer graphene sheets (Iijima, 1991).

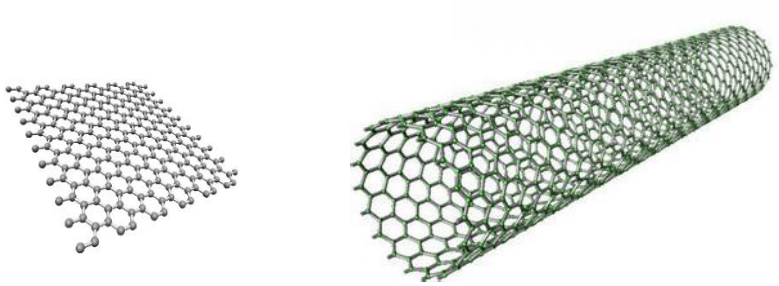

Figure 1.1 Structure of graphene and single walled carbon nanotube.

Due to their excellent thermal and electrical conductivities, high mechanical strength, large surface area, relatively high oxidation stability, surface chemical flexibility and porous structure (Fu, 2007), CNTs can be excellent supports for catalytic nanoparticles, including Pt, Pd, Ru, Pt, Ag, Au, Fe, Co, Ni, MoO_x, and various semiconductors (Fu, 2007).

1.4.2 CNT as Catalyst Support for CO_2 Reduction

Although it has been less than 30 years since CNTs were invented (Iijima, 1991), its advantages as catalyst supports for a number of heterogeneous catalysis processes, including DR, have been identified. Donphai et al. (Donphai, 2014) researched DR over Ni/CNT and Ni/SiO_2 catalysts. They observed approximately the same conversions from the two catalysts, but Ni/CNT showed much better stability. Khavarian et al. (2015) applied Co/CNT and Co/MgO for DR. Higher CH_4 conversions were observed from Co/CNT, which also had lower carbon deposition rate and less catalyst deactivation.

No references were found about CNT supported metal catalyst for RWGS. But as RWGS is one of the side reactions of DR, the possibilities for RWGS over CNT-supported catalysts are worthy of study.

1.5 Objectives

In this study, Ru/CNT and Pt/Pd-CNT catalysts were produced by novel methods by the group led by co-advisor Dr. S. Mitra at the NJIT Chemistry Department. This research includes running experiments of CH_4 DR over the Ru/CNT and Pt/Pd-CNT catalysts, RWGS over Pt/Pd-CNT catalyst, data collection and analyses, reactor modeling and comparison to experimental data, and detailed reaction mechanism study by *Chemkin*® model (2013).

The experimental apparatus will be introduced in Chapter 3. During the tests of DR and RWGS, both mass of catalyst and reaction pressure are fixed. Appropriate temperatures are selected for these experiments. For DR, two groups of experiments are done for every temperature. In the first group, the total flow rate of reactants was fixed, while the feed ratio of CH_4/CO_2 is varied. In the second part, while keeping the ratio CH_4/CO_2 constant, the total flow rate was varied. For RWGS, the total flow rate of reactants was fixed, and the feed ratio of CH_4/CO_2 is varied. On-line gas chromatography was used to detect and measure gas species.

The major goals of this project were to demonstrate the catalytic activity of novel CNT based catalysts for both DR and RWGS, and to reveal reaction kinetics. Results from DR over Ru/CNT and Pt/Pd-CNT catalysts will be shown in Chapter 6 and 7. The calculation of carbon balance between inlet and outlet components will show how the carbon deposition tendency of our catalysts. Conversions of reactants will be analyzed with the influence of feed molar ratio, reaction temperature, and inlet flow rate. Comparison of equilibrium and experimental results will demonstrate how far or close the experimental results are from equilibrium. Selective models will be processed to

reveal reaction kinetics. Power law is the simplest model, but it could most visually show the overall activation energy and reflect how concentrations of reactants affect the overall reaction rates. Multiple reaction models are presented. These are more complicated than power law, and divide the global reaction network into several semi-global steps including the main reaction and side reactions. It shows how the magnitude of each reaction changes with different conditions. *Chemkin*® (2013) model is the most complex detailed mechanism steps including all gas and surface species, which will be applied on *Chemkin-Pro*® software (2013) with reaction conditions, catalyst site density, and catalyst surface area. Extra DR tests over Pt/Pd-CNT without Zeolite (added to the catalyst for inert bulk) were finished as blank tests, results of which will be discussed in Chapter 8. Result for RWGS over Pt/Pd-CNT catalyst will be shown in Chapter 9, following the research strategy used for the DR analysis. Chapter 10 considers any mass transfer limitations, catalyst bed isothermality, and the integral reactor model.

CHAPTER 2

CATALYST

2.1 Catalyst Synthesis and Preparation

All catalysts used in this study were prepared by the research group directed by Prof. Somenath Mitra of the Chemistry and Environmental Science Department of NJIT. The catalyst synthesis begins with the functionalization in which carboxyl groups (-COOH) are chemically attached to the CNT. Then, the metal is added. Both steps use a microwave reaction technique (Chen, 2008).

Multi-wall CNT (Length 10-30μm, Outer diameter 20-30 nm) were purchased from Cheap Tubes Inc. Other chemicals were purchased from Sigma-Aldrich Inc. A microwave-accelerated reaction system (Mode: CEM Mars) fitted with internal temperature and pressure controls was used. The 100 mL reaction chamber was lined with Teflon PFA® (Perfluoroalkoxy) with an operating range of 0~473 K and 0~200 psi.

In a typical synthesis of carboxylated CNTs, 100 mg of CNTs were added to the reaction vessel together with 40 mL of 3:1 concentrated H_2SO_4 and HNO_3 acids. This mixture was subjected to microwave radiation at a preset temperature of 413 K for 40 min. The resulting solid from filtration using a 0.45 μm Teflon membrane was washed with deionized (DI) water until the filtrate reached a neutral pH. The functionalized carbon nanotubes (f-CNT) were dried in a vacuum oven at 343 K for 12 h. This was used for further synthesis of the platinum-palladium carbon nanotube hybrid.

To add Pt/Pd, 100 mg of the f-CNT was added to a microwave vessel with 30 mL of 12.5 each mM $PtCl_2$ and $PdCl_2$ in ethanol, and the reaction vessel was subjected to

1600 Watts of microwave radiation to achieve a synthesis temperature of 463 K. The reaction was carried out for 10 min. Once the reactor contents were cooled down, the mixture was filtered, then washed with 0.5 N HCl solution and DI water separately. The product was dried at room temperature in the vacuum oven for 12 h.

For Ru/CNT synthesis, f-CNTs were dispersed in diethylene glycol by sonication with 30 mL of 12.5 mM $RuCl_3$. The remaining steps were the same as those for Pt/Pd-CNT.

In this study, 0.5 gram Pt/Pd-CNT, 0.5 gram Ru/CNT, and 0.5 gram f-CNT were prepared. To increase the bulk volume, each of the three materials were mixed with 2.0 grams Y-zeolite, respectively. Two grams each of Pt/Pd-CNT/zeolite and Ru/CNT-zeolite were used for the catalysis processes experiments; 2.0 grams of f-CNT/zeolite were used for blank tests. The remaining 0.5 grams of each material was saved for characterizations.

2.2 Catalyst Characterization

Characterizations were done to obtain key catalyst parameters to facilitate the kinetic analysis that is the focus of this dissertation.

The Brunauer–Emmett–Teller (BET) tests show the catalyst surface area of the Pt/Pd/CNT/zeolite is 14 m^2/gram; the surface area of the Ru/CNT-zeolite is 23 m^2/gram.

The CO chemisorption tests revealed an active site density of Pt/Pd/CNT/zeolite of 1.06×10^{-5}mole/gram; the active site density of Ru/CNT-zeolite is 1.25×10^{-5}mole/gram. Using the BET areas, the site densities can also be reported as $7.6x10^{12}$ and $5.4x10^{12}$ sites/cm^2 for the Pt/Pd/CNT/zeolite and Ru/CNT/zeolite, respectively.

Energy-dispersive X-ray spectroscopy (EDS) was also done for the Pt/Pd-CNT and Ru/CNT before mixing with the zeolite. The atom contents from the EDS are shown in Table 2.1.

Table 2.1 Atoms Content of Pt/Pd-CNT and Ru/CNT

Element	Atomic Content (%)	Element	Atomic Content (%)
C	92.87	C	83.90
O	0.30	O	7.30
Pt	4.56	Ru	8.80
Pd	2.27	—	—

Figure 2.1 shows the SEM and TEM images of the catalysts. The data showed the presence of Pt and Pd on the CNTs. The SEM image shows Pt/Pd-CNT where the CNTs were 20-30 nm diameters. The TEM images under 100X and 500X magnification show well distributed Pt and Pd nanoparticles.

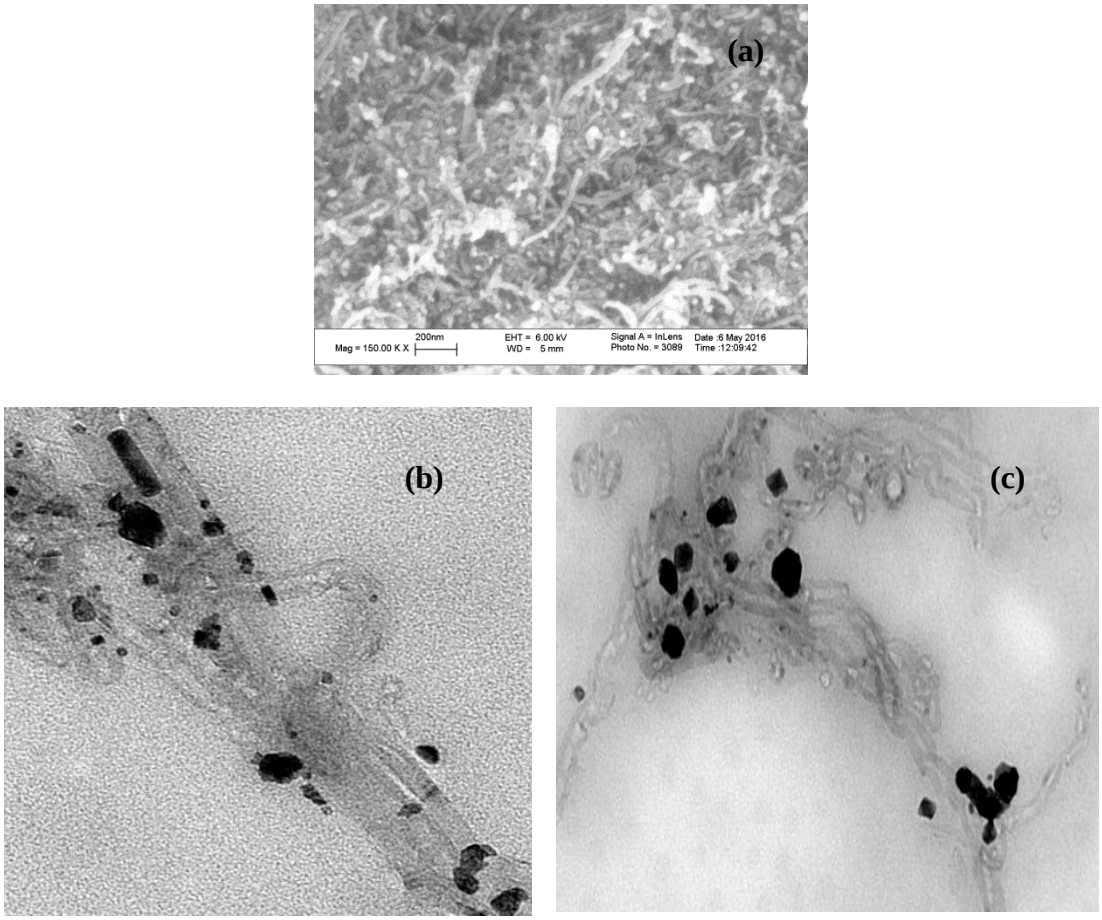

Figure 2.1 (a) SEM image of Pt/Pd-CNT under 150K magnification, (b) TEM of Pt/Pd-CNT (black) under 100,000, 500,000, (c) TEM of Pt/Pd-CNT (black) under 500,000 magnification.

CHAPTER 3

ORIGINAL EXPERIMENTS

3.1 Experimental Apparatus

All experiments for this study are conducted with the apparatus shown in Figure 3.1. The apparatus consists of mass flow control and delivery; a stainless steel tubular packed bed reactor (PBR); an electric furnace; and an on-line sampling and analysis. For each process, as Table 3.1 shows, different reactant gases and diluent helium (He) are fed through mass flow controllers. The analyzing instrument is a gas chromatograph with thermal conductivity detector (GC/TCD).

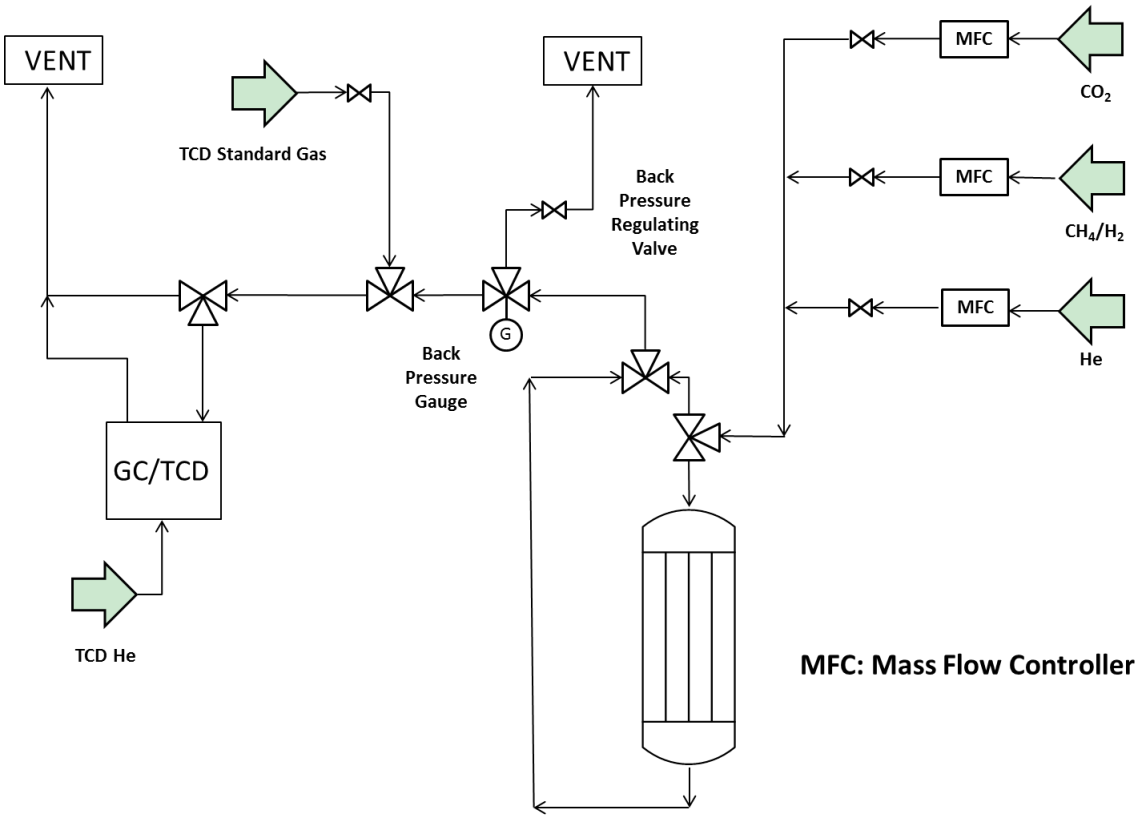

Figure 3.1 Experimental system block diagram.

Table 3.1 Reactant Gases for Each Processes Studied

Process	Reactant Gases		Dilution
DR	CH_4	CO_2	He
RWGS	H_2	CO_2	

3.1.1 Gas Flow Control

The flow rate of reactants (CH_4, CO_2 and H_2) and diluent (He) are well maintained by calibrated mass flow controllers. He for the GC is controlled by two fine regulating valves. The pressure in the flow system is monitored by a pressure gauge; a fine regulating valve is installed to manually adjust the system pressure. Two 3-way valves allow the operator to direct either feed gas (reactor bypass) or reactor effluent for on-line sampling for GC/TCD analysis.

3.1.2 Reactor Configuration

The packed bed reactor (PBR) is prepared with a (1/2 inch OD) stainless steel tube. The tube is located vertically in a robust 3-zone, temperature-controlled electric furnace. An axial thermocouple is inserted inside the tube to the catalyst bed. Excellent isothermal reactor conditions were obtained, as are described later in Chapter 10.

The CNT supported catalysts (Pt/Pd-CNT and Ru/CNT) were synthesized by Dr. Mitra's group from the NJIT Chemistry Department. Because the initial amounts of synthesized CNT catalysts were small, this material was admixed with zeolite Y. Later testing described in Chapter 10 show that this extender was chemically inert under our conditions.

The catalyst was directly plugged into the tube and well fixed by quartz wool plugs on both ends. The length of Pt/Pd-CNT/zeolite and Ru/CNT-zeolite catalyst beds were both 4 cm, therefore the pressure drops for these tests are not obvious. This wool+powder zone constitutes the PBR.

3.1.3 Gas Analysis

A model 5890 Hewlett-Packard GC with TCD is used. For all experiments, He is the carrier flow gas for the GC/TCD at 30 standard cubic centimeters per minute (sccm). The GC He source regulated pressure is 80 psig. The GC oven temperature is kept at 303 K, attenuation at 0, and range at 3. The peaks are recorded by and quantified on a laboratory PC using the Vernier Logger-Pro software.

A gas standard was used to calibrate the CG/TCD. It contains CO (1.024%, mole fraction, similarly hereinafter), CO_2 (1.002%), O_2 (1.048%), H_2 (4.044%), and CH_4 (2.040%), with balance He. In the calibration experiments, standard sample is delivered on-line into the GC/TCD. As mole fractions of all components are all known, we get the fraction-area function for every gaseous component (except water vapor). Regulated pressure of the standard cylinder is 30 psig. A gas sample valve is used for injecting a known amount of gas, collected into a sample loop, into the GC/TCD. This sample loop is always filled to the SAME pressure and temperature for both calibration and experimental samples. This ensures consistent chromatographic analysis.

3.2 Experimental Procedure

In order to keep the reaction pressure constant, a back pressure gauge and a regulating valve are applied. The regulating valve should be manually adjusted to keep reaction

pressure at 30 psig. For safety consideration, relief gas and all effluent are discharged to vent. Any leak of the system will lead to inaccurate experimental results, or even safety risks in lab. Therefore, seal tests are done for the whole system before any experiment. Inspections are focused on connections of tubes or flow meters, where any leaks are most likely to exist.

Before running experiments, all gas sources are checked for sufficiency. To protect the catalyst, only feed He flows through the reactor when heating up the furnace. During the DR and RWGS experiments reactant CO_2 and CH_4 (or H_2) is added once reactor temperature is achieved.

3.2.1 Dry Reforming Tests

Dry reforming is tested over Pt/Pd-CNT/zeolite and Ru/CNT-zeolite catalysts. Reaction temperature ranges from 500 ^oC to 700 ^oC, feed molar ratio CH_4/CO_2 ranges from 0.5 to 2.0, total inlet flow rate ranges from 46.67 sccm to 166.67sccm. For each run, the following protocol is followed:

1. Raise the reactor temperature to the set-point desired.
2. Switch the two 3-way valves to direct CH_4, CO_2 and He to bypass the reactor.
3. Sample the feed by GC/TCD analysis.
4. Redirect the feed through the reactor.
5. Wait several minutes till the effluent flushes the whole post-reactor piping.
6. Sample the effluent by GC/TCD.
7. When appropriate, convert the peak areas of products and unreacted reactants into mole fractions.

3.2.2 Reverse Water Gas Shift Tests

The RWGS is tested over the Pt/Pd-CNT/zeolite catalyst. Reaction temperature ranges from 500 ^{o}C to 700 ^{o}C, feed molar ratio CO_2/H_2 ranges from 0.5 to 2.0, while total inlet flow rate is kept at 66.67 sccm. The 7-step procedure of experiment described above is the same as for the DR tests, only to change the inlet from CH_4 and CO_2 into H_2 and CO_2.

3.2.3 Blank Tests

To rule out the catalytic effect of steel tube and zeolite, three sets of blank test are being conducted.

1. CH_4 and CO_2 go through empty steel tube reactor with same reaction conditions of previous DR tests.
2. CH_4 and CO_2 go through pure zeolite packed bed in steel tube reactor with same reaction conditions of previous DR tests.
3. CH_4 and CO_2 go through Pt/Pt-CNT without zeolite packed bed in steel tube reactor with same reaction conditions of previous DR tests.

CHAPTER 4

DATA ANALYSIS

4.1 Experimental Gas Composition

For each workday, a GC/TCD calibration test is done as the first experiment. Subsequent analysis of mole fractions is based on the result of this calibration experiment. Table 4.1 lists typical sample data of a calibration test. In all cases, the TCD response (peak area) is linear with gas concentration.

Table 4.1 Sample data of calibration experiment

Species	Composition (x) (mole %)	Retention time (s)	Peak area (y) (mv ·s)	Calibration Relations
H_2	4.044	~115	2.591	y=0.6407x
CO	1.024	~176	129.9	y=126.66x
CH_4	2.040	~313	205.6	y=100.93x
CO_2	1.002	~779	148.3	y=148x

The compositions (x) in Table 4.1 are already known, since they are based on calibrated mixtures obtained from gas vendors. The measured GC/TCD peak areas, are taken as y. The GC/TCD is known to be linear over a wide range; so a one-point calibration is sufficient.

4.1.1 Dry Reforming Gas Composition

Table 4.2 lists a typical sample of experiment results from CH_4 DR over Pt/Pd-CNT/zeolite reactor feed (bypass) test and reactor effluent test as measured by GC/TCD. Reaction conditions were 923 K and 30 psig. Total flow rate was 66.67 standard cubic centimeters (sccm), flow rate of He is 56.67 sccm, gas hourly space velocity (GHSV) =2000 ml/(gram of catalyst·hr). For precision, every GC/TCD run was repeated.

Table 4.2 Sample Data of CH_4 DR Experiment

	#	Species	Retention time (s)	Peak area (mv ·s)	Composition (mole %)
Bypass Experiments	1	CH_4	~313	874.4	8.57
		CO_2	~779	852.2	5.78
	2	CH_4	~313	880.9	8.64
		CO_2	~779	858.1	5.82
Reaction	1	H_2	~115	6.924	5.34
		CO	~176	677.8	5.37
		CH_4	~313	507.6	4.98
		CO_2	~779	355.9	2.41
	2	H_2	~115	7.623	4.83
		CO	~176	669.6	5.31
		CH_4	~313	510.9	5.01
		CO_2	~779	359.8	2.44

Since each run was repeated, the mean was taken as the final result. The result is shown as Table 4.3.

Table 4.3 Sample Mean Composition of CH_4 DR– Reactor Feed and Effluent

	Species	Composition (% mole)
Feed	CH_4	8.61
	CO_2	5.80
Effluent	H_2	5.55
	CO	5.34
	CH_4	5.00
	CO_2	2.43

From Table 4.3, the inlet CH_4/CO_2 ratio = 8.61/5.80 = 1.48. The H_2O vapor content is estimated based on the O atom balance since CO and CO_2 are accurately measured, and CO_2 is the only oxygen atom source in the feed. For the case in Table 4.3, the H_2O composition is calculated as 1.4%.

According to the principle of TCD, the bigger the difference of thermal conductivity between sample gas and the carrier gas (He), the more sensitive the detector will be for the sample gas, as long as the carrier conductivity is larger than the sample gas value. Table 4.4 shows the thermal conductivities of all gas species in our research at TCD temperature. The thermal conductivity of H_2 is close and even greater than that of He. That explains why the relatively small and negative peak area of H_2 observed in our TCD tests, which will amplify the uncertainty when converting peak area into mole

fraction. Therefore, for DR data analysis, as compositions of CH_4, CO_2, and CO are accurately measured, composition of H_2O is well estimated, H_2 content is estimated based on H atom balance. For the case in Table 4.3, the H_2 composition is calculated as 5.82%. All results of CH_4 DR are listed in Appendix F and M.

Table 4.4 Thermal Conductivities of Gas Species at 400 K

Gas Species	Thermal Conductivity [mW/(m·K)]
He	190.6
H_2	230.4
CO	32.3
CH_4	49.1
CO_2	25.1

Source: http://www.engineersedge.com/heat_transfer/thermal-conductivity-gases.htm

4.1.2 Reverse Water Gas Shift Gas Composition

Table 4.5 lists a typical sample of experiment results from RWGS over Pt/Pd-CNT/zeolite reactor feed (bypass) test and reactor effluent test as measured by GC/TCD. Reaction conditions were 923 K and 30 psig. Total flow rate was 66.67 sccm, flow rate of He is 56.67 sccm, gas hourly space velocity (GHSV) =2000 ml/(gram of catalyst·hr). In order to ensure accuracy, every GC/TCD run was repeated.

Table 4.5 Sample Data of RWGS Experiment

	#	Species	Retention time (s)	Peak area (mv ·s)	Composition (mole %)
Bypass Experiments	1	H_2	~115	12.37	9.39
		CO_2	~779	666.2	4.65
	2	H_2	~313	12.69	9.46
		CO_2	~779	665.5	4.64
Reaction	1	H_2	~115	7.769	5.90
		CO	~176	241.3	1.97
		CH_4	~313	31.1	0.31
		CO_2	~779	375.6	2.62
	2	H_2	~115	8.206	6.23
		CO	~176	241.9	1.98
		CH_4	~313	32.11	0.32
		CO_2	~779	368.0	2.57

The mean results are shown as Table 4.6.

Table 4.6 Sample Mean Composition of RWGS– Reactor Feed and Effluent

	Species	Composition (% mole)
Inlet	H_2	9.43
	CO_2	4.65
Outlet	H_2	6.07
	CO	1.98
	CH_4	0.32
	CO_2	2.60

From Table 4.6, the inlet CO_2/H_2 ratio = 4.65/9.43 = 0.49. The H_2O vapor content is also estimated based on the O atom balance. For the case in Table 4.6, the H_2O composition is calculated as 2.12%.

Our RWGS tests take relatively high content H_2 as reactant, which leads to a relatively bigger H_2 peak area. Snavely (1998) showed that the linear range for H_2 was 6-32.5% when using He as carrier gas. Therefore, the inlet H_2 composition is converted from peak area. As a certain amount of H_2 is consumed in RWGS test, peak area of outlet H_2 is shrunk. Therefore, outlet H_2 content is estimated based on H atom balance. For the case in Table 4.6, the H_2 composition is calculated as 6.67%. All results of RWGS are listed in Appendix Table Q.1.

4.2 Uncertainty Estimation

The results of DR and RWGS needs an indication of the uncertainty (precision) in the experimental data. Since the results involves outlet compositions of H_2O (y_{H_2O}) and H_2 (y_{H_2}), which are calculated quantities based on measured inlet compositions of CH_4 ($y_{CH_4\,0}$), CO_2 ($y_{CO_2\,0}$), and H_2 ($y_{H_2\,0}$) with outlet compositions of CH_4 (y_{CH_4}), CO_2 (y_{CO_2}), and CO (y_{CO}), a propagation of errors analysis is appropriate.

4.2.1 Dry Reforming Results

For all experiments, the reactants flow rates were all calibrated against bubble flow meter. Therefore, all reactants flow rates are supposed to be right. The H_2O composition is calculated by:

$$y_{H_2O} = 2\left(y_{CO_2\,0} - y_{CO_2}\right) - y_{CO} \tag{4.1}$$

For DR results, the +/- uncertainties in compositions of inlet CH_4 ($\sigma_{y_{CH_4\,0}}$), outlet CH_4 ($\sigma_{y_{CH_4}}$), inlet CO_2 ($\sigma_{y_{CO_2\,0}}$), outlet CO_2 ($\sigma_{y_{CO_2}}$), and outlet CO ($\sigma_{y_{CO}}$) are determined by the difference from first test and repeated test. The +/- uncertainties in compositions of H_2O composition (y_{H_2O}) is given by:

$$(\sigma_{y_{H_2O}})^2 = \left(\frac{\partial\, y_{H_2O}}{\partial y_{CO_2\,0}}\right)^2 \left(\sigma_{y_{CO_2\,0}}\right)^2 + \left(\frac{\partial\, y_{H_2O}}{\partial y_{CO_2}}\right)^2 \left(\sigma_{y_{CO_2}}\right)^2 + \left(\frac{\partial\, y_{H_2O}}{\partial y_{CO}}\right)^2 \left(\sigma_{y_{CO}}\right)^2 \tag{4.2}$$

Plug equation 4.1 into 4.2:

$$(\sigma_{y_{H_2O}})^2 = (2)^2 \left(\sigma_{y_{CO_2\,0}}\right)^2 + (-2)^2 \left(\sigma_{y_{CO_2}}\right)^2 + (-1)^2 \left(\sigma_{y_{CO}}\right)^2 \tag{4.3}$$

$$(\sigma_{y_{H_2O}})^2 = 4\left[\left(\sigma_{y_{CO_2\,0}}\right)^2 + \left(\sigma_{y_{CO_2}}\right)^2\right] + \left(\sigma_{y_{CO}}\right)^2 \tag{4.4}$$

The outlet H_2 composition is calculated by:

$$y_{H_2} = 2\left(y_{CH_4\,0} - y_{CH_4}\right) - y_{H_2O} \tag{4.5}$$

Plug Equation 4.1 into 4.5:

$$y_{H_2} = 2\left(y_{CH_4\,0} - y_{CH_4}\right) - \left[2\left(y_{CO_2\,0} - y_{CO_2}\right) - y_{CO}\right] \tag{4.6}$$

The +/- uncertainty in H_2 composition (y_{H_2}) is given by:

$$(\sigma_{y_{H_2}})^2 = \left(\frac{\partial\, y_{H_2}}{\partial y_{CH_4\,0}}\right)^2 \left(\sigma_{y_{CH_4\,0}}\right)^2 + \left(\frac{\partial\, y_{H_2}}{\partial y_{CH_4}}\right)^2 \left(\sigma_{y_{CH_4}}\right)^2 + \left(\frac{\partial\, y_{H_2}}{\partial y_{CO_2\,0}}\right)^2 \left(\sigma_{y_{CO_2\,0}}\right)^2 +$$

$$\left(\frac{\partial\, y_{H_2}}{\partial y_{CO_2}}\right)^2 \left(\sigma_{y_{CO_2}}\right)^2 + \left(\frac{\partial\, y_{H_2}}{\partial y_{CO}}\right)^2 \left(\sigma_{y_{CO}}\right)^2 \tag{4.7}$$

$$(\sigma_{y_{H_2}})^2 = 4\left[\left(\sigma_{y_{CH_4\,0}}\right)^2 + \left(\sigma_{y_{CH_4}}\right)^2 + \left(\sigma_{y_{CO_2\,0}}\right)^2 + \left(\sigma_{y_{CO_2}}\right)^2\right] + \left(\sigma_{y_{CO}}\right)^2 \tag{4.8}$$

Based on Equation 4.4 and 4.8, $\sigma_{y_{H_2O}}$ and $\sigma_{y_{H_2}}$ for DR could be determined. Uncertainty analysis on results of DR over Pt/Pd-CNT/zeolite at 873 K are selected as typical example, and is shown in Table 4.7.

Table 4.7 Uncertainty Analysis on Results of DR over Pt/Pd-CNT/zeolite at 873 K

Feed CH_4/CO_2	$\sigma_{y_{CH_4\,0}}$	$\sigma_{y_{CO_2\,0}}$	$\sigma_{y_{CH_4}}$	$\sigma_{y_{CO_2}}$	$\sigma_{y_{CO}}$	$\sigma_{y_{H_2O}}$	$\sigma_{y_{H_2}}$
0.47	0.12	0	0.01	0.05	0.07	0.12	0.27
0.72	0.06	0.07	0.02	0.04	0	0.15	0.20
0.99	0.04	0.03	0.01	0.03	0.03	0.10	0.13
1.46	0.06	0.02	0.02	0.03	0.03	0.08	0.15
1.96	0.04	0.02	0	0	0	0.04	0.19

As is shown in Table 4.7, the uncertainty of H_2O and H_2 are obviously higher than those of other species. To further demonstrate the impact, uncertainties are compared

with experimental measured values. The relative uncertainty σ_{y_i} /y_i are of the same case are shown in Table 4.8.

Table 4.8 Relative Uncertainty on Results of DR over Pt/Pd-CNT/zeolite at 873 K

Feed CH_4/CO_2	$\frac{\sigma_{y_{CH_4\,0}}}{y_{CH_4\,0}}$ (%)	$\frac{\sigma_{y_{CO_2\,0}}}{y_{CO_2\,0}}$ (%)	$\frac{\sigma_{y_{CH_4}}}{y_{CH_4}}$ (%)	$\frac{\sigma_{y_{CO_2}}}{y_{CO_2}}$ (%)	$\frac{\sigma_{y_{CO}}}{y_{CO}}$ (%)	$\frac{\sigma_{y_{H_2O}}}{y_{H_2O}}$ (%)	$\frac{\sigma_{y_{H_2}}}{y_{H_2}}$ (%)
0.47	2.55	0	0.30	0.64	2.06	12.00	16.07
0.72	0.95	0.80	0.43	0.47	0	11.11	10.36
0.99	0.53	0.39	0.17	0.75	0.90	8.47	5.75
1.46	0.67	0.33	0.28	0.75	0.96	7.62	5.62
1.96	0.40	0.39	0	0	0	2.63	8.56

According to Table 4.8, the relative uncertainties of species, which are directly measured from TCD, are very small. The relative uncertainties of H_2O and H_2 are obviously higher than other species. Generally speaking, the uncertainties of all species are acceptable. Uncertainty estimates are conducted for all DR data. All results are listed in Appendix A and presented with multiple reaction model in Sections 6.5.4 and 7.5.4.

4.2.2 Reverse Water Gas Shift Results

For RWGS results, the +/- uncertainties in compositions of inlet H_2 ($\sigma_{y_{H_2\,0}}$), outlet CH_4 ($\sigma_{y_{CH_4}}$), inlet CO_2 ($\sigma_{y_{CO_2\,0}}$), outlet CO_2 ($\sigma_{y_{CO_2}}$), and outlet CO ($\sigma_{y_{CO}}$) are determined by the difference from first test and repeated test. The +/- uncertainties in compositions of H_2O composition (y_{H_2O}) is also given by Equation 4.4.

The outlet H_2 composition is calculated by:

$$y_{H_2} = y_{H_2\,0} - y_{H_2O} - 0.5y_{CH_4} \tag{4.9}$$

Plug equation 4.1 into 4.9:

$$y_{H_2} = y_{H_2\,0} - 2\left(y_{CO_2\,0} - y_{CO_2}\right) + y_{CO} - 0.5y_{CH_4} \tag{4.10}$$

The +/- uncertainty in H_2 composition (y_{H_2}) is given by:

$$(\sigma_{y_{H_2}})^2 = \left(\frac{\partial\, y_{H_2}}{\partial y_{H_2\,0}}\right)^2 \left(\sigma_{y_{H_2\,0}}\right)^2 + \left(\frac{\partial\, y_{H_2}}{\partial y_{CH_4}}\right)^2 \left(\sigma_{y_{CH_4}}\right)^2 + \left(\frac{\partial\, y_{H_2}}{\partial y_{CO_2\,0}}\right)^2 \left(\sigma_{y_{CO_2\,0}}\right)^2 +$$

$$\left(\frac{\partial\, y_{H_2}}{\partial y_{CO_2}}\right)^2 \left(\sigma_{y_{CO_2}}\right)^2 + \left(\frac{\partial\, y_{H_2}}{\partial y_{CO}}\right)^2 \left(\sigma_{y_{CO}}\right)^2 \tag{4.11}$$

$$(\sigma_{y_{H_2}})^2 = \left(\sigma_{y_{H_2\,0}}\right)^2 + 0.25\left(\sigma_{y_{CH_4}}\right)^2 + 4\left[\left(\sigma_{y_{CO_2\,0}}\right)^2 + \left(\sigma_{y_{CO_2}}\right)^2\right] + \left(\sigma_{y_{CO}}\right)^2 \tag{4.12}$$

Based on Equations 4.4 and 4.12, $\sigma_{y_{H_2O}}$ and $\sigma_{y_{H_2}}$ for RWGS could be determined. Uncertainty analysis on results of RWGS over Pt/Pd-CNT/zeolite at 923 K is selected as typical example, and is shown in Table 4.9.

Table 4.9 Uncertainty analysis on results of RWGS over Pt/Pd-CNT/zeolite at 923 K

Feed CO_2/H_2	$\sigma_{y_{CO_2\,0}}$	$\sigma_{y_{H_2\,0}}$	$\sigma_{y_{CO_2}}$	$\sigma_{y_{CH_4}}$	$\sigma_{y_{CO}}$	$\sigma_{y_{H_2O}}$	$\sigma_{y_{H_2}}$
0.49	0.01	0.25	0.05	0.01	0.01	0.10	0.27
0.76	0	0.36	0.01	0.01	0	0.02	0.36
1.02	0.03	0.16	0.03	0	0.01	0.09	0.18
1.51	0.01	0.09	0.01	0	0.04	0.05	0.10
1.99	0.03	0.10	0	0	0.03	0.07	0.12

According to Table 4.9, the uncertainty of inlet H_2 is obviously higher than those of other directly measured species, because of the relatively smaller peak area of H_2. The uncertainty of outlet H_2 is almost as same as that of inlet H_2. The uncertainty of H_2O is lower than that of inlet and outlet H_2, but still higher than other spices. Relative uncertainties are also estimated for the same case, and shown in Table 4.10.

Table 4.10 Relative Uncertainty on Results of RWGS over Pt/Pd-CNT/zeolite at 923 K

Feed CO_2/H_2	$\frac{\sigma_{y_{CO_{2\,0}}}}{y_{CO_{2\,0}}}$ (%)	$\frac{\sigma_{y_{H_{2\,0}}}}{y_{H_{2\,0}}}$ (%)	$\frac{\sigma_{y_{CO_2}}}{y_{CO_2}}$ (%)	$\frac{\sigma_{y_{CH_4}}}{y_{CH_4}}$ (%)	$\frac{\sigma_{y_{CO}}}{y_{CO}}$ (%)	$\frac{\sigma_{y_{H_2O}}}{y_{H_2O}}$ (%)	$\frac{\sigma_{y_{H_2}}}{y_{H_2}}$ (%)
0.49	0.22	2.65	1.92	3.13	0.51	4.83	4.05
0.76	0.00	4.60	0.27	4.17	0.00	0.94	6.91
1.02	0.44	2.39	0.66	0.00	0.43	4.05	4.24
1.51	0.12	1.65	0.16	0.00	1.67	2.65	2.99
1.99	0.34	2.23	0.00	0.00	1.35	4.22	4.27

Table 4.10 shows relative uncertainties for all species. The values of them are generally limited. Uncertainty estimates are also conducted for all RWGS data. All results are listed in Appendix A and presented with multiple reaction model in Section 9.5.3.

CHAPTER 5

MULTIPLE REACTION MODEL FOR METHANE DEHYDROAROMATIZATION

5.1 Introduction of Methane Dehydroaromatization

The necessity of alternative nature gas (mostly CH_4) utilization has been discussed in Section 1.2.1. Typically, CH_4 is first converted to synthesis gas either by reforming or partial oxidation. In the second step, various chemical products are made from the synthesis gas (Cheng, 2017). However, because CH_4 is an extremely stable molecule, requiring relatively severe reaction conditions to activate the C−H bond, the preparation and compression of synthesis gas typically accounts for about 60−70% of the capital cost and almost all of the energy consumption to operate the plant (Kosinov, 2017). Consequently, direct conversion of CH_4 into desired chemical products is an important goal to reduce cost and energy consumption relative to conventional processing (Kosinov, 2017). A number of processes have been proposed for direct conversion of CH_4 to valuable chemicals or liquid hydrocarbon fuels, including direct partial oxidation of CH_4 to methanol and formaldehyde, oxidative coupling of CH_4 to ethylene, and dehydroaromatization to aromatics (Ma, 2013). Compared to oxidative processes, methane dehydroaromatization (MDA) could achieve higher benzene selectivity with the oxygen-free conditions (Kosinov, 2017). The ideal overall stoichiometry of MDA is shown as Equation 5.1(Karakaya, 2015):

$$6CH_4 \rightarrow C_6H_6 + 9H_2 \quad \Delta H_{298K} = 89 \text{ kJ/mol} \tag{5.1}$$

The challenges facing this promising process are still considerable, including high endothermicity requiring relatively high temperatures (900-1100 K) and

equilibrium-limited conversions (e.g., ~ 21% at 1000 K) (Karakaya, 2015), (Li, 2002).

Though out of topic, this chapter describes a computational study done to establish a global multi-reaction model technique developed and used for the modeling of the DR and RWGS data – the primary topics. This effort begins with the consideration of a multiple elementary reaction model for MDA. The model, taken from the literature, will be used to generate *simulated* experimental data. These data are then used to calibrate a short global reaction model.

5.2 Multiple Reaction Model

Evaluation of the detailed catalytic MDA reaction mechanism, which contains all gaseous and adsorbed reacting species, is demanding. For example, a proper detailed mechanism set requires a mechanism computational tool such as *Chemkin*® (2013) or *Cantera*® (Goodwin, 2016). The full mechanism does not lend itself to quick engineering calculations, for which the following 3-reaction scheme (Karakaya, 2015) is better suited.

The 3-reaction scheme, shown in Table 3.1, contains only gaseous species, though the reactions occur on a solid catalyst. The first reaction is the critical activation of CH_4 to ethylene (C_2H_4), while the second is the aromatization to the desired benzene (C_6H_6). The third step is the continued, though undesired, molecular weight growth to even larger species, represented by naphthalene ($C_{10}H_8$). All three reactions are reversible. Their forward rates are taken to be first order in each relevant reactant, with the net rates represented through the use of the approach to equilibrium η_i. The goal of this 3-reaction model study was the estimation of the Arrhenius parameters for each reaction in Table 3.1: $k_{fi} = A_i exp(-E_i/(RT))$. These Arrhenius parameters do not exist in the literature.

The original study (Li, 2002) proposing this 3-reaction set was run at only a single temperature 950 K.

Table 5.1 Three Global Reaction Scheme with Accompanying Rates

Rxn #	Stoichiometry	Kinetic Rate Expression	Approach to Equilibrium
1	$2\ CH_4 \rightleftharpoons C_2H_4 + 2\ H_2$	$r_1 = k_{f1} P_{CH4}(1-\eta_1)$	$\eta_1 = \frac{P_{C2H4} P_{H2}^2}{P_{CH4}^2 K_{p1}}$
2	$3\ C_2H_4 \rightleftharpoons C_6H_6 + 3\ H_2$	$r_2 = k_{f2} P_{C2H4}(1-\eta_2)$	$\eta_2 = \frac{P_{C6H6} P_{H2}^3}{P_{C2H4}^3 K_{p2}}$
3	$C_6H_6 + 2\ C_2H_4 \rightleftharpoons C_{10}H_8 + 3\ H_2$	$r_3 = k_{f3} P_{C2H4} P_{C6H6}(1-\eta_3)$	$\eta_3 = \frac{P_{C10H8} P_{H2}^3}{P_{C6H6} P_{C2H4}^2 K_{p3}}$

5.3 Model Testing and Results

In order to estimate the Arrhenius parameters, the global 3-reaction set must be evaluated against quality data. Experimental MDA data over a temperature range (948-1023 K) obtained in a *laboratory* packed bed reactor (PBR) were used to validate a detailed 54-reaction MDA mechanism shown in Appendix C (Karakaya, 2016). Their PBR simulation accounted for real reactor non-idealities such as axial dispersion. Therefore, in the current study where six Arrhenius parameters are desired, it is more appropriate to evaluate the 3-reaction set against idealized data obtained using the published MDA mechanism rather than the actual experimental MDA data (Karakaya, 2016) since the elementary mechanism represents pure catalytic chemistry without any complications such as transport effects.

In this study, an idealized calibration database was generated with which to evaluate the 3-reaction set to obtain Arrhenius parameters. The detailed MDA mechanism (Karakaya, 2016) was exercised with an *ideal* PBR (modeled as a plug flow reactor)

simulation using the *Chemkin-Pro*® package (2013). The simulation conditions were the experiment values reported by Karakaya et al. (2016). These are in Table 5.2 in two parametric groups. The primary data collected from the new simulations were the mole fractions y_j of the five major species in Table 5.1.

Table 5.2 Parameters for the *Chemkin*® Simulations Using the Full MDA Mechanism

Run name	I	II	III	IV
WHSV (cm^3/g_{cat}-hr)	750	750	750	750
v_o (sccm)	12.3	12.3	12.3	12.3
T (K)	948	973	998	1023

Run name	V	VI	VII	VIII
WHSV (cm^3/g_{cat}-hr)	1500	1500	1500	1500
v_o (sccm)	24.7	24.7	24.7	24.7
T (K)	948	973	998	1023

Run name	IX	X	XI	XII
WHSV (cm^3/g_{cat}-hr)	2250	2250	2250	2250
v_o (sccm)	36.9	36.9	36.9	36.9
T (K)	948	973	998	1023

Run name	XIII	XIV	XV	XVI
WHSV (cm^3/g_{cat}-hr)	3000	3000	3000	3000
v_o (sccm)	49.3	49.3	49.3	49.3
T (K)	948	973	998	1023

Other important parameters used in the *Chemkin-Pro*® PBR simulations were: feed 95 mole% CH_4, balance He; 4 cm bed length; 1.23 cm^2 net cross-section; 2.5E5 cm^2/cm surface area/unit bed length; and 14.5 psia reactor pressure. These are consistent with those reported by Karakaya et al. (2016), whose catalytic reactor bed consisted of 2.5 total grams of catalyst (1 gram of Mo/zeolite, balance inert SiC). All species fractions from *Chemkin-Pro*® simulations for the 16 runs above are listed in Appendix Table B.1.

5.3.1 Programing for Reaction Rate Constants

The 3-reaction set (Table 5.1) was evaluated within an ideal PBR simulation as defined in Table 5.3. For a given temperature, the species balances were integrated with a *Matlab*® program. All relevant inlet PBR mole fraction data from the *Chemkin-Pro* simulations at a given temperature were supplied to the *Matlab*® program. The integration was repeated within a regression loop that optimized the rate constants k_{fi} at that temperature. This entire integration / regression procedure was performed for each temperature.

Table 5.3 Key Equations of PBR Simulation of 3-reaction Global Model

PBR Species j Balances	Net Rates r_j	Mole Fractions y_j	Partial Pressures
$dF_j/dW = r_j$ At W = 0, F_{jo} = value	$r_{CH4} = -2r_1$ $r_{C2H4} = r_1 - 3r_2 - 2r_3$ $r_{C6H6} = r_2 - r_3$ $r_{C10H8} = r_3$ $r_{H2} = 2r_1 + 3r_2 + 3r_3$	$y_j = \frac{F_j}{\sum_j F_j}$ Total molar rate includes inert	$P_j = y_j P$

The algorithm of the *Matlab*® program briefly concluded and shown in Figure 5.1.

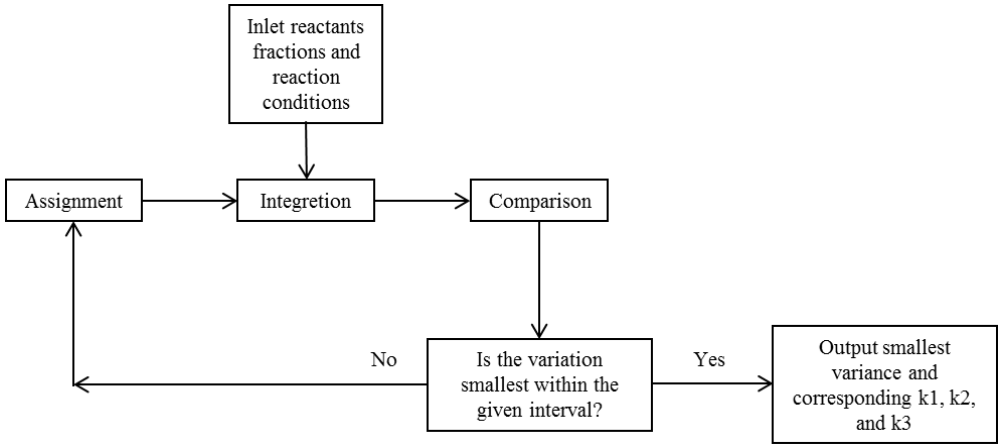

Figure 5.1 Flow chart of *Matlab*® program algorithm

Before simulation, a certain interval of k_{fi} and step size are defined. Then *Matlab*® assigns k_{f1}, k_{f2}, and k_{f3} within the interval. Integration by *Matlab*® is executed with the same inlet components and reaction conditions as *Chemkin*®. Then *Matlab*® compares the outlet fractions of all species to the simulation results from *Chemkin*® by calculating variations between them. *Matlab*® conducts this process for every step within the interval defined at first, and then outputs the smallest variation and corresponding values of k_{f1}, k_{f2}, and k_{f3}. The *Matlab*® program code for solving values of k_{fi} at 1023 K is selected as example and listed in Appendix D. Similar *Matlab*® program codes were applied for 948, 973, and 998 K. All k_{fi} values for each temperature were determined based on this algorithm.

5.3.2 Arrhenius Plots

Completion of the *Matlab*® integration / regression routine at each temperature yielded rate constants k_{fi}, which are listed in Table 5.4, for each of the three global MDA reactions.

Table 5.4 Rate Constant k_{fi} for 3-Global Reactions

T/K	1/T*1000	k_1	lnk_1	k_2	lnk_2	k_3	lnk_3
948	1.054852	0.064	-2.74887	0.080	-2.52573	2.61	0.959350
973	1.027749	0.074	-2.60369	0.091	-2.39690	2.46	0.900161
998	1.002004	0.093	-2.37516	0.096	-2.34341	2.35	0.854415
1023	0.977517	0.117	-2.14558	0.108	-2.22562	2.16	0.770108

These optimized k_{fi} were then correlated, in Figure 5.2, to obtain the Arrhenius parameters A_i, E_i for each reaction, as presented in Table 5.5. Assuming a bed density of 0.51 g/cm^3, based on the bed dimensions and total catalyst mass reported by Karakaya et al. (2016), the A_i values are also reported on a catalyst mass basis. The activation

energies for Reactions 1 and 2 are both positive, but negative for Reaction 3. The negative activation energy is because of that the reaction rates are declining with increasing temperature in this model. The equilibrium constant profile of reaction 3 is k_{ep}=exp (1398.3/T+8.2224), which is also decreasing with increasing temperature.

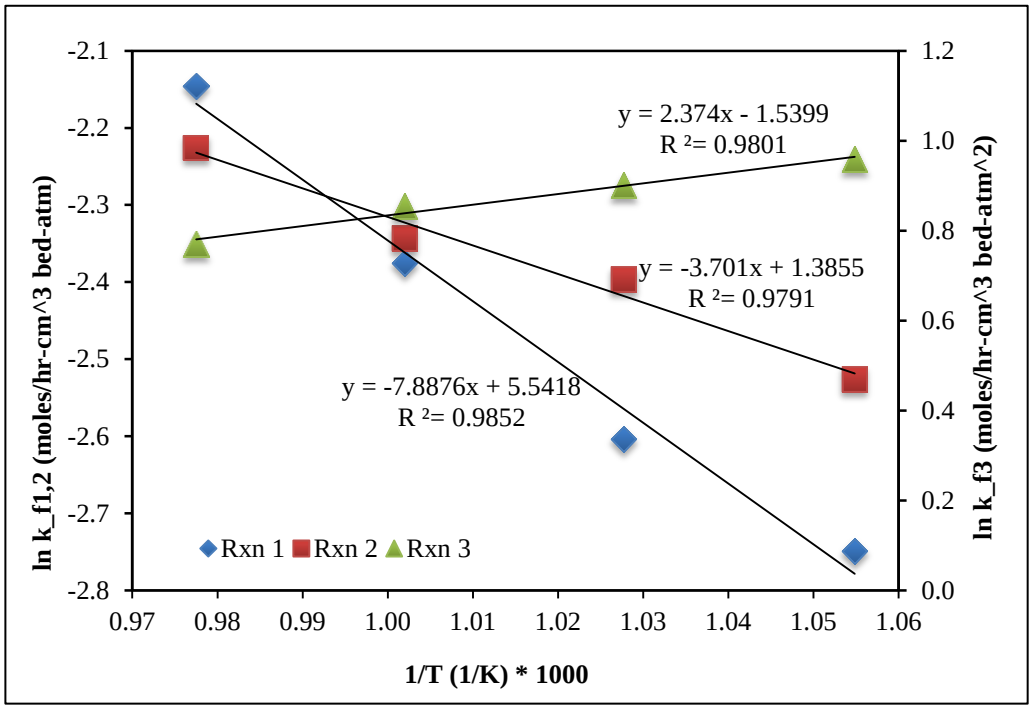

Figure 5.2: Arrhenius plot of forward rate constants k_{fi} for reactions in Table 5.1.

Table 5.5: Arrhenius Parameters for 3 Global Reactions

Reaction i	Parameter A_i (mole, hr,cm^3 bed, atm)	Parameter A_i (mole, hr, g cat, atm)	Parameter E_i (kJ)
1	255.1	500.3	65.58.
2	3.997	7.837	30.84.
3	0.214	0.420	-19.74.

5.3.3 Assessment of Multiple Reaction Model

With Arrhenius parameters obtained, the 3-reaction set was tested against the mechanism-based data for selected cases from Table 5.2. The ideal PBR simulation based on Table 5.3 was evaluated in *Polymath*®. A typical *Polymath* code, at 948 K, is listed in Appendix E.

As an example, Figure 5.3 compares the key species profiles as a function of PBR bed length for Run XI.

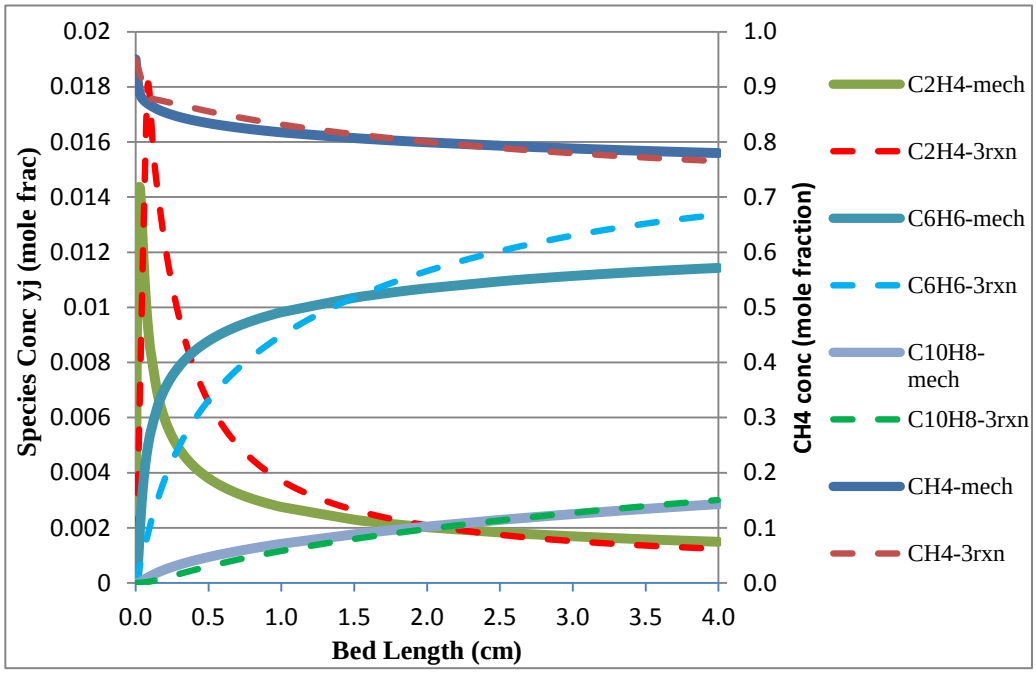

Figure 5.3 Comparison of mechanism-based and 3-reaction model-based concentrations for fixed temperature (998 K), feed rate (36.9 sccm) – Run XI from Table 5.2.

Figure 5.4 presents PBR outlet (4 cm) mole fractions for key species as functions of temperature at constant flow rate. The agreement is reasonable, with a modest difference (~10%) for C_6H_6. The CH_4 conversion increases with higher temperature,

while C_6H_6 and $C_{10}H_8$ also rise. The intermediate C_2H_4 is very small since it is consumed by two subsequent reactions, and rises very slightly with temperature.

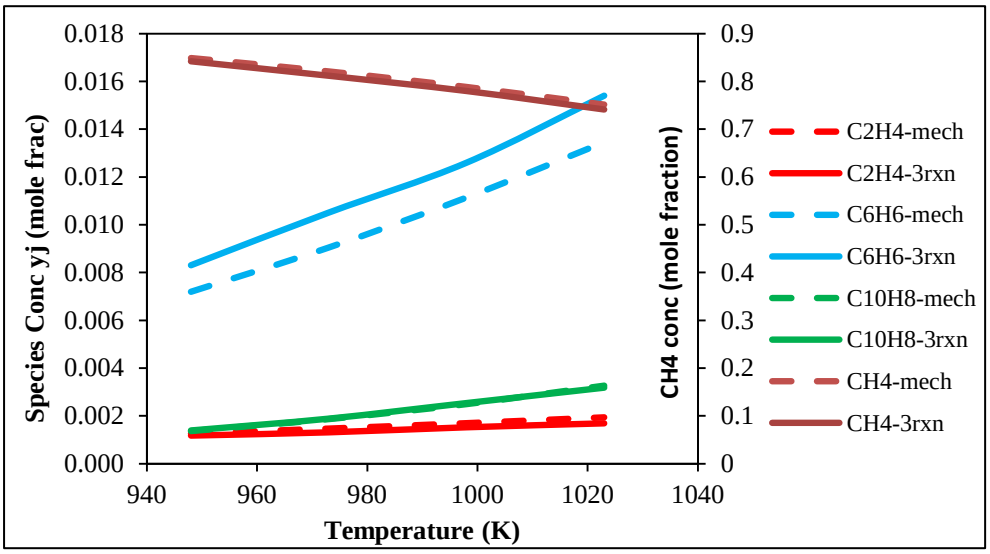

Figure 5.4 Comparison of mechanism-based and 3-reaction model-based concentrations for fixed feed rate (49.3 sccm) – Runs XIII-XVI from Table 5.2 – for PBR 4 cm.

Figure 5.5 presents similar results as functions of flow rate at constant temperature. Again, the agreement between the mechanism-based data and the 3-reaction model is also reasonable. As feed rate increases, the reduced residence time results in less CH_4 conversion, and lower amounts of product C_6H_6 and $C_{10}H_8$. Intermediate C_2H_4 modestly rises as a result.

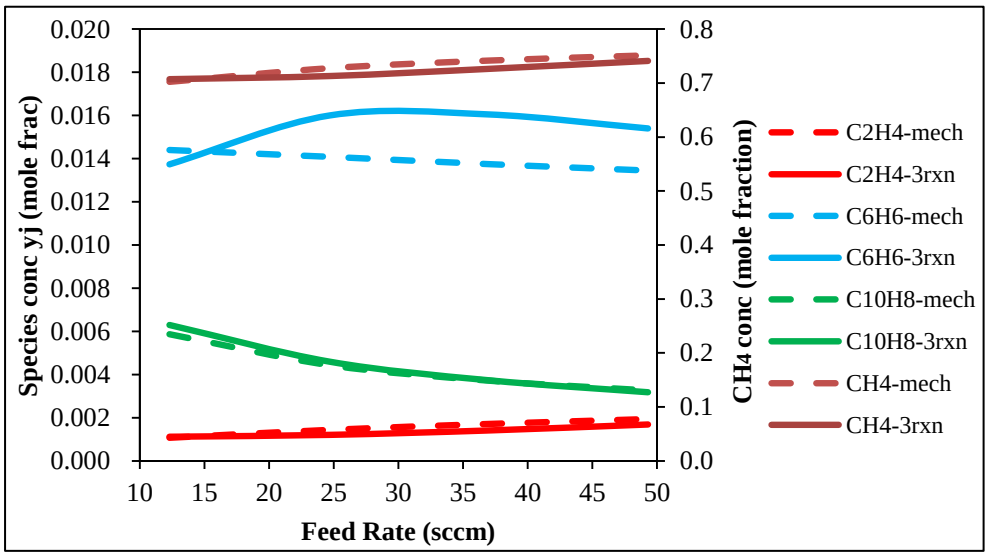

Figure 5.5 Comparison of mechanism-based and 3-reaction model-based concentrations at fixed temperature (1023 K) – Runs IV, VIII, XII, XVI – for PBR (4 cm).

It is notable that the *Chemkin*® simulations with the MDA mechanism are computationally challenging, especially in time waiting for the solution. Typical wait times in this study with *Chemkin*® (Release 17.2) running on a Windows 7 (Enterprise) PC (4 GB ram, 2.93 GHz Intel Core) were ~10 minutes for the 4 cm PBR. Evaluation of the 3-reaction set on *Polymath* takes ~ 1 second.

Though not directly related to the topic "CO_2 Reduction", this chapter describes a computational study done in this study to establish the global multi-reaction model technique developed and used for the modeling of the dry reforming and reverse water gas shift data.

CHAPTER 6

DRY REFORMING OVER PT/PD-CNT/ZEOLITE

6.1 Observed Carbon Balance

The overall DR reaction stoichiometry can be taken as:

$$CH_4 + bCO_2 \rightarrow cCO + dH_2 + eH_2O \quad (6.1)$$

The carbon atoms from CH_4 and CO_2 should convert to CO, so the CO moles should be close to the moles of sum of converted CH_4 and CO_2. Such a carbon balance is a good test of the experimental method, as well as a test for any possible carbon deposits on the catalyst. Figure 6.1 shows the comparison between feed carbon and outlet carbon for all runs in parity graphic. All runs shown on this figure were done with the same catalyst, which was not regenerated or changed.

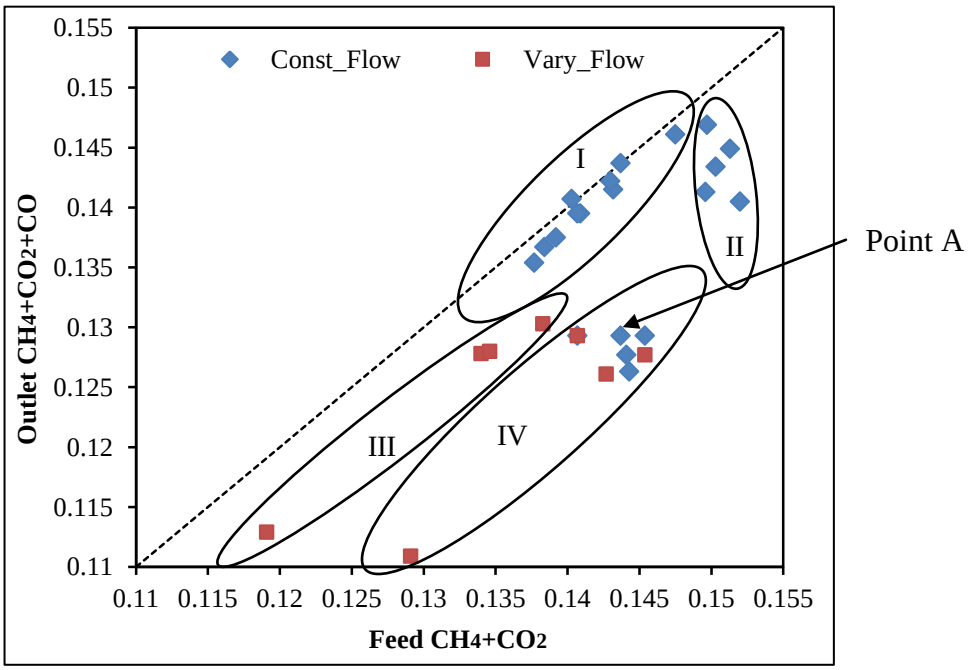

Figure 6.1 Carbon balance for all runs over Pt/Pd-CNT/zeolite.

In Figure 6.1, all spots are at or under the parity line, which means the carbon deposit is occurring during the DR reaction. A closer look of the spots distribution in the graphic could reveal the law of carbon loss in our study:

1. All runs at 773 and 823 K, as shown in circle I. The carbon loss level is obviously lower than cases at higher temperatures.

2. Circle II reflects the five constant flow runs at 873K. Result of the five spots shows that within the CH_4/CO_2 range of 0.5-2.0, the higher the feed molar ratio CH_4/CO_2 is, the more carbon loss during reaction will be.

3. Circle III shows the various flow rate runs with CH_4/CO_2=1.0 at 873 K. The level of carbon loss are very similar to circle II

4. Circle IV shows all varies flow and constant flow runs at 923 K. The level of carbon loss is more serious than cases of lower temperatures.

The carbon difference between inlet and outlet is also found in equilibrium calculations. For example, for the same reaction conditions with point A in Figure 6.1, 923 K with CH_4/CO_2 =0.5 and 66.7 sccm total flow, the feed mole fraction of CH_4+CO_2 is 0.144, the outlet mole fraction of $CH_4+CO_2+CH_4$ is 0.0817. The carbon deposit is 0.0632. All equilibrium calculation code will be shown in Section 6.3.

To sum up, for the application of Pt/Pd-CNT/zeolite, the carbon loss level is dependent on temperature and inlet CH_4/CO_2. The higher the temperature is, the serious the carbon loss will be; the higher the CH_4/CO_2, the more the carbon lost observed. Various inlet flow rate has no obvious influence on carbon loss.

6.2 Methane and Carbon Dioxide Conversion, H_2/CO

To calculate CH_4 conversions (X_A), we have:

$$X_A = \frac{\text{Moles of Converted } CH_4}{\text{Moles of Feed } CH_4} \tag{6.1}$$

Since there is a negligible change of total moles in current system as the feed is highly diluted by He, then Equation 4.1 reduces to:

$$X_A = \frac{\text{Feed } CH_4 \text{ Mole Fraction} - \text{Outlet } CH_4 \text{ Mole Fraction}}{\text{Feed } CH_4 \text{ Mole Fraction}} \tag{6.2}$$

Equation 6.2 is used to calculate conversions CH_4 for all cases in this chapter.

Similarly, CO_2 conversions (X_B) can be calculated by:

$$X_B = \frac{\text{Feed } CO_2 \text{ Mole Fraction} - \text{Outlet } CO_2 \text{ Mole Fraction}}{\text{Feed } CO_2 \text{ Mole Fraction}} \tag{6.3}$$

Equation 6.3 is used to calculate conversions CO_2 for all cases in this chapter.

Product H_2/CO is expressed as:

$$H_2/CO = \frac{\text{Outlet } H_2 \text{ Mole Fraction}}{\text{Outlet CO Mole Fraction}} \tag{6.4}$$

6.2.1 Influence of Feed Molar Ratio

Experiments were run at 773, 823, 873 and 923 K. Reactor pressure is kept at 30 psig. The total flow rate is set at 66.67 sccm, with the flow rate of He of 56. 7 sccm (85% diluent). Based on the volume of the catalyst bed, the gas hourly space velocity (GHSV) is 2000 ml/(g_{cat} hr). All calculated CH_4 and CO_2 conversions are shown as X_A, X_B vs. feed molar ratio CH_4/CO_2 plots at each temperature. In the following figures, unless specifically stated, the lines are only used for the sake of clarity for the presentation of the experimental data points, and do not represent any modeling or regression.

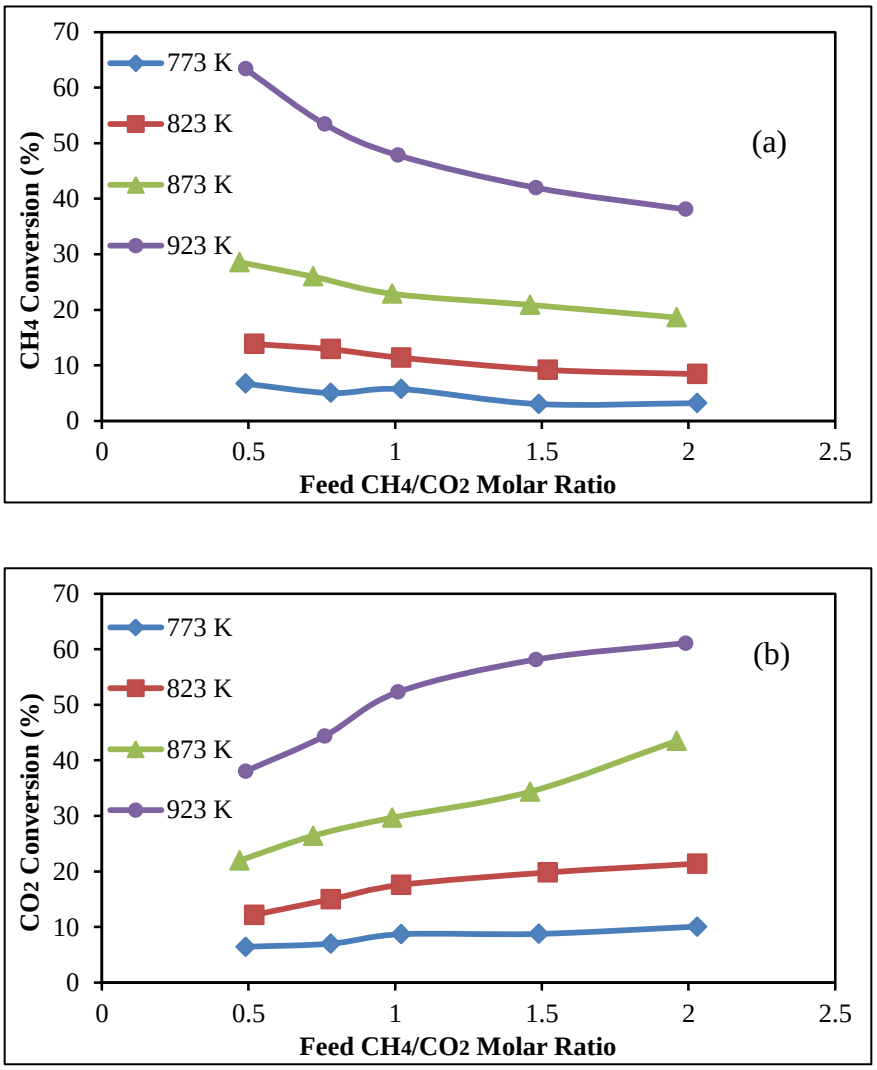

Figure 6.2 (a) CH_4 and (b) CO_2 conversion vs. feed molar ratio CH_4/CO_2 at each temperature.

Figure 6.2 shows the different CH_4 and CO_2 conversions at various molar ratios CH_4/CO_2 under each temperature. The molar ratio CH_4/CO_2 has a significant influence on both conversions. CH_4 conversion decreases with increasing molar ratio CH_4/CO_2. The higher the reaction temperature is, the bigger the drop will be. The CO_2 conversion increases with increasing feed molar ratio. These results are not necessarily surprising since, as feed CH_4/CO_2 increases, there is a shift in which is the limiting reactant.

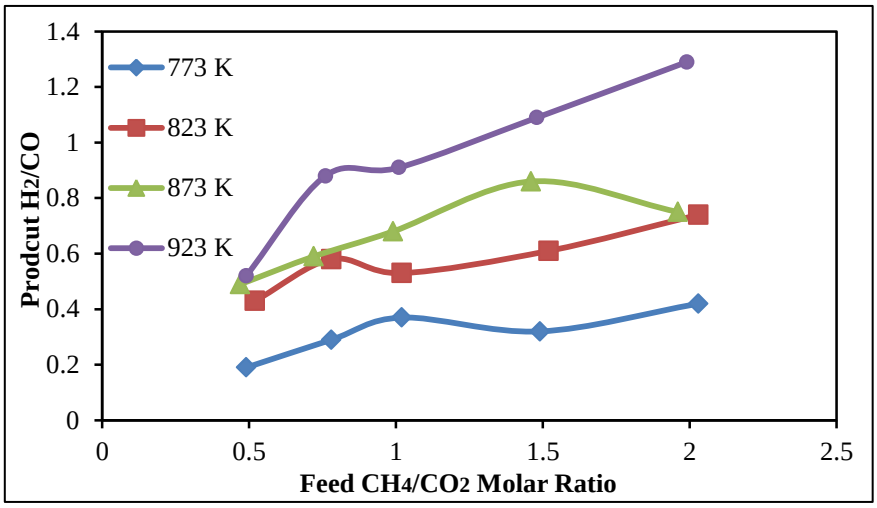

Figure 6.3 Product H_2/CO vs. feed molar ratio CH_4/CO_2 at each temperature.

Figure 6.3 shows product H_2/CO ratio changes with the feed molar ratio. Since higher CH_4/CO_2 mean more H atoms input, a higher H_2/CO ratio results.

6.2.2 Influence of Temperature

To investigate the influence of reaction temperature, the constant flow experimental results are shown in same feed molar ratio of CH_4/CO_2.

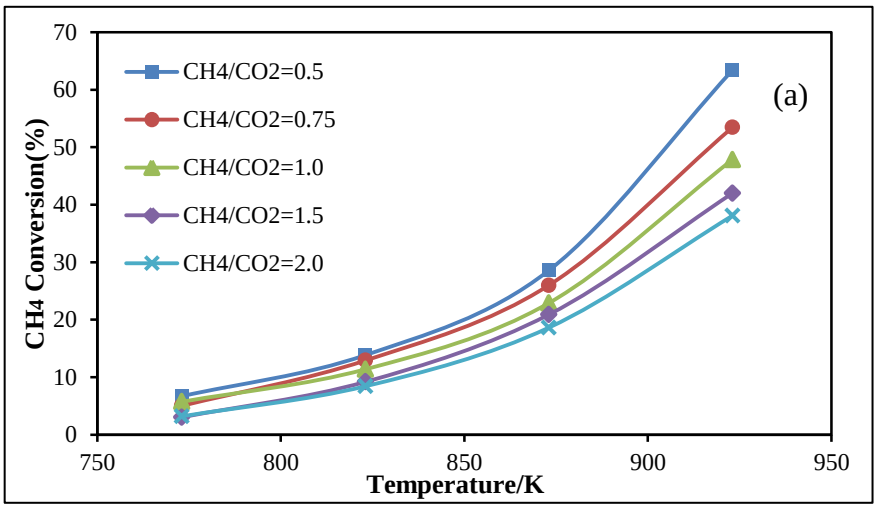

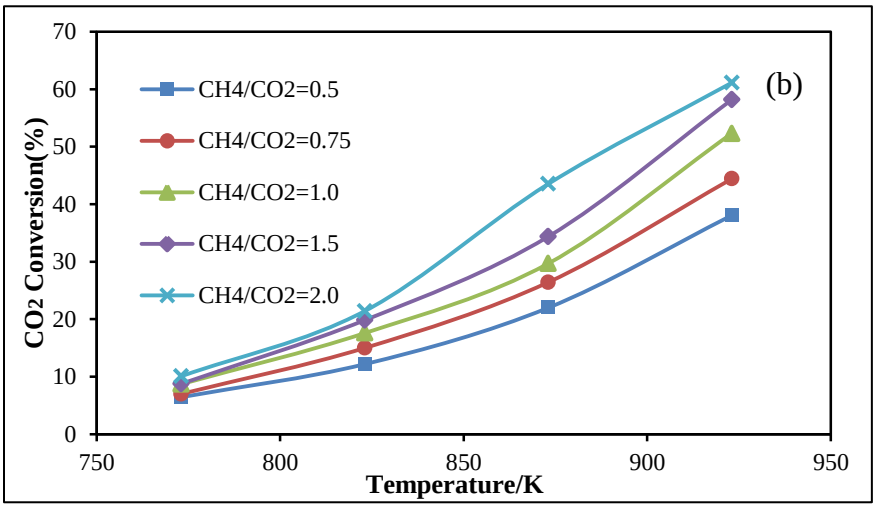

Figure 6.4 (a) CH_4 and (b) CO_2 conversion vs. temperature at each feed molar ratio CH_4/CO_2.

From Figure 6.4, both CH_4 and CO_2 conversions are affected strongly by temperature. With an increasing temperature from 773 to 923 K, both conversions rapidly rise from below 10% to over 60%. The higher the temperature is, the more rapidly the conversions will increase.

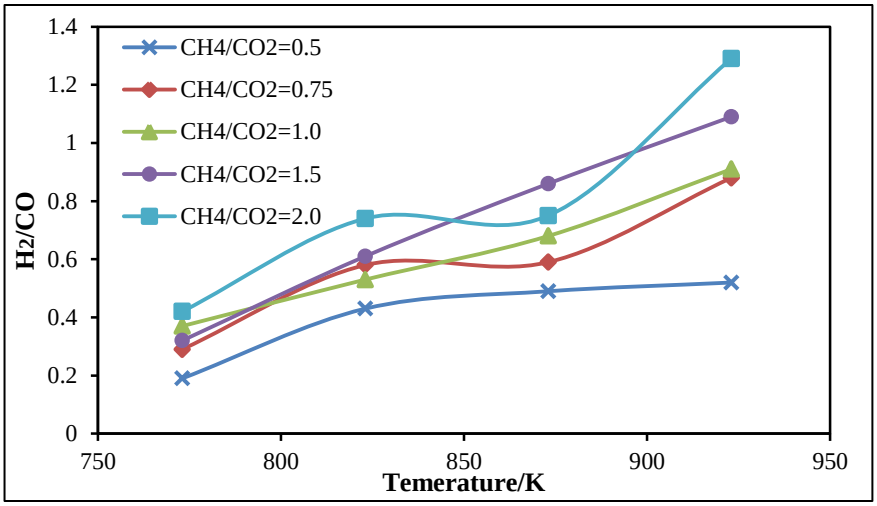

Figure 6.5 Product H_2/CO vs. feed molar ratio CH_4/CO_2 at each temperature.

The effect of reaction temperature on product H_2/CO ratio is also strong. From Figure 6.5, the H_2/CO ratio is favored at higher temperature. When above 900 K, the H_2/CO ratio exceeds 1.0, which is the stoichiometric H_2/CO ratio from the ideal overall DR reaction (Equation 1.1). This suggests that a closer examination will be needed, especially in the thermodynamics and kinetic modeling.

6.2.3 Influence of Total Flow Rate

A number of experiments were run with constant molar ratio of CH_4/CO_2, but variable total flow rate. Reaction conditions of these experiments were 30 psig, and molar feed CH_4/CO_2=1.0. Reaction temperatures were 873 and 923 K.

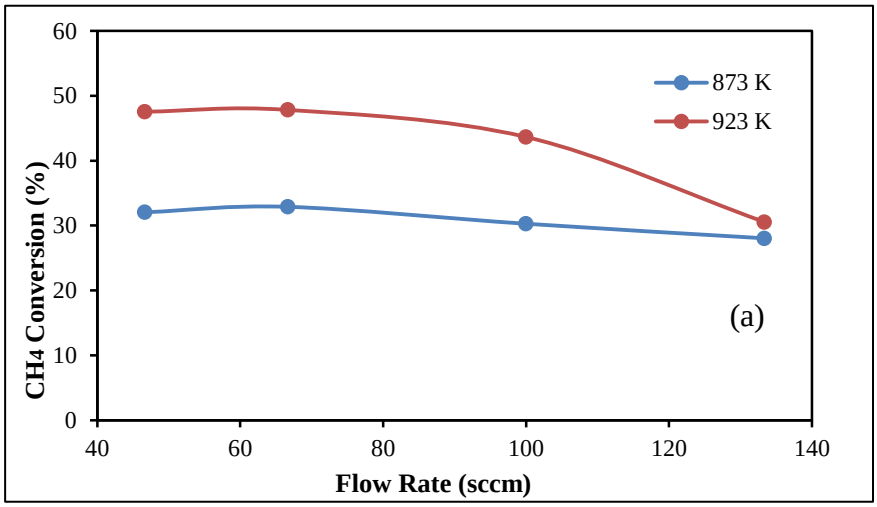

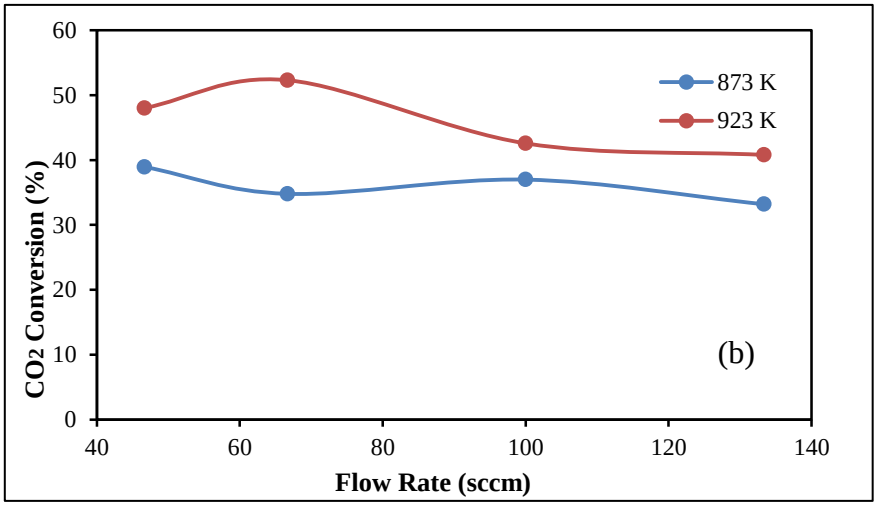

Figure 6.6 (a) CH_4 and (b) CO_2 conversion vs. total flow rate at 873 and 923 K.

From Figure 6.6, the total flow rate does not affect CH_4 conversion significantly at 873K. But the CH_4 conversion drops with an increasing total inlet flow rate at 923K. For both 873 and 923 K, effects from various flow rates to CO_2 conversion are minor.

6.3 Equilibrium Calculation

A reaction equilibrium calculation is independent of any reaction mechanism or kinetics. Equilibrium results show the upper limit of reactant conversions, revealing the potential to improve conversions in catalysis processes. Therefore, it is instructive to compare experimental vs. equilibrium data. In this study, the equilibrium calculations were performed by using *Chemkin-Pro*®.

6.3.1 Chemical Equilibrium Calculation Procedures

Chemkin-Pro® provides an efficient algorithm for minimizing the free energy of the mixture to find the equilibrium state. The user specifies the following input information:

- Constraints: e.g. constant T and P (this study)
- Starting T and P
- Starting composition

The equilibrium solver determines the ending composition that minimizes the Gibbs free energy of the system, subject to the constraints provided by the user. The *Chemkin-Pro*® graphical user interfaces for the equilibrium calculations are show in Appendix J. Reaction conditions were 773 K and 30 psig. Total flow rate was 66.67 sccm, flow CH_4/O_2 =0.5. Flow rate of He is 56.67 sccm. As is discussed in Section 6.1, solid carbon C(s) is a byproduct in our reaction. Thus, for the equilibrium calculation, C(s) is also chosen as a product.

This equilibrium tool is used for all cases. The only numerically significant species are H_2, H_2O, CH_4, CO, CO_2, He, and C(s). All results are listed in Appendix Table F.5 and F.6.

6.3.2 Equilibrium vs. Experimental Values

The experimental and equilibrium conversions of the highest (2.0) and lowest (0.5) feed CH_4/CO_2 ratio cases, constant GHSV = 2 L/h-g_{cat}, at all temperatures are shown in Figure 6.7. All conversions are simply based on inlet and outlet mole fractions. Both CH_4 and CO_2 equilibrium conversions exceeded observed values, with the equilibrium values less sensitive to temperature. CH_4 equilibrium conversions are higher than those of CO_2, and very close to 100%. Trends for the other feed ratios tested were similar and fell in between the 0.5 and 2.0 curves.

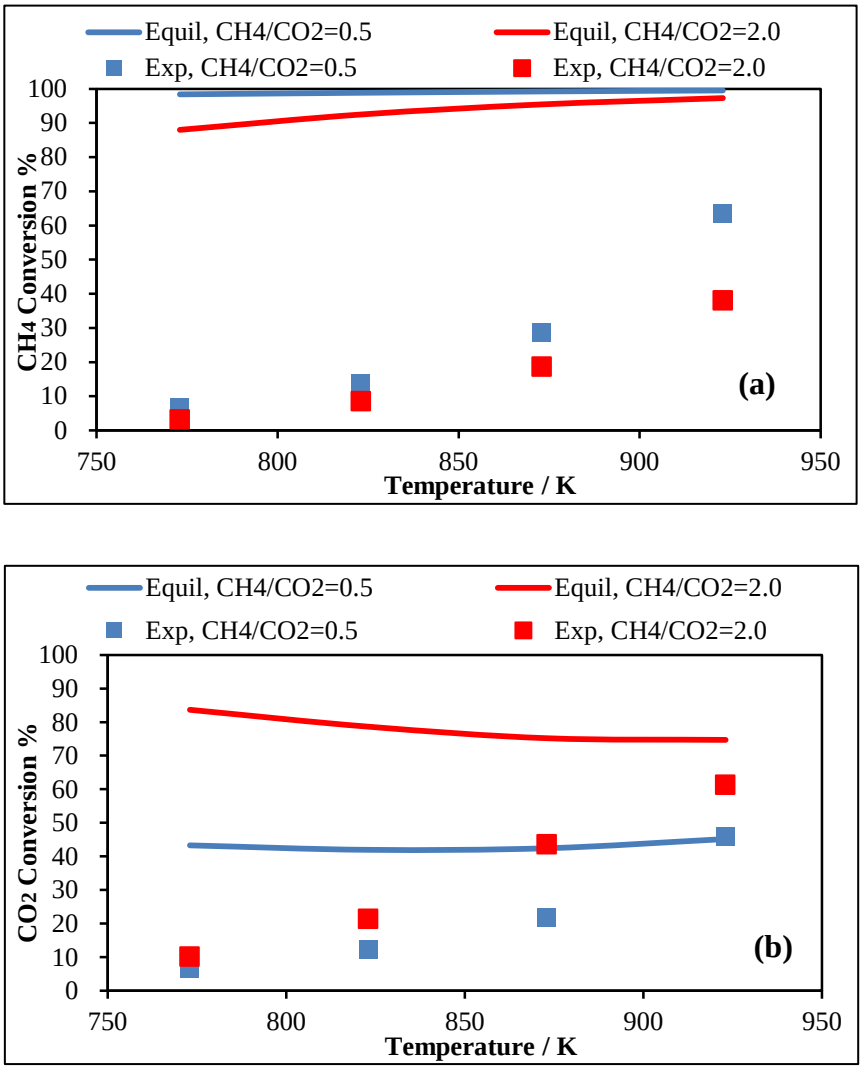

Figure 6.7 Comparison of equilibrium and experimental conversions of (a) CH_4 and (b) CO_2 at GHSV = 2 L/h-g_{cat}; feed CH_4/CO_2 = 0.5 and 2.0.

The experimental and equilibrium conversions of the highest (923 K) and lowest (773 K) temperatures, at constant GHSV = 2 L/h-g_{cat}, as functions of feed CH_4/CO_2 are shown in Figure 6.12. The equilibrium conversions exceeded observed values. The CH_4 equilibrium conversions are higher than those of CO_2, and do not change much with CH_4/CO_2. The CO_2 equilibrium conversions gradually increased with CH_4/CO_2. Trends for the other temperatures tested are similar and fall in between

the high and low values.

A limited number of experiments were run at 308kPa at constant feed ratio CH_4/CO_2 = 1.0, but variable total flow rates at 873 and 923 K. Both CH_4 and CO_2 conversions decreased very slightly with increasing total flow rate. Once again, the observed conversions were consistently less than equilibrium values.

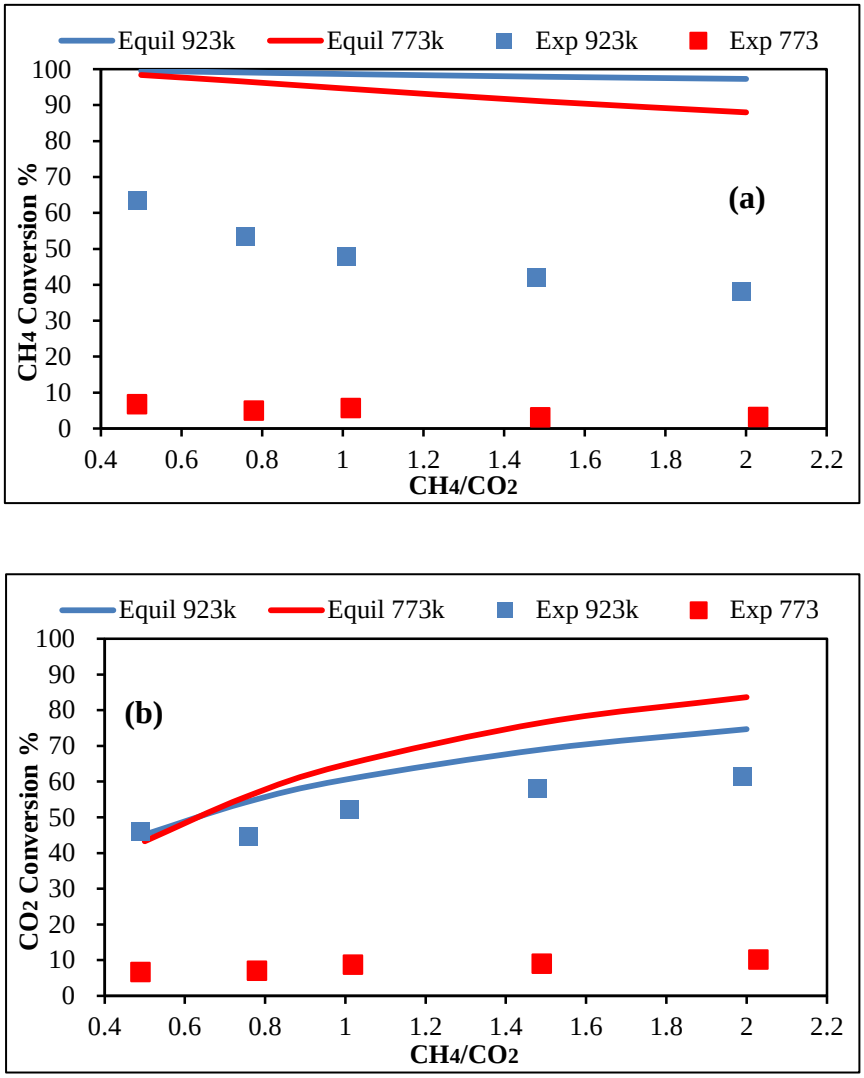

Figure 6.8 Comparison of equilibrium and experimental conversions of (a) CH_4 and (b) CO_2 at GHSV = 2 L/h-g_{cat}; temperature=773 and 923 K.

The product mole fraction ratio H_2/CO is an important measure of reforming catalyst effectiveness since many industrial processes prefer high syngas H_2/CO ratios (Bartholomew, 1997). All H_2/CO results from equilibrium are above 1.0. From Figure 6.9, the equilibrium H_2/CO increases with inlet CH_4/CO_2, which is consistent with experimental results. The equilibrium H_2/CO, strongly drops with increasing temperature.

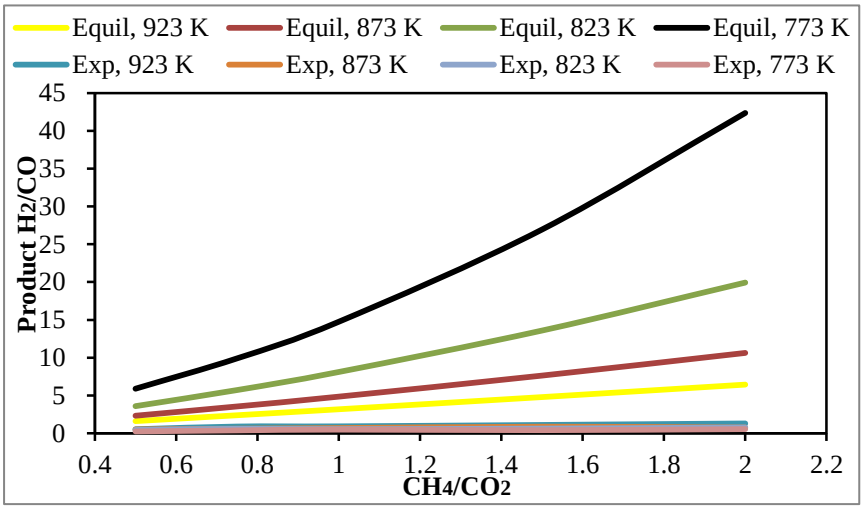

Figure 6.9 Equilibrium H_2/CO at GHSV = 2 L/h-g_{cat} at all temperatures.

According to Figure 6.9, the equilibrium H_2/CO at each temperature is much higher than experimental H_2/CO. Moreover, the equilibrium H_2/CO decreases with increasing temperature, which is different to the trend of experimental H_2/CO. The differences between equilibrium and catalysis experiments indicate that the catalyst provides a different path for CH_4 and CO_2 conversions.

6.4 Power Law Model

The power law model can be a useful tool for design and engineering studies. To determine the power law kinetic rate equations, there is no need to present any fundamental or exhaustive reaction mechanisms. Over the range of their calibration, the accuracy of power law models can be as good as more complex models. Their relative simplicity makes them useful for comparing the behavior of different catalyst materials (Hla, 2011). Their usefulness has been demonstrated and recommended as a tool for an integrated and optimized simulation (Hla, 2011).

6.4.1 Model Selection and Derivation

Data in Section 6.2 show that the CH_4 conversions are sufficiently high (> 10%) that a simple differential reactor model is not appropriate. Rather, an integral packed bed reactor (PBR) model is used. It begins with:

$$r_A' = \frac{dF_A}{dW} \tag{6.2}$$

where r_A' is the molar reaction rate (based on catalyst mass), W is mass of catalyst, and F_A is the CH_4 molar flow rate.

The global reaction can be written as:

$$CH_4 + bCO_2 \rightarrow cCO + dH_2 + eH_2O \tag{6.3}$$

where A is assigned to CH_4, and B is assigned to CO_2. A global reaction rate form, the power law model, is assumed:

$$r_A' = kC_A^{\alpha}C_B^{\beta} \tag{6.4}$$

where k is the overall rate constant, C_j are molar gas-phase concentrations, and α and β are kinetic orders. The immediate objective is to derive F_A (molar flow rate of A),

C_A, and C_B in terms of mole fraction y_A, the mole fraction of CH_4.

The volumetric flow rate of gas v depends on local temperature T, pressure P, and total molar rate F_T. Subscript o refers to the inlet condition; i.e., preheated to reaction temperature in the experimental furnace, at the entrance to the catalyst bed. Based on the ideal gas law,

$$v = v_0 \left(\frac{P_0}{P}\right)\left(\frac{T}{T_0}\right)\left(\frac{F_T}{F_{T0}}\right) \tag{6.5}$$

As the feed reactants are highly diluted by He (85%), $F_T \approx F_{To}$. The length of catalyst bed is short enough that the pressure drop across the catalyst bed is small. This resulted $P \approx P_o$. Due to the preheat, $T \approx T_o$. Then, Equation 6.5 reduces to:

$$v = v_0 \tag{6.6}$$

For the reactants molar flow rates, F_B depends on stoichiometry and the consumption of A:

$$F_B = F_{B0} - b(F_{A0} - F_A) \tag{6.7}$$

The flow rates F_A and F_B relate to the total F_T using the mole fractions y_j.

$$F_A = y_A F_T \text{ and } F_B = y_B F_T \tag{6.8}$$

For the reactants concentrations, using the ideal gas law:

$$C_A = \frac{P}{RT} y_A \tag{6.9}$$

where R is the ideal gas constant.

Using Equation 6.7, the mole fraction of B is:

$$y_B = \frac{F_B}{F_T} = \frac{F_{B0} - b(F_{A0} - F_A)}{F_T} \tag{6.10}$$

Due to high dilution, $F_T \approx F_{To}$. Equation 6.10 becomes:

$$y_B = \frac{F_{B0}}{F_{T0}} - b\left(\frac{F_{A0}}{F_{T0}}\right) + b\left(\frac{F_A}{F_{T0}}\right) = y_{B0} - by_{A0} + by_A \tag{6.11}$$

Defining $y_0 = \left(\frac{y_{B0}}{b} - y_{A0}\right)$, Equation 6.11 becomes:

$$y_B = b(y_0 + y_A) \tag{6.12}$$

The molar concentration of B is now:

$$C_B = \frac{F_B}{v} = \frac{y_B F_T}{v} = y_B \frac{P}{RT} \tag{6.13}$$

Substituting Equation 6.12 into 6.13 yields:

$$C_B = (y_0 + y_A)\frac{bP}{RT} \tag{6.14}$$

Substituting C_A and C_B (Equations 6.9 and 6.13, respectively) into Equation 6.4, we have:

$$-r'_A = k\left(\frac{P}{RT}\right)^{\alpha+\beta} y_A^{\alpha}(y_0 + y_A)^{\beta} b^{\beta} \tag{6.15}$$

Using Equation 6.8 together with $F_T \approx F_{To}$,

$$F_A \approx y_A F_T \tag{6.16}$$

Finally, substituting Equations 6.15 and 6.16 into the PBR species balance (Equation 6.2) yields a working model that could be used directly for data regression.

$$\frac{dy_A}{dW} = \frac{-k}{F_{T0}}\left(\frac{P}{RT}\right)^{\alpha+\beta} y_A^{\alpha}(y_0 + y_A)^{\beta} b^{\beta} \tag{6.17}$$

To obtain a better perspective, Equation 6.17 can be put in terms of CH_4 conversion X_A. Using the definition, $X_A \equiv (F_{A0} - F_A)/F_{A0}$, $F_A = y_A F_{To}$, and $F_T \approx F_{To}$, the y_A is:

$$y_A = \frac{F_{A0}(1-X_A)}{F_{T0}} \tag{6.18}$$

Substituting Equation 6.18 into 6.17, and with manipulations, the working model becomes:

$$\frac{dX_A}{dW} = \frac{k}{F_{A0}}\left(\frac{Py_{A0}}{RT}\right)^{\alpha+\beta}(1 - X_A)^{\alpha}\left(\frac{y_{B0}}{by_{A0}} - X_A\right)^{\beta} b^{\beta} \tag{6.19}$$

The final form of the CH_4 conversion model is Equation 6.19. The quantities W, F_{T0}, P, T, y_A, and y_0 are all known. The parameters k, α and β are all unknown.

The CO_2 conversion could be determined by:

$$X_B = \frac{bX_A y_{A0}}{y_{B0}} \tag{6.20}$$

The value of b could be determined by:

$$\text{b} = \frac{\text{Moles of Converted } CO_2}{\text{Moles of Converted } CH_4} \tag{6.21}$$

Since there is a negligible change of total moles in current system as the feed is highly diluted by He, then Equation 6.21 reduces to:

$$\text{b} = \frac{\text{Feed } CO_2 \text{Mole Fraction} - \text{Outlet } CO_2 \text{Mole Fraction}}{\text{Feed } CH_4 \text{ Mole Fraction} - \text{Outlet } CH_4 \text{ Mole Fraction}} \tag{6.22}$$

Equation 6.22 is used to calculate the value of b for all cases in this study. The approach will be to numerically integrate Equation 6.19 with assumed values of k, α and β for a given run. The calculated X_A and X_B are compared to the experimental X_A and X_B. If they cannot match well, the assumed values of k, α and β are altered, until a good fit is found. This procedure is repeated over all the experimental runs.

6.4.2 Model Testing

As a reasonable start, the orders α and β of the reaction rate were both set to be one. Equation 6.4 becomes:

$$r'_A = kC_A C_B \tag{6.23}$$

The second assumption is the value of k, which is assumed to be temperature dependent.

A typical sample case is temperature at 923 K, feed molar ratio CH_4/CO_2 of 1.01, reaction pressure at 30 psig, total flow rate is 66.67 sccm, flow rate of He is 56.67 sccm,

and W=2.0 grams. Experimental CH_4 conversion is 47.82%, experimental CO_2 conversion is 52.30%. The assumed value of k is 5×10^6 cm^6/ (min gram mol).

The solution tool used to integrate Equation 6.19 for the runs is the software package Polymath®. The calculated CH_4 conversion is 28.90%, CO_2 conversion is 31.52%, which are quite too low compared with the experimental conversions. Different k values are tried until the difference between the predicted and experimental conversions is small enough.

Finally, when $k=1.24\times10^7$ cm^6/ (min gram mol), the predicted X_A=49.52% X_B=54.00, which are very close to the experimental conversions X_A=47.82%, X_B=52.30%. The original Polymath® code for solving this case, with assumptions, α=1, β=1 and $k=1.24\times10^7$ is listed in Appendix G. The calculation report is shown in Figure 6.10. Four more runs with various molar ratios of CH_4/CO_2 were also made at 923 K.

POLYMATH Report
Ordinary Differential Equations

Calculated values of DEQ variables

	Variable	Initial value	Minimal value	Maximal value	Final value
1	W	0	0	2.	2.
2	yA	0.0706	0.0356392	0.0706	0.0356392
3	XA	0	0	0.495195	0.495195
4	yAo	0.0706	0.0706	0.0706	0.0706
5	b	1.0828	1.0828	1.0828	1.0828
6	yBo	0.0701	0.0701	0.0701	0.0701
7	FTo	0.002725	0.002725	0.002725	0.002725
8	yo	-0.0058604	-0.0058604	-0.0058604	-0.0058604
9	P	3.040816	3.040816	3.040816	3.040816
10	R	82.1	82.1	82.1	82.1
11	T	923.	923.	923.	923.
12	alpha	1.	1.	1.	1.
13	beta	1.	1.	1.	1.
14	k	1.24E+07	1.24E+07	1.24E+07	1.24E+07
15	FAo	0.0001924	0.0001924	0.0001924	0.0001924
16	FBo	0.000191	0.000191	0.000191	0.000191
17	FA	0.0001924	9.712E-05	0.0001924	9.712E-05
18	yB	0.0701	0.0322445	0.0701	0.0322445
19	FB	0.000191	8.787E-05	0.000191	8.787E-05
20	XB	0	0	0.5400217	0.5400217

Figure 6.10 Sample Polymath report for power law evaluation.

The power law simulation shows a good fit with the experimental CH_4 and CO_2 conversions for this case with $\alpha=1$, $\beta=1$ and $k=1.24\times10^7$. Moreover, after further testing, we are satisfied with the other three results. Figure 6.11 shows the excellent comparison between experimental conversions and model-simulated conversions at 923 K for five different feed CH_4/CO_2 ratios, with $\alpha=1$, $\beta=1$and $k=1.24\times10^7$ $cm^6/$ (min gram mol).

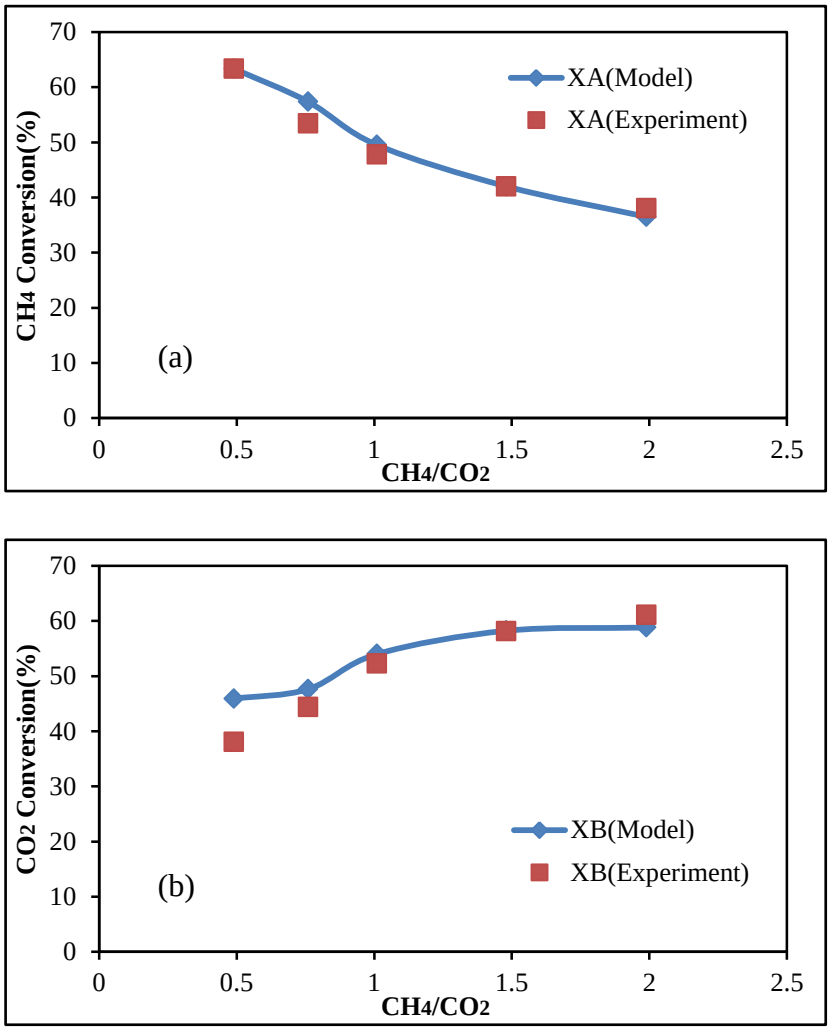

Figure 6.11 Power law model conversions vs. experimental conversions: (a) CH_4 (b) CO_2 at 923 K.

Figure 6.11 shows that the model with assumptions α=1, β=1and k=1.24 ×10^7 cm^6/ (min gram mol) works well. Similarly, for runs at other temperatures, α=1 and β=1 were used. Values for k were assumed at 773, 823, and 873 K until the "best fits" were found. Comparisons between experimental conversions and model conversions for the other three temperatures are shown as Figures 6.12-6.14. It should be pointed out that the

apparent lack of smoothness in some of the power law model curves results from the use of actual experimental conditions (e.g., flow rates) at each abscissa value. These actual values, nominally constant, vary slightly from run to run.

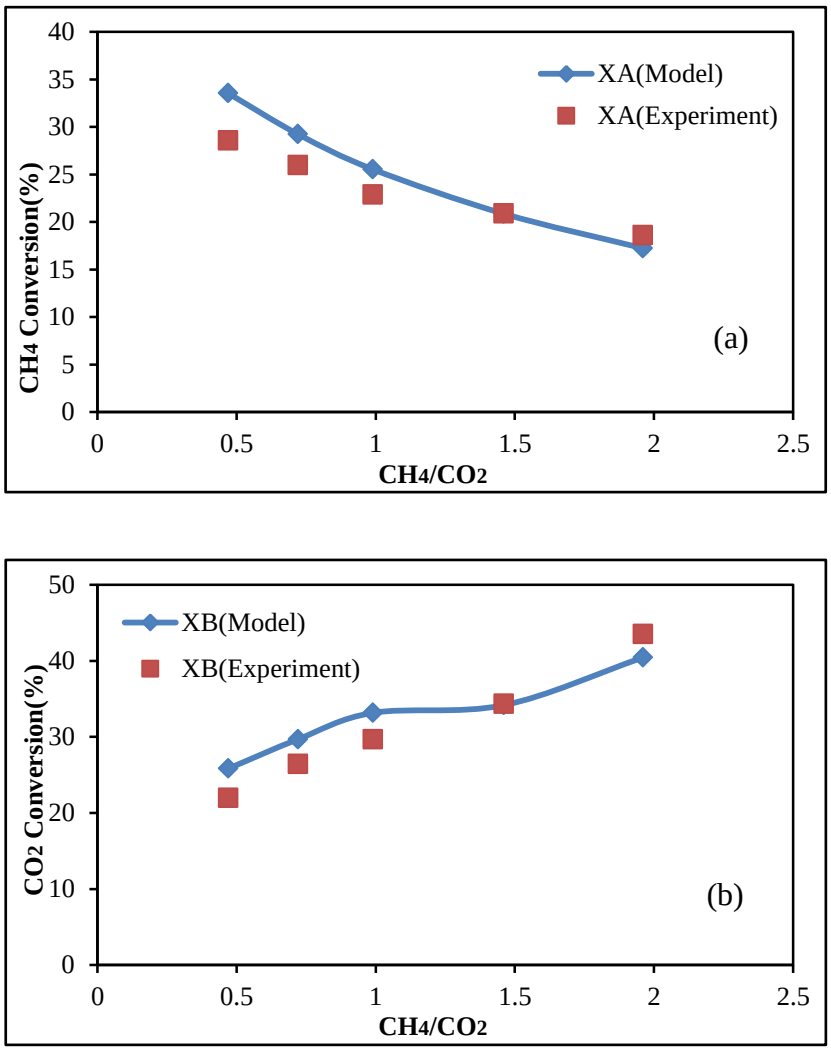

Figure 6.12 Power law model conversions vs. experimental conversions: (a) CH_4 (b) CO_2 at 873 K.

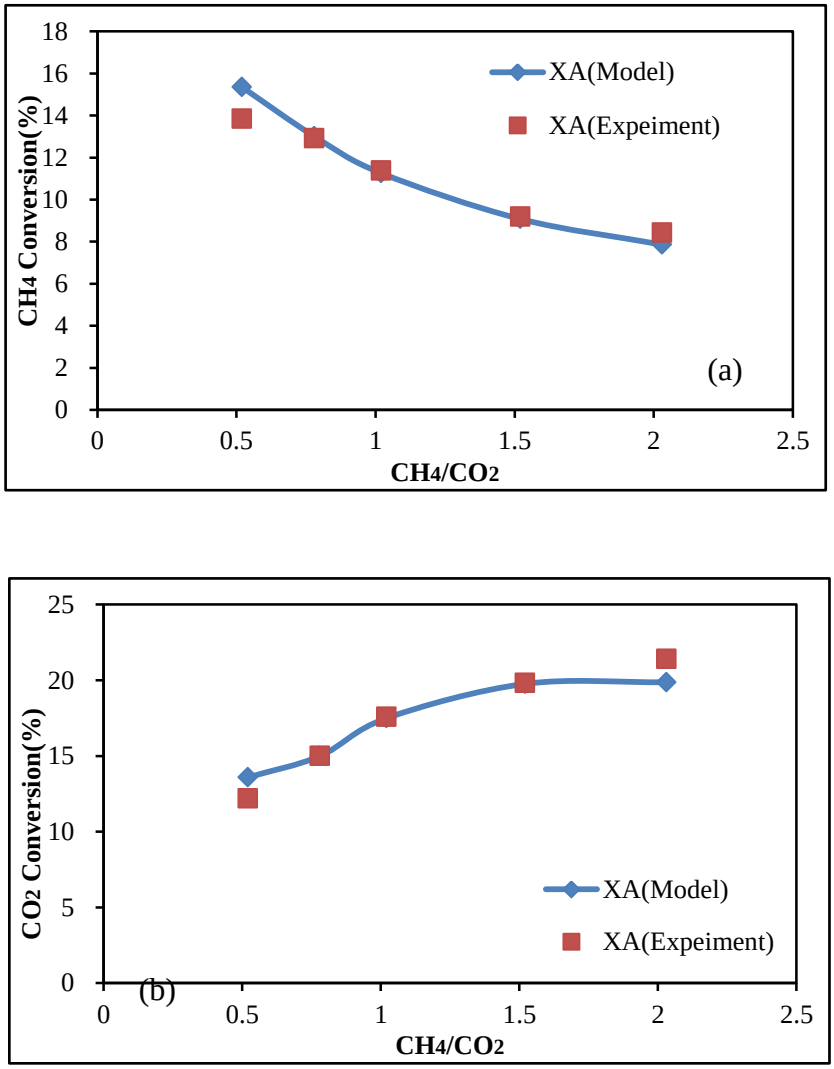

Figure 6.13 Power law model conversions vs. experimental conversions: (a) CH_4 (b) CO_2 at 823 K.

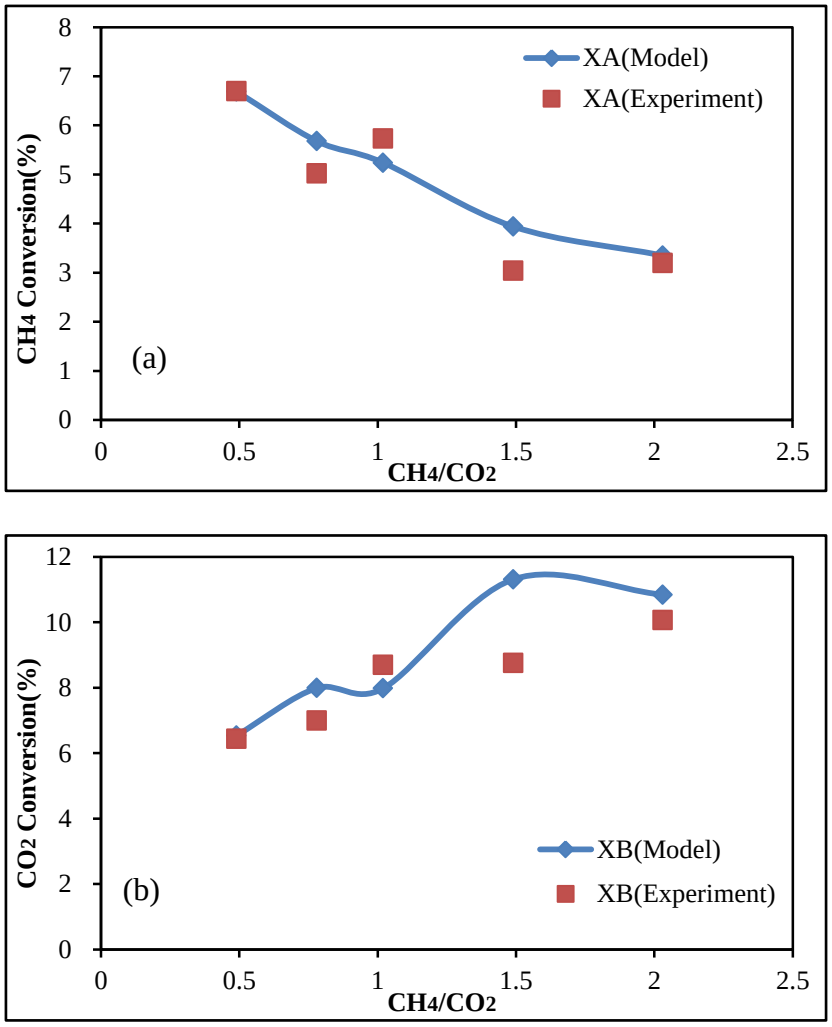

Figure 6.14 Power law model conversions vs. experimental conversions: (a) CH_4 (b) CO_2 at 773K.

Figures 6.12-6.14 (constant total flow rate for all plots) show us a generally good fit between model-simulated conversions and experimental conversions assuming both α and β are 1. Trial-and-error process estimates k, for the given four temperatures, that predicts X_A and X_B values similar to observed X_A and X_B for each molar ratio of CH_4/CO_2. In the next section, the dependence of the k values is examined as a function of temperature.

6.4.3 Arrhenius Plot

The "best fit" k values described in the previous section are presented in Table 6.1.

Table 6.1 Arrhenius Plot Data

k [m^6/ (s ŧkg ŧmol)]	T (K)	lnk	1/T
7.50×10^{-6}	773	-11.8006	0.001294
2.17×10^{-5}	823	-10.7397	0.001215
6.00×10^{-5}	873	-9.72117	0.001145
2.07×10^{-4}	923	-8.4844	0.001083

Based on the data in Table 6.1, an Arrhenius-type plot is made, shown as Figure 6.15.

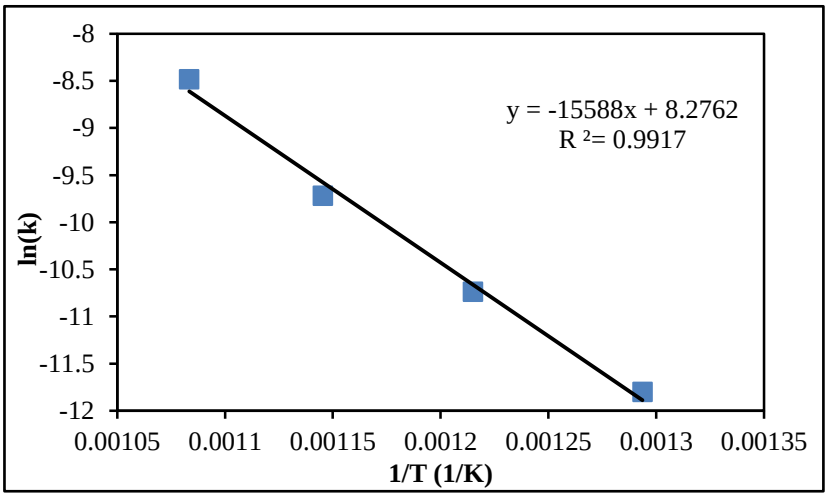

Figure 6.15 Arrhenius plot of "best fit" empirical, global rate constant k.

Figure 6.15 presents an excellent linear relationship between ln(k) and 1/T. Therefore, the Arrhenius equation is built up as: $k = 3.9 \times 10^3 e^{\frac{-1.3\times10^5}{RT}}$ (m^6 /moles s ŧkg catalyst).

6.4.4 Assessment of Power Law Approach

The power law model was derived and tested above shows good agreement with results of the constant flow rate runs. To further assess the power law model, a limited number of experiments were run with constant molar ratio of CH_4/CO_2, but variable total flow rate. Reaction conditions of these experiments were 30 psig, and molar feed CH_4/CO_2=1.0. Reaction temperatures were 873 and 923 K. The power law model was then run using the corresponding k values presented in Table 6.1, to see how the model would predict the CH_4 and CO_2 conversions in the variable total flow rate experiments. Comparisons between experimental conversions and model conversions are shown as Figures 6.16 and 6.17. In the two figures, both equilibrium CH_4 and CO_2 conversions are constant with total flow rate, and higher than experimental conversions.

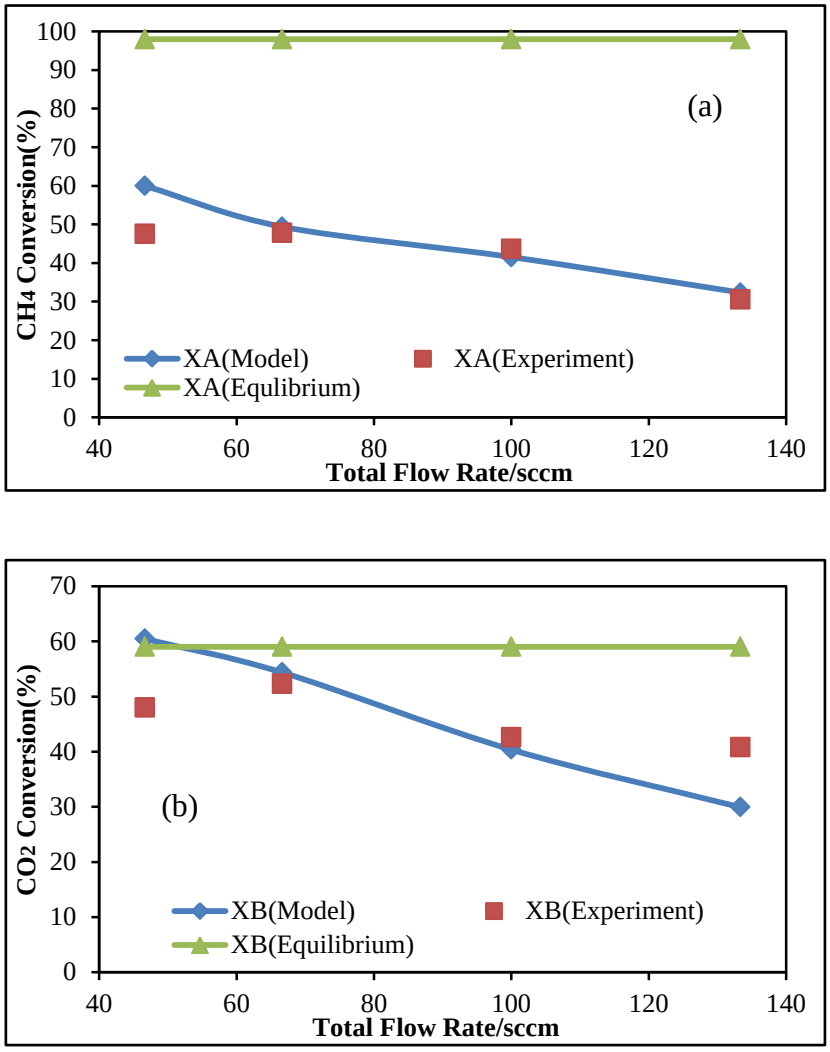

Figure 6.16 Model conversions vs. experimental conversions: (a) CH_4 (b) CO_2 at 923K and CH_4/CO_2=1.0.

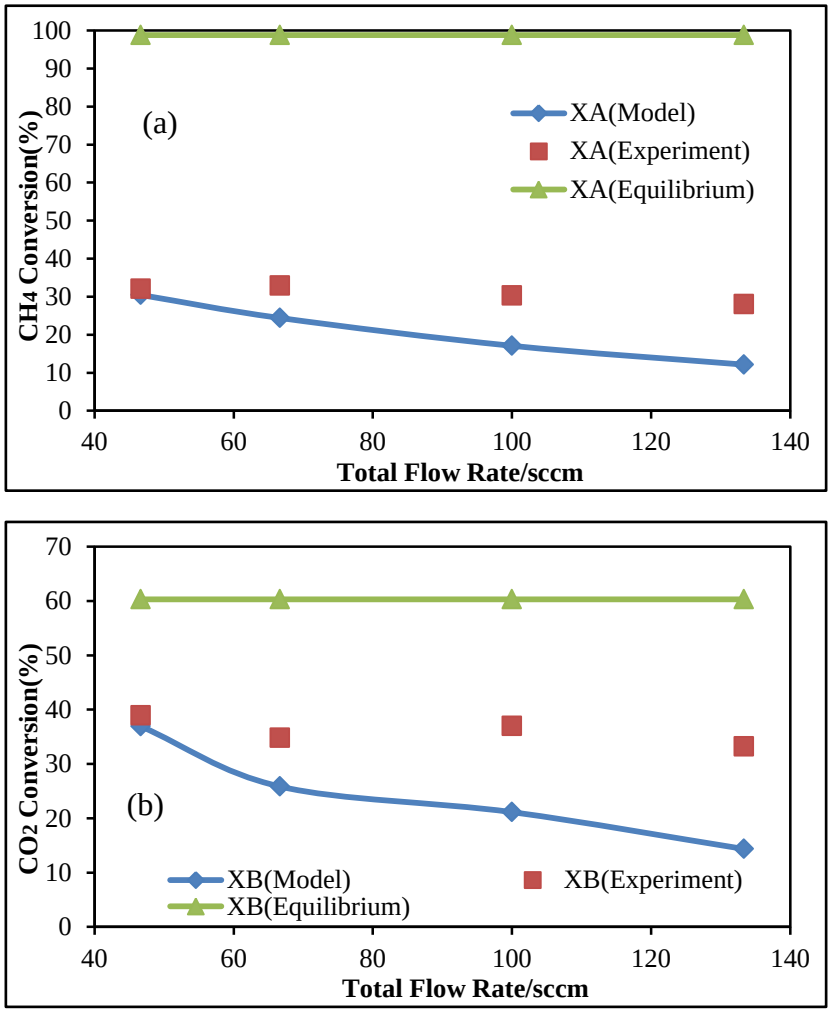

Figure 6.17 Model conversions vs. experimental conversions: (a) CH_4 (b) CO_2 at 873K and CH_4/CO_2=1.0.

Figure 6.16 shows us a generally decent-to-good fit for 923 K between model conversions and experimental conversions assuming both α and β are 1. But the fit in Figure 6.17 for 873 K is unacceptable. Combined with Figures 6.11-6.14, the conclusion can be made that this model (Equation 6.19) shows promise in the prediction of CH_4 and CO_2 conversions in constant total flow rate experiments. But it poorly models the variable flow rate experiments. Although the scope of application for

power law model is limited in our study, it demonstrates its convenience in directly showing how reactions rates are affected by reactants concentrations and rapid calculation of reaction rates. To make both constant flow runs and variable flow runs fit well, a better model, which should be more complex, is proposed below.

6.5 Multiple Reaction Model

As is discussed in Section 5.2, a multiple reaction model, which includes the main reaction with several side reactions, is more complicated than the power law model, and it should lead to a better prediction. On the other hand, the multiple reaction model is much simpler than the detailed reaction mechanism, which is not useful for quick engineering calculations.

6.5.1 Candidate Reactions to Consider

The choice of DR (Equation 1.1) is obvious. RWGS (Equation 1.4) is known to occur during both DR and steam reforming (Wei and Iglesia, 2004). Reactions 1 and 2 together predict $H_2/CO < 1$, which is coincident with most spots in Figure 6.3 and Figure 6.5. According to the two figures, however, there are several instances of observed $H_2/CO > 1$. This might be explained by either the CH_4 decomposition (MD, Equation 1.2) generating more H_2, or Boudouard reaction (Equation 1.3) consuming more CO. The equilibrium constant for MD increases at higher temperatures, while that for Boudouard decreases. Moreover, according to Section 6.1, higher temperature favors carbon deposite. Therefore, it is felt that MD is more likely in this study. The MD is also consistent with the claim (Wei and Iglesia, 2004) that DR occurs through a catalytic decomposition of CH_4 to adsorbed C and H atoms. The selected reactions for

the multiple reaction model are summarized in Table 6.2.

Table 6.2 Reactions in multiple reaction, where $k_{fi} = A_i exp[-E_i/(RT)]$.

Reaction	*Rate Expression r_i*	*Approach to Equil. η_i*
Dry Reforming $CH_4 + CO_2 = 2CO + 2H_2$	$r_1 = k_{f1} P_{CH4} P_{CO2} (1 - \eta_1)$	$\eta_1 = \frac{P_{CO}^2 P_{H2}^2}{P_{CH4} P_{CO2} K_{p1}}$
Reverse Water Gas Shift $CO_2 + H_2 = CO + H_2O$	$r_2 = k_{f2} P_{CO2} (1 - \eta_2)$	$\eta_2 = \frac{P_{CO} P_{H2O}}{P_{H2} P_{CO2} K_{p2}}$
Methane Decomposition $CH_4 = Cs + 2H_2$	$r_3 = k_{f3} P_{CH4} (1 - \eta_3)$	$\eta_3 = \frac{P_{H2}^2}{P_{CH4} K_{p3}}$

The equilibrium constants K_{pi} in Table 6.2, as functions of temperature, are obtained from an on-line database calculator (http://www.crct.polymtl.ca/reacweb.htm). The kinetic parameters A_i and E_i will be determined from analysis of the experimental data. For Reactions 1 and 3, the first order dependencies on CH_4 are inspired by Wei and Iglesia (2004). This reference also suggested a zero order dependency on CO_2. However, as will be seen shortly, the regression analysis done in this study on the data for the Pt/Pd-CNT catalyst yielded generally better results with a first order dependence on CO_2. In addition, the first order dependence on CO_2 in Reaction 2 is inspired by Foppa et al. (2016).

6.5.2 Programing for reaction rate constant

The DR experiments in the current study were simulated with a packed bed reactor (PBR) model as described in Table 6.3. The goal of the simulation was to obtain Arrhenius parameter pairs (A_i, E_i) by determining k_{fi}. The species balances were integrated with an original *Matlab*® program (see Appendix H). All available experimental mole fraction and flow rate data at a given temperature were supplied to

the program. As was done in Chapter 5, the integration was repeated within a regression loop that optimized the three rate constants k_i at that temperature.

Table6.3 Key equations of PBR simulation of 3-reaction global model

PBR Balances Species j	*Net Rates r_j*	*Mole Fractions y_j*	*Partial Pressures*
$dF_j/dW = r_j$ At W = 0, F_{jo} = value	$r_{CH4} = -r_1 - r_3$ $r_{CO2} = -r_1 - r_2$ $r_{CO} = 2r_1 + r_2 + r_3$ $r_{H2} = 2r_1 - r_3 + 3r_3$ $r_{H2O} = r_2 - r_3$	$y_j = \frac{F_j}{\sum_j F_j}$ Total molar rate includes inert gas	$P_j = y_j P$ P = total pressure

The *Matlab*® program code for solving values of k_{fi} at 923 K is shown in Appendix H. Similar *Matlab*® program codes were also applied for 773, 823, and 873 K, both constant flow and variable flow cases. All k_{fi} values for each temperature were determined based on this algorithm.

6.5.3 Arrhenius Plots

Completion of the integration / regression routine at each temperature yielded the rate constant k_{fi}, which are listed in Table 6.4, for each of the three global reactions.

Table 6.4: Rate Constant k_{fi} for 3-Global Reactions

T/K	1/T*1000	k_1	$\ln k_1$	k_2	$\ln k_2$	k_3	$\ln k_3$
773	0.001294	0.0046	-5.3817	0.0016	-6.43775	0.00012	-9.02802
823	0.001215	0.012	-4.42285	0.0034	-5.68398	0.00054	-7.52394
873	0.001145	0.031	-3.47377	0.0119	-4.43122	0.0022	-6.1193
923	0.001083	0.070	-2.65926	0.029	-3.54046	0.0082	-4.80362

Figure 6.18 presents the Arrhenius plots of the global rate constants k_i vs. reaction temperatures based on Table 6.4. The Arrhenius fits are quite linear over the temperature

range (773-923 K).

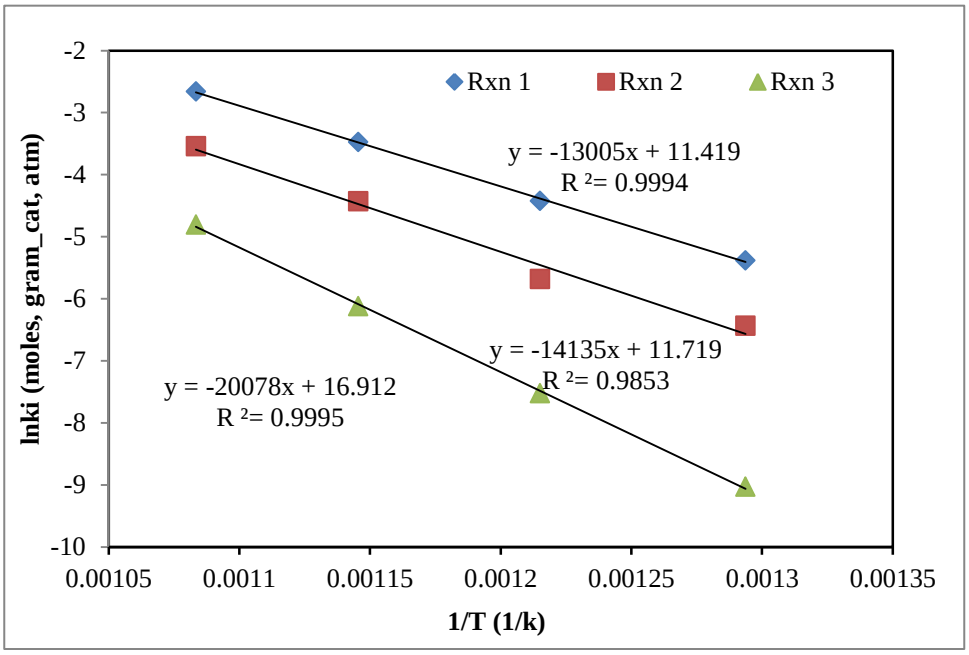

Figure 6.18 Arrhenius plots of forward rate constants k_i.

Based on Figure 6.18, Arrhenius parameters are presented in Table 6.5. Not surprisingly, the CH_4 decomposition (Reaction 3) has the largest barrier among the three reactions.

Table 6.5: Arrhenius Parameters

Reaction i	*Parameter A_i (mole, hr, g_cat, atm)*	*Parameter E_i (cal/mole)*
1	9.104E4	25840
2	1.229E5	28090
3	2.212E7	39890

6.5.4 Model Testing

With Arrhenius parameters observed, the 3-reaction set was tested against the experimental data for the cases from Table 6.2. The PBR simulation based on Table 6.3 was evaluated in *Polymath*®. A typical *Polymath* code, at 923 K, is shown in Appendix I:

Similar *Polymath*® codes are also applied for 873, 823, and 773 K. Then molar flow rates of all species determined from *Polymath*® are converted into concentrations. All results are listed in Appendix Table F.9 and F.10. For constant flow runs, outlet concentrations of all species from 3-reaction model and experiments are compared in Figures 6.19-6.22.

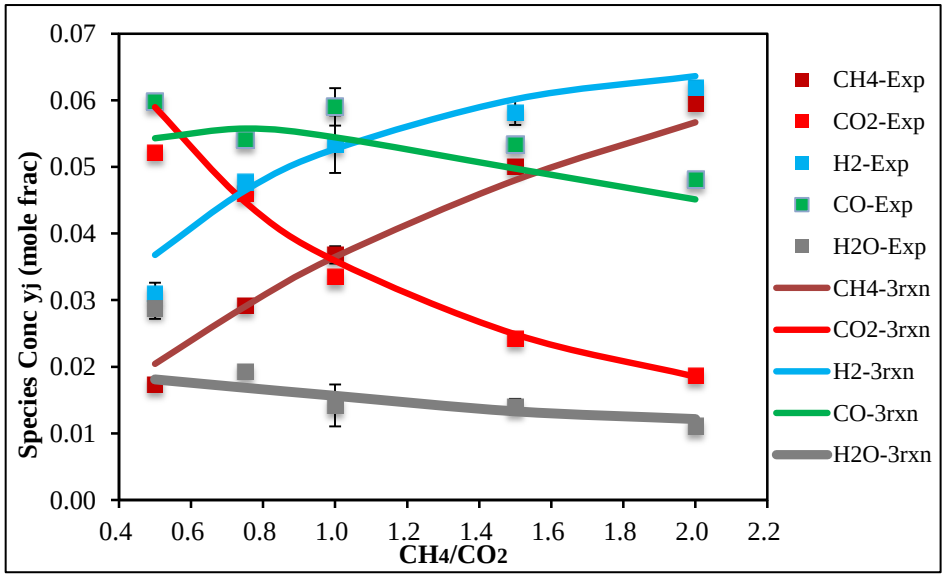

Figure 6.19 Comparison of 3-reaction model-based concentrations and experimental concentrations at 923 K.

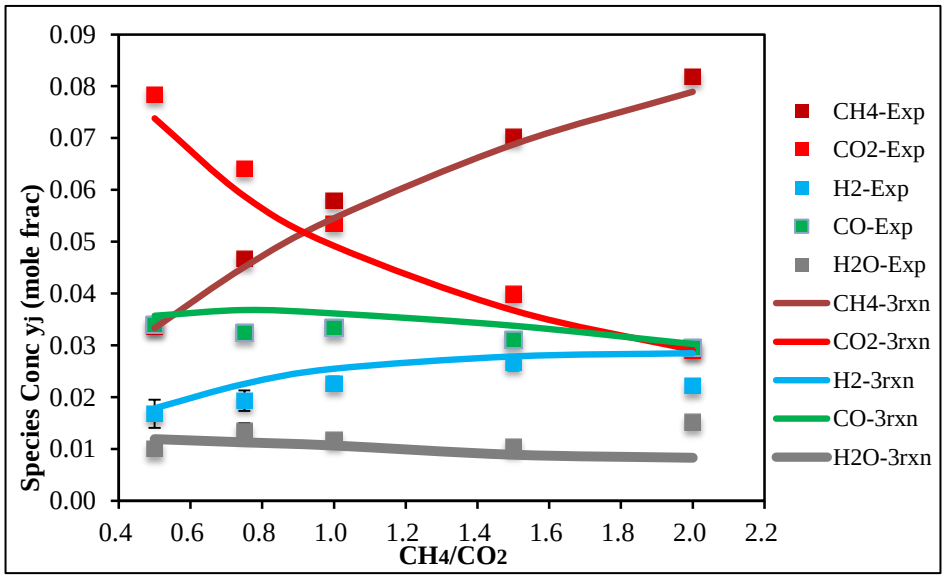

Figure 6.20 Comparison of 3-reaction model-based concentrations and experimental concentrations at 873 K.

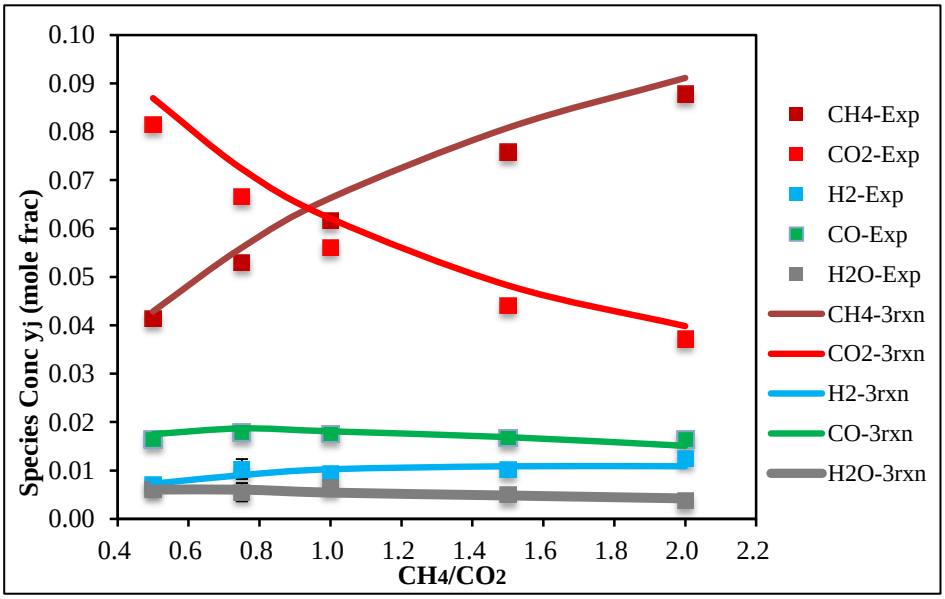

Figure 6.21 Comparison of 3-reaction model-based concentrations and experimental concentrations at 823 K.

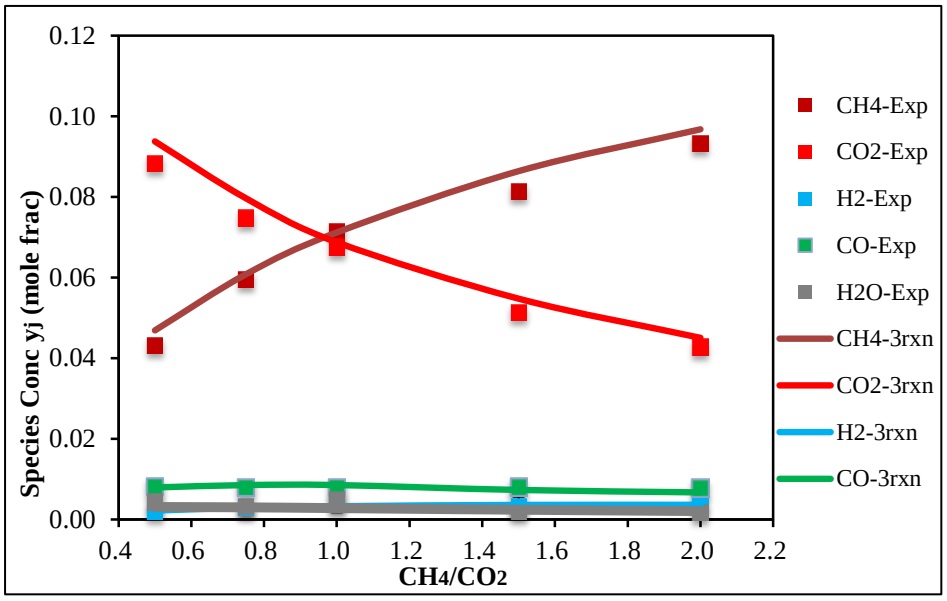

Figure 6.22 Comparison of 3-reaction model-based Concentrations and experimental concentrations at 773 K.

Figure 6.19-6.22 shows concentrations of all species as functions of feed molar ratio CH_4/CO_2. The 3-reaction model surprisingly did a good job on outlet concentration prediction for all species at each temperature with constant total inlet flow rate.

6.5.5 Assessment of Multiple Reaction Model

To fully assess the accuracy of multiple reaction model in this study, the comparison of outlet species concentrations between model results and experimental data for variable flow rate runs are shown in Figures 6.23 and 6.24.

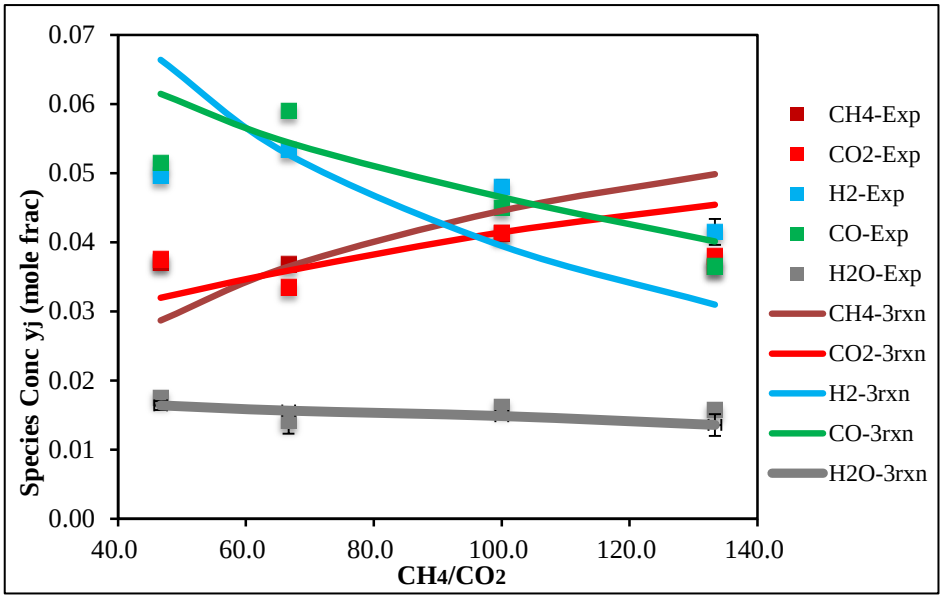

Figure 6.23 Comparison of 3-reaction model-based concentrations and experimental concentrations at 923 K with CH_4/CO_2=1.0 and variable flow rate.

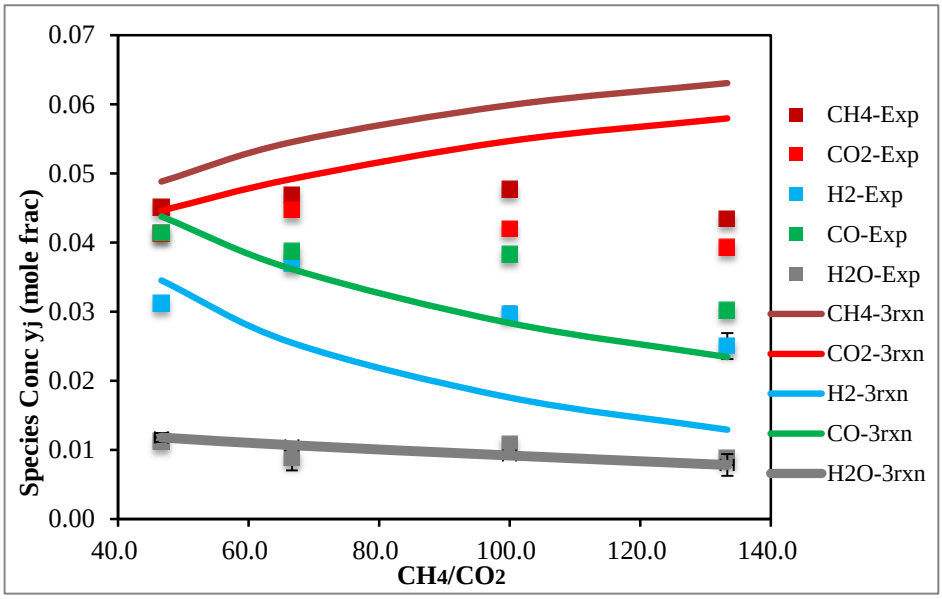

Figure 6.24 Comparison of 3-reaction model-based concentrations and experimental concentrations at 873 K with CH_4/CO_2=1.0 and variable flow rate.

Figure 6.23 shows the comparison at 923 K with an equal molar inlet of CH_4 and CO_2. In this figure, outlet concentrations of all species from 3-reaction model and experiment fit decently. Figure 6.24 shows the comparison at 873 K also with CH_4/CO_2=1.0. The fit for outlet H_2O concentrations is still excellent as before, but the prediction of 3-reaction model for CH_4, CO_2, CO and H_2 are not very good especially at higher flow rate. Among all cases have been tested, this is the only one without a good fit. Generally speaking, the 3-reaction model is good on the outlet prediction for all species in this DR study, especially for constant flow runs.

6.6 Chemkin® Model

Chemkin® is a powerful computational tool for chemical engineering calculations and simulations. It provides many reactor simulations provided a reaction mechanism is supplied. Users select the proper processes, with the required reactants, reactor size and reaction conditions. In this dissertation, *Chemkin*® has already been applied on equilibrium calculations and the MDA study. For this study of DR, a PBR model is selected. Also, a detailed mechanism is also required.

6.6.1Detailed Reaction Mechanism

In this study, a Ni-based catalyst detailed mechanism was used within *Chemkin*®. This mechanism was initially developed and validated by Janardhanan et al. (2005) to describe steam-assisted catalytic partial oxidation of methane in small-channel monolith reactors using Ni supported on alumina, and was tested by Hecht (2006) and Delgado (2015) with accurate predictions observed for methane partial oxidation and reforming. The full mechanism is listed in Appendix K.

No exact detailed elementary reaction mechanism exists for DR on Pt/Pd/CNT heterogeneous catalysts. However, it was felt that general trends within the DR experimental data in this study could be tested using an existing DR mechanism, while looking for gross agreement and possibly some catalytic insights.

6.6.2 Chemkin® Simulation

To proceed with the *Chemkin*® simulation, the required parameters are plugged into the software via the graphical user interface. Experimental conditions are used as fully as possible. The reactor length is 5 cm, reactor inner diameter is 1 cm. An independent chemisorption test done on Pt/Pd-CNT/zeolite reported the active catalytic site density as 6.4×10^{18} sites/gram. With the surface area 14 m^2/gram, which was observed from the BET test, the active site density of 7.57×10^{-11} mole/cm^2, was input. As 2 grams catalyst was uploaded for our study, the internal surface area per unit length was calculated as: 14×10^4 cm^2/gram $\times$ 2 grams/5cm = 5.6×10^4cm. The case of CH_4/CO_2=2.0 with total flow rate = 66.67 sccm at 932 K is chosen as a typical example to present the simulation process, which is shown in Appendix J.

A similar process was applied for all experimental runs including constant flow rate cases and variable flow rate cases. Then, as a sensitivity, the active density was changed to 2.66×10^{-9} mole/cm^2, which is the original active site density of Ni from reference, published with the detailed mechanism. All the PBR simulations were repeated. All *Chemkin*® results including higher active site density (Ni) simulation and lower active site density (Pt/Pd) are listed in Appendix Table F.11-F.18.

6.6.3 Chemkin® Simulation Results Discussion

The *Chemkin*® simulation results, including CH_4 and CO_2 conversions and product H_2/CO, based on higher and lower active site density are compared with those from experimental data. Figure 6.25-6.28 show comparisons for constant flow runs.

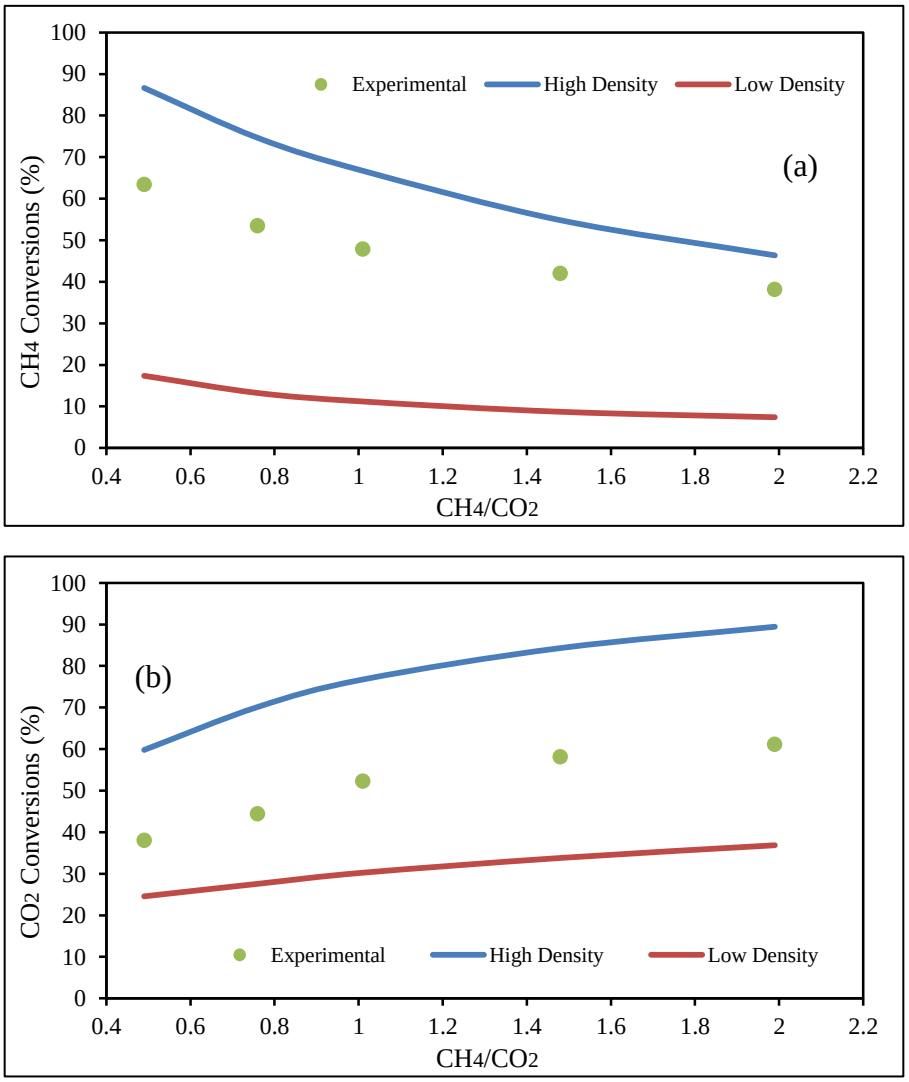

Figure 6.25 Comparison of *Chemkin*® simulation results and experimental results on (a) CH_4 conversions and (b) CO_2 conversions at 923 K and 66.7 sccm.

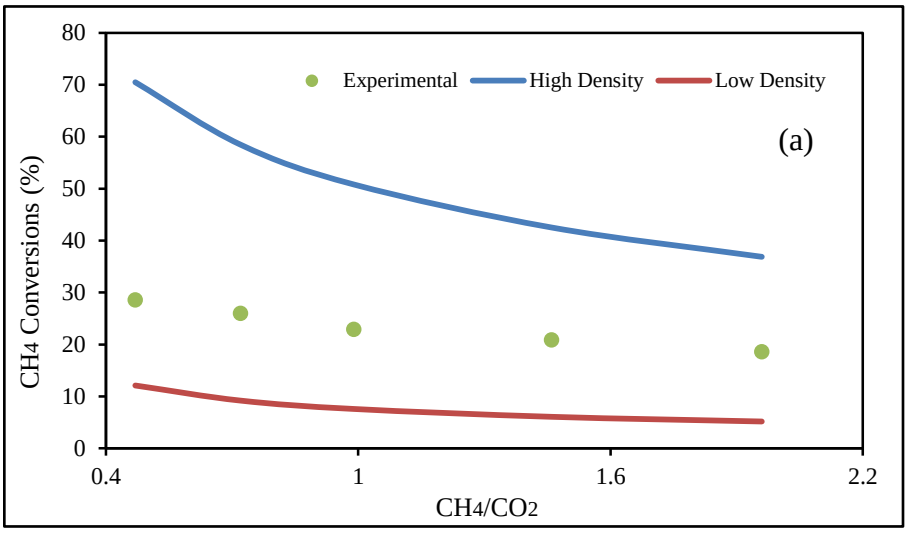

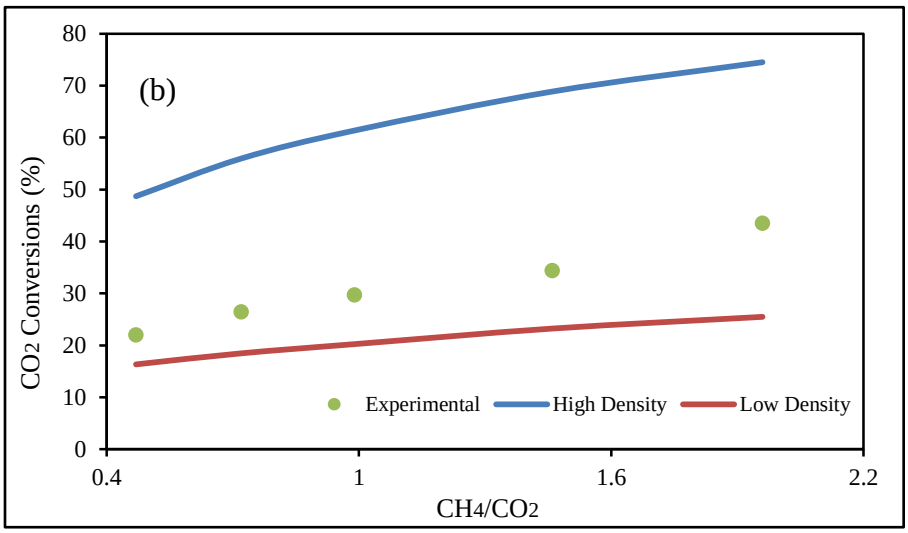

Figure 6.26 Comparison of *Chemkin*® simulation results and experimental results on (a) CH_4 conversions and (b) CO_2 conversions at 873 K and 66.7 sccm.

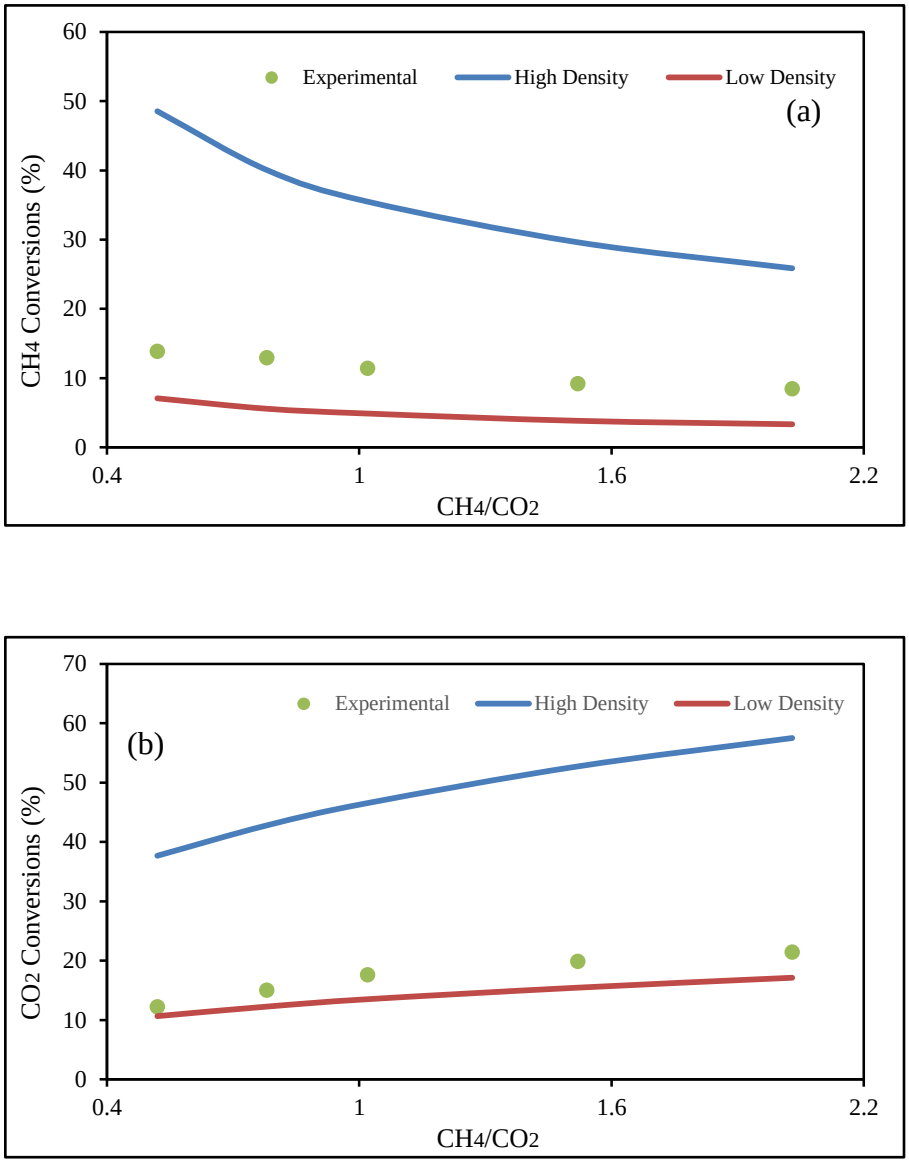

Figure 6.27 Comparison of *Chemkin*® simulation results and experimental results on (a) CH_4 conversions and (b) CO_2 conversions at 823 K and 66.7 sccm.

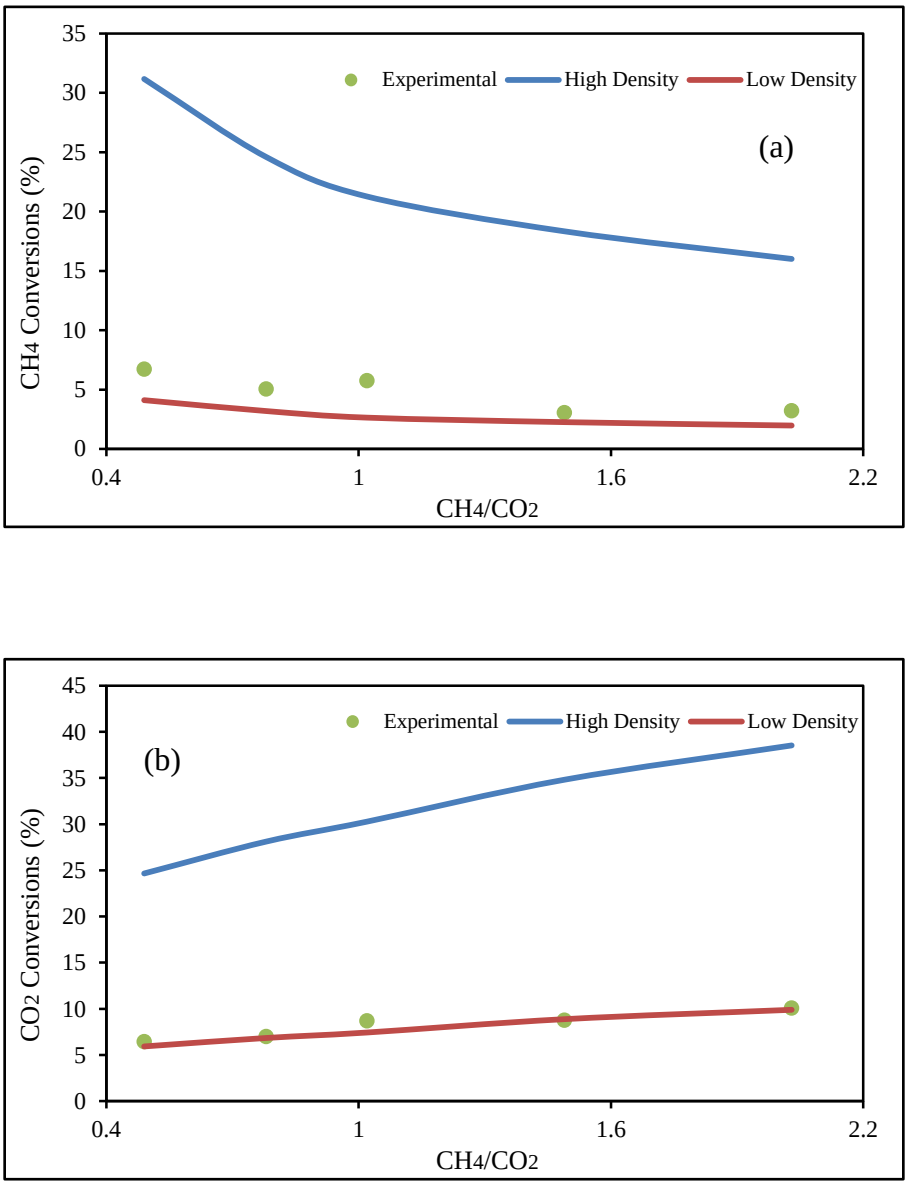

Figure 6.28 Comparison of *Chemkin*® simulation results and experimental results on (a) CH_4 conversions and (b) CO_2 conversions at 773 K and 66.7 sccm.

According to Figures 6.25-6.28, the *Chemkin*® simulation conversions of CH_4 and CO_2 are sensitive to active site density. The higher the density is, the higher the conversions. The simulation CH_4 conversions decline with the feed molar ratio CH_4/CO_2; while the simulation CO_2 conversions increase with CH_4/CO_2. Such

tendency is consistent with experimental CH_4 and CO_2 conversions. The *Chemkin*® simulation conversions of CH_4 and CO_2 based on higher and lower active site density effectively bracket the experimental CH_4 and CO_2 conversions for all tested temperatures at constant flow. For lower active site density simulations, the employed active site density is exact the value of our Pt/Pd-CNT catalyst, but the conversions of CH_4 and CO_2 are obviously lower than experimental conversions. What is more, the simulation conditions are as same as experimental conditions. Such observation implies that the activity of our Pt/Pd-CNT/zeolite is higher than Ni based catalyst. At 773 K, the experimental conversions of CH_4 and CO_2 are almost as same as those from lower active site density simulations. At 923 K, however, the experimental conversions of CH_4 and CO_2 are much closer to those from higher active site density simulations. Therefore, the activity of Pt/Pd-CNT/zeolite is more temperature dependent than Ni based catalyst.

The *Chemkin*® simulation product H_2/CO is compared with those obtained from the experiments. As H_2/CO from lower active site density simulation are all below 0.02, only H_2/CO from the higher active site density simulation and experiments are presented in Figure 6.29-6.32.

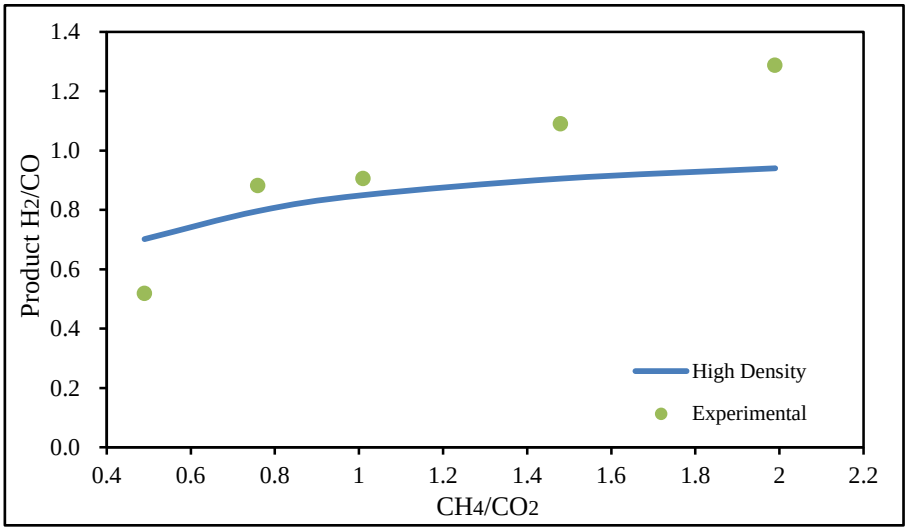

Figure 6.29 Comparison of *Chemkin*® simulation results and experimental results on H_2/CO at 923 K and 66.7 sccm.

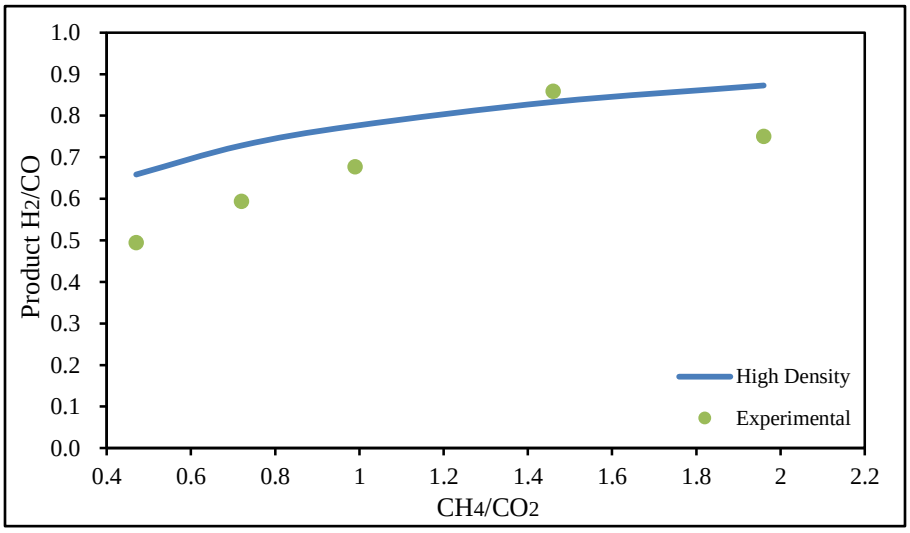

Figure 6.30 Comparison of *Chemkin*® simulation results and experimental results on H_2/CO at 873 K and 66.7 sccm.

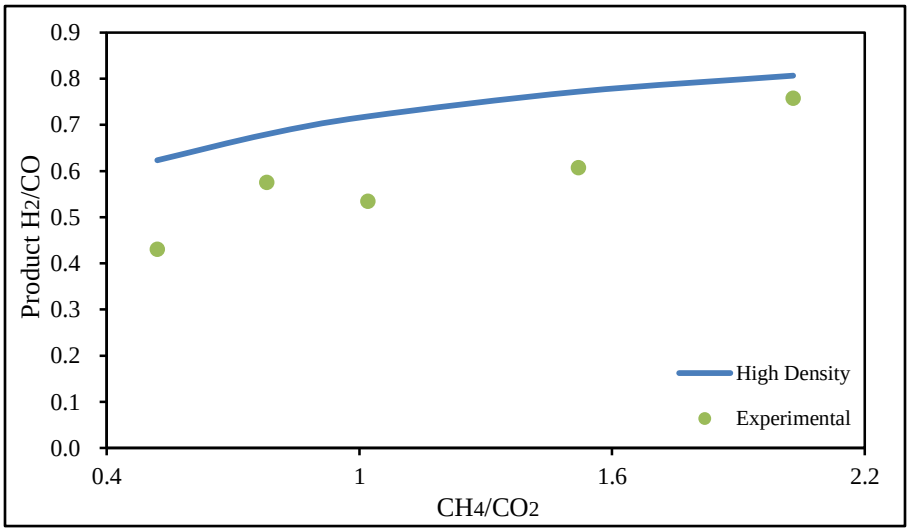

Figure 6.31 Comparison of *Chemkin*® simulation results and experimental results on H_2/CO at 823 K and 66.7 sccm.

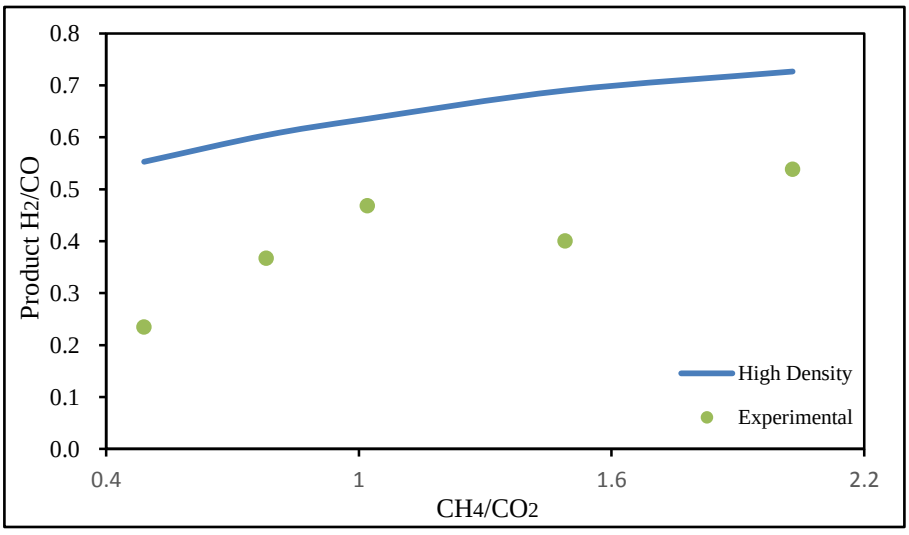

Figure 6.32 Comparison of *Chemkin*® simulation results and experimental results on H_2/CO at 773 K and 66.7 sccm.

Figures 6.29-6.32 shows comparison between simulation H_2/CO and experimental H_2/CO. The simulation H_2/CO increase with CH_4/CO_2, which is consistent with experimental H_2/CO. Higher temperature favors higher simulation H_2/CO from *Chemkin*®, but the experimental H_2/CO is more dependent on temperature than that of simulation. It is noticed that several experimental H_2/CO data points are above 1.0. The simulation H_2/CO could approach 1.0 due to higher CH_4/CO_2 or higher temperature, but it never reaches 1.0. It should be pointed out that the Ni mechanism does NOT include carbon deposits, unlike the equilibrium calculation or the 3-rxn model. Without the chance for solid carbon, there is no pathway for $H_2/CO > 1$.

Chemkin® simulations were also conducted on variable flow rate cases. Comparison of CH_4 and CO_2 conversions at $CH_4/CO_2=1.0$ between simulation and experiment are shown in Figure 6.33 and 6.34.

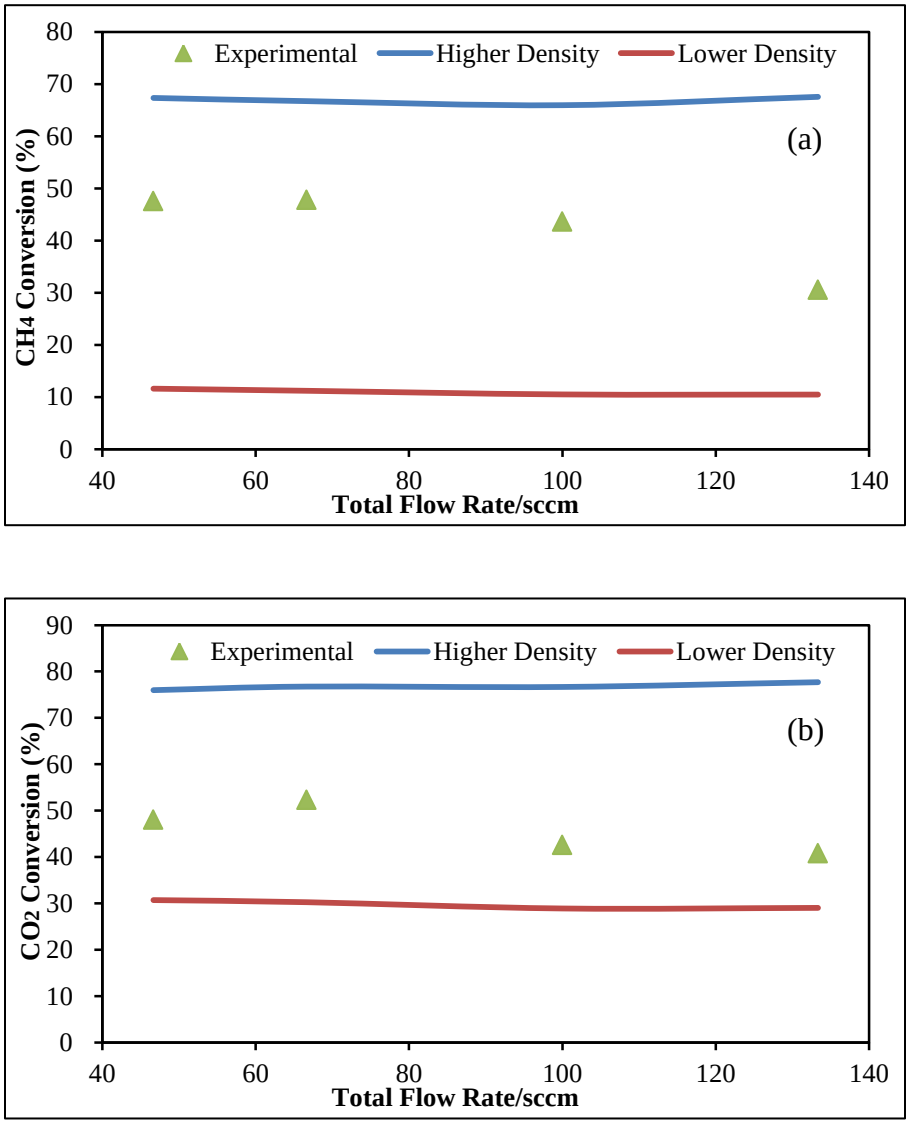

Figure 6.33 Comparison of *Chemkin*® simulation results and experimental results on (a) CH_4 conversions and (b) CO_2 conversions at 923 K and CH_4/CO_2=1.0.

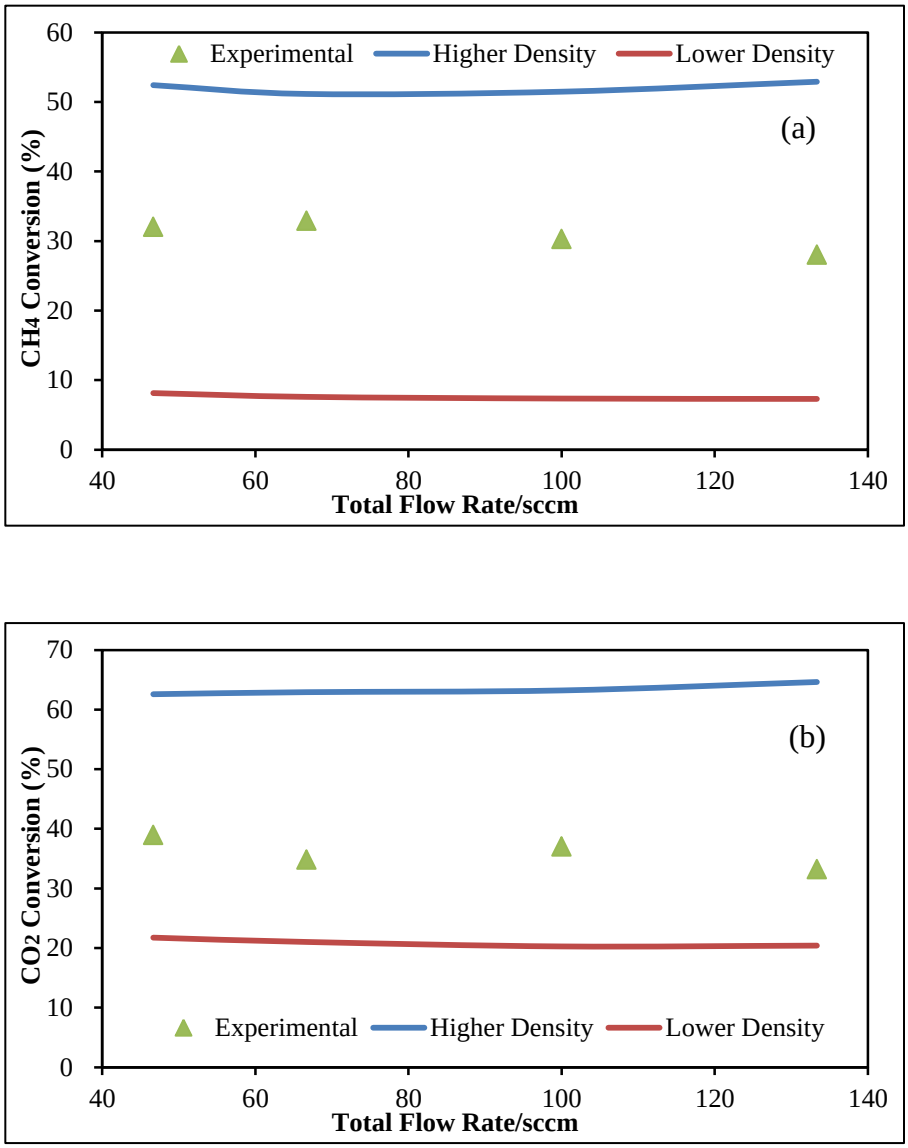

Figure 6.34 Comparison of *Chemkin*® simulation results and experimental results on (a) CH_4 conversions and (b) CO_2 conversions at 873 K and CH_4/CO_2=1.0.

According to Figures 6.33 and 6.34, the *Chemkin*® simulation conversions of CH_4 and CO_2 based on higher and lower active site density also bracket the experimental CH_4 and CO_2 conversions. The simulation CO_2 conversions are also higher than simulation CH_4 conversions with the feed CH_4/CO_2=1.0. At 923 and 873 K,

the simulation CH_4 and CO_2 conversions are almost constant with variable flow rates. The difference of total flow rate could rarely affect simulation CH_4 and CO_2 conversions, which is similar to experimental CH_4 and CO_2 conversions. For the all three models we have studied, *Chemkin*® did the best job in predicting the trend of conversions vs. flow rate.

Chemkin® is a very useful tool to show how the detailed reaction mechanism could simulate the reaction results. Although without the Pt/Pd-based CNT catalyst detailed mechanism applied, the simulations on Ni-based catalyst mechanism are still valuable. The very similar trend of simulations curves and experimental curves suggest strongly that the mechanism of Pt/Pd-CNT catalyst is very similar to that of Ni-based catalyst. The different levels of those curves suggest that Pt/Pd-CNT has a higher activity than Ni-based catalyst. As temperature rises, however, the experimental data seems to move from being closer to "low density" lines toward the "high density" lines. This suggests that the Pt/Pd catalyst system has a higher activation energy than the Ni case.

CHAPTER 7

DRY REFORMING OVER RU/CNT-ZEOLITE

7.1 Observed Carbon Balance

Similar to the analysis of Pt/Pd-CNT/zeolite experimental results for carbon balance, the parity graphic is also plotted for Ru/CNT-zeolite experimental results. Figure 7.1 shows the comparison between feed carbon and outlet carbon for all runs with Ru/CNT-zeolite. The same Ru/CNT-zeolite catalyst was used in all runs, there was no change or regeneration.

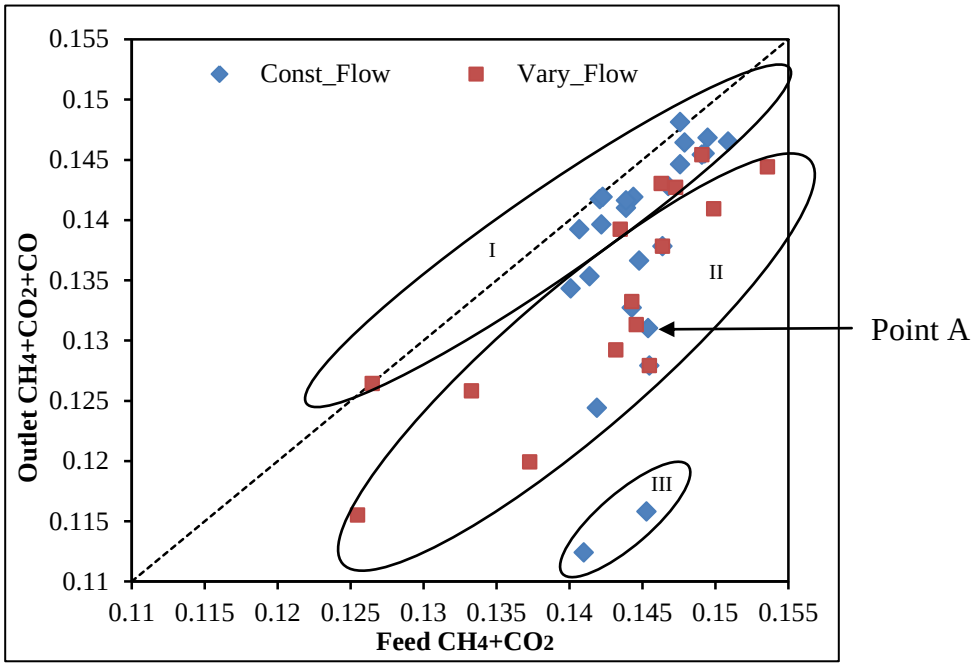

Figure 7.1 Carbon balance for all runs over Ru/CNT-zeolite

In Figure 7.1 all markers are at or under the parity line, which means carbon deposition has occurred during the DR reaction. A closer look of the marker

distribution in the graphic reveals:

1. Circle I shows the runs at 773, 823, and 873 K, including constant flow runs and variable flow runs. These spots are very close or even at the parity line. It means little carbon deposition occurred at the lower temperatures.

2. Circle II and III present the runs at 923 and 973K including constant flow runs and variable flow runs. Compared to circle I, higher temperature favors coke formation.
3. Circle III shows two cases at 973 K. They are even further from the parity line than the other runs at 973K due to higher feed CH_4/CO_2. The same observation is obtained from other temperatures. Therefore, higher CH_4/CO_2 also favors coke formation.

4. For all runs, the further below the parity line, higher H_2/CO is observed. It is implied that the formation of H_2 is coincident with coke formation.

5. Variable total flow rates has very little influence on coke formation.

The comparison of carbon difference is also made to equilibrium calculations. For example, for the same reaction conditions with point A in Figure 7.1, 973 K with CH_4/CO_2 =0.75 and 66.7 sccm total flow, the feed mole fraction of CH_4+CO_2 is 0.145, the outlet mole fraction of $CH_4+CO_2+CH_4$ is 0.0768. The carbon deposit is 0.0682.

7.2 Methane and Carbon Dioxide Conversion, H_2/CO

The methods for calculation of conversions X_A, X_B, and H_2/CO are the same as those for Pt/Pd-CNT/zeolite as discussed in Section 6.2.

7.2.1 Influence of Feed Molar Ratio

Experiments were run at 773, 823, 873, 923 and 973 K. Reactor pressure is kept at 30 psig. The total flow rate is set at 66.7 sccm, with the flow rate of He of 56.7 sccm (85% diluent). Based on the volume of the catalyst bed, the gas hourly space velocity (GHSV) is 2000 ml/(g_{cat} hr). All calculated CH_4 and CO_2 conversions are shown as X_A, X_B vs.

feed molar ratio CH_4/CO_2 plots at each temperature. In the following figures, unless specifically stated, the lines are only used for the sake of clarity for the presentation of the experimental data points, and do not represent any modeling or regression.

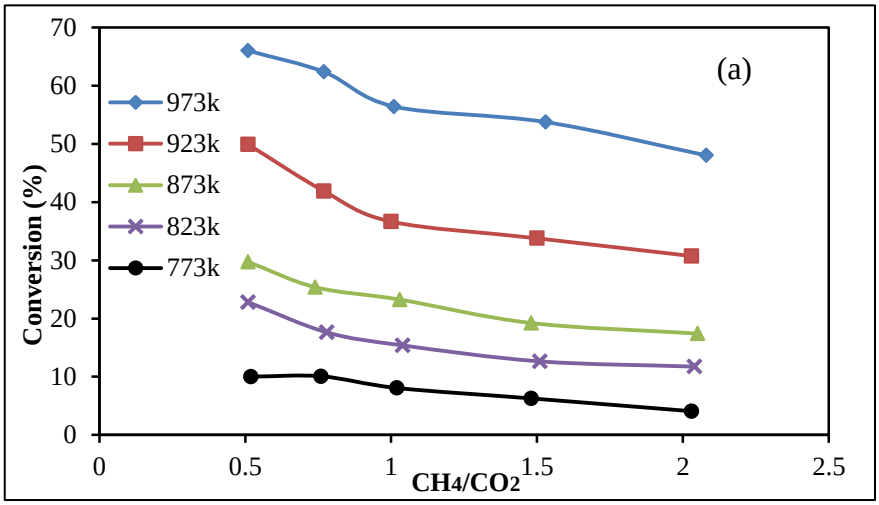

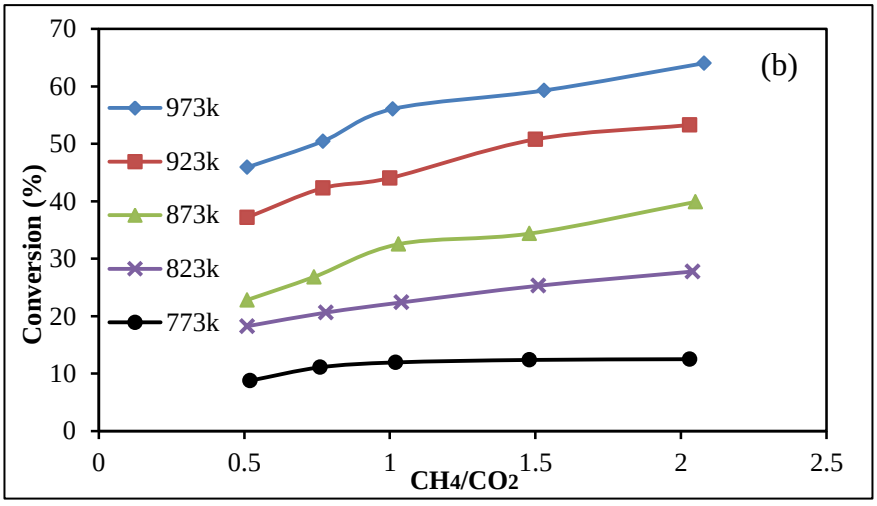

Figure 7.2 (a) CH_4 and (b) CO_2 conversion vs. feed molar ratio CH_4/CO_2 at each temperature

Figures 7.2 shows the different CH_4 and CO_2 conversions at various molar ratios CH_4/CO_2 under each temperature. The feed molar ratio CH_4/CO_2 impacts both conversions. The CH_4 conversion decreases with increasing molar ratio CH_4/CO_2. The higher the reaction temperature is, the bigger the drop will be. The CO_2 conversion increases with increasing feed molar ratio.

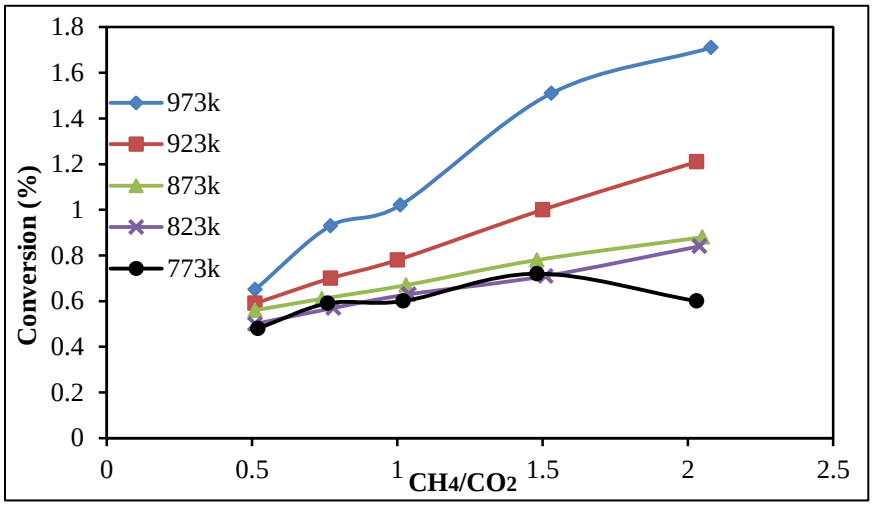

Figure 7.3 Product H_2/CO vs. feed molar ratio CH_4/CO_2 at each temperature

Figure 7.3 shows product H_2/CO ratio generally increases with feed molar ratio. Higher CH_4/CO_2 mean more H atoms input, so a higher H_2/CO ratio can be observed.

7.2.2 Influence of Temperature

To investigate the influence of reaction temperature, the constant flow experimental results are shown in same feed molar ratio of CH_4/CO_2.

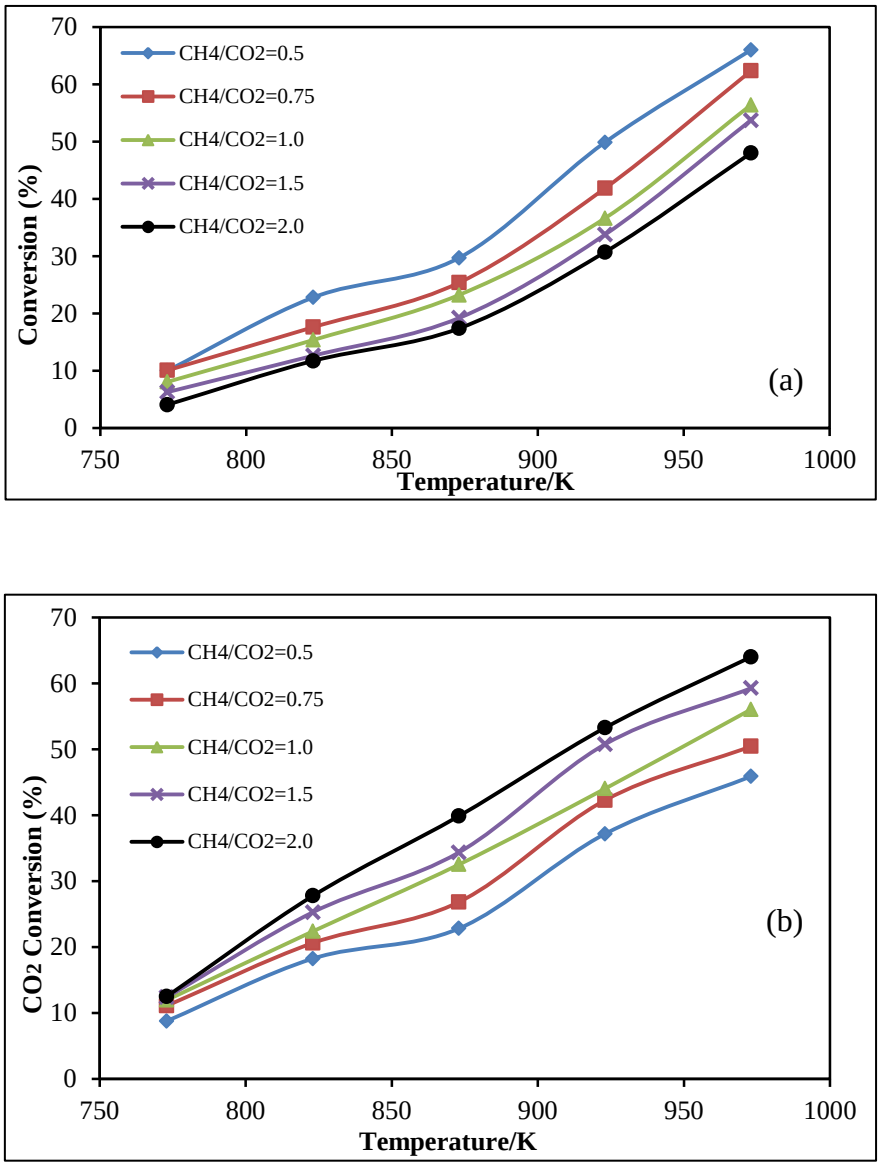

Figure 7.4 (a) CH_4 and (b) CO_2 conversion vs. temperature at each feed molar ratio CH_4/CO_2.

From Figure 7.4, both CH_4 and CO_2 conversions are strongly affected by temperature. With an increasing temperature from 773 to 923 K, both conversions rapidly rise from below 10% to over 60%. Both conversions increase faster after 873K.

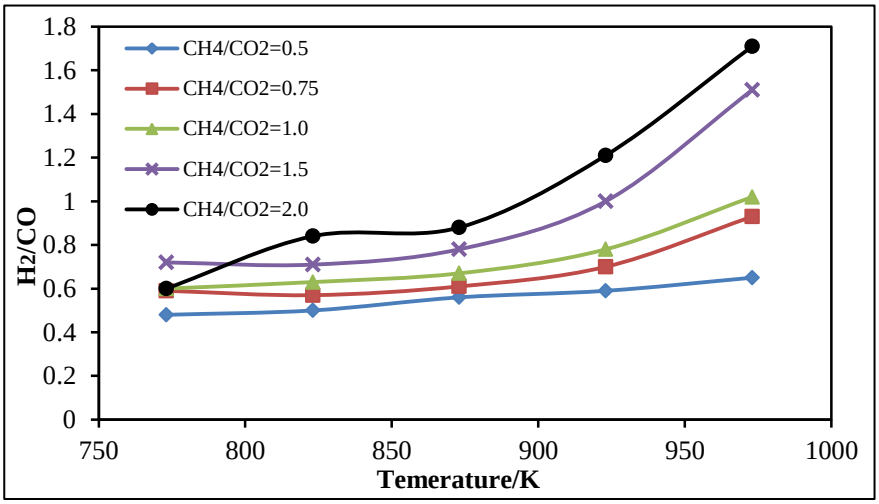

Figure 7.5 Product H_2/CO vs. feed molar ratio CH_4/CO_2 at each temperature.

The effect of reaction temperature on product H_2/CO ratio is also strong. From Figure 7.5, the H_2/CO ratio is favored at higher temperature. When above 900 K, the H_2/CO ratio exceeds 1.0, which is the stoichiometric H_2/CO ratio from the ideal overall DR reaction (Equation 1.1). With the increasing temperature, H_2/CO even reaches 1.7. A closer examination is needed, especially in the thermodynamics and kinetic modeling.

7.2.3 Influence of Total Flow Rate

A number of experiments were run with constant molar ratio of CH_4/CO_2, but variable total flow rate. Reaction conditions of these experiments were 30 psig, and molar feed CH_4/CO_2=1.0. Reaction temperatures were 873, 923 and 973 K.

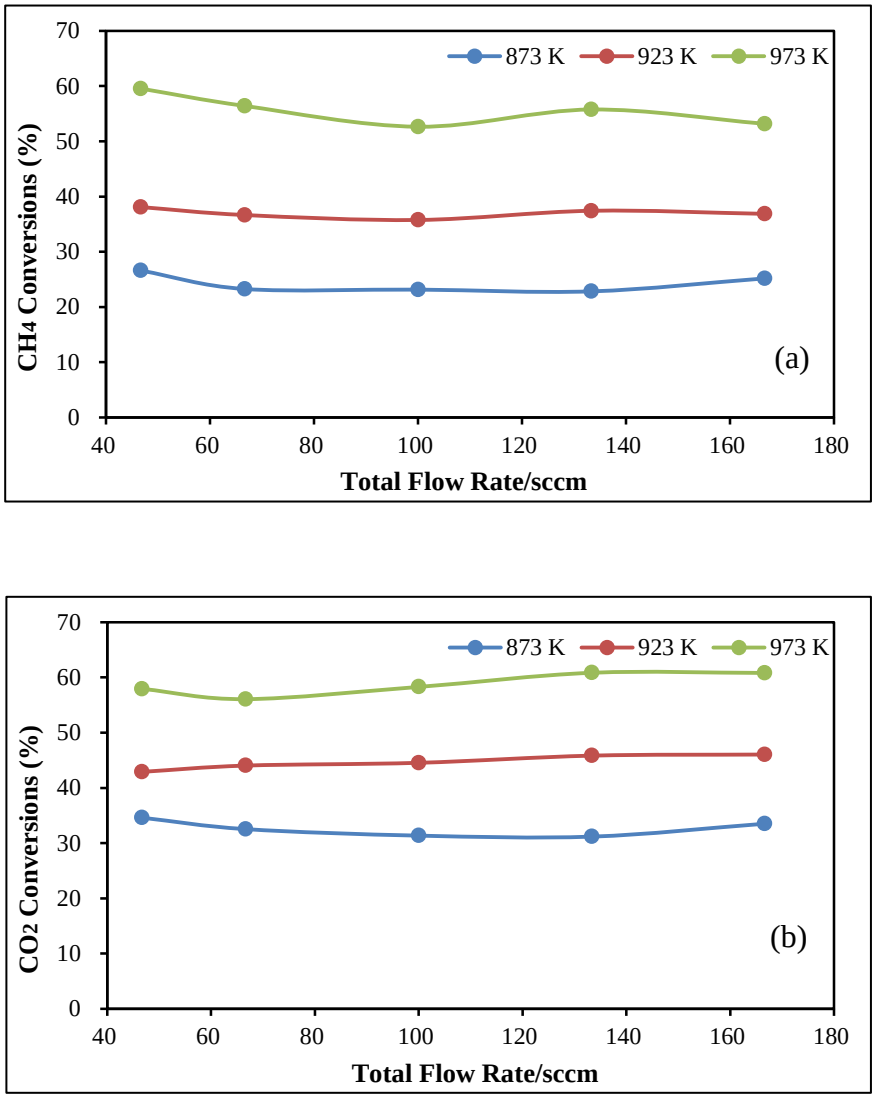

Figure 7.6 (a) CH_4 and (b) CO_2 conversion vs. total flow rate with CH_4/CO_2 at 873, 923 and 973 K.

From Figure 7.6, the influence of temperature on both CH_4 and CO_2 conversions is strong. Both conversions are barely affected by the total flow rate over a wide range, though a slight impact at the highest temperature 973 K is observed.

7.3 Equilibrium Calculation

Same as the analysis in Section 6.3, equilibrium calculations for Ru/CNT catalyst runs were also performed by *Chemkin*® with the same procedures. All equilibrium results are listed in Appendix M.

7.3.1 Equilibrium vs. Experimental Values

The experimental and equilibrium conversions of the highest (2.0) and lowest (0.5) feed CH_4/CO_2 ratio cases, at constant GHSV = 2 L/h-g_{cat}, with all temperatures are shown in Figure 7.7. All conversions are simply based on inlet and outlet mole fractions. Both CH_4 and CO_2 equilibrium conversions exceeded observed values, with the equilibrium values less sensitive to temperature. The CH_4 equilibrium conversions are higher than those of CO_2, and very close to 100%. The experimental conversions approach the equilibrium values as temperature increases. Trends for the other feed ratios tested were similar and fell in between the 0.5 and 2.0 curves.

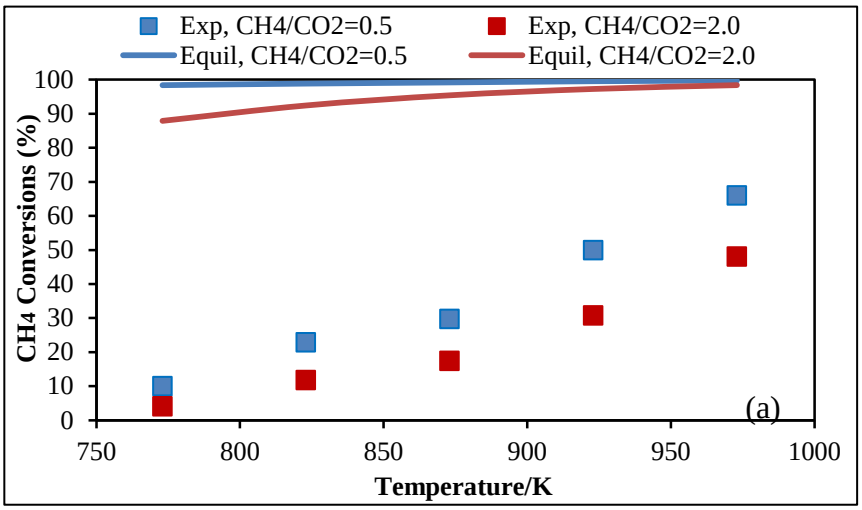

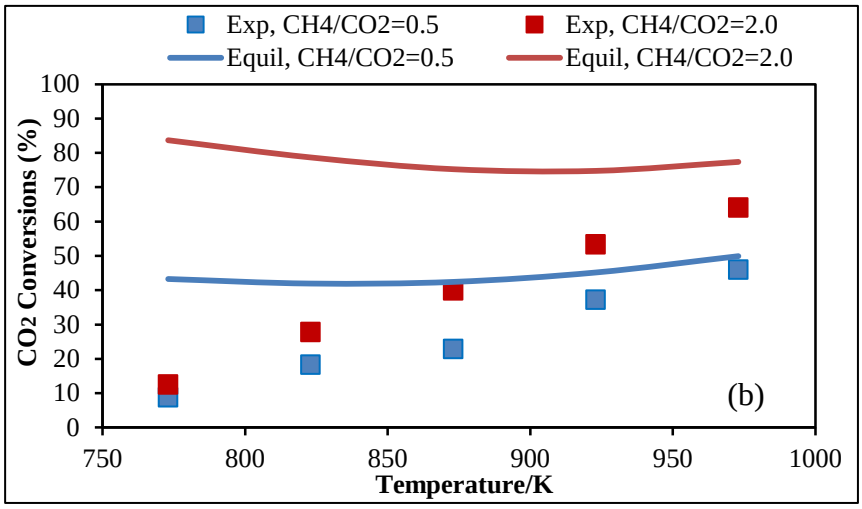

Figure 7.7 Comparison of equilibrium and experimental conversions of (a) CH_4 and (b) CO_2 at GHSV = 2 L/h-g_{cat}; feed CH_4/CO_2 = 0.5 and 2.0.

The experimental and equilibrium conversions of the highest (973 K) and lowest (773 K) temperatures, at GHSV = 2 L/h-g_{cat}, as functions of feed CH_4/CO_2 are shown in Figure 7.8. The equilibrium conversions exceeded observed values. The CH_4 equilibrium conversions are higher than those of CO_2, and do not change much with CH_4/CO_2. The CO_2 equilibrium conversions gradually increased with CH_4/CO_2. Trends

for the other temperatures tested are similar and fall in between the high and low values.

A limited number of experiments were run at 308 kPa at constant feed ratio CH_4/CO_2 = 1.0, but variable total flow rates at 873 and 923 K. Both CH_4 and CO_2 conversions decreased very slightly with increasing total flow rate. Once again, the observed conversions were consistently less than equilibrium values.

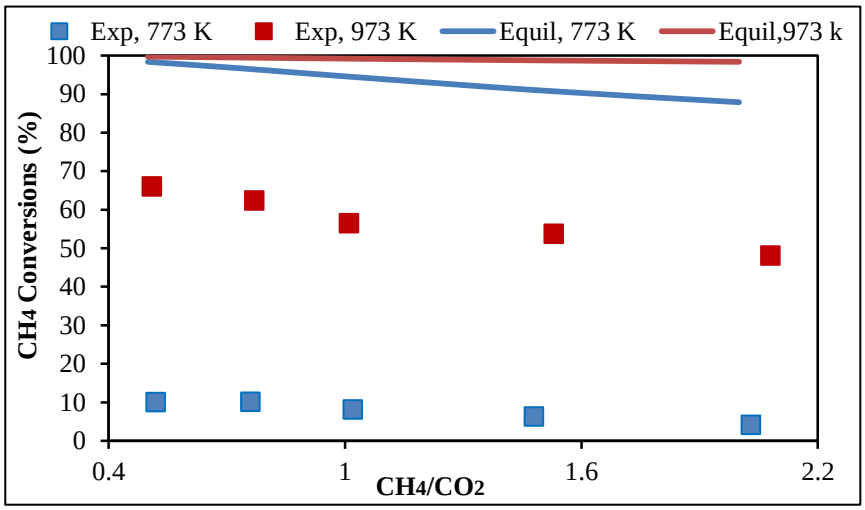

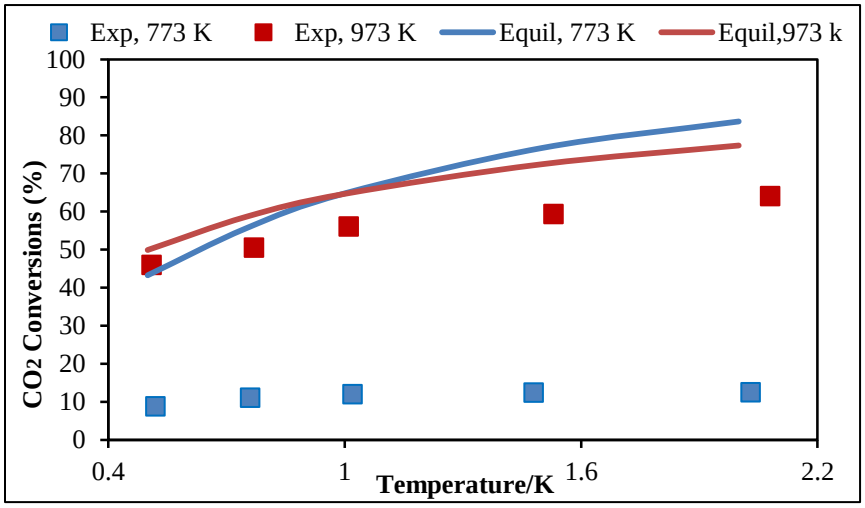

Figure 7.8 Comparison of equilibrium and experimental conversions of (a) CH_4 and (b) CO_2 at GHSV = 2 L/h-g_{cat}; temperature=773 and 973 K.

From Figure 7.9, the equilibrium H_2/CO increases with inlet CH_4/CO_2, which is consistent with experimental results. The equilibrium H_2/CO, strongly drops with increasing temperature. Comparing Figure 7.9 to Figure 7.3, we could found the equilibrium H_2/CO is much higher than experimental H_2/CO.

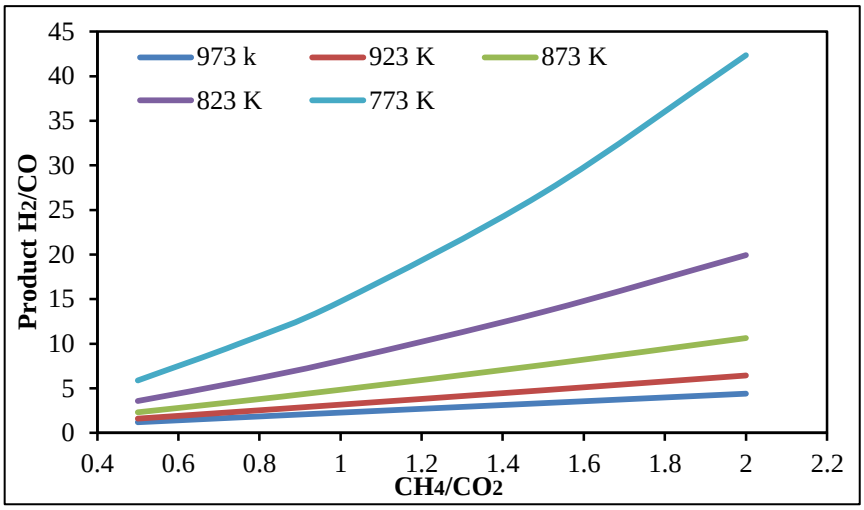

Figure 7.9 Equilibrium H_2/CO at GHSV = 2 L/h-g_{cat} at all temperatures.

It is also found in Figure 7.9, the equilibrium H_2/CO decreases with increasing temperature. But the experimental H_2/CO increases with temperature. It is because in the equilibrium test (without catalyst), the magnitude of DR is much less than that of catalysis experiments at low temperature. Therefore, CH_4 decomposition is more favored, and production of H_2 is much higher than CO. With the increasing temperature, DR is more favored in equilibrium test, so H_2/CO drops. Such different observation between equilibrium and catalysis experiments also reveals the effect of catalyst. The analysis of the comparison between equilibrium calculations and catalytic reactions suggests that the catalyst reaction system is not nearly at equilibrium for CH_4 and CO_2 conversions. This maybe suggests even more opportunity to improve syngas yields and quality.

7.4 Power Law Model

Due to its decent accuracy and simplicity, the power law model is a useful for comparing the behavior of different catalysts, and so is also applied to the Ru/CNT data.

7.4.1 Model Testing

The model derivation and testing process are same as what we have done in Sections 6.4.1 and 6.4.2 for Pt/Pd/CNT. Equation 6.19 is integrated with the reaction conditions of the Ru/CNT experiments. The orders α and β of the reaction rate are both determined as 1. Values of k are determined for each temperature. The *Polymath*® code for integration is listed in Appendix N. Comparisons between experimental conversions and model conversions for all temperatures are shown as Figures 7.10-7.14. As with the Power Law model results in Sections 6.4, the model curves here are not "smooth" since they are simulating actual experimental runs.

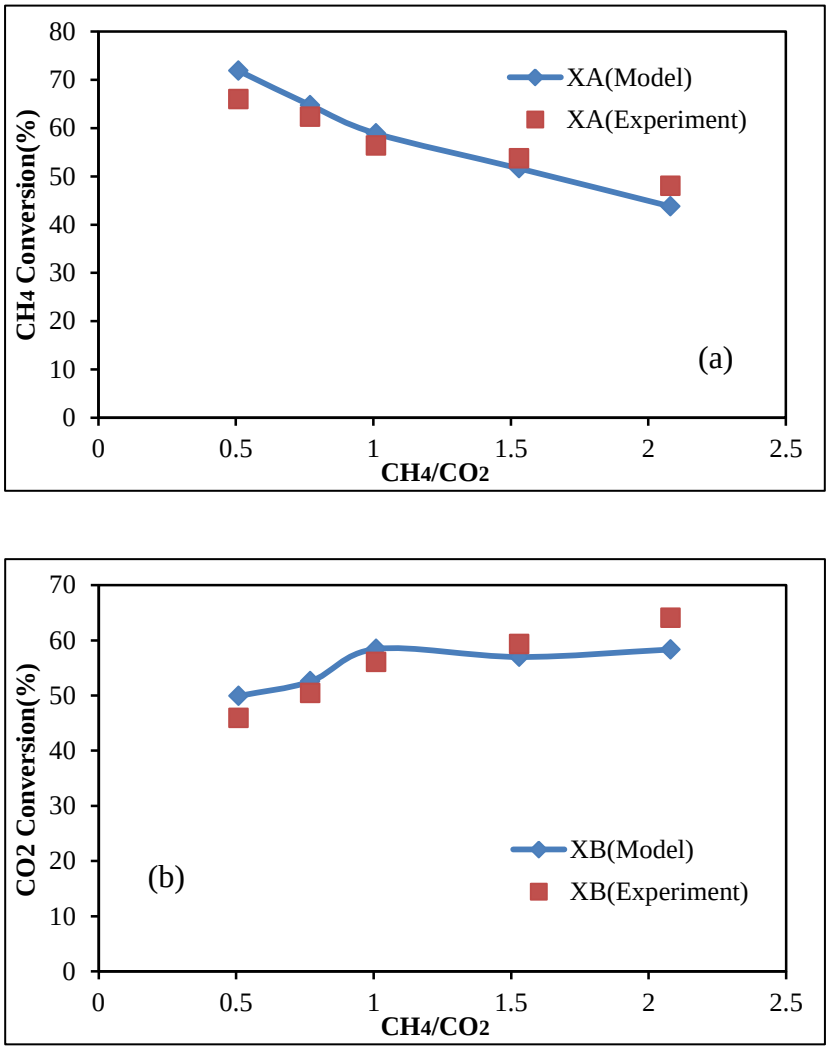

Figure 7.10 Model conversions vs. experimental conversions: (a) CH_4 (b) CO_2 at 973K.

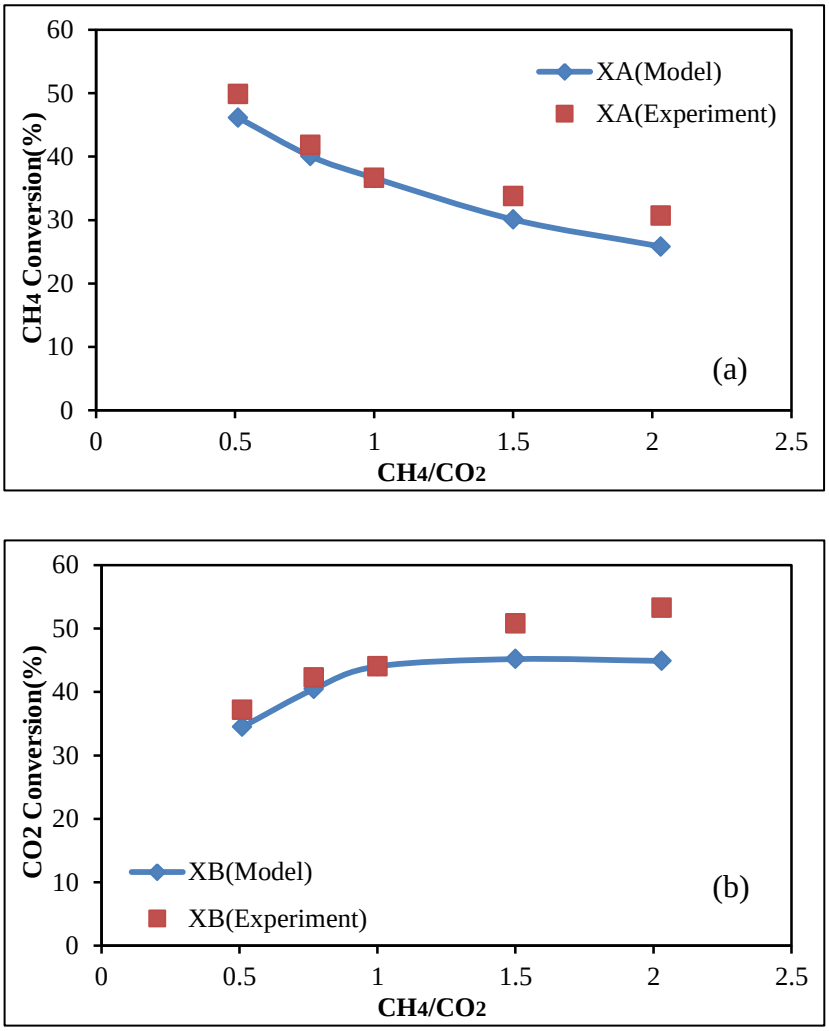

Figure 7.11 Model conversions vs. experimental conversions: (a) CH_4 (b) CO_2 at 923K.

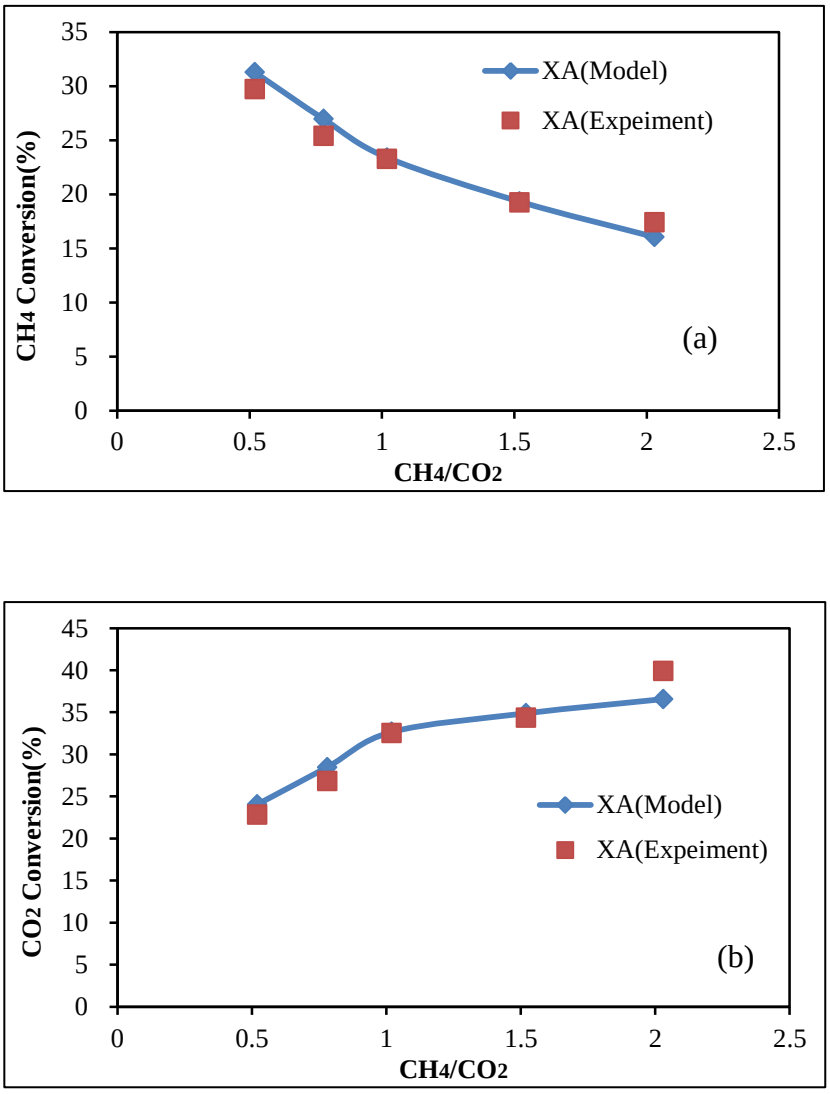

Figure 7.12 Model conversions vs. experimental conversions: (a) CH_4 (b) CO_2 at 873K.

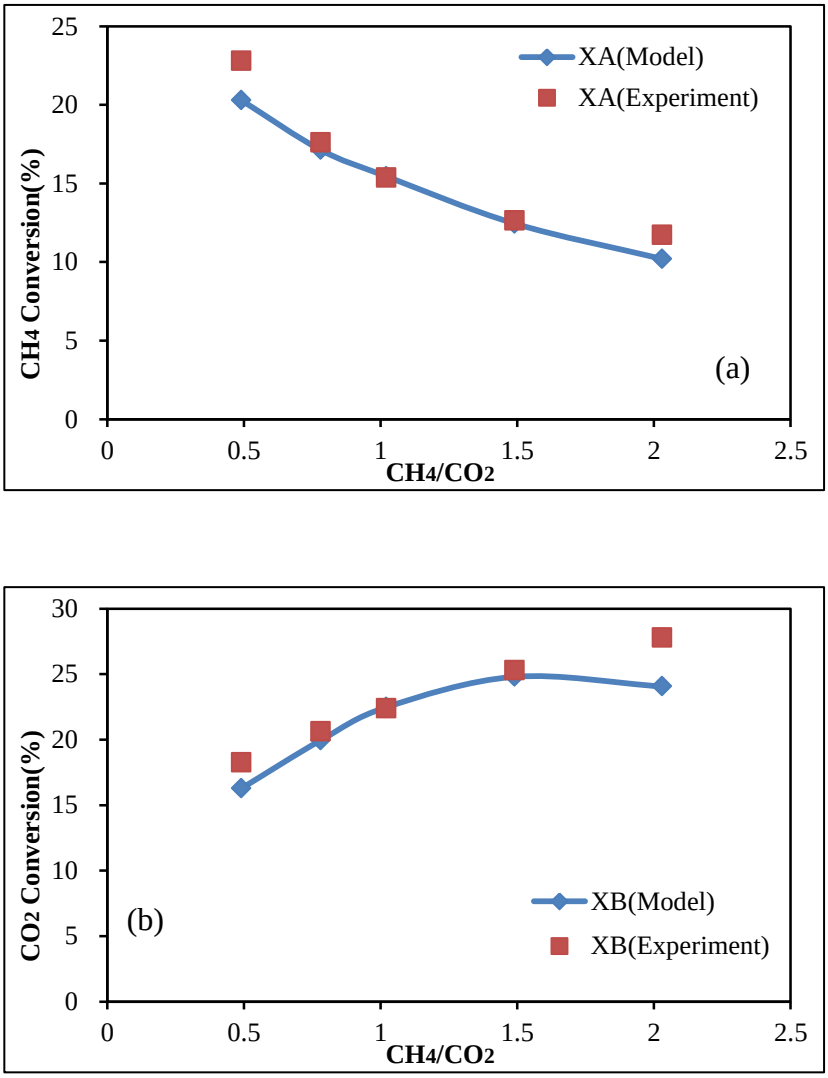

Figure 7.13 Model conversions vs. experimental conversions: (a) CH_4 (b) CO_2 at 823K.

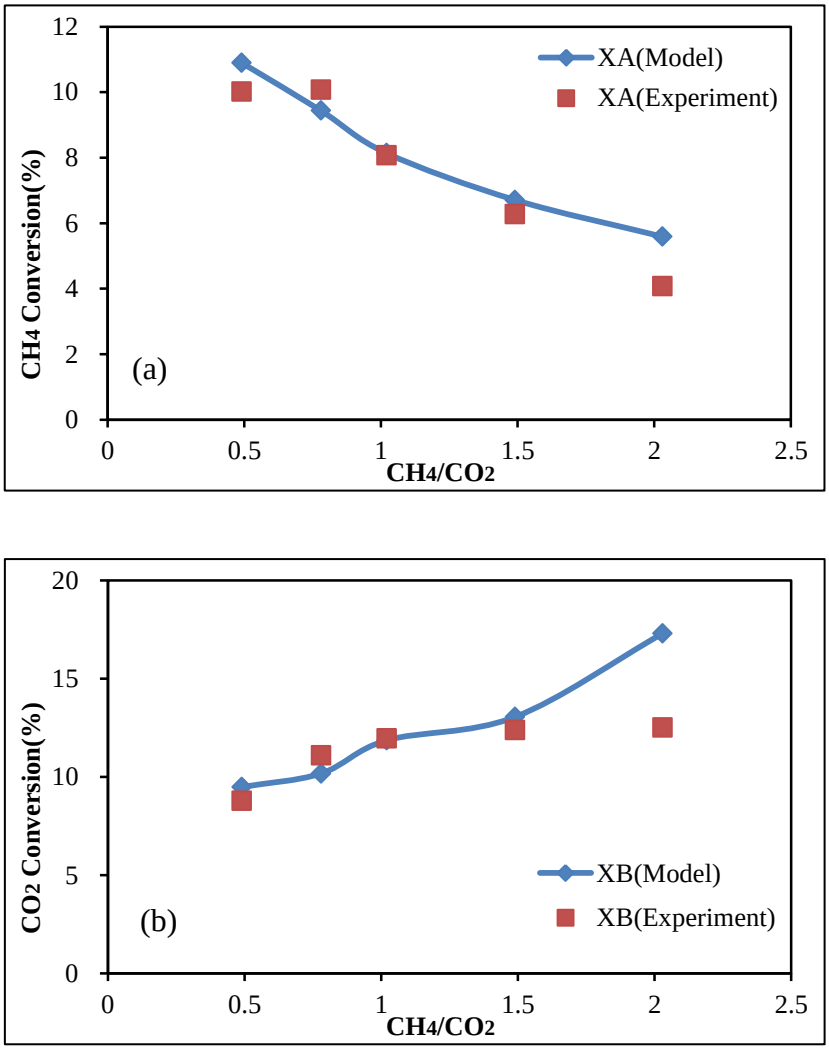

Figure 7.14 Model conversions vs. experimental conversions: (a) CH_4 (b) CO_2 at 773K.

Figures 7.10-7.14 (constant total flow rate at 66.7 sccm for all plots) show us a reasonable fit between model-simulated conversions and experimental conversions assuming both α and β are 1. Trial-and-error process estimates k, for the given four temperatures, that predicts X_A and X_B values similar to observed X_A and X_B for each molar ratio of CH_4/CO_2. In the next section, the dependence of the k values is examined as a function of temperature.

7.4.2 Arrhenius Plot

The "best fit" k values described in the previous section are presented in Table 7.1.

Table 7.1 Arrhenius Plot Data

k [m^6/ (s ⋅kg ⋅mol)]	T (K)	lnk	1/T
1.28×10^{-5}	773	-11.2635	0.001294
2.92×10^{-5}	823	-10.4425	0.001215
5.58×10^{-5}	873	-9.7931	0.001145
1.18×10^{-4}	923	-9.0420	0.001083
2.49×10^{-4}	973	-8.2974	0.001028

Based on the data in Table 7.1, an Arrhenius-type plot is made, shown as Figure 7.15.

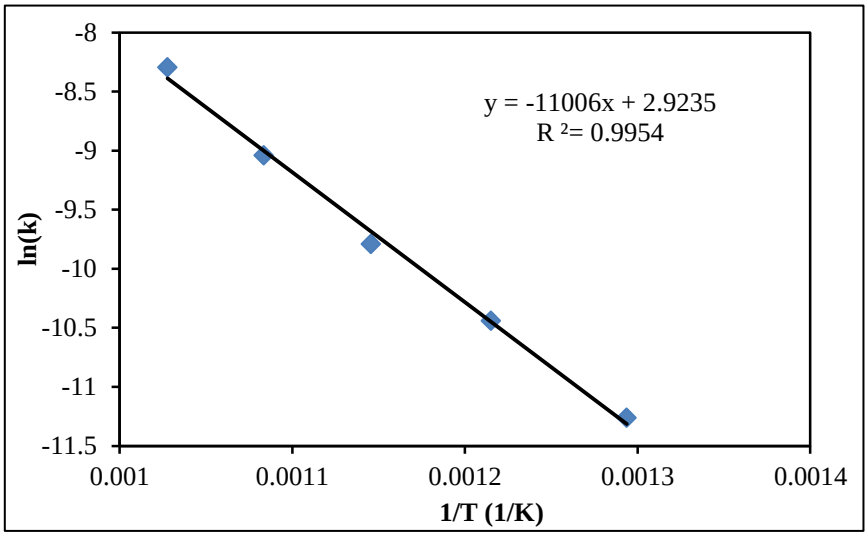

Figure 7.15 Arrhenius plot of "best fit" empirical, global rate constant k.

Figure 7.15 presents an excellent linear relationship between ln(k) and 1/T. Therefore, the Arrhenius equation is built up as: $k = 18.61e^{\frac{-9.15\times10^4}{RT}}$ (m^6 /moles s kg catalyst).

7.4.3 Assessment of Power Law Approach

The power law model above showed decent agreement with results of the constant flow rate runs. To further assess the power law model, the variable flow rate runs with constant molar ratio of CH_4/CO_2. Reaction conditions were 30 psig, and molar feed CH_4/CO_2=1.0. Reaction temperatures were 873, 923, and 973 K. The power law model was applied using the corresponding k values presented in Table 7.1. Comparisons between experimental conversions and model conversions are shown as Figures 7.16-7.18.

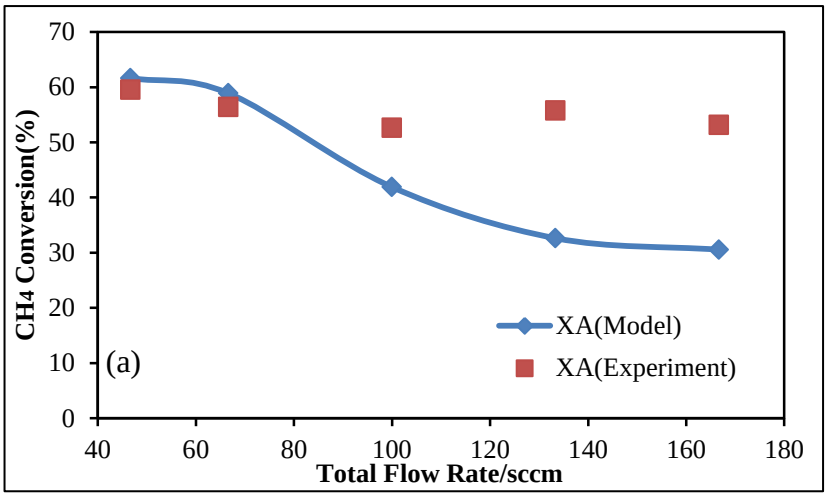

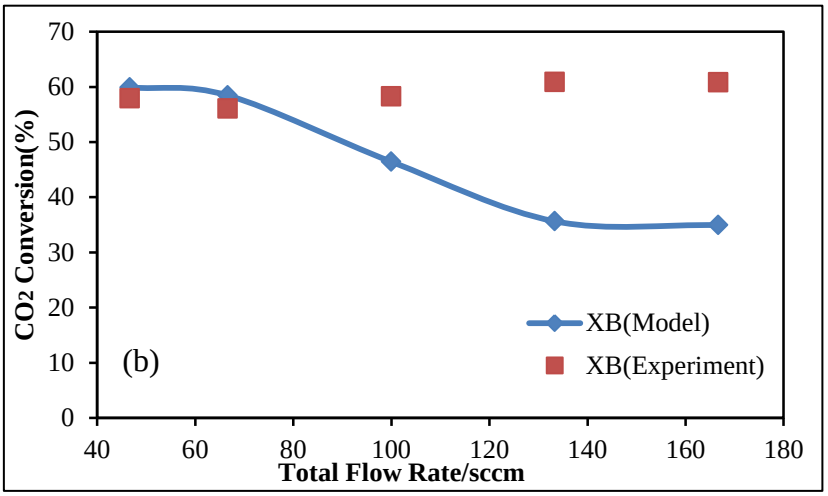

Figure 7.16 Model conversions vs. experimental conversions: (a) CH_4 (b) CO_2 at 973K and CH_4/CO_2=1.0.

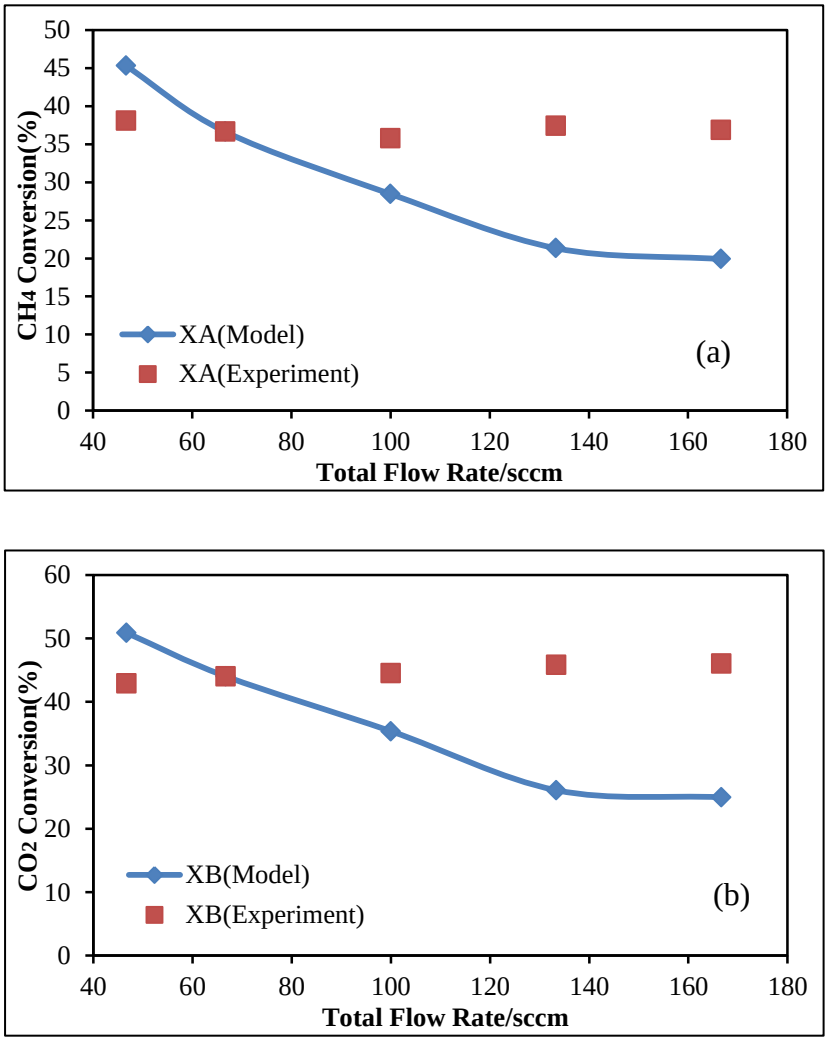

Figure 7.17 Model conversions vs. experimental conversions: (a) CH_4 (b) CO_2 at 923K and CH_4/CO_2=1.0.

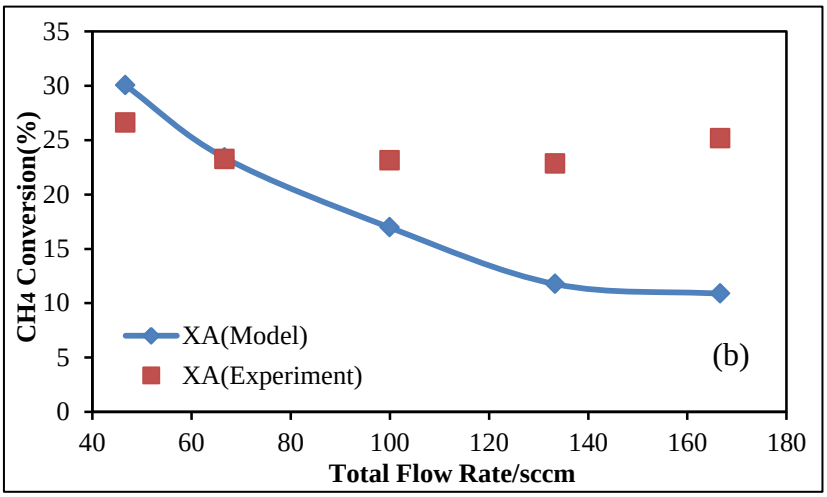

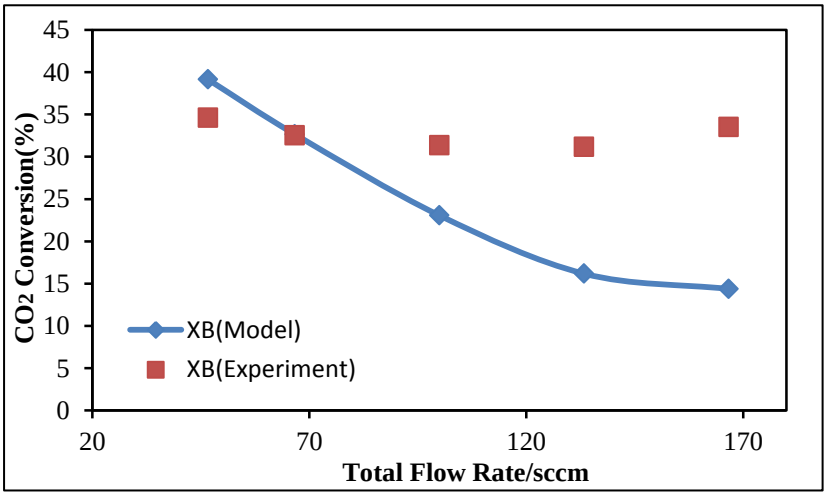

Figure 7.18 Model conversions vs. experimental conversions: (a) CH_4 (b) CO_2 at 873K and CH_4/CO_2=1.0.

According to Figures 7.16-7.18, the power law model predicts that both conversions decline with the total flow rate for all temperatures. However, the experimental conversions are barely influenced by flow rate. Combined with Figures 7.10-7.14, the conclusion can be made that this model (Equation 6.19) shows promise in the prediction of CH_4 and CO_2 conversions at total feed rates at or below 67 sccm. But it badly underpredicts the observed conversions at higher flow rates.

7.5 Multiple Reaction Model

For pursuing more accurate prediction, as what we have done in Section 6.5, a multiple reaction global model is also applied for the Ru/CNT-zeolite. As it was also a DR process, the candidates for the multiple reaction model for Ru/CNT are the same as those for Pt/Pd-CNT. The selected reactions for multiple reaction model are summarized in Table 6.2.

7.5.1 Programing for Reaction Rate Constant

The DR experiments in the current study were also simulated with a packed bed reactor (PBR) model as described in Table 6.3. The goal of the simulation was to obtain Arrhenius parameter pairs (A_i, E_i) by determine k_{fi}. The species balances were integrated with an original *Matlab*® program. All available experimental mole fraction and flow rate data at a given temperature were supplied to the program. The *Matlab*® program code for solving values of k_{fi} at 973 K is selected as example and shown in Appendix O.

The *Matlab*® program codes were applied for all experimental temperatures, using data from both constant flow and variable flow cases. All k_{fi} values for each temperature were determined based on the algorithm and *Matlab*® code.

7.5.2 Arrhenius Plots

Completion of the integration / regression routine at each temperature yielded the rate constants k_{fi}, which are listed in Table 7.2, for each of the three global reactions.

Table 7.2 Rate Constant k_{fi} for 3-Global Reactions

T/K	1/T	k_1	lnk_1	k_2	lnk_2	k_3	lnk_3
773	0.001294	0.0086	-4.75599	0.00138	-6.58567	0.00016	-8.74034
823	0.001215	0.0198	-3.92207	0.0044	-5.42615	0.00071	-7.25025
873	0.001145	0.032	-3.44202	0.006	-5.11600	0.0012	-6.72543
923	0.001083	0.065	-2.73337	0.0243	-3.71728	0.0043	-5.44914
973	0.001028	0.129	-2.04794	0.05	-2.99573	0.0109	-4.51899

Figure 7.19 presents the Arrhenius plot of the global rate constants k_{fi} vs. temperature based on Table 7.2. The Arrhenius fits are quite linear over the 773-973 K range.

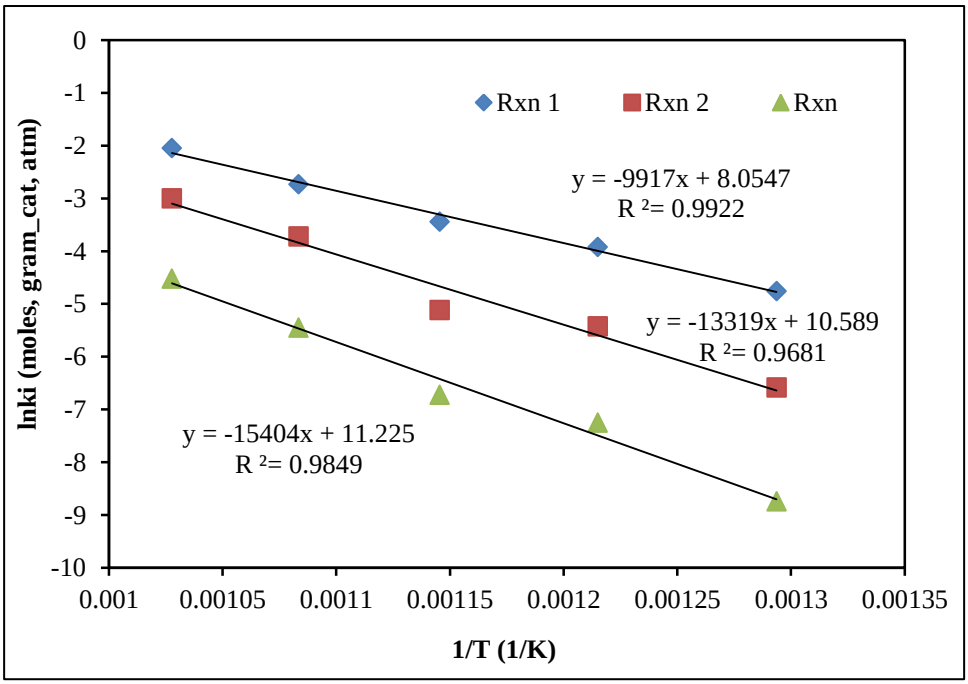

Figure 7.19. Arrhenius plots of forward rate constants k_i.

Based on Figure 7.19, Arrhenius parameters are presented in Table 7.3. As with over Pt/Pd-CNT/zeolite, CH_4 decomposition has the largest barrier among the three reactions.

Table 7.3 Arrhenius Parameters

Reaction i	*Parameter A_i (mole, hr, g_cat, atm)*	*Parameter E_i (cal/mole)*
1	3.149E3	19705
2	3.970E4	26445
3	7.498E4	30608

7.5.3 Model Testing

With the obtained Arrhenius parameters, the 3-reaction global set was tested against the experimental data for cases from Table 6.2. The PBR simulation based on Table 6.3 was evaluated in *Polymath*®. A typical *Polymath*®code, at 923 K, is shown in Appendix P.

The *Polymath*® code is applied to all the collected data. Then molar flow rates of all species determined from *Polymath*® are converted into concentrations. All results are listed in Appendix M. For constant flow runs, outlet concentrations of all species from 3-reaction model and experiments are compared in Figures 7.20-7.24.

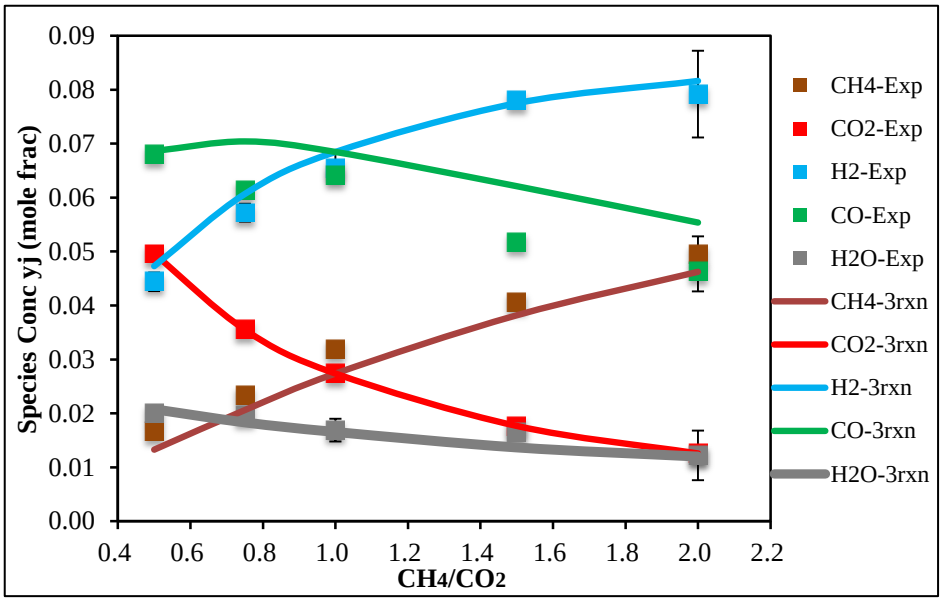

Figure 7.20 Comparison of 3-reaction model-based concentrations and experimental concentrations at 973 K.

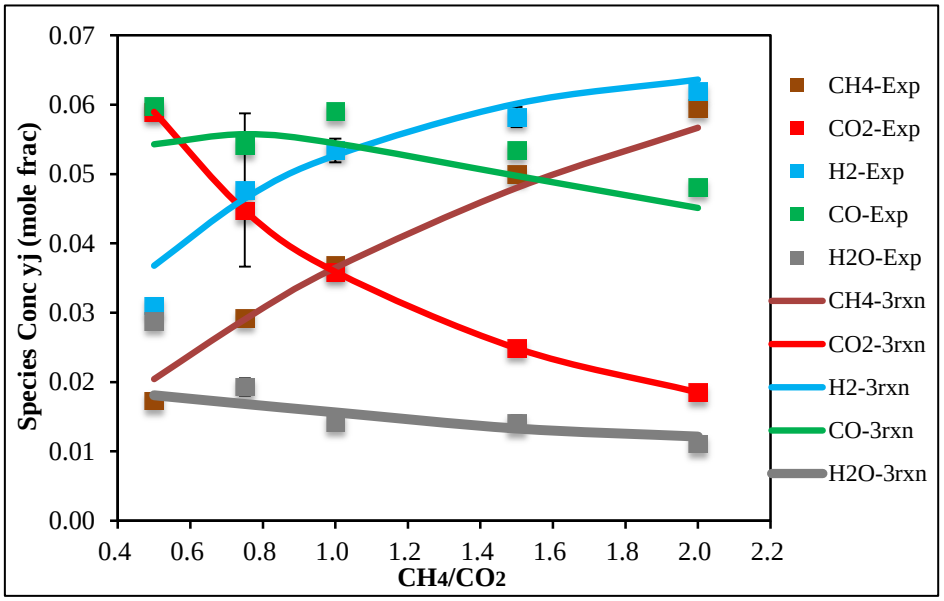

Figure 7.21 Comparison of 3-reaction model-based concentrations and experimental concentrations at 923 K.

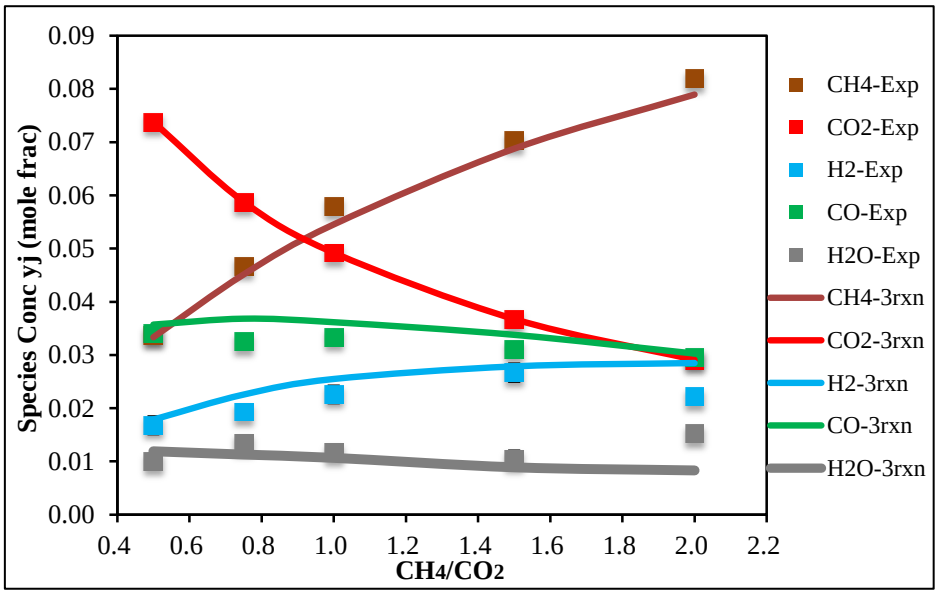

Figure 7.22 Comparison of 3-reaction model-based concentrations and experimental concentrations at 873 K.

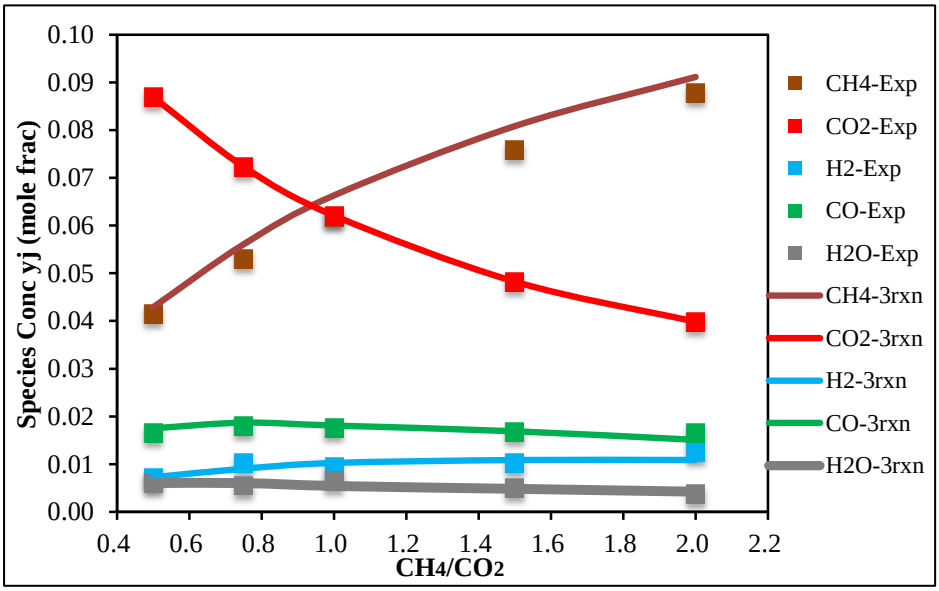

Figure 7.23 Comparison of 3-reaction model-based concentrations and experimental concentrations at 823 K.

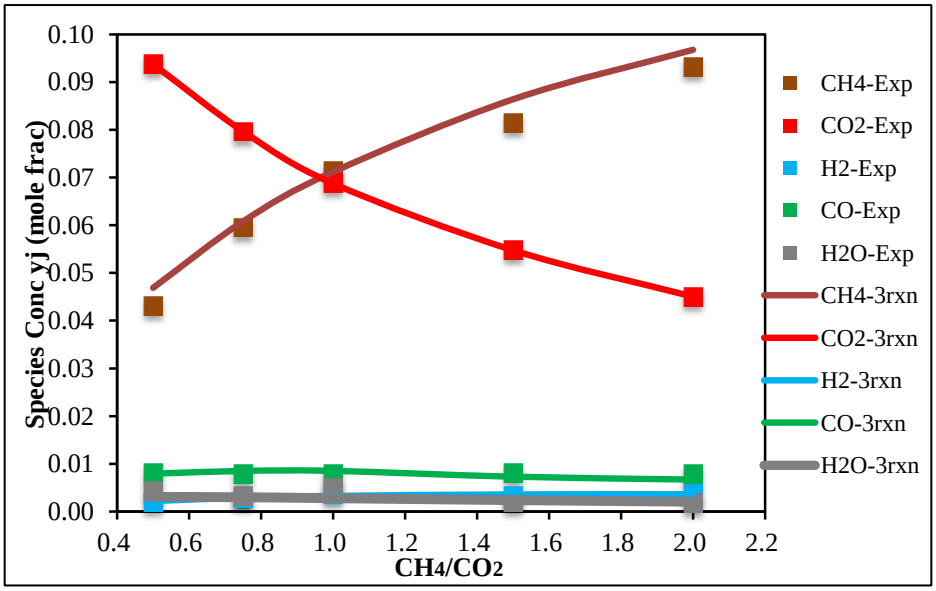

Figure 7.24 Comparison of 3-reaction model-based concentrations and experimental concentrations at 773 K.

Figures 7.20-7.24 shows concentrations as functions of feed molar ratio CH_4/CO_2. Similar to Section 6.5, the 3-reaction model did a good job on outlet concentration prediction for all species at each temperature with constant total inlet flow rate (66.7 sccm).

7.5.4 Assessment of Multiple Reaction model

To fully assess multiple reaction model in this study, the comparison of outlet species concentrations between 3-reaction global model results and experimental data for the variable flow rate runs are shown in Figures 7.25-7.27 at constant feed ratio CH_4/CO_2=1.0.

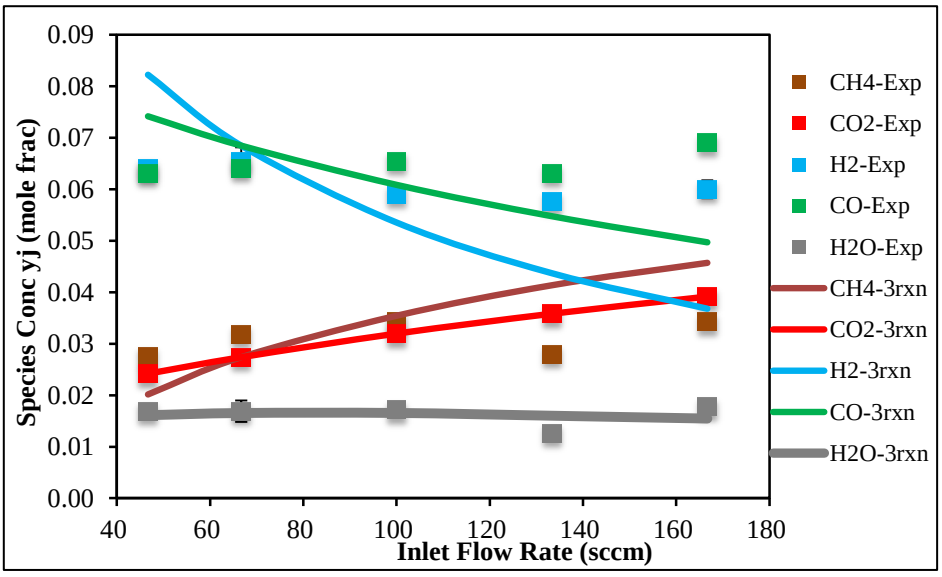

Figure 7.25 Comparison of 3-reaction model-based concentrations and experimental concentrations at 973 K with CH_4/CO_2=1.0 and variable flow rate.

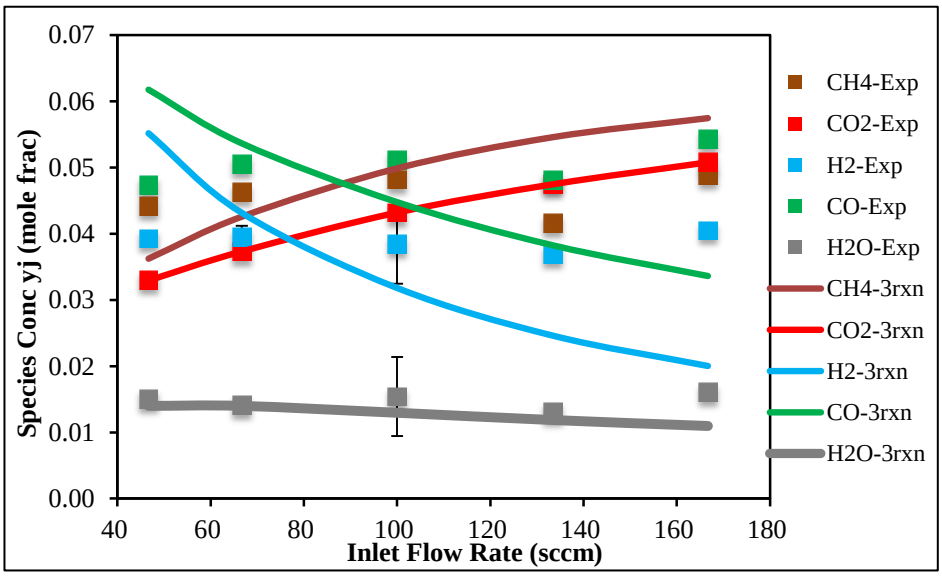

Figure 7.26 Comparison of 3-reaction model-based concentrations and experimental concentrations at 923 K with CH_4/CO_2=1.0 and variable flow rate.

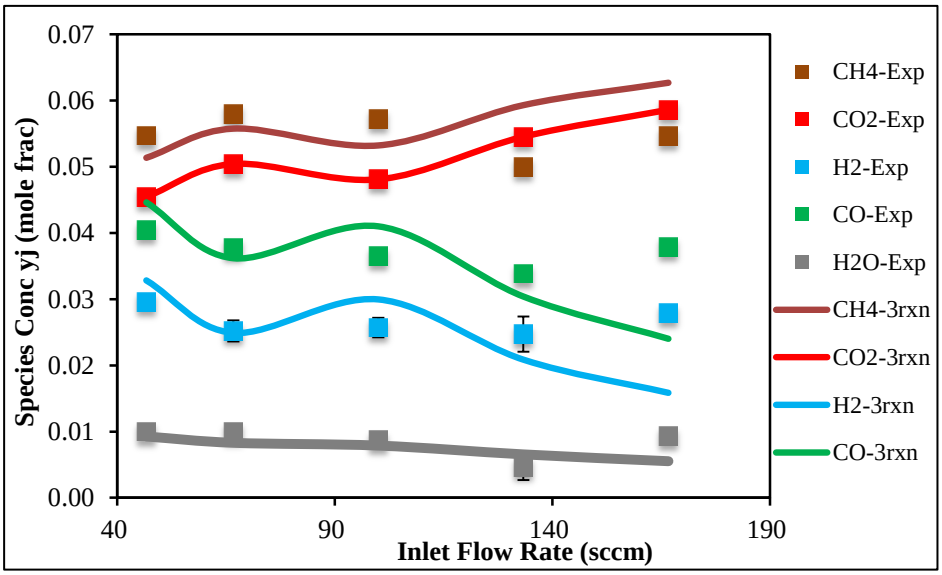

Figure 7.27 Comparison of 3-reaction model-based concentrations and experimental concentrations at 873 K with CH_4/CO_2=1.0 and variable flow rate.

Figures 7.25-7.27 show that the fits for outlet H_2O concentrations are as excellent as constant flow runs. The performance of the 3-reaction model for CH_4, CO_2, CO and H_2 is mixed. Some curve waviness observed against the experimental results. As power law could only show the prediction conversions X_A and X_B, however, the 3-

reaction model includes all species mole fractions, and also the coking process.

7.6 Chemkin® Model

Chemkin® is a powerful computational tool for chemical engineering calculations and simulations, and will be applied on DR over Ru/CNT-zeolite with the same PBR model and detailed mechanism as what was done on Pt/Pd-CNT/zeolite. As before, it must be recognized that there is no detailed mechanism for Ru/CNT. The mechanism applied here is the same Ni mechanism used in Section 6.6.

7.6.1 Chemkin® Simulation

To proceed the *Chemkin*® simulation, the required parameters need to be plugged into the software. The catalyst bed length is 5 cm, with reactor inner diameter 1 cm. A chemisorption test was done on Ru/CNT-Zeolite, the active site density was measured as 7.51×10^{18} sites/gram. With a measured BET surface area 23 m^2/gram, the active site density converts to 5.42×10^{-11} mole/cm^2, which was inserted into detailed mechanism. As 2 grams catalyst was uploaded for our study, the internal surface area per unit catalyst bed length calculates as: 23×10^4 cm^2/gram $\times2$ grams /5cm = 9.2×10^4cm.

The first round *Chemkin*® simulation process is the same as that for Pt/Pd-CNT/zeolite, including constant flow rate cases and variable flow rate cases, in which the Ru/CNT site density above is used, and referred to as the "lower" site density. Then the *Chemkin*® calculations were repeated with the "higher" active density 2.66×10^{-9} mole/cm^2, which is the original active Ni site density. All *Chemkin*® results including higher active site density (Ni) simulation and lower active site density (Ru) are listed in Appendix M.

7.6.2 Chemkin® Simulation Results Discussion

The *Chemkin*® simulation results, including CH_4 and CO_2 conversions and product H_2/CO, based on higher and lower active site density are compared with those from the experimental data. Figure 7.28-7.32 show comparisons for the constant flow runs.

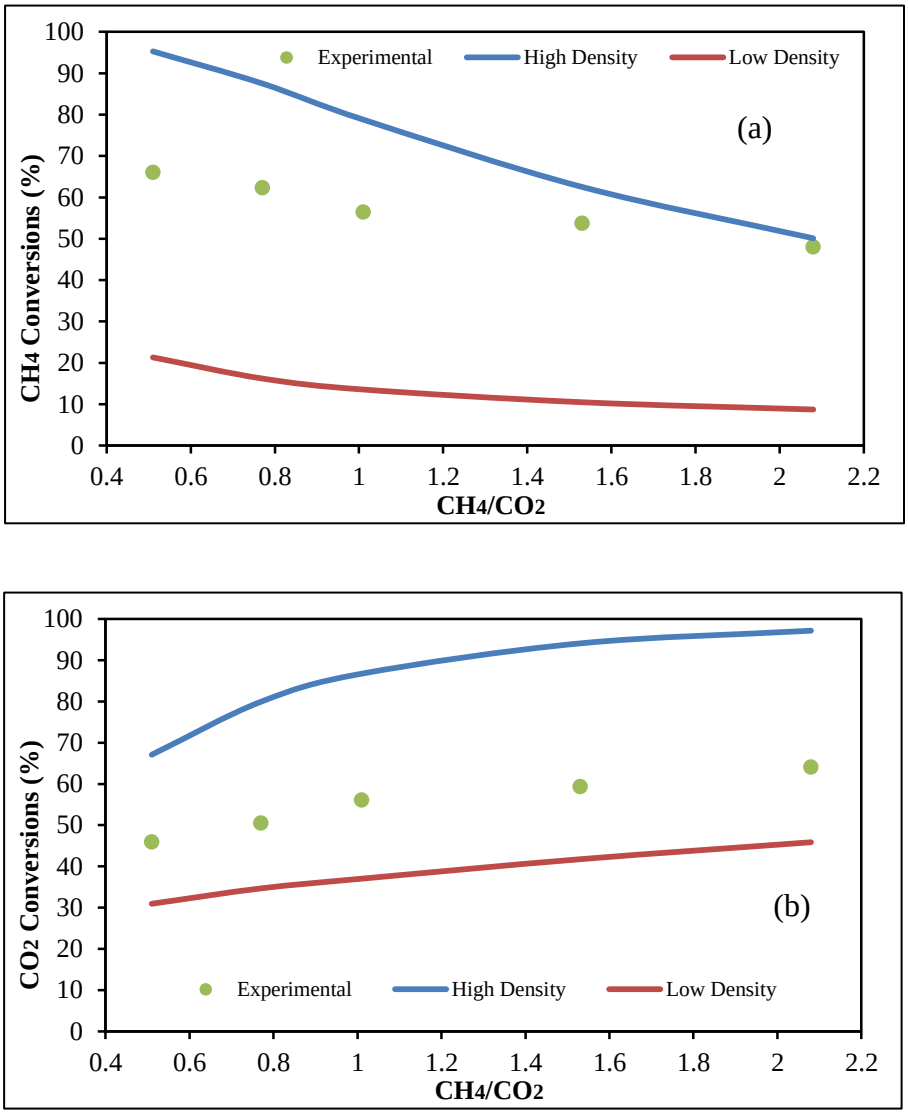

Figure 7.28 Comparison of *Chemkin*® simulation results and experimental results on (a) CH_4 conversions and (b) CO_2 conversions at 973 K and 66.7 sccm.

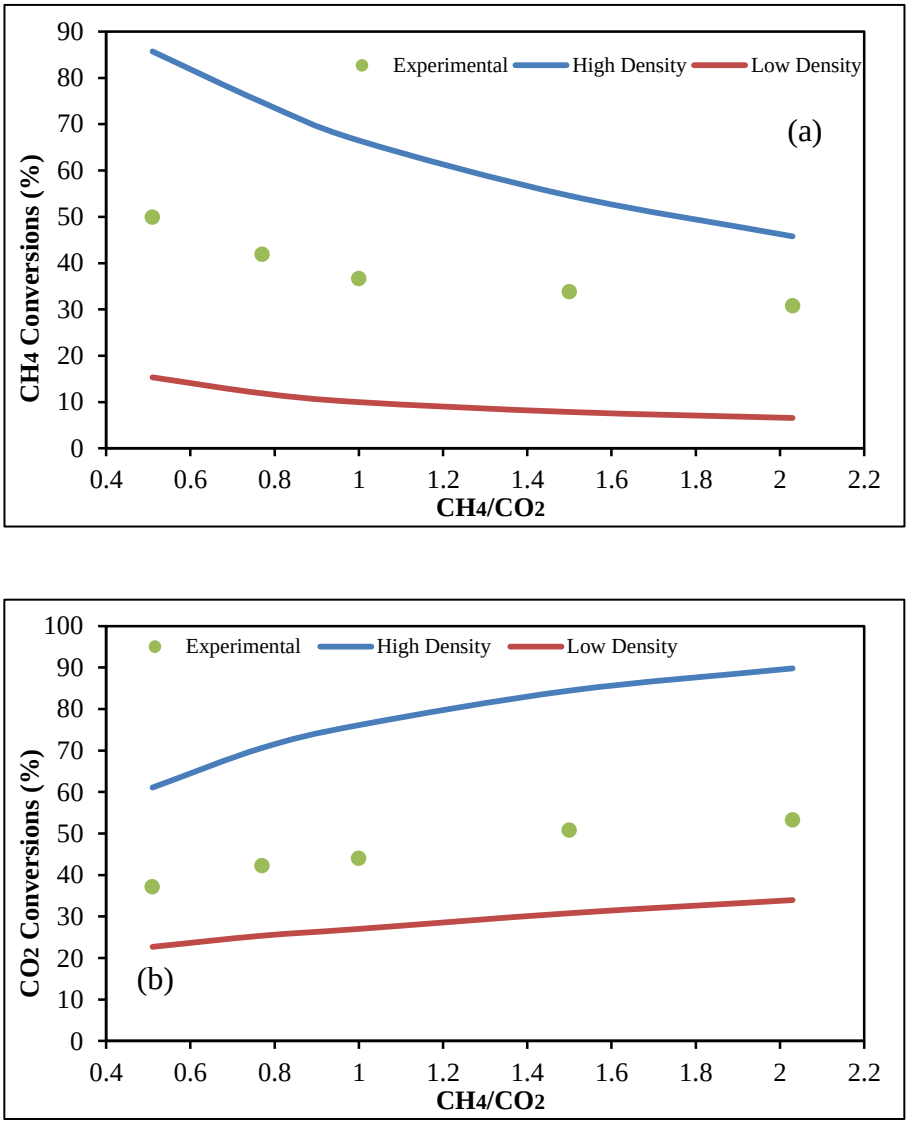

Figure 7.29 Comparison of *Chemkin*® simulation results and experimental results on (a) CH_4 conversions and (b) CO_2 conversions at 923 K and 66.7 sccm.

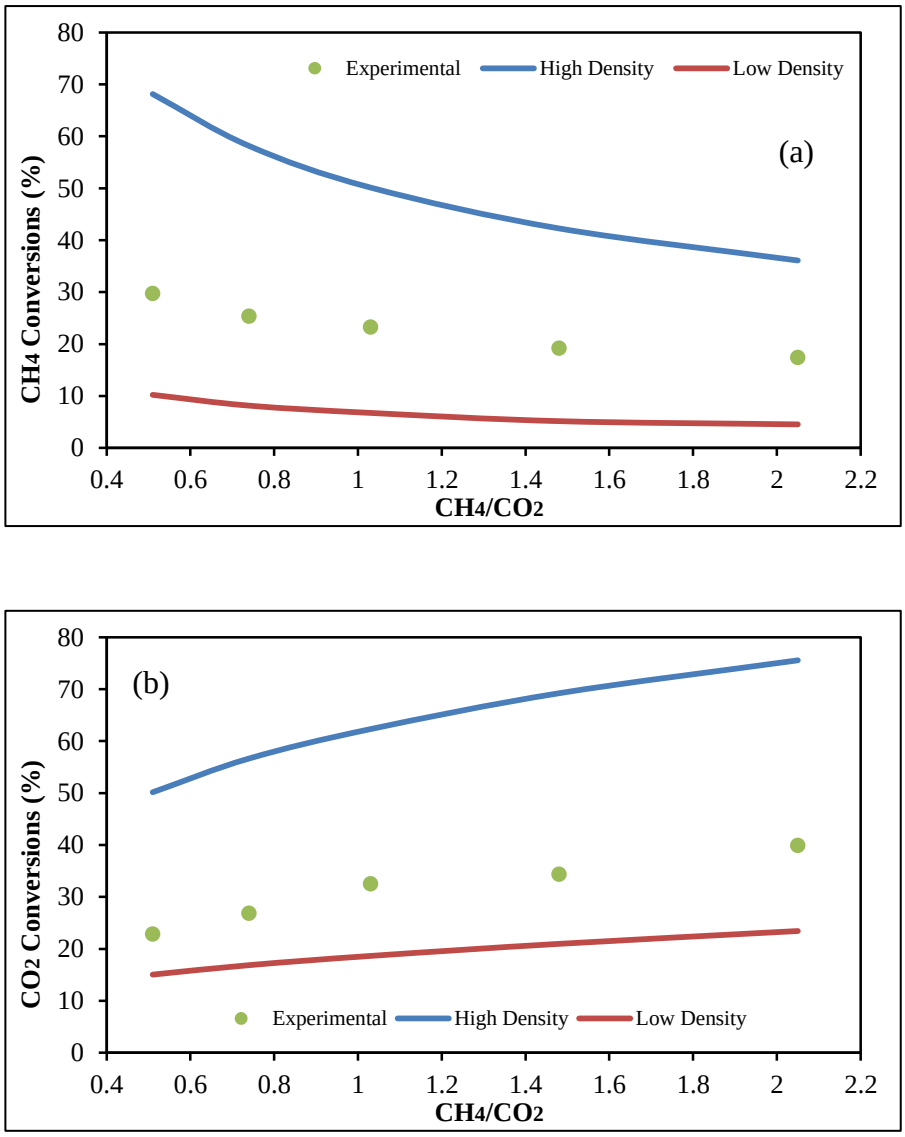

Figure 7.30 Comparison of *Chemkin*® simulation results and experimental results on (a) CH_4 conversions and (b) CO_2 conversions at 873 K and 66.7 sccm.

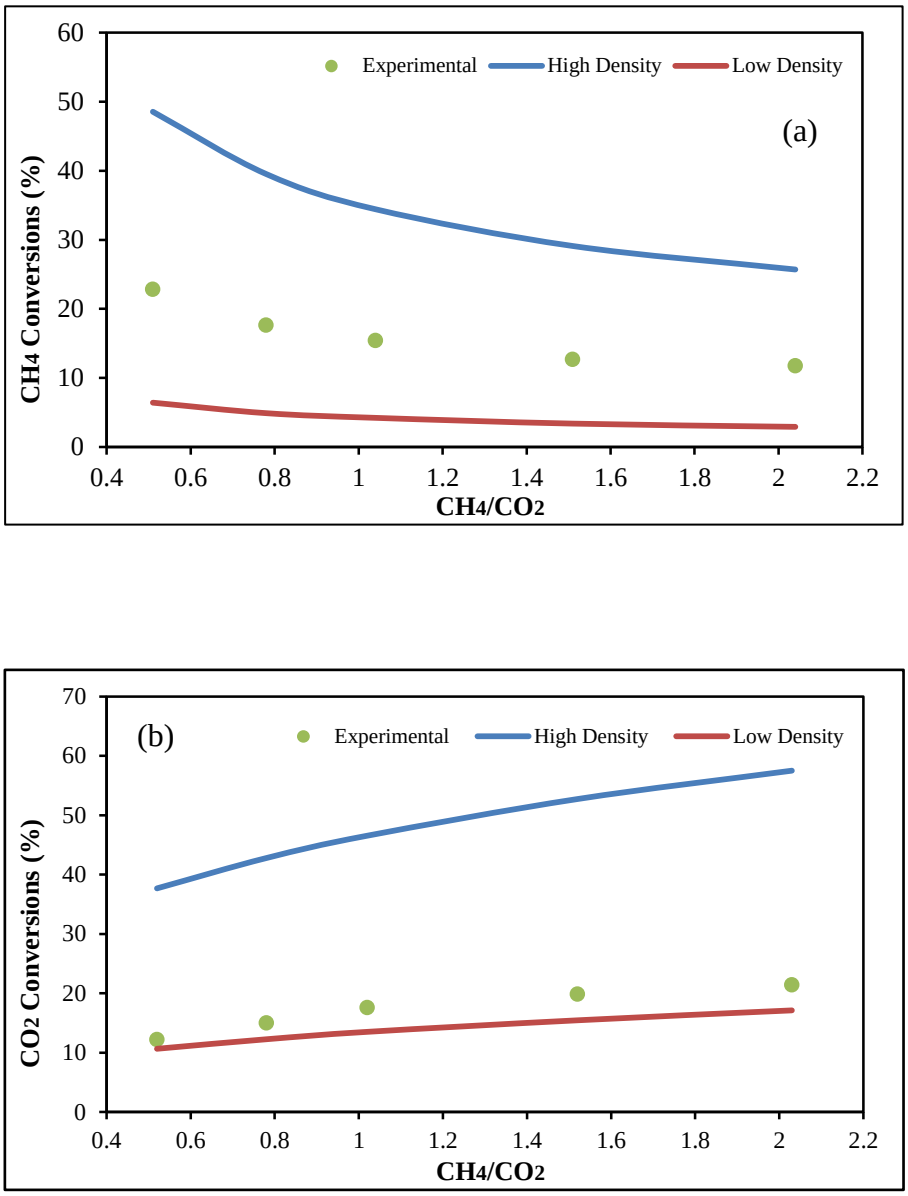

Figure 7.31 Comparison of *Chemkin*® simulation results and experimental results on (a) CH_4 conversions and (b) CO_2 conversions at 823 K and 66.7 sccm.

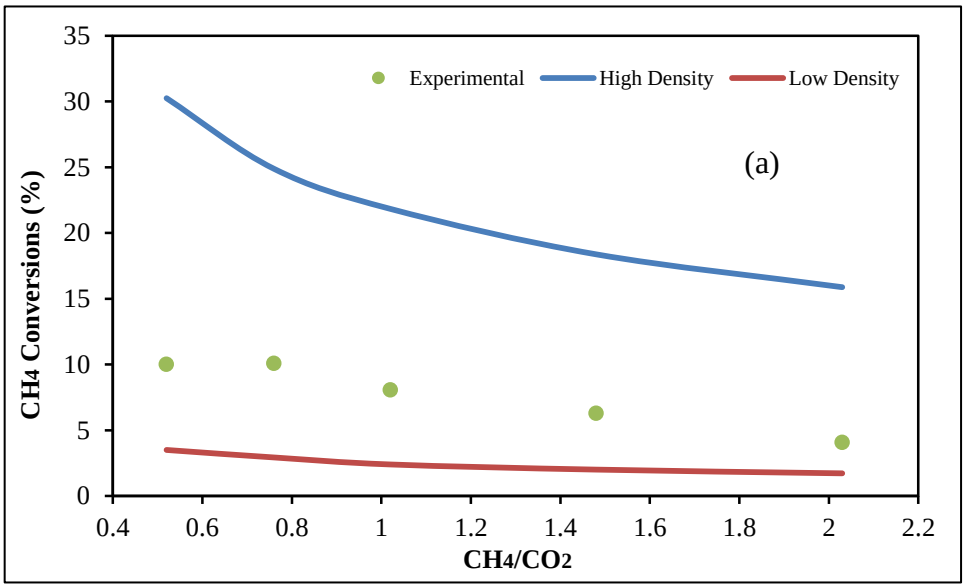

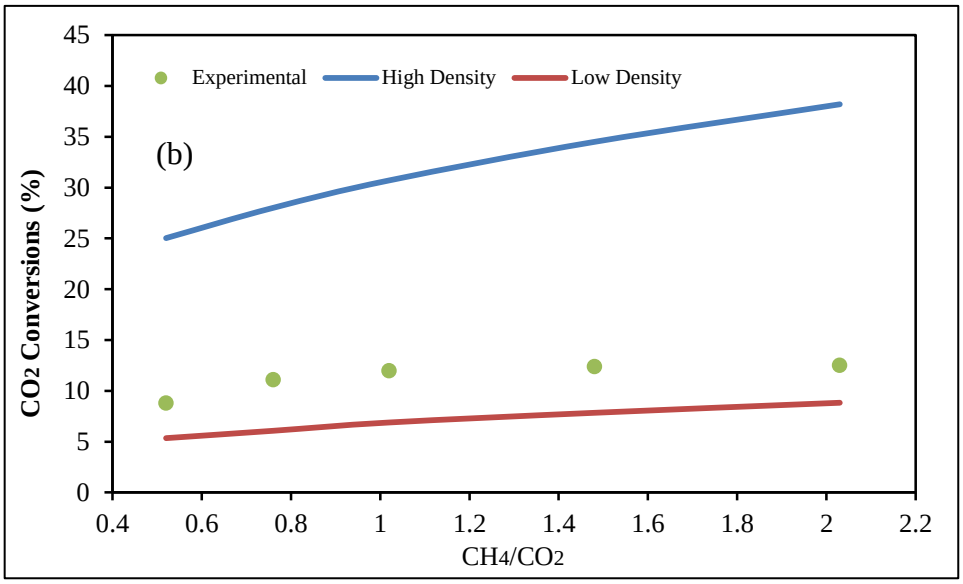

Figure 7.32 Comparison of *Chemkin*® simulation results and experimental results on (a) CH_4 conversions and (b) CO_2 conversions at 773 K and 66.7 sccm.

According to Figure 7.28-7.32, the *Chemkin*® simulation conversions of CH_4 and CO_2 are sensitive to active site density. The higher the density is, the higher the conversions. The simulation CH_4 conversions decline with the feed molar ratio

CH_4/CO_2; while the simulation CO_2 conversions increase with CH_4/CO_2. Such tendency is consistent with experimental CH_4 and CO_2 conversions. The *Chemkin*® simulation conversions of CH_4 and CO_2 based on higher and lower active site density effectively bracket the experimental CH_4 and CO_2 conversions for all tested temperatures at constant flow. For lower active site density simulations, the employed active site density is exact the value of our Ru/CNT catalyst, but the conversions of CH_4 and CO_2 are obviously lower than experimental conversions. What is more, the simulation conditions are as same as experimental conditions.

Such observation implies that the activity of our Ru/CNT-zeolite is higher than Ni based catalyst. At 773 and 823 K, the experimental conversions of CH_4 and CO_2 are close to those from lower active site density simulations. At 923 K, however, the experimental conversions of CH_4 and CO_2 are much closer to those from higher active site density simulations, especially the CH_4 conversion at CH_4/CO_2=2.0, as it almost coincides with the conversion from the simulation. Therefore, the activity of Ru/CNT-zeolite is also more temperature dependent than Ni based catalyst.

The *Chemkin*® simulation product H_2/CO is compared with those obtained from the experiments. As H_2/CO from lower active site density simulation are all below 0.02, only H_2/CO from the higher active site density simulation and experiments are presented in Figures 7.33-7.37.

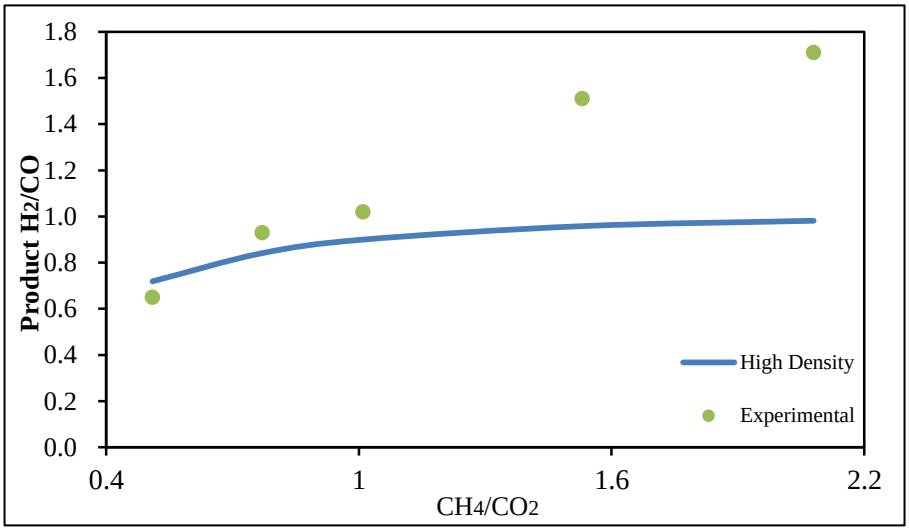

Figure 7.33 Comparison of *Chemkin*® simulation results and experimental results on H_2/CO at 973 K and 66.7 sccm.

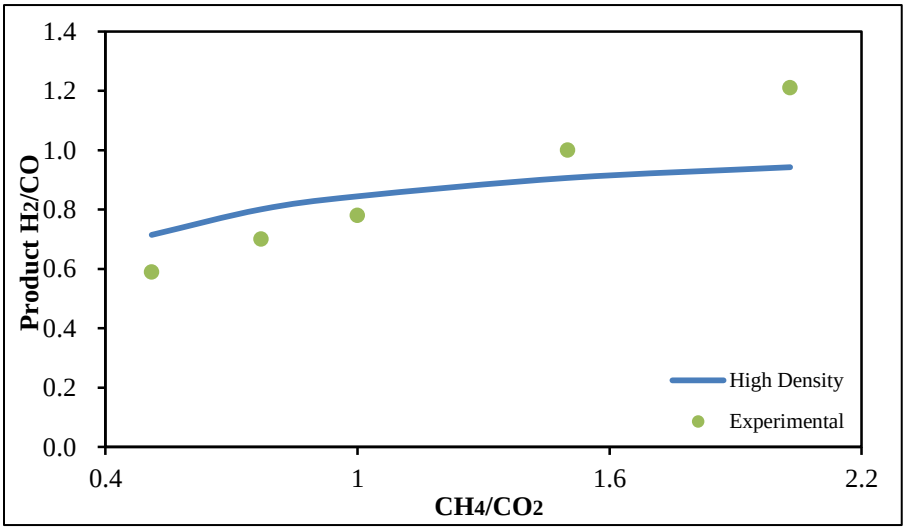

Figure 7.34 Comparison of *Chemkin*® simulation results and experimental results on H_2/CO at 923 K and 66.7 sccm.

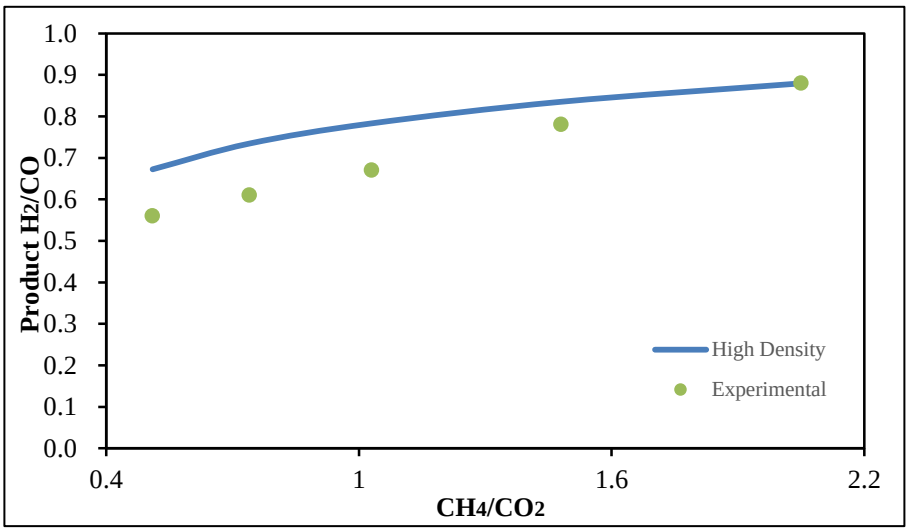

Figure 7.35 Comparison of *Chemkin*® simulation results and experimental results on H_2/CO at 873 K and 66.7 sccm.

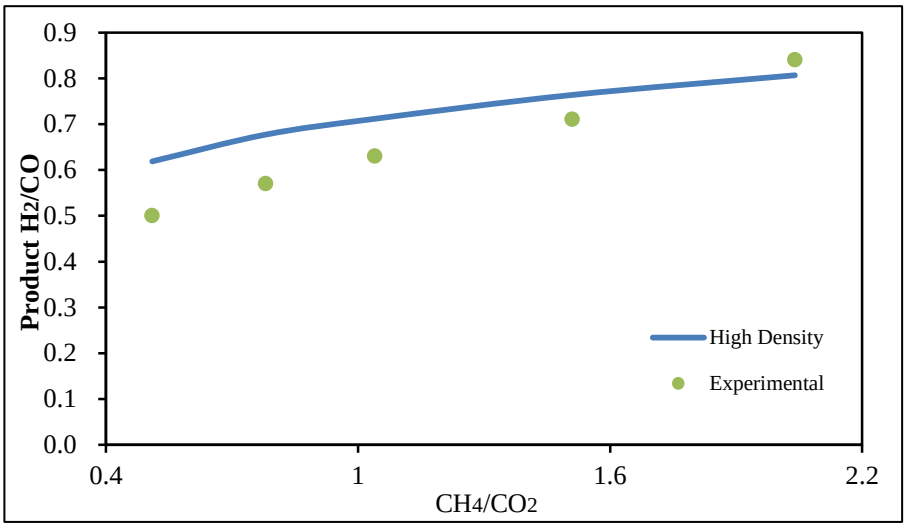

Figure 7.36 Comparison of *Chemkin*® simulation results and experimental results on H_2/CO at 823 K and 66.7 sccm.

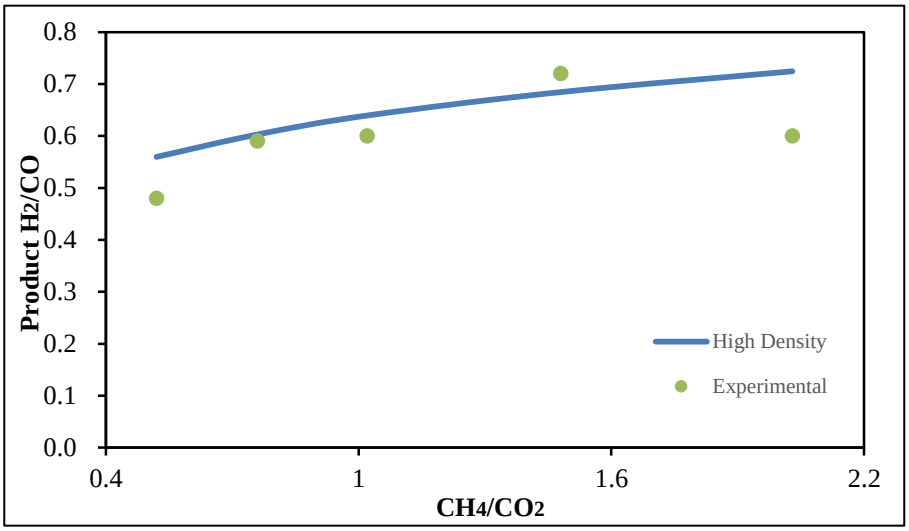

Figure 7.37 Comparison of *Chemkin*® simulation results and experimental results on H_2/CO at 773 K and 66.7 sccm.

Figures 7.34-7.37 shows comparison between simulation H_2/CO and experimental H_2/CO. The simulation H_2/CO increase with CH_4/CO_2, which is consistent with experimental H_2/CO. Higher temperature favors higher simulation H_2/CO from *Chemkin*®, but the experimental H_2/CO is more dependent on temperature than that of simulation. It is noticed that several experimental H_2/CO data points are above 1.0. The simulation H_2/CO could approach 1.0 due to higher CH_4/CO_2 or higher temperature, but it never reaches 1.0. Again, the Ni mechanism does NOT include carbon deposits, unlike the equilibrium calculation or the 3-rxn model. Without the chance for solid carbon, there is no pathway for $H_2/CO > 1$.

Chemkin® simulations were also conducted on the variable flow rate cases. Comparison of CH_4 and CO_2 conversions at CH_4/CO_2=1.0 between simulation and experiment are shown in Figures 7.38-7.40.

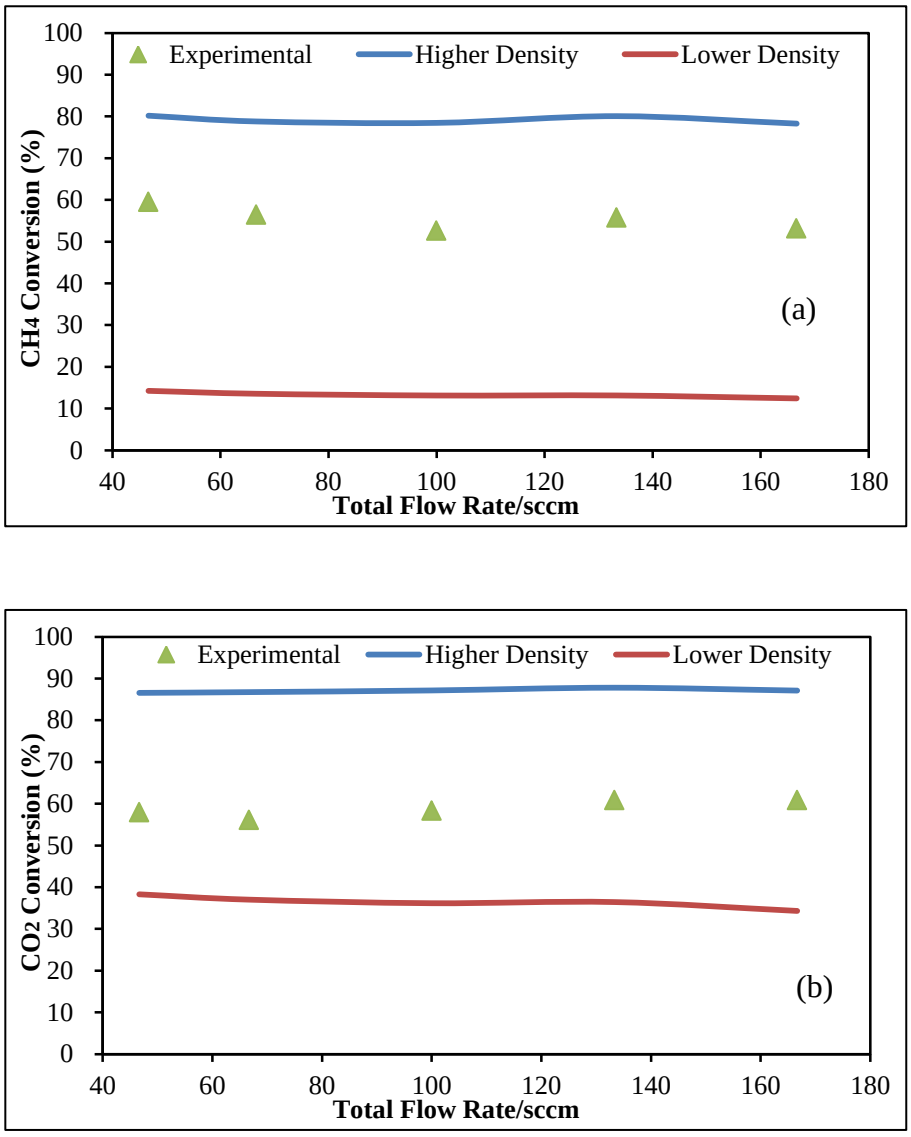

Figure 7.38 Comparison of *Chemkin*® simulation results and experimental results on (a) CH_4 conversions and (b) CO_2 conversions at 973 K and CH_4/CO_2=1.0.

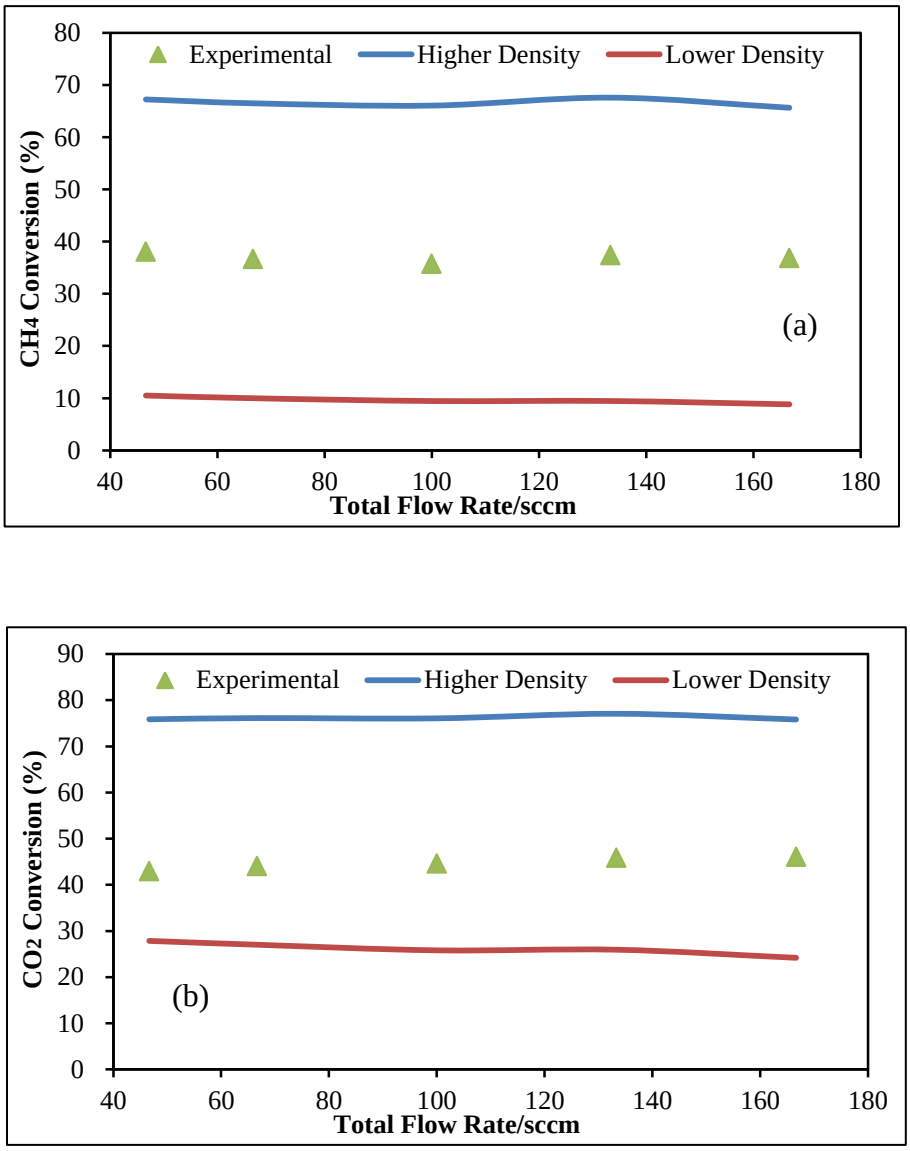

Figure 7.39 Comparison of *Chemkin*® simulation results and experimental results on (a) CH_4 conversions and (b) CO_2 conversions at 923 K and CH_4/CO_2=1.0.

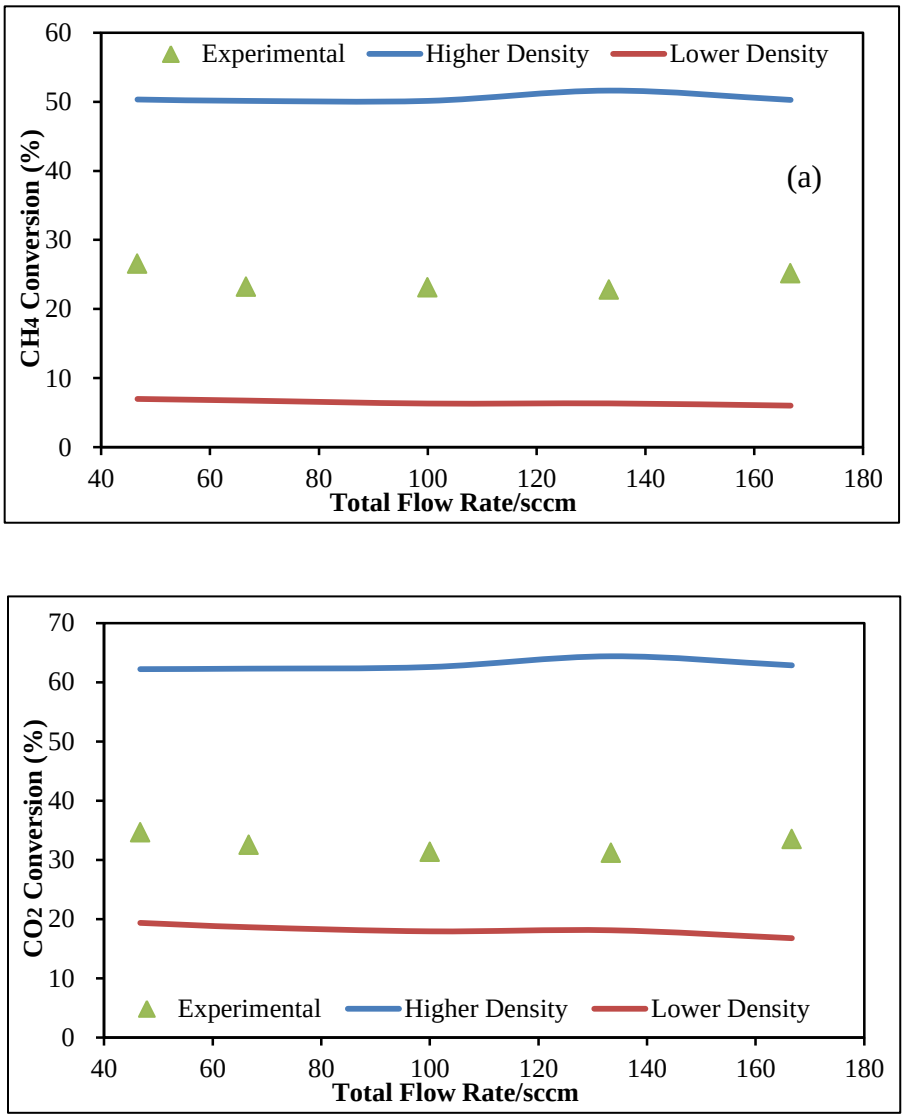

Figure 7.40 Comparison of *Chemkin*® simulation results and experimental results on (a) CH_4 conversions and (b) CO_2 conversions at 873 K and CH_4/CO_2=1.0.

According to Figures 7.39 and 7.40, the *Chemkin*® simulation conversions of CH_4 and CO_2 based on higher and lower active site density also bracket the experimental CH_4 and CO_2 conversions. The simulation CO_2 conversions are also higher than simulation CH_4 conversions with the feed CH_4/CO_2=1.0. At 973, 923, and

873 K, the simulation CH_4 and CO_2 conversions are almost constant with variable flow rates. The total flow rate has almost no effect on the simulation CH_4 and CO_2 conversions, which is similar to experimental CH_4 and CO_2 conversions.

The very similar trend of *Chemkin*® simulations curves and experimental curves strongly suggest that the mechanism of Ru/CNT catalyst is very similar to that of Ni-based catalyst. The different levels of those curves suggest that Ru/CNT has a higher activity than Ni-based catalyst.

7.7 Comparison of Pt/Pd-CNT and Ru/CNT

For the DR studies, 2.0 grams of each Pt/Pd-CNT/zeolite (Chapter 6) and Ru/CNT-zeolite (Chapter 7) were applied. The active site densities of the two kinds of catalysts are also similar: 6.4×10^{18} sites/gram (Pt/Pd/CNT) and $7.5\text{x}10^{18}$sites/gram (Ru/CNT). According to the analysis above, the two catalysts show similar coking tendencies, and similar influences from temperature and feed CH_4/CO_2 on reactants conversions and H_2/CO. The results from 3-reaction modeling and *Chemkin*® simulations are similar. Therefore, Pt/Pd-CNT/zeolite and Ru/CNT-zeolite likely have similar DR mechanisms.

A closer comparison between the results of the two catalysts, however, could reveal some different characteristics.

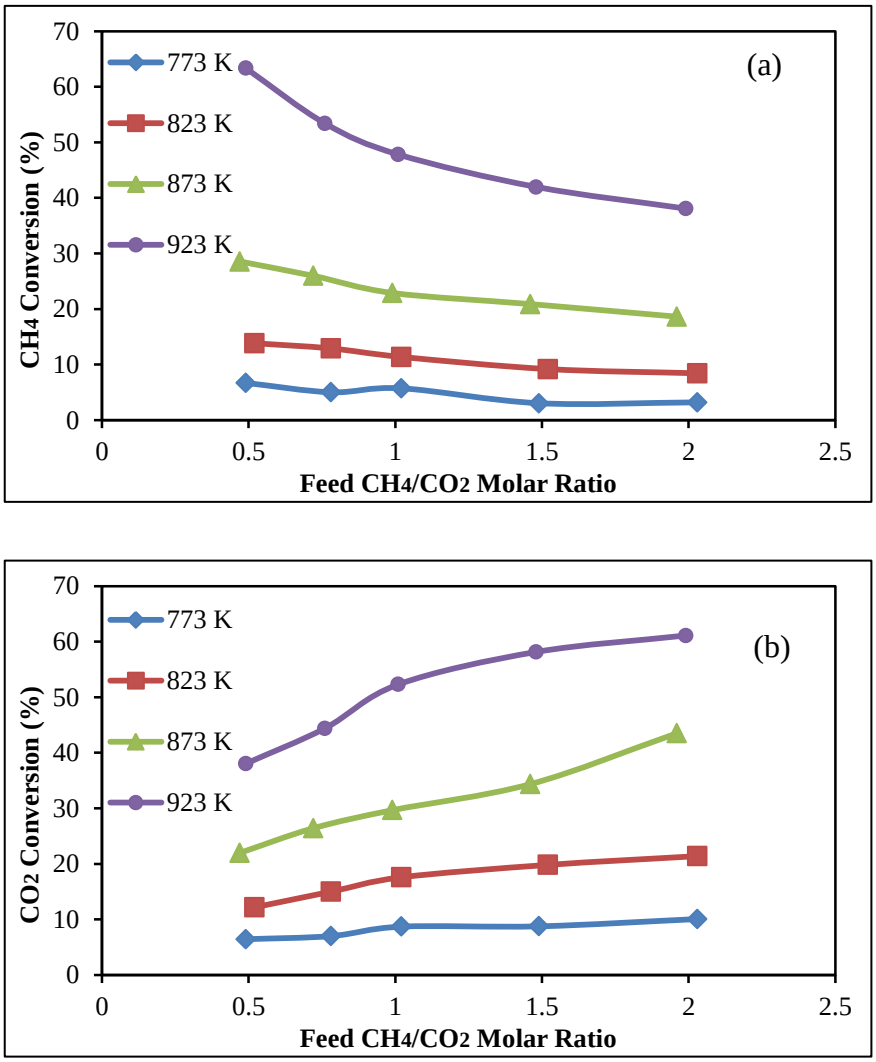

Figure 6.2 (a) CH_4 and (b) CO_2 conversion vs. feed molar ratio CH_4/CO_2 at each temperature.

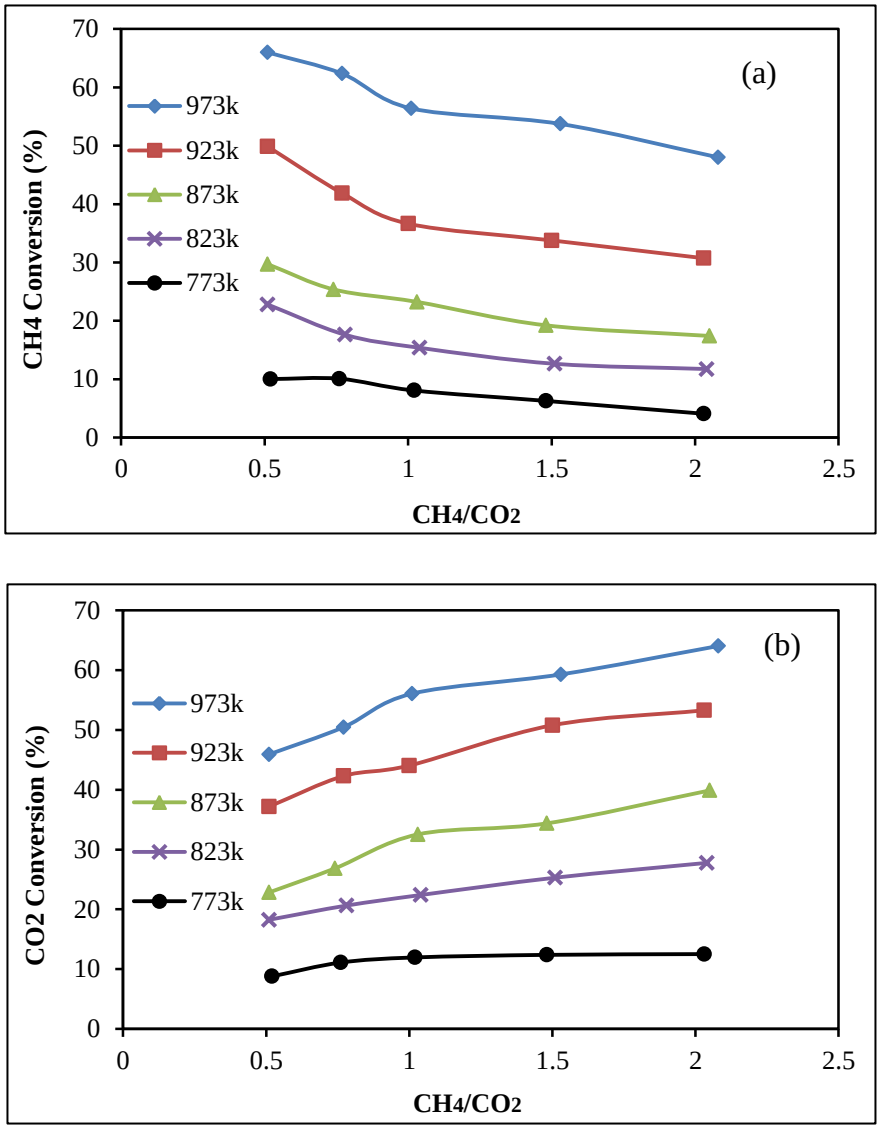

Figure 7.2 (a) CH_4 and (b) CO_2 conversion vs. feed molar ratio CH_4/CO_2 at each temperature.

Comparing Figures 6.2 and 7.2, both conversions of CH_4 and CO_2 from Pt/Pd-CNT/zeolite are higher than those from Ru/CNT-zeolite at 773 and 823 K. When 873 K, however, conversions of CH_4 and CO_2 from the two catalysts are about the same. Conversions of CH_4 and CO_2 from Pt/Pd-CNT/zeolite at 923 K are about same as those from Ru/CNT-zeolite at 973 K. Therefore, activity of Pt/Pd-CNT/zeolite is more temperature dependent than that of Ru/CNT-zeolite. Such conclusion coincides with the results from modeling: the Pt/Pd-CNT/zeolite activation energies on DR from the power law and 3-reaction model are both higher than those of Ru/CNT-zeolite.

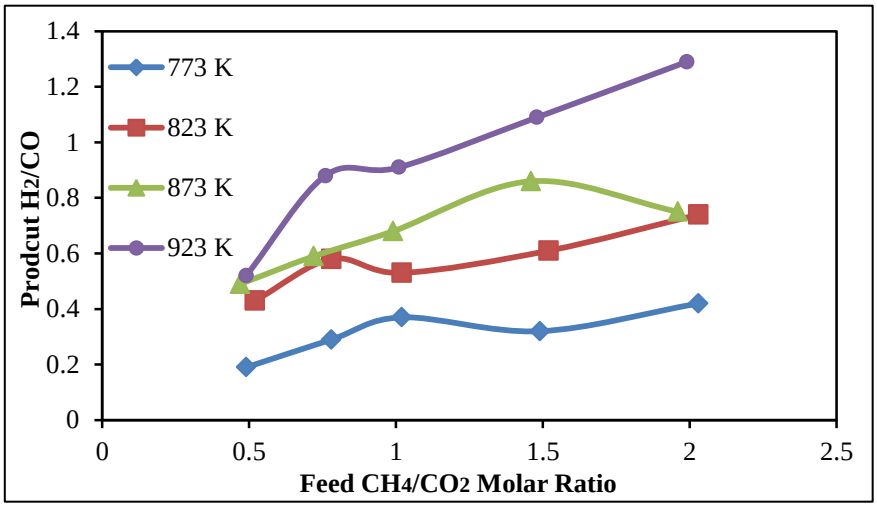

Figure 6.3 Product H_2/CO vs. feed molar ratio CH_4/CO_2 at each temperature.

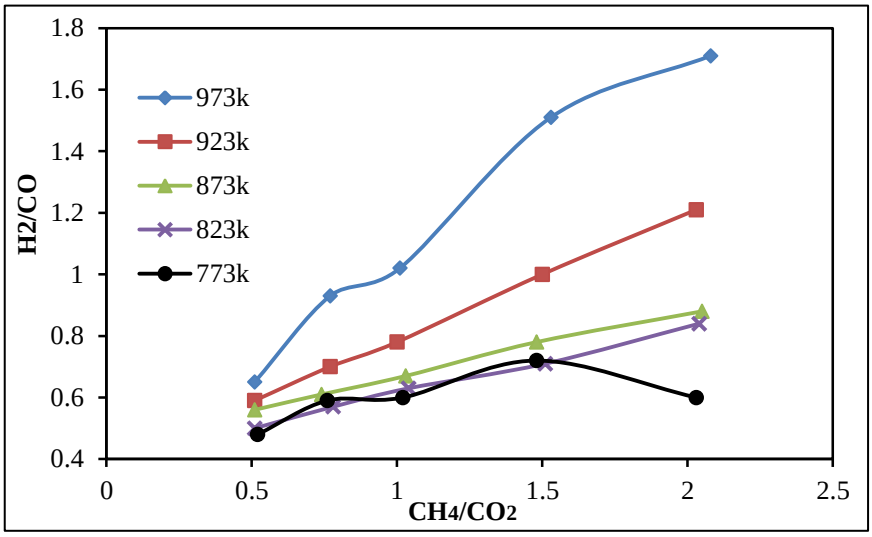

Figure 7.3 Product H_2/CO vs. feed molar ratio CH_4/CO_2 at each temperature.

Comparing Figures 6.3 and 7.3, within the temperature range 773- 823K, product H_2/CO from Pt/Pd-CNT/zeolite is lower than that from Ru/CNT-zeolite at 823 K. When 823 and 873 K, however, H_2/CO from Pt/Pd-CNT/zeolite is about same as that from Ru/CNT-zeolite. The H_2/CO from Pt/Pd-CNT/zeolite is higher than that from Ru/CNT-zeolite at 923 K. Therefore, product H_2/CO from Pt/Pd-CNT/zeolite is more temperature dependent than that from Ru/CNT-zeolite.

CHAPTER 8

DRY REFORMING OVER PT/PD-CNT W/O ZEOLITE

8.1 Objectives

Chapter 6 and 7 introduced DR over Pt/Pd-CNT/zeolite and Ru/CNT-zeolite. As was mentioned in Chapter 2, zeolite was mixed with the metal/CNT to increase the bulk volume to make for an easier upload. Therefore, blank tests were required to see if either the CNT and/or the zeolite contribute any intrinsic catalytic reactivity.

Blank tests were done over equivalent amounts of CNT/zeolite and pure zeolite under the DR conditions of this study. No CH_4 or CO_2 conversion was observed in either blank test. Finally, a group of tests over metal/CNT were run to rule out any impact of zeolite. In previous tests, 0.4 gram of Pt/Pd-CNT/zeolite mixed with 1.6 grams of zeolite, totaling 2.0 grams catalyst was uploaded into reactor. For this test, an amount 0.1 gram of fresh Pt/Pd-CNT was mixed with plain CNT, which could increase bulk volume, and uploaded into reactor. The total mass was 1.0 gram. Selected tests were run with same DR conditions of experiments done over Pt/Pd-CNT/zeolite.

8.2 Experimental Result and Discussion

Experiments over Pt/Pd-CNT were run with 66.7 sccm total inlet (85% He dilution) at 873 and 923 K. The feed conditions are shown in Table 8.1. Results are shown in Table 8.2.

Table 8.1 Pt/Pd-CNT Experiment Results

Temperature (K)	Inlet CH_4/CO_2	Inlet Mole Fractions (%)	
		CH_4	CO_2
923	1.05	7.45	7.12
923	2.00	9.75	4.88
873	1.04	7.38	7.12
873	2.00	9.76	4.89

According to Table 8.2, both CH_4 and CO_2 conversions increase with temperature. The CH_4 conversion declines with increasing inlet CH_4/CO_2, while CO_2 conversion increases with increasing inlet CH_4/CO_2. Product H_2/CO increases with temperature and inlet CH_4/CO_2. Such observations are consistent with those in Section 6.2 with Pt/Pd-CNT/zeolite. The 3-reaction model simulations, with kinetic parameters from Chapter 6 based on Pt/Pd-CNT/zeolite data, of these experiments were also made for the Pt/Pd-CNT runs. These results are also shown in Table 8.2.

Table 8.2 Experimental and 3-Reaction Model Simulation Results

Temperature (K)	Inlet CH_4/CO_2	Experimental Results			3-Reaction Model Results		
		X_A (%)	X_B (%)	H_2/CO	X_A (%)	X_B (%)	H_2/CO
923	1.05	4.46	8.00	0.34	4.15	7.28	0.42
923	2.00	3.49	11.07	0.51	3.32	8.38	0.71
873	1.04	2.87	5.45	0.28	1.63	3.23	0.31
873	2.00	2.46	8.18	0.42	1.24	3.72	0.54

Figure 8.1-8.3 shows the comparison of data in Table 8.2.

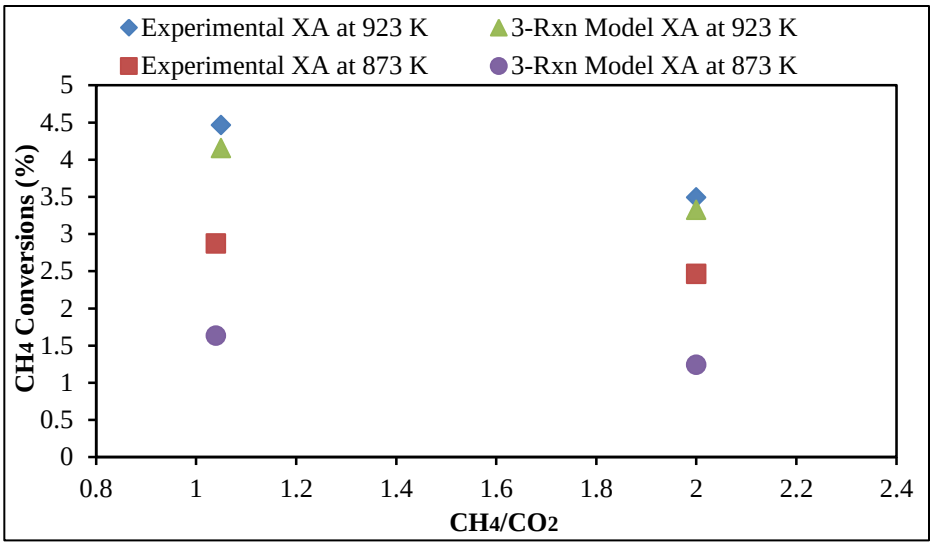

Figure 8.1 Comparison of Experimental and Model CH_4 Conversions at 923 and 873 K.

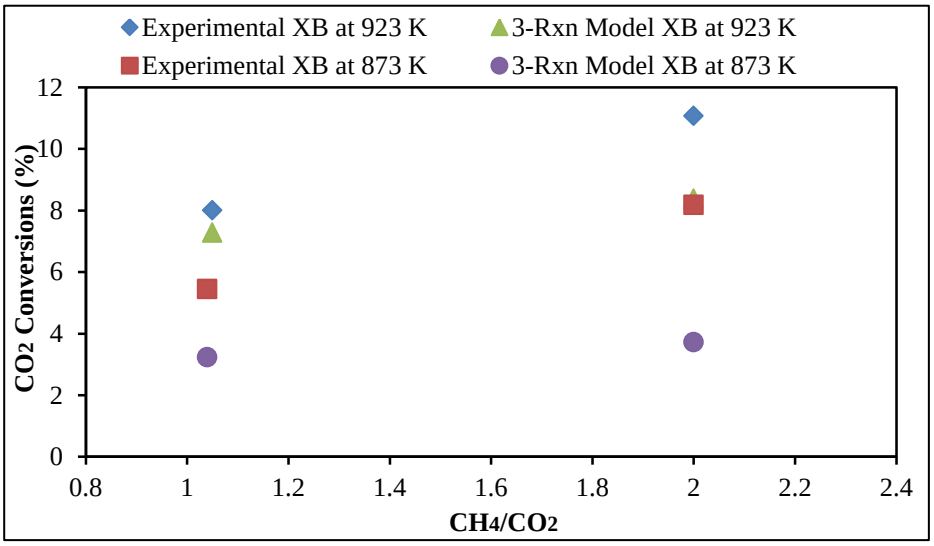

Figure 8.2 Comparison of Experimental and Model CO_2 Conversions at 923 and 873 K.

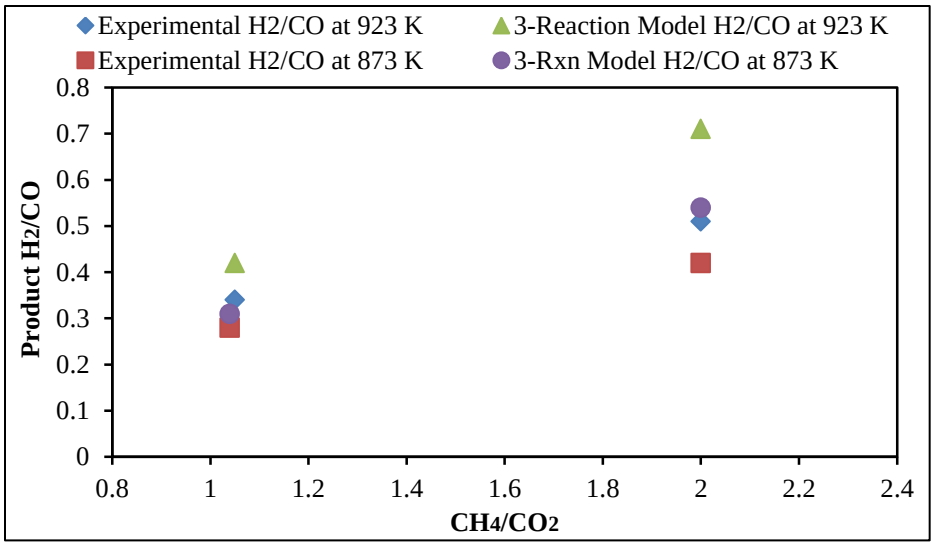

Figure 8.3 Comparison of Experimental and Model H_2/CO at 923 and 873K.

According to Figures 8.1-8.3, we could find that the experiment results are similar to the simulation results. The conversions X_A and X_B from Pt/Pd-CNT are a little higher than those from 3-reaction model simulations. The experimental H_2/CO from Pt/Pd-CNT is a little lower than those from 3-reaction model simulations. Therefore, the activity of Pt/Pd-CNT is a little higher than that of Pt/Pd-CNT/zeolite; the Pt/Pd-CNT/zeolite has a higher CH_4 decomposition tendency, which leads to a higher product H_2/CO. The impact of zeolite exists, but not big.

CHAPTER 9

REVERSE WATER GAS SHIFT OVER PT/PD-CNT/ZEOLITE

9.1 Observed Carbon Balance

The overall reverse water gas shift (RWGS) reaction stoichiometry is shown in Equation 1.4. The carbon atoms from CO_2 should convert to CO, so the CO moles should be close to the moles of converted CO_2. Such a carbon balance is a good test of the experimental method, as well as a test for any possible carbon deposits on the catalyst. Figure 9.1 shows compares the feed carbon and outlet carbon for all RWGS runs in as a parity graphic.

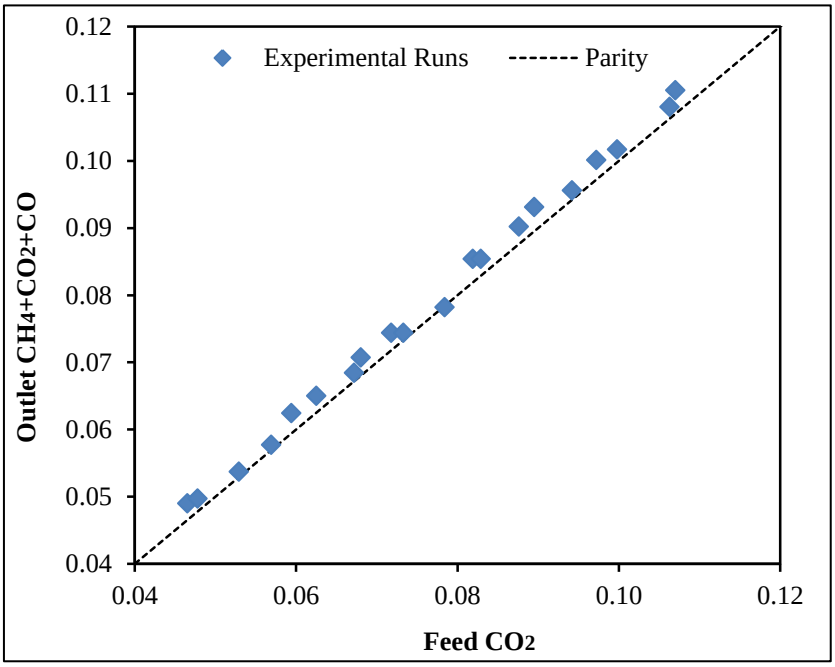

Figure 9.1 Carbon balance for all runs over Pt/Pd-CNT/zeolite.

In Figure 9.1 all markers are at or above the parity line. Since feed rates and reactor effluent analyses are calibrated this result suggests that additional carbon is

releasing into the flow during the RWGS reaction. These RWGS experiments were done with Pt/Pd-CNT/zeolite spent DR catalyst. It is hypothesized that, the deposited carbon reacted with the H_2 or CO_2. This effect will be considered in the multiple reaction model.

9.2 Hydrogen and Carbon Dioxide Conversion

To calculate H_2 conversions (X_A), we have:

$$X_A = \frac{\text{Moles of Converted } H_2}{\text{Moles of Feed } H_2} \tag{9.1}$$

Since there is a negligible change of total moles in current system as the feed is highly diluted by He, then Equation 9.1 reduces to:

$$X_A = \frac{\text{Feed } H_2 \text{ Mole Fraction} - \text{Outlet } H_2 \text{ Mole Fraction}}{\text{Feed } H_2 \text{ Mole Fraction}} \tag{9.2}$$

Equation 9.2 is used to calculate conversions H_2 for all cases in this chapter.

Similarly, CO_2 conversions (X_B) can be calculated by:

$$X_B = \frac{\text{Feed } CO_2 \text{ Mole Fraction} - \text{Outlet } CO_2 \text{ Mole Fraction}}{\text{Feed } CO_2 \text{ Mole Fraction}} \tag{9.3}$$

Equation 9.3 is used to calculate conversions CO_2 for all cases in this chapter.

9.2.1 Influence of Feed Molar Ratio

Experiments were run at 773, 823, 873 and 923 K. Reactor pressure was kept at 30 psig. The total flow rate was set at 66.7 sccm, with the flow rate of He of 56.7 sccm (85% diluent). Based on the volume of the catalyst bed, the gas hourly space velocity (GHSV) was 2000 ml/(g_{cat} hr). All calculated H_2 and CO_2 conversions are shown as X_A, X_B vs. feed molar ratio CO_2/H_2 plots at each temperature.

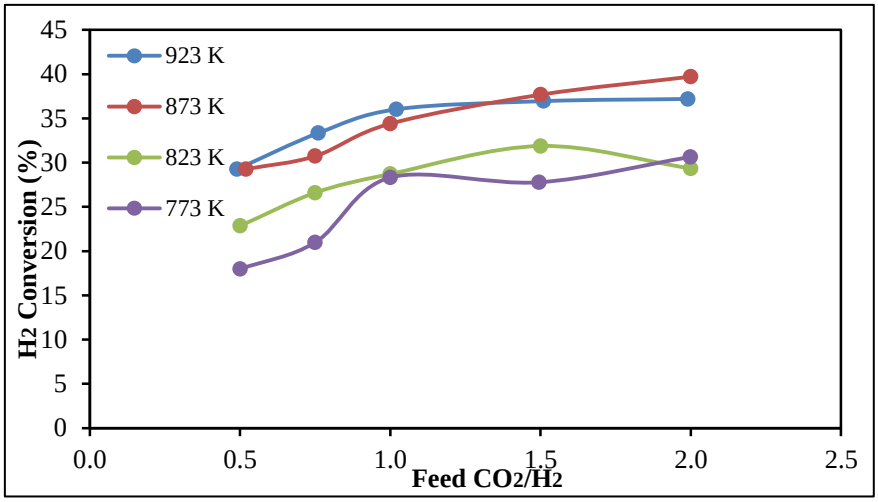

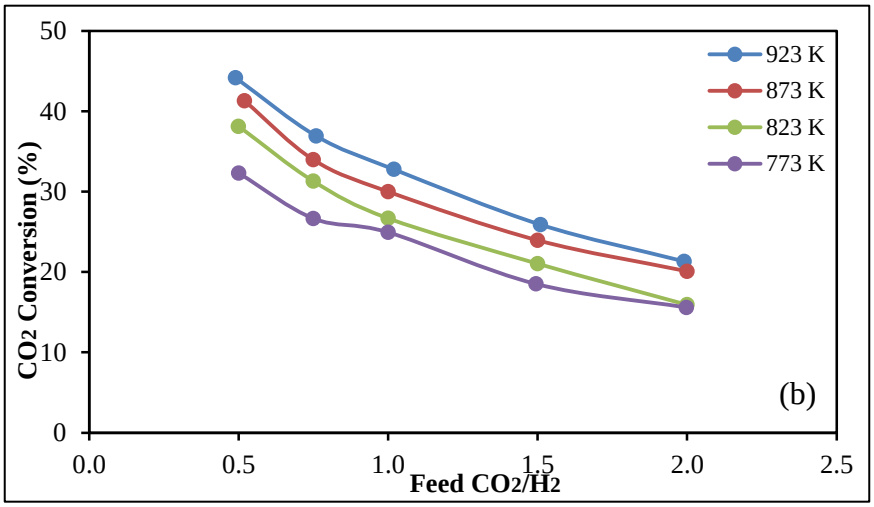

Figure 9.2 (a) H_2 and (b) CO_2 conversion vs. feed molar ratio CO_2/H_2 at each temperature.

Figure 9.2 shows the different H_2 and CO_2 conversions at various molar ratios CO_2/H_2 under each temperature. The lines connecting the markers are shown only for the sake of clarity. The molar ratio CO_2/H_2 has a significant influence on both conversions. The H_2 conversion increases with increasing molar ratio CO_2/H_2, while the CO_2 conversion declines with increasing feed molar ratio.

9.2.2 Influence of Temperature

To investigate the influence of reaction temperature, the constant flow experimental results are shown in same feed molar ratio of CO_2/H_2.

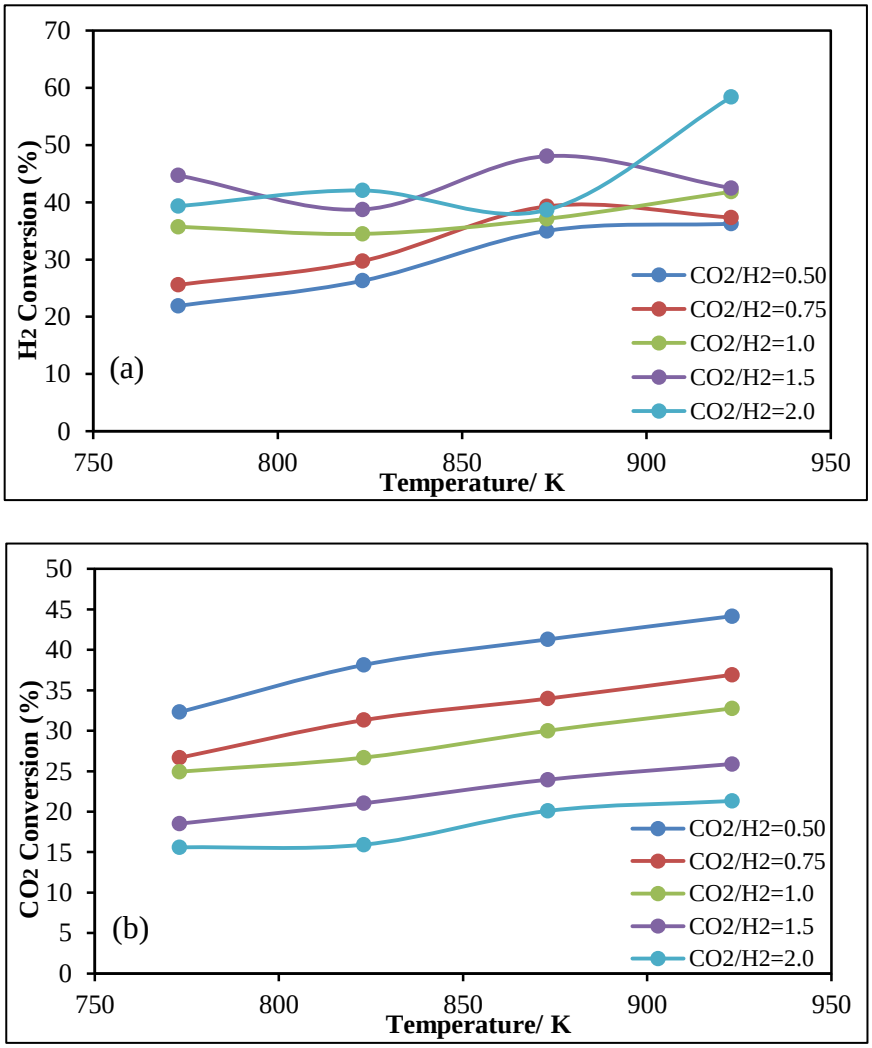

Figure 9.3 (a) H_2 and (b) CO_2 conversion vs. temperature at each feed molar ratio CO_2/H_2.

From Figure 9.3, both H_2 and CO_2 conversions somewhat increase within the temperature range 773 to 923 K. Comparing to the results of DR, conversions of reactants in RWGS has a lower temperature dependence.

9.3 Equilibrium Calculation

As with the analysis for DR, equilibrium calculations for RWGS runs were also performed by *Chemkin* ® with the same procedures. All equilibrium results are listed in Appendix Q

9.3.1 Equilibrium vs. Experimental Values

The experimental and equilibrium conversions of the highest (2.0) and lowest (0.5) feed CO_2/H_2 ratio cases, at constant GHSV = 2 L/h-g_{cat}, with all temperatures are shown in Figure 9.4. All conversions are simply based on inlet and outlet mole fractions. Both H_2 and CO_2 equilibrium conversions exceed observed values. The H_2 equilibrium conversions are higher than those of CO_2 and declining with increasing temperature. The CO_2 conversions are almost independent with temperature. The experimental CO_2 conversions are quite close to equilibrium values for feed ratio CO_2/H_2=2.0. Trends for the other feed ratios tested are similar and fall in between the 0.5 and 2.0 curves.

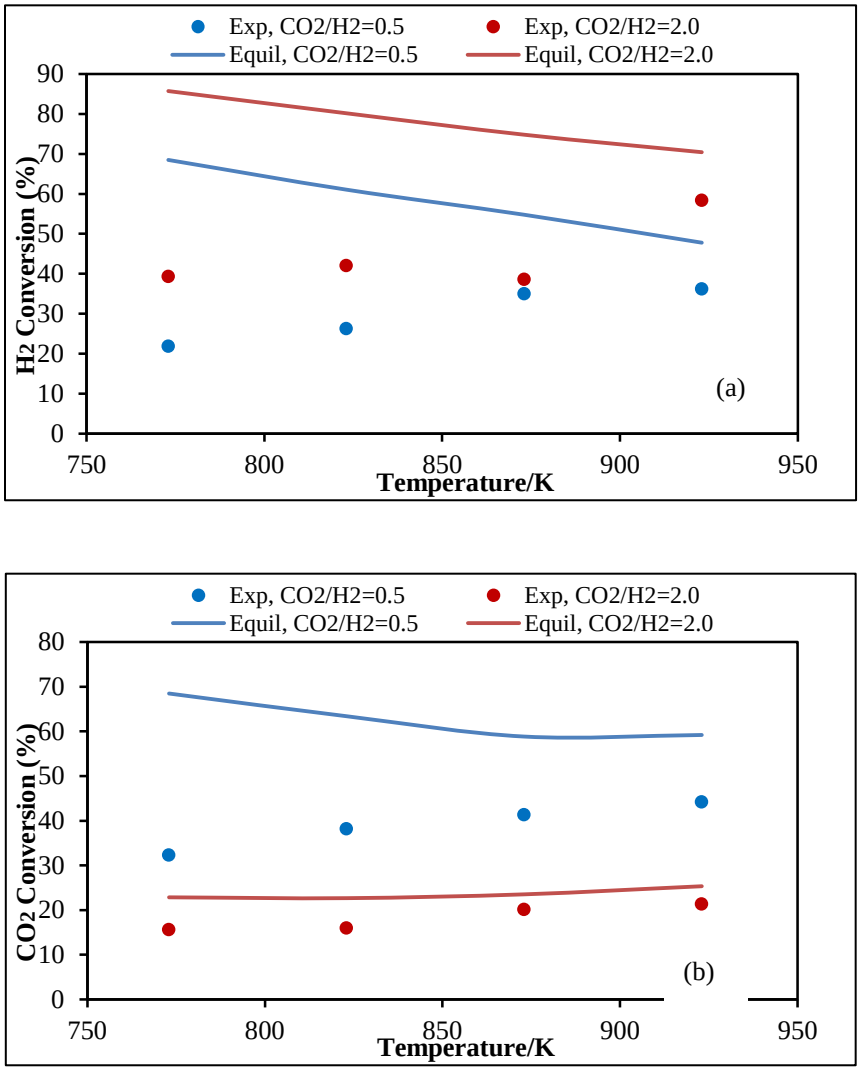

Figure 9.4 Comparison of equilibrium and experimental conversions of (a) H_2 and (b) CO_2 at GHSV = 2 L/h-g_{cat}; feed CO_2/H_2 = 0.5 and 2.0.

The experimental and equilibrium conversions of highest (923 K) and lowest (773 K) temperature, GHSV = 2 L/h-g_{cat}, with all feed CO_2/H_2 are shown in Figure 9.5. The equilibrium conversions exceeded observed values. The H_2 equilibrium conversions gradually increase with CO_2/H_2, while CO_2 equilibrium conversions decrease with CO_2/H_2. The experimental and equilibrium conversions get close together

at higher temperatures. Trends for the other temperatures tested are similar and fall in between the high and low values.

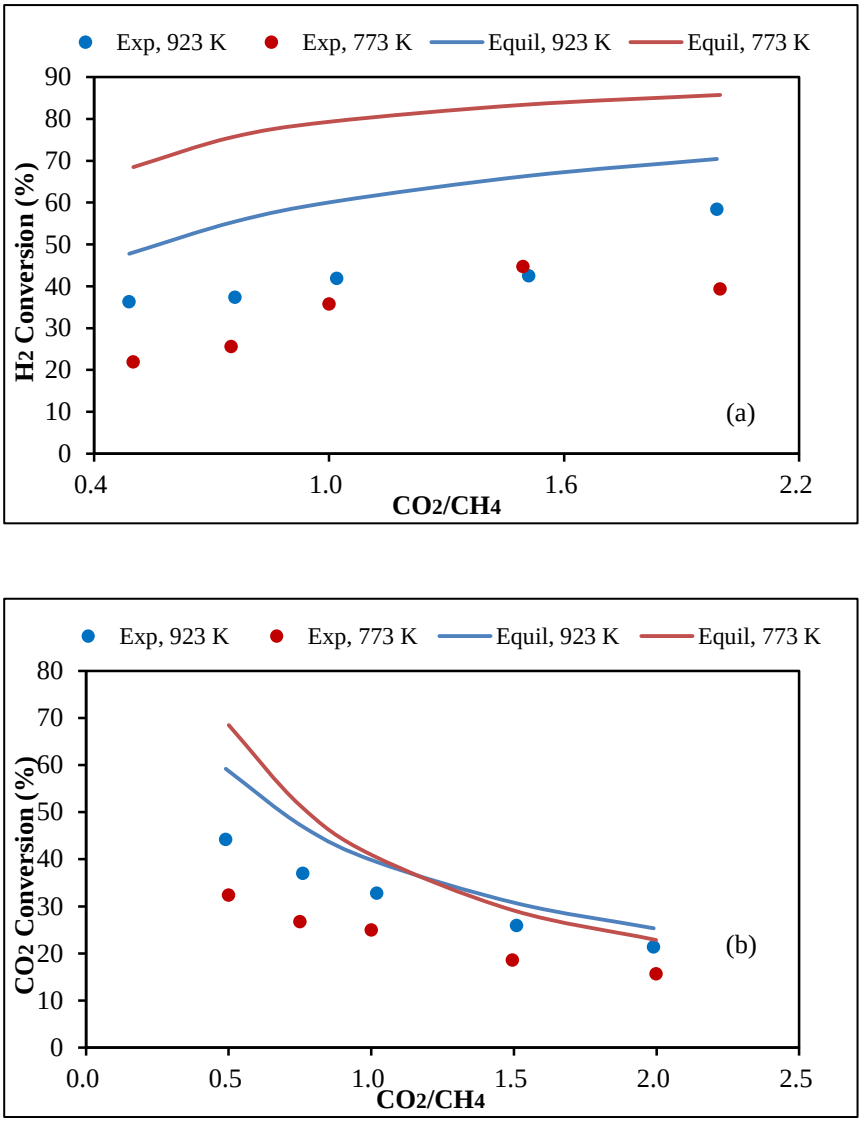

Figure 9.5. Comparison of equilibrium and experimental conversions of (a) H_2 and (b) CO_2 at GHSV = 2 L/h-g_{cat}; temperature=773 and 923 K.

9.4 Power Law Model

As was done for the DR analysis, a simple power law model is applied for RWGS due to its decent accuracy and simplicity for comparing the behavior of different catalysts.

9.4.1 Model Selection and Derivation

The data in Section 9.2 show that the H_2 and CO_2 conversions are sufficiently high (> 10%) that a simple differential reactor model is not appropriate. Rather, an integral packed bed reactor (PBR) model is used. It begins with:

$$r_A' = \frac{dF_A}{dW} \tag{9.2}$$

where A is H_2, r_A' is the molar reaction rate (based on catalyst mass), W is mass of catalyst, and $F_A$is H_2 molar flow rate.

The global reaction can be written as:

$$H_2 + bCO_2 \rightarrow cCO + dH_2O + eCH_4 \tag{9.3}$$

where A is assigned to H_2, and B is assigned to CO_2. CH_4 is included in this stoichiometry because CH_4 was experimentally observed during the RWGS experiments.

A global reaction rate form, the power law model, is assumed:

$$r_A' = kC_A^{\alpha}C_B^{\beta} \tag{9.4}$$

where k is the rate constant, and C_j are molar gas-phase concentrations and orders α and β are to be determined. The immediate objective is to derive F_A (molar flow rate of A), C_A, and C_B in terms of mole fraction y_A, the mole fraction of H_2.

The derivation is applied for this process, which is very similar to Section 6.4.1. After derivation, the final form of the H_2 conversion model is Equation 9.5:

$$\frac{dX_A}{dW} = \frac{k}{F_{A0}}\left(\frac{Py_{A0}}{RT}\right)^{\alpha+\beta}(1-X_A)^{\alpha}\left(\frac{y_{B0}}{by_{A0}} - X_A\right)^{\beta} b^{\beta} \tag{9.5}$$

The quantities W, F_{T0}, P, T, y_A, and y_0 are all known. The parameters k, α and β

are all unknown. As in Section 6.4, the CO_2 conversion is determined by:

$$X_B = \frac{bX_A y_{A0}}{y_{B0}} \tag{9.6}$$

The value of b could be determined by:

$$\text{b} = \frac{\text{Moles of Converted } CO_2}{\text{Moles of Converted } H_2} \tag{9.7}$$

Since there is a negligible change of total moles in current system as the feed is highly diluted by He, then Equation 9.7 reduces to:

$$\text{b} = \frac{\text{Feed } CO_2 \text{Mole Fraction} - \text{Outlet } CO_2 \text{Mole Fraction}}{\text{Feed } H_2 \text{ Mole Fraction} - \text{Outlet } H_2 \text{ Mole Fraction}} \tag{9.8}$$

Equation 9.8 is used to calculate the value of b for all cases in this study. The approach will be to numerically integrate Equation 9.5 with assumed values of k, α and β for a given run by Polymath. The calculated X_B is also output-based using Equation 9.6. The calculated X_A and X_B from Polymath are compared to the experimental X_A and X_B. If they do not match well, the assumed values of k, α and β are altered, until good fits for both X_A and X_B are found. This procedure is repeated over all the experimental runs. The Polymath code is listed in Appendix R.

9.4.2 Model Testing

The testing process is same as was done during DR modeling. Equation 9.5 is integrated with the reaction conditions of the Pt/Pd-CNT RWGS experiments. The "best fit" orders α and β of the reaction rate are both determined as 1. Values of k are also determined for each temperature. The *Polymath*® code at 873 K is listed in Appendix R as example. Comparisons between experimental conversions and model conversions for all temperatures are shown as Figures 9.6-9.9. The model lines might not appear "smooth" since the evaluations at each condition used actual values.

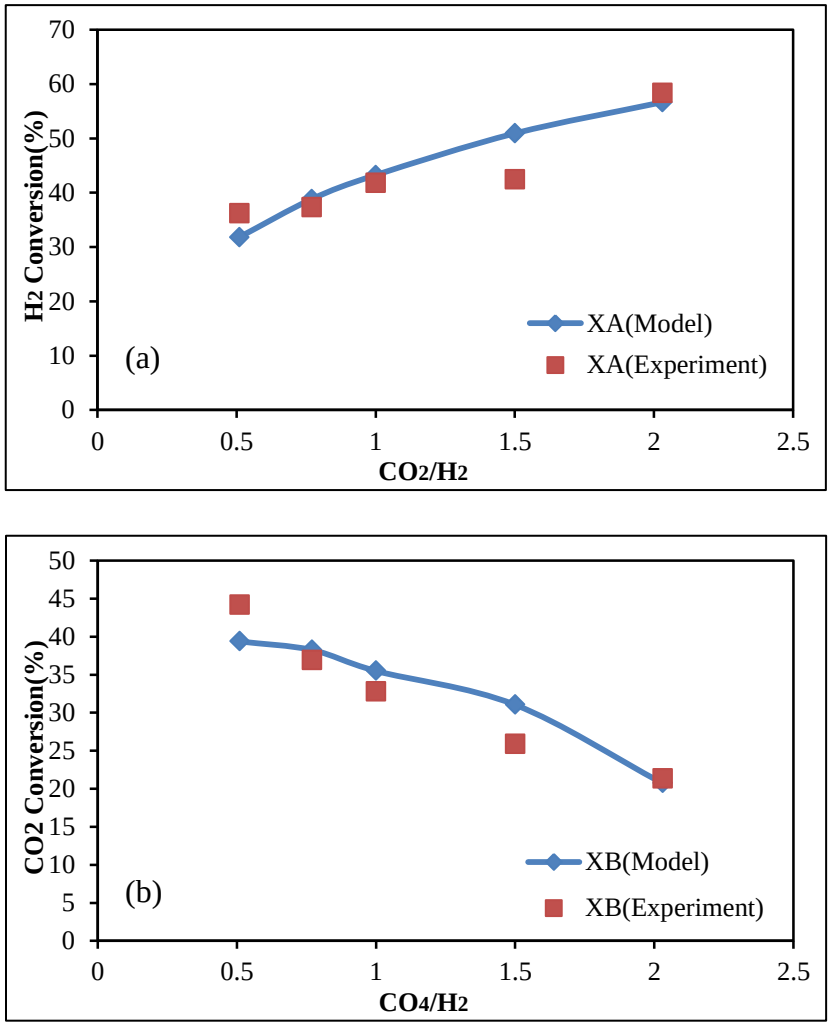

Figure 9.6 Model conversions vs. experimental conversions: (a) H_2 (b) CO_2 at 923K.

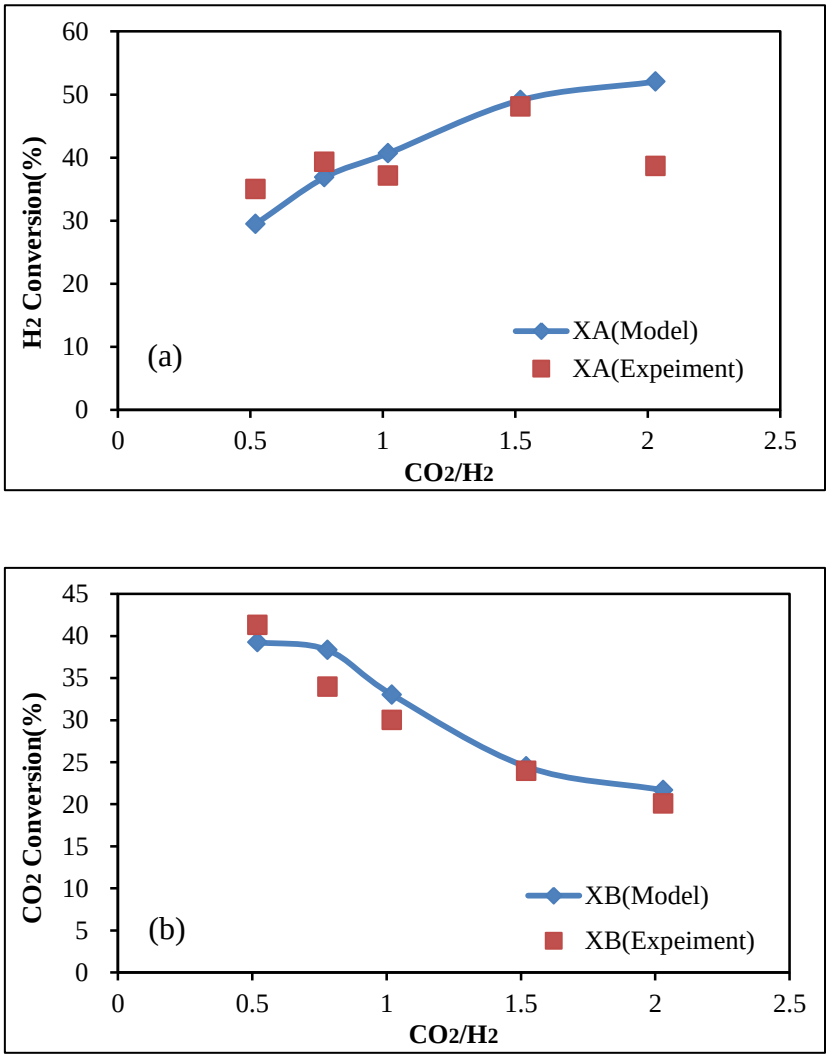

Figure 9.7 Model conversions vs. experimental conversions: (a) CH_4 (b) CO_2 at 873K.

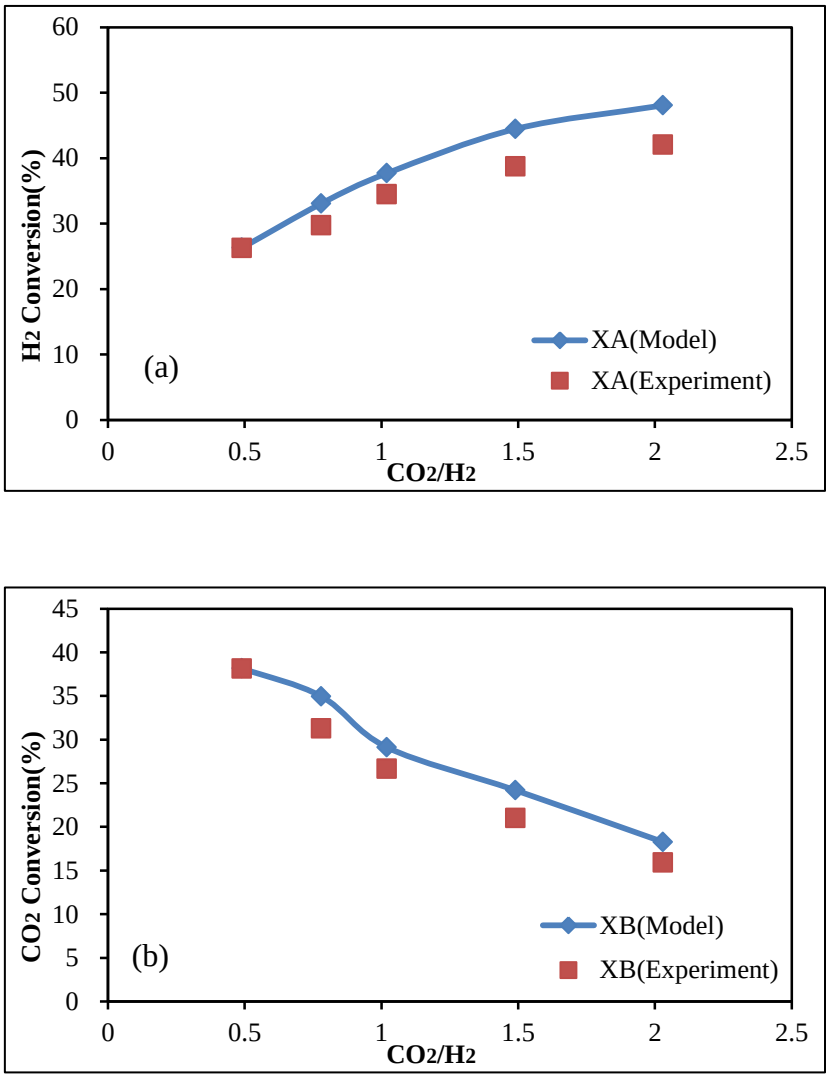

Figure 9.8 Model conversions vs. experimental conversions: (a) CH_4 (b) CO_2 at 823K.

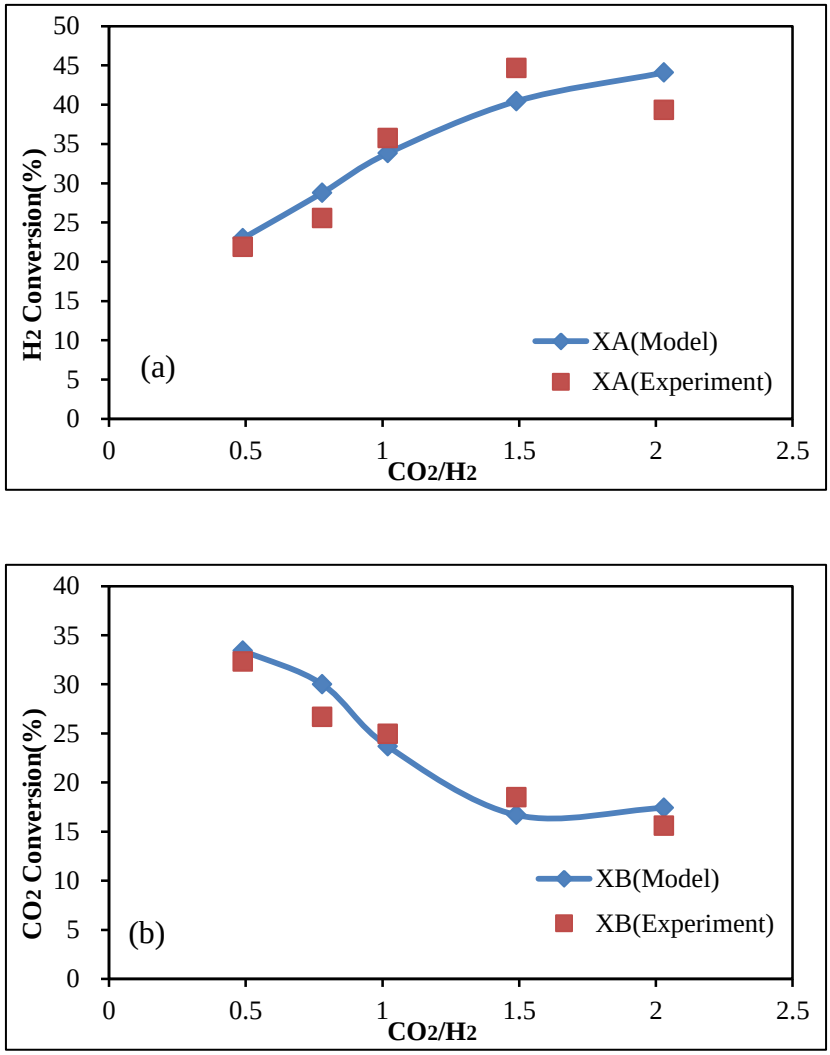

Figure 9.9 Model conversions vs. experimental conversions: (a) CH_4 (b) CO_2 at 773K.

Figures 9.6-9.9 show a generally good fit between power law model-simulated conversions and experimental conversions assuming both α and β are 1. The trial-and-error process yields estimates of k at each temperature such that predicted X_A and X_B values are similar to observed X_A and X_B values for each molar ratio of CH_4/CO_2. In the next section, the dependence of the k values is examined as a function of temperature.

9.4.3 Arrhenius Plot

The "best fit" k values described in the previous section are presented in Table 9.1.

Table 9.1 Arrhenius Plot Data

k [m^6/ (s ƙg mol)]	T (K)	lnk	1/T
6.00×10^{-5}	773	-9.72117	0.001294
7.67×10^{-5}	823	-9.47604	0.001215
1.13×10^{-4}	873	-9.08518	0.001145
1.50×10^{-4}	923	-8.80488	0.001083

Based on the data in Table 9.1, an Arrhenius-type plot is made, shown as Figure 9.10.

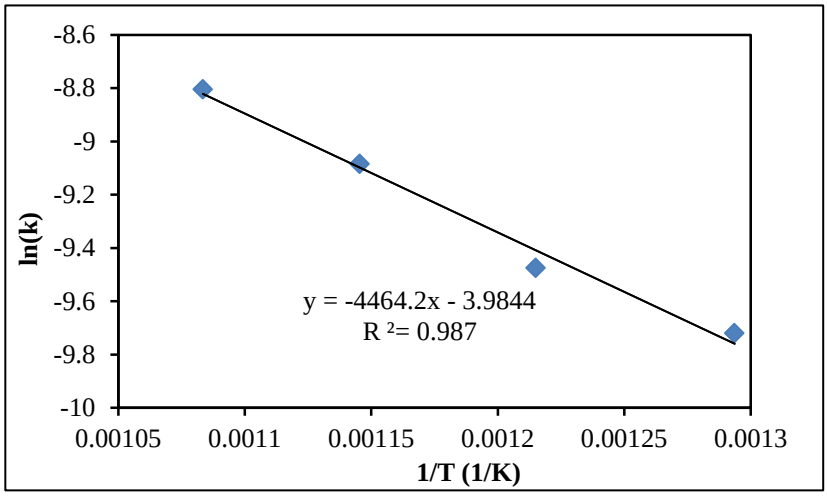

Figure 9.10 Arrhenius plot of "best fit" empirical, global rate constant k.

Figure 9.10 presents an excellent linear relationship between ln(k) and 1/T. Therefore, the Arrhenius equation is: $k = 1.86 \times 10^{-2} e^{\frac{-3.7 \times 10^4}{RT}}$ (m^6 /moles s ƙg catalyst).

9.5 Multiple Reaction Model

For an ideal RWGS reaction, the product should be CO and H_2O. The RWGS experiments, however, show the generation of CH_4. The parity plot in Section 9.1 suggests that carbon might be releasing from the catalyst. Therefore, a multiple reaction model is employed to offer an explanation.

9.5.1 Candidate Reactions to Consider

The choice of RWGS (Equation 1.1) is clear. As is discussed in Section 9.1, existing (i.e. from old DR experiments) deposited carbon reacted with H_2 or CO_2:

$$C + 2H_2 \rightarrow CH_4 \quad \Delta H_{298K} = -86.3 kJ/mol \tag{9.1}$$

$$C + CO_2 \rightarrow 2CO \quad \Delta H_{298K} = 159.9 kJ/mol \tag{9.2}$$

The experimental data in Appendix Table Q.1 show that the higher the temperature, the more the carbon in the outlet than inlet. So an endothermic reaction should be considered. In addition, the difference between inlet and out carbon increases with CO_2/H_2. Therefore, Equation 9.2 is selected. The typical side reactions of RWGS Equation 1.7 and 1.8 are also considered, as production of CH_4 increases with H_2 inlet.

Table 9.2 Potential Candidate Reactions

Set I	Set II
$CO_2 + H_2 = CO + H_2O$	$CO_2 + H_2 = CO + H_2O$
$C + CO_2 \rightarrow 2CO$	$C + CO_2 \rightarrow 2CO$
$3H_2 + CO \rightarrow CH_4 + H_2O$	$4H_2 + CO_2 \rightarrow CH_4 + 2H_2O$

Two groups of simulation were done based on Reaction Set I, includes Equation 1.1, 9.2, and 1.7, and Reaction Set II, includes Equation 1.1, 9.2 and 1.8. Set I did not give a good fit on all species, while reasonable agreement was observed with Set II. Therefore, Equation 1.8 should be included. Reaction Set 2 is presented in Table 9.3.

Table 9.3 Reactions in Multiple Reaction Model, where $k_{fi} = A_i exp[-E_i/(RT)]$

Reaction	*Rate Expression* r_i	*Approach to Equil.* η_i
Reverse Water Gas Shift $CO_2 + H_2 = CO + H_2O$	$r_1 = k_{f1}P_{H2}P_{CO2}(1-\eta_1)$	$\eta_1 = \frac{P_{CO}P_{H2O}}{P_{H2}P_{CO2}K_{p1}}$
Reverse Boudouard $C + CO_2 \rightarrow 2CO$	$r_2 = k_{f2}P_{CO2}(1-\eta_2)$	$\eta_2 = \frac{P^2{}_{CO}}{P_{CO2}K_{p2}}$
Sabatier reaction $4H_2 + CO_2 \rightarrow CH_4 + 2H_2O$	$r_3 = k_{f3}P_{H2}(1-\eta_3)$	$\eta_3 = \frac{P_{CH4}P^2_{H2O}}{P^4{}_{H2}P_{CO2}K_{p3}}$

The equilibrium constants K_{pi} in Table 9.3, as functions of temperature, are obtained from same calculator as used in Section 6.5. The kinetic parameters A_i and E_i are determined from analysis of the experimental data. For Reaction 1, the first order dependence on CO_2 is consistent with DR modeling. However, the regression analysis done in this study on the data of RWGS yielded generally better results with a first order dependence also on H_2. The experimental results in Appendix Table Q.1 show that the CH_4 production declines with CO_2/H_2, which inspires the first order dependence on H_2 and zero order dependence on CO_2 in Reaction 3.

9.5.2 Programing for Reaction Rate Constants

The RWGS experiments in the current study were simulated with a packed bed reactor (PBR) model as described in Table 9.4. The goal of the simulation was to obtain Arrhenius parameter pairs (A_i, E_i) by determination of k_{fi} for the reactions in Table 9.3.

The species balances were integrated with an original *Matlab*® program. All available experimental mole fraction and flow rate data at a given temperature were supplied to the program. As was done in Chapter 5, the integration was repeated within a regression loop that optimized the three rate constants k_{fi} at that temperature.

Table 9.4 Key Equations of PBR Simulation of 3-Reaction Global Model

PBR Balances Species j	*Net Rates r_j*	*Mole Fractions y_j*	*Partial Pressures*
$dF_j/dW = r_j$ At W = 0, F_{jo} = value	$r_{H2} = -r_1 - 3r_3$ $r_{CO2} = -r_1 - r_2$ $r_{CO} = r_1 + 2r_2 - r_3$ $r_{H2O} = r_1 + r_3$ $r_{CH4} = r_3$	$y_j = \frac{F_j}{\sum_j F_j}$ Total molar rate includes inert gas	$P_j = y_j P$ P = total pressure

The *Matlab*® program code for solving values of k_{fi} at 923 K is selected as example and shown in Appendix S. Similar *Matlab*® program codes were also applied for 773, 823, and 873 K, for both the constant and variable flow cases. All k_{fi} values for each temperature were determined based on this algorithm.

9.5.3 Arrhenius Plots

Completion of the integration / regression routine at each temperature yielded a rate constant k_{fi}, which are listed in Table 9.5, for each of the three global reactions.

Table 9.5 Rate Constant k_{fi} for 3-Global Reactions

T/K	1/T	k_1	$\ln k_1$	k_2	$\ln k_2$	k_3	$\ln k_3$
773	0.001294	0.045	-3.10109	0.0007	-7.26443	0.0003	-8.11173
823	0.001215	0.052	-2.95651	0.0009	-7.01312	0.0005	-7.6009
873	0.001145	0.06	-2.81341	0.0012	-6.72543	0.001	-6.90776
923	0.001083	0.071	-2.64508	0.0015	-6.50229	0.0019	-6.2659

Figure 9.11 presents the Arrhenius plots of the global rate constants k_i with reaction temperatures based on Table 9.5. The Arrhenius fits are quite linear over the temperature range (773-923 K).

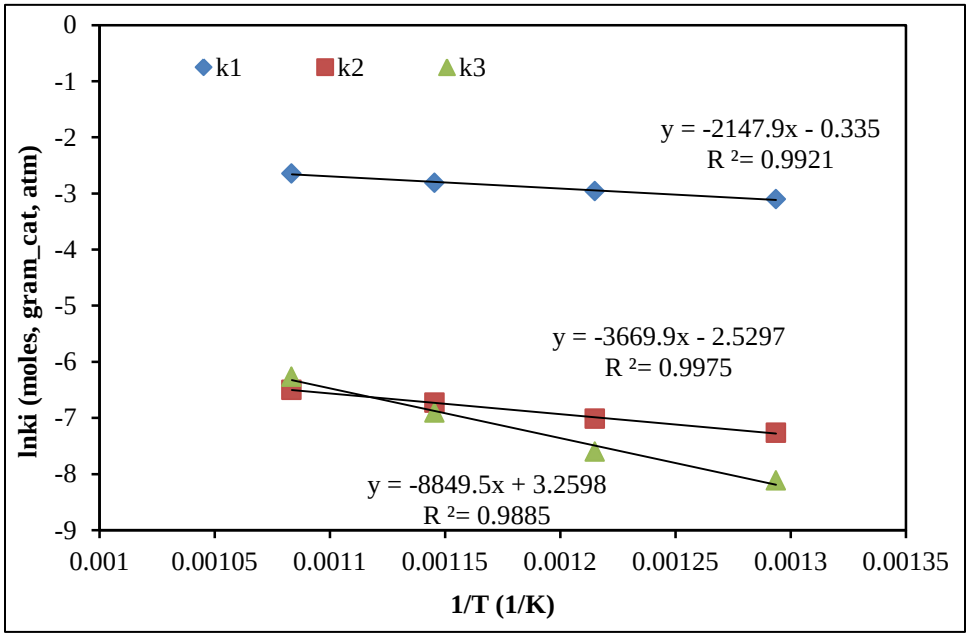

Figure 9.11. Arrhenius plots of forward rate constants k_{fi}.

Based on Figure 9.11, Arrhenius parameters are presented in Table 9.6. The Sabatier reaction (r_3) has the largest barrier among the three reactions.

Table 9.6 Arrhenius Parameters

Reaction i	*Parameter A_i (mole, hr, g_cat, atm)*	*Parameter E_i (cal/mole)*
1	7.153E-1	4268
2	7.968E-2	7292
3	2.604E1	17584

9.5.4 Model Testing

With Arrhenius parameters obtained, the 3-reaction set was tested against the experimental RWGS data. The PBR simulation based on Table 9.4 was evaluated in *Polymath*®. A typical *Polymath* code, at 923 K, is shown in Appendix T.

Similar *Polymath*® codes are also applied for 873, 823, and 773 K. Then the molar flow rates of all species determined from *Polymath*® are converted into concentrations. All results are listed in Appendix Q. For constant flow runs, outlet concentrations of all species from the 3-reaction model and experiments are compared in Figures 9.12-9.15.

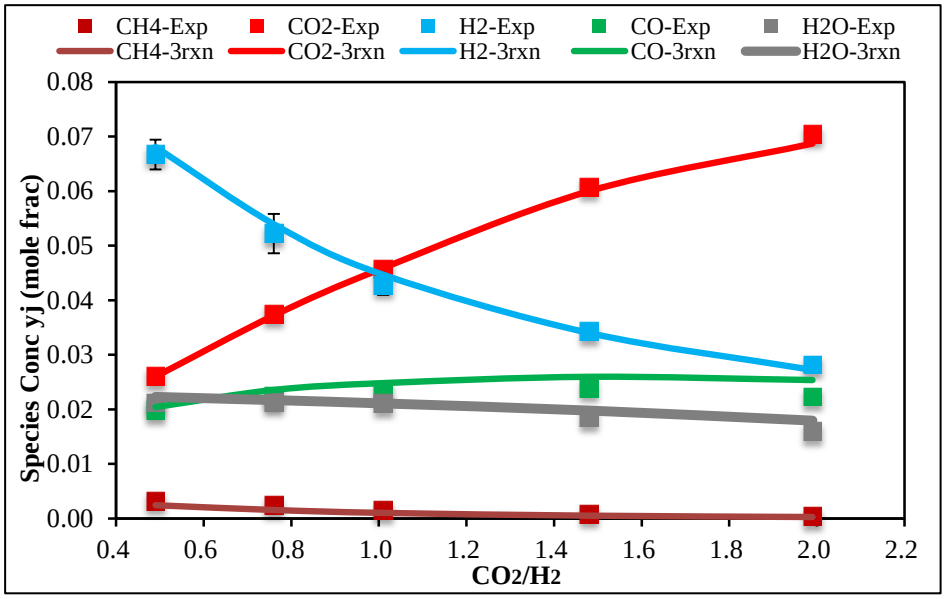

Figure 9.12 Comparison of 3-reaction model-based concentrations and experimental concentrations at 923 K.

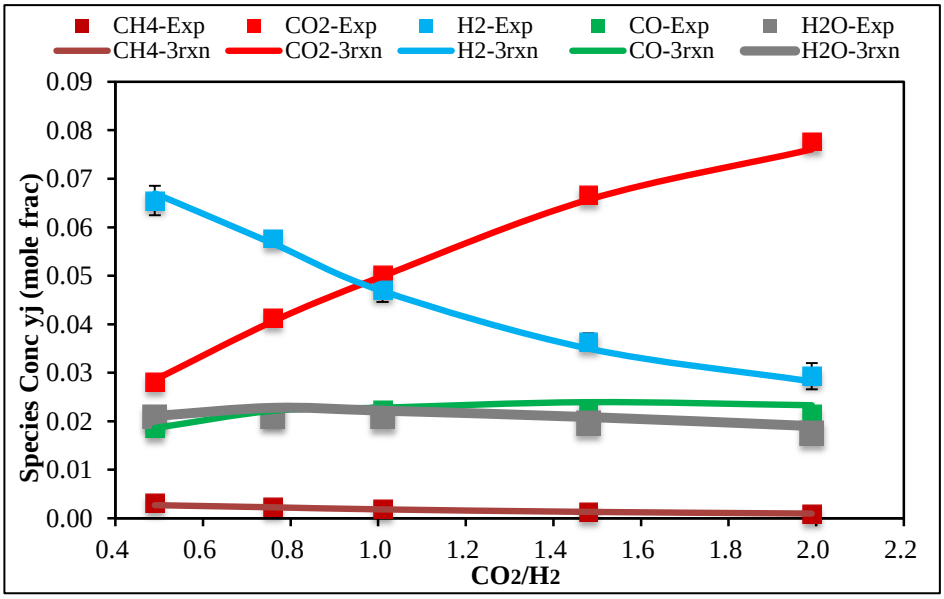

Figure 9.13 Comparison of 3-reaction model-based concentrations and experimental concentrations at 873 K.

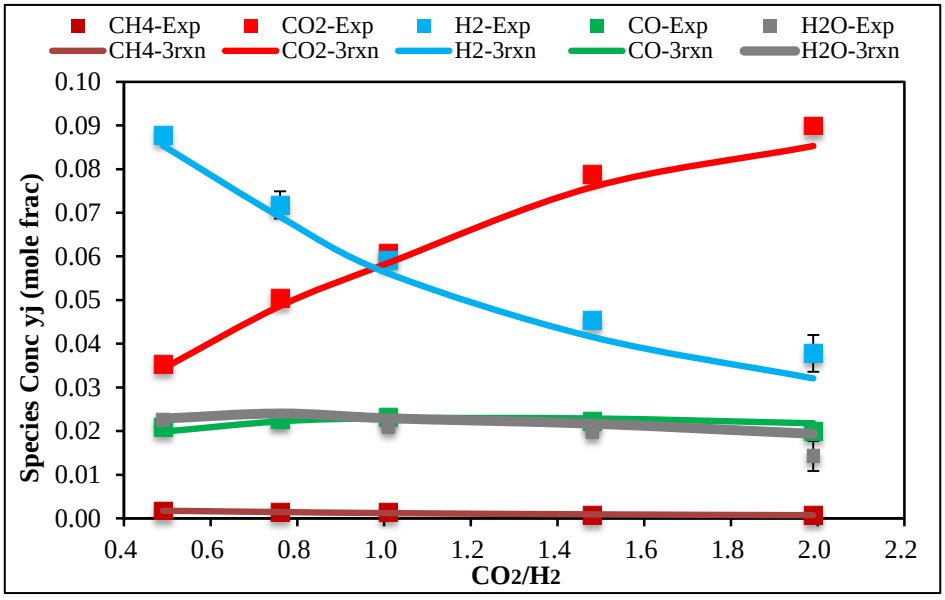

Figure 9.14 Comparison of 3-reaction model-based concentrations and experimental concentrations at 823 K.

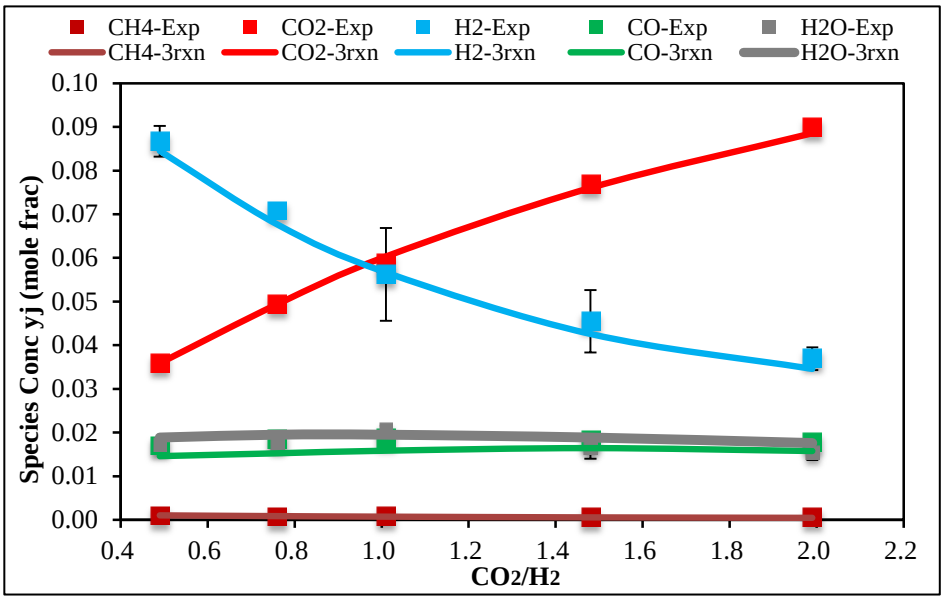

Figure 9.15 Comparison of 3-reaction model-based concentrations and experimental concentrations at 773 K.

Figures 9.12-9.15 show concentrations of all species as functions of feed molar ratio CO_2/H_2. The 3-reaction model did a good job on outlet concentration prediction for all species at each temperature with constant total inlet flow rate. Uncertainty estimation for experimental outlet fractions are shown as error bars in Figures 9.12-9.15. Uncertainty of CO_2, CO, and CH_4 are too limited and the error bars are too small to show. As was discussed in Section 4.1, the application of He as carrier gas results in relative small peak area of H_2. Therefore, the uncertainty of H_2 and H_2O outlet fraction is obviously bigger than other species. Error bars of H_2 are found in Figures 9.12-9.15; error bars of H_2O are observed in Figures 9.14 and 9.15. The H_2 and H_2O outlet mole fractions consistently fall within the uncertainty band of the experimental mole fractions for every point.

9.6 Chemkin® Model

Chemkin® is a powerful computational tool for chemical engineering calculations and simulations. It was applied for DR analysis with a Ni-based detailed mechanism. As is introduced in Section 6.6, the mechanism was originally built up for CH_4 partial oxidation, and also validated with DR research. For this section, this Ni-based detailed mechanism is applied with *Chemkin*® to see whether it could work for RWGS.

9.6.1 Chemkin® Simulation Results Discussion

The *Chemkin*® simulation results, including H_2 and CO_2 conversions, based on higher and lower active site density are compared with those from the RWGS experimental data. Figures 9.16-9.19 show comparisons for the constant flow runs.

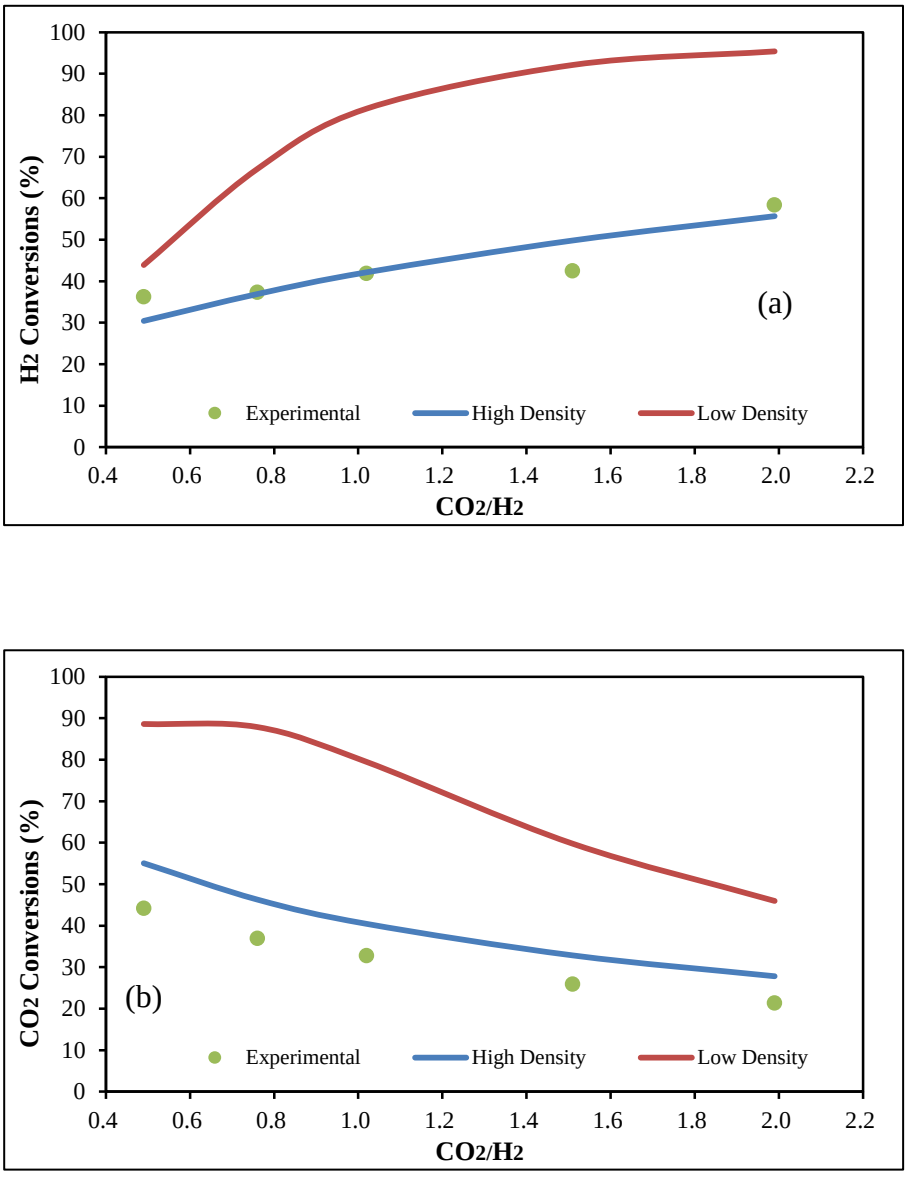

Figure 9.16 Comparison of *Chemkin*® simulation results and experimental results on (a) CH_4 conversions and (b) CO_2 conversions at 923 K and 66.7 sccm.

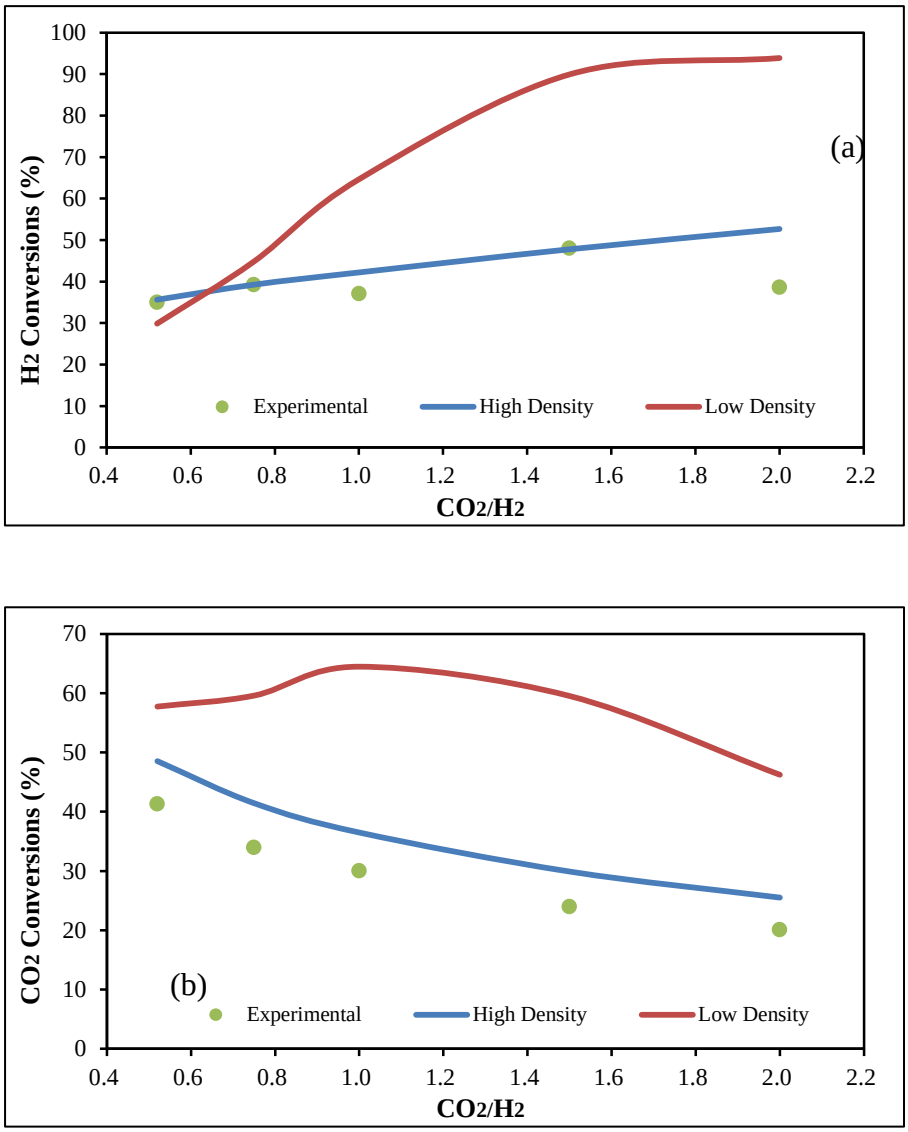

Figure 9.17 Comparison of *Chemkin*® simulation results and experimental results on (a) CH_4 conversions and (b) CO_2 conversions at 873 K and 66.7 sccm.

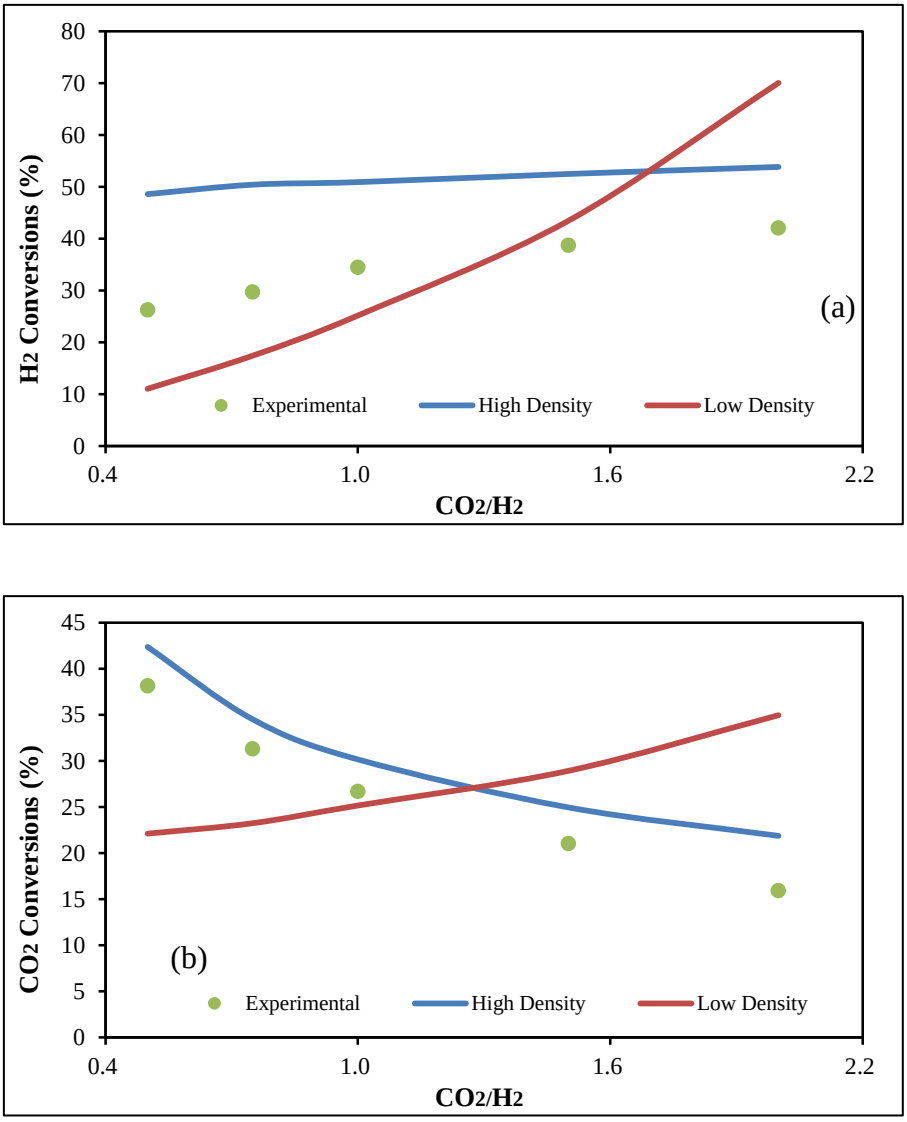

Figure 9.18 Comparison of *Chemkin*® simulation results and experimental results on (a) CH_4 conversions and (b) CO_2 conversions at 823 K and 66.7 sccm.

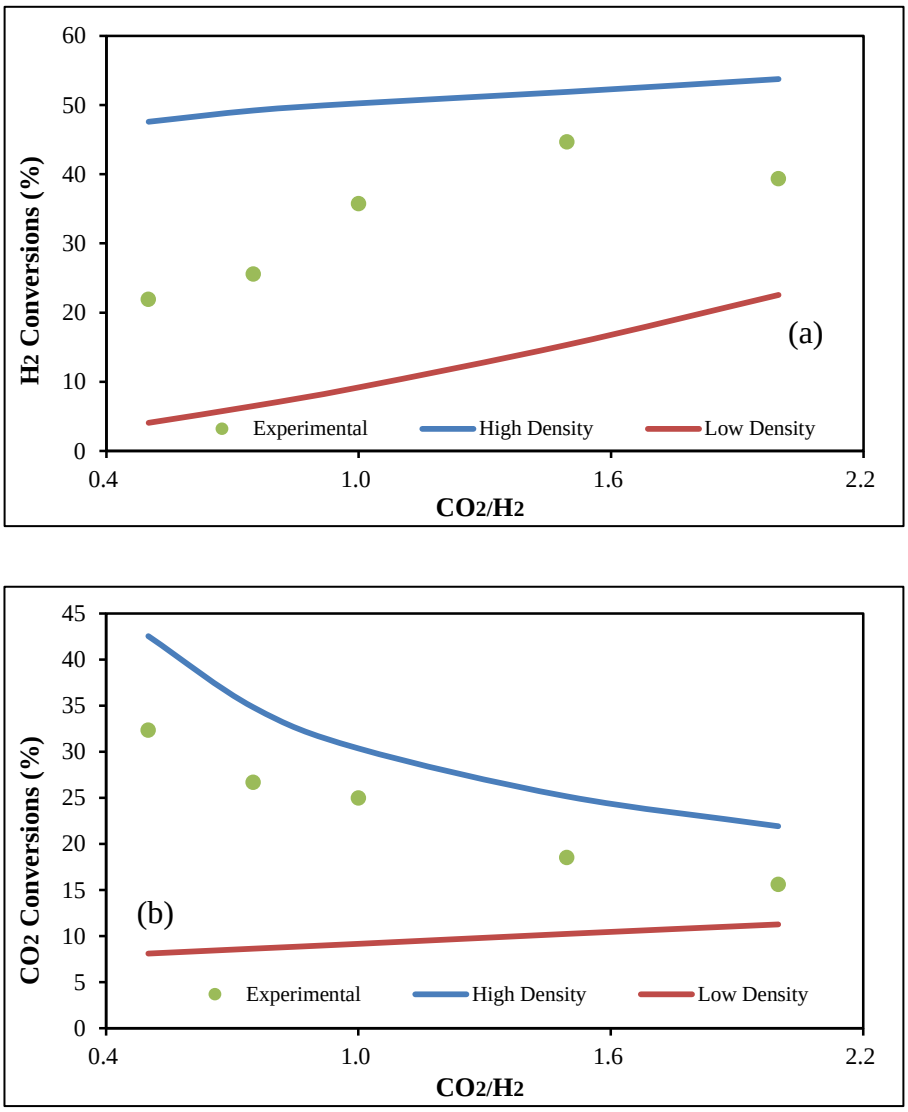

Figure 9.19 Comparison of *Chemkin*® simulation results and experimental results on (a) CH_4 conversions and (b) CO_2 conversions at 773 K and 66.7 sccm.

According to Figures 9.16-9.19, the *Chemkin*® simulation conversions of H_2 and CO_2 show different trends with experimental conversions. The simulation conversions from the higher active site density are less than those from the lower active site density at the highest temperature studied. But this pattern reverses as the temperature is lowered. There is some general trend agreement between the

experimental conversions and the higher density simulations, but not the consistent bracketing as observed with the DR work. It is concluded that the Ni-based detailed mechanism for CH_4-based reactions, including DR and Partial Oxidation, and is not reliable for the RWGS simulation. To pursue a better prediction on RWGS, a more appropriate mechanism is needed.

CHAPTER 10

TESTS OF SELECTED ASSUMPTIONS IMPORTANT FOR KINETIC ANALYSES

10.1 Tests for Mass Transfer Limitations

A heterogeneous catalysis reaction rate could be controlled by internal diffusion, external mass transfer, or intrinsic surface kinetics. Ideally, catalyst kinetics studies should be based in the kinetics-controlled regime. Qualitatively speaking, in this study, the catalyst beds were composed of powders with very small particles. In addition, reaction temperatures were relatively low. Therefore, the processes should be kinetic-controlled. To verify this, the Mears criterion test was performed for Pt/Pd-CNT/zeolite and Ru/CNT-zeolite catalysts.

Mears (1971) proposed that external diffusion resistance in a gas/solid catalyst system is negligible if the following criterion were true:

$$\frac{Rr_p n}{C_b k_c} < 0.15 \tag{10.1}$$

where R = observed reaction rate per unit particle volume, r_p = particle radius, n = reaction order, C_b = reactant molar concentration in bulk fluid, and k_c = mass transfer coefficient. This expression was modified for the existing problem:

$$\frac{r' \rho_c r_p n}{C_b k_c} < 0.15 \tag{10.2}$$

where ρ_c = bulk mass density of the bed, and r' = observed reaction rate per unit catalyst mass. The mass transfer coefficient k_c was estimated from the correlation for gas flow in packed beds developed by Dwivedi and Upadhyay (1977):

$$\varepsilon J_d \equiv \varepsilon \frac{Sh}{Sc^{1/3} Re} = \frac{0.4548}{Re^{0.4069}} \tag{10.3}$$

where ε = bed void fraction, J_d = mass transfer factor, Sh = Sherwood number $\equiv k_c d_p / D_{AB}$, Sc = Schmidt number $\equiv \mu / (\rho D_{AB})$, Re = Reynolds number $\equiv d_p G / \mu$, d_p = particle diameter, D_{AB} = gaseous diffusion coefficient, G = superficial mass velocity, μ = dynamic viscosity, and ρ = gas mass density.

The cases with CH_4/CO_2 or H_2/CO_2=1.0 are selected at each temperature. Reaction rates are estimated by power law model results. For the estimated bed parameters ($d_p \approx 0.003$ cm, $\varepsilon \approx 1$), fluid pressure (3 atm), temperature range (573-973 K), and flow rate (66.7 sccm), the estimated Mears criterion (Equation 10.2) are shown in Table 10.1.

Table 10.1 Mears Criterion Value for All Processes

Temperature (K)	Mears Criterion Value		
	RWGS over Pt/Pd-CNT/zeolite	DR over Pt/Pd-CNT/zeolite	DR over Ru/CNT-zeolite
773	2.75×10^{-5}	3.33×10^{-6}	5.39×10^{-6}
823	3.22×10^{-5}	7.80×10^{-6}	1.13×10^{-5}
873	3.68×10^{-5}	2.06×10^{-5}	1.90×10^{-5}
923	4.09×10^{-5}	5.90×10^{-5}	3.50×10^{-5}
973	—	—	6.52×10^{-4}

According to Table 10.1, Mears Criterion values of all three processes at each temperature are all much below 0.15. Therefore, none of the reactions in this study were controlled by external diffusion.

Here is additional evidence to support the above claim that the results in this study are free from external diffusion limitations. Fogler (2005) states that when a reaction is controlled by external diffusion, the reaction rate will increase with the square root of superficial velocity; when a reaction is controlled by kinetics, the reaction rate will be independent with square root of stream velocity The reaction rates (CH_4/CO_2=1.0 at 873 and 923 K) of DR over Pt/Pd-CNT/zeolite and Ru/CNT-zeolite are potted against square root of stream velocity U (m/s), and are shown in Figures 10.1 and 10.2.

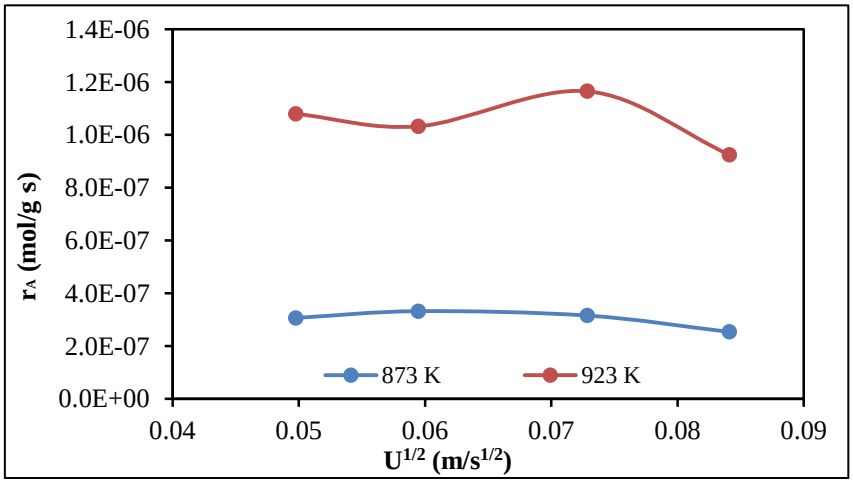

Figure 10.1 Test for external mass transfer resistance during DR over Pt/Pd-CNT/zeolite.

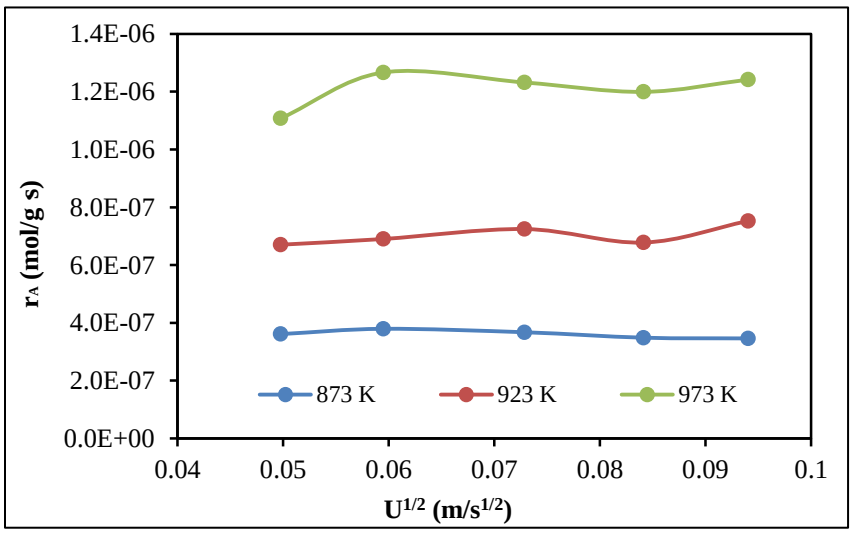

Figure 10.2 Test for external mass transfer resistance during DR over Ru-CNT/zeolite.

Figures 10.1 and 10.2 show that the rate DR reaction rate is effectively independent of gas flow rate. This is further evidence that the data observed in this study are free from any external mass transfer limitations.

Weisz and Prater (1954) proposed that internal diffusion resistance in a heterogeneous catalyst system is negligible if the following criterion were true:

$$\frac{r'\rho_c r_p^2}{D_e C_{As}} \ll 1 \qquad (10.3)$$

where ρ_c = bulk mass density of the bed, r' = observed reaction rate per unit catalyst mass, r_p = particle radius, D_e = effective diffusivity, C_{As} = concentration of A at catalyst surface. For this study, as resistance from external diffusion has been eliminated, C_{As} could be treated as C_A, the concentration in the bulk flow; and D_e is taken as D_{AB}. The cases with CH_4/CO_2 or H_2/CO_2=1.0 are selected at each temperature. The estimated Weisz-Prater criterion (Equation 10.3) are shown in Table 10.2.

Table 10.2 Weisz-Prater Criterion Value for All Processes

Temperature (K)	Mears Criterion Value		
	RWGS over Pt/Pd-CNT/zeolite	DR over Pt/Pd-CNT/zeolite	DR over Ru/CNT-zeolite
773	3.70×10^{-7}	4.37×10^{-8}	7.04×10^{-8}
823	4.27×10^{-7}	9.92×10^{-8}	1.44×10^{-7}
873	4.72×10^{-7}	2.65×10^{-7}	2.38×10^{-7}
923	5.07×10^{-7}	7.31×10^{-7}	4.38×10^{-7}
973	—	—	7.98×10^{-7}

According to Table 10.2, the Weisz-Prater criteria of all three processes at each temperature are all much less than 1. Therefore, none of reactions in this study were controlled by internal diffusion.

10.2 Tests for Catalyst Bed Isothermality

Reaction temperature is a crucial parameter when analyzing reaction kinetics. All analyses above are based on the assumption of an isothermal catalyst bed. An independent experimental test for catalyst bed isothermality is necessary.

The catalyst bed isothermality validating test was done with the Ru/CNT-zeolite. As was introduced in Section 3.1, the reactor temperature was measured by a thermocouple with digital readout. The position of the thermocouple in the previous experiments is shown in Figure 10.3.

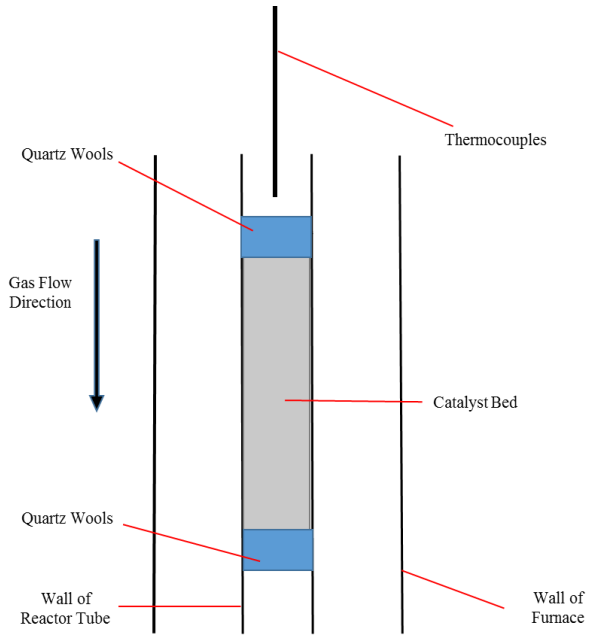

Figure 10.3 Thermocouple setup in previous experiments.

In previous experiments, as shown in Figure 10.3, the catalyst bed was fixed by quartz wool plugs. The reaction temperature was measured by the thermocouple placed just at the inlet side of the reactor but not contacting quartz wool or catalyst bed. But this arrangement could raise an uncertainty: the thermocouple is outside the reaction bed, and DR and RWGS are both endothermic reactions. Is the bed temperature the same as that reported by the single thermocouple in Figure 10.3? To answer this question, an additional thermocouple was added, and both were inserted into the bed at each end, as shown in Figure 10.4. Keep in mind that the furnace is 3-zone, with each zone having its own independent controller and thermocouple (not shown) outside the reactor tube.

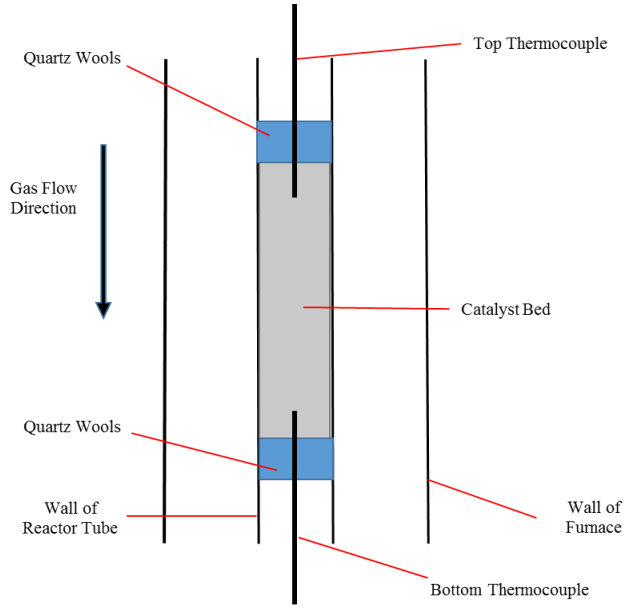

Figure 10.4 Thermocouple setup in isothermality test.

After the modification of reactor, several catalytic runs were repeated at 923 and 873 K. During these tests, the measurements from the two thermocouples were the same within 3 degrees C. In addition, the temperature readings inside the bed were the

same as that of the thermocouple placed just upstream of the upper quartz wool plug. These results confirm that all temperatures reported in this study are valid as bed temperatures, and that the catalytic beds were all isothermal.

CHAPTER 11

CONCLUSIONS

Experiments and modeling have been performed to test the activity of metal-CNT catalysts, independently synthesized by a microwave reaction technique, for CO_2 reduction. An isothermal, packed bed, integral reactor was used for data collection. The catalyst operated under kinetically-limited conditions.

In this study, 2.0 grams of Pt/Pd-CNT/zeolite and 2.0 grams of Ru/CNT-zeolite were applied for CH_4 dry reforming (ideal: $CH_4 + CO_2 \rightarrow 2CO + 2\ H_2$). Experiments were run at 773-973 K primarily at a GHSV of 2000 ml/(g_{cat} ·hr) with a CH_4/CO_2 feed molar ratio range of 0.5-2.0.

The two catalysts showed impressive activity in CO_2 reduction and CH_4 conversions at modest temperatures. The main influencing factors are reaction temperature and feed molar ratio of CH_4/CO_2. Higher reaction temperature favors higher CH_4 and CO_2 conversions and higher product ratios H_2/CO. Higher feed molar ratios of CH_4/CO_2 also favor production of CO_2 conversions and H_2/CO, but at the expense of CH_4 conversion. A limited number of tests run at a constant $CH_4/CO_2 = 1$, showed that CH_4 and CO_2 conversions were insignificantly influenced by total flow rate.

The same 2.0 grams of Pt/Pd-CNT/zeolite used for the dry reforming tests were also tested for the reverse water gas shift reaction (ideal: $CO_2 + H_2 \rightarrow CO + H_2O$) at 773-923 K and a GHSV of 2000 ml/(g_{cat} ·hr). Reasonable catalytic activity was observed. Both H_2 and CO_2 conversions are favored by higher temperatures. The higher CO_2/H_2 favors H_2 conversion but lowers CO_2 conversion.

Thorough out the whole study, the metal-CNT catalysts showed very good activity and stability in the temperature range 773-973 K. Based on the analysis of the experimental data, a small amount of carbon deposition was observed during dry reforming, and it was enhanced by temperature and higher CH_4/CO_2. This observation is consistent with observed $H_2/CO > 1$ at the highest temperatures and higher CH_4/CO_2, which are consistent with equilibrium calculations only if solid carbon is allowed. Therefore, it can be concluded that the observed performance and subsequent kinetic analyses of the Pt/Pd-CNT/zeolite and Ru/CNT-zeolite catalysts for tested for dry reforming correspond to a non-fresh (though NOT spent) catalyst.

No catalyst regeneration was performed during this study. The non-fresh Pt/Pd-CNT/zeolite catalyst was also used for the reverse water gas shift. Methane was observed as a product – an unexpected result. This suggests that old carbon from the dry reforming was possibly being gasified during the reverse shift. As with the dry reforming, the results for the reverse shift correspond to a non-fresh (though NOT spent) catalyst.

In general, observed conversions of reactants of during the dry reforming and reverse shift are considerably below non-equilibrium level values. This suggests room to improve conversions and product yield.

One advantage of integral reactor data is the opportunity to observe catalysts under conditions more closely associated with larger scale. A disadvantage is that the generally simple kinetic modeling (e.g., Langmuir-Hinshelwood) possible with differential reactor data is very difficult, if not impossible. Therefore, isothermal integral packed bed reactor species balances were applied to model all the experiments.

A simple power law rate model was applied to account for reactant conversions

and temperature dependencies. Empirical reaction rate constants, as well as global kinetic orders for these rate expressions, were determined from regression of data fitted to this numerical model. Analysis indicates a first order dependence on each of reactant for both dry reforming and reverse shift. The global reaction rates of both are second-order. Strong linear Arrhenius plots are observed over the global rate constants.

In order to account for both reactant and product species concentrations, semi-global multiple reaction models were developed for the dry reforming and reverse shift, based on the regression of experimental species outlet concentrations. For the dry reforming, the three reactions are dry reforming (ideal), reverse water gas shift, and methane decomposition. For the reverse shift experiments, the model included the reverse shift (ideal), reverse Boudouard, and Sabatier. The multiple reaction models adequately represent the observed species profiles as functions of temperature and feed flow rate. Linear Arrhenius plots are observed for each reaction in the models. The kinetics modeling shows that Pt/Pd-CNT/zeolite is more temperature dependent than Ru/CNT-zeolite for dry reforming activity.

Detailed reaction mechanism simulations were applied for the dry reforming and reverse shift experiments using a Ni-based detailed mechanism for methane reforming or partial oxidation. The simulation results indicate a decent agreement with experimental data for the dry reforming. Both of Pt/Pd-CNT/zeolite and Ru/CNT-zeolite show higher activity and more temperature dependence than the Ni catalysts. Not surprisingly, results were inconclusive for the reverse shift, indicating a different mechanism is needed.

APPENDIX A

UNCERTAINTY ESTIMATION DATA

Table A.1 to A.5 show uncertainty estimation data in Chapter 4.

Table A.1 Uncertainty Analysis on DR over Pt/Pd-CNT/zeolite at Constant Flow

T/K	Feed CH_4/CO_2	$\sigma_{y_{CH_4 0}}$ (%)	$\sigma_{y_{CO_2 0}}$ (%)	$\sigma_{y_{CH_4}}$ (%)	$\sigma_{y_{CO_2}}$ (%)	$\sigma_{y_{CO}}$ (%)	$\sigma_{y_{H_2O}}$ (%)	$\sigma_{y_{H_2}}$ (%)
923	0.49	0	0.08	0	0.01	0.02	0.16	0.16
	0.76	0.02	0.02	0	0.02	0.01	0.06	0.07
	1.01	0.07	0.04	0.13	0.06	0.28	0.31	0.43
	1.48	0.07	0.04	0.03	0.03	0.06	0.12	0.19
	1.99	0.02	0.03	0.01	0.03	0.02	0.09	0.10
873	0.47	0.12	0	0.01	0.05	0.07	0.12	0.27
	0.72	0.06	0.07	0.02	0.04	0	0.15	0.20
	0.99	0.04	0.03	0.01	0.03	0.03	0.10	0.13
	1.46	0.06	0.02	0.02	0.03	0.03	0.08	0.15
	1.96	0.04	0.02	0	0	0	0.04	0.19
823	0.52	0	0.02	0.01	0.02	0.01	0.06	0.06
	0.78	0.03	0.02	0.03	0.09	0.04	0.19	0.21
	1.02	0.01	0.01	0.01	0	0	0.02	0.03
	1.52	0.02	0.01	0.03	0.03	0	0.06	0.10
	2.03	0.03	0	0.02	0.01	0.02	0.03	0.08
773	0.49	0.06	0.03	0.02	0.02	0.01	0.07	0.15
	0.78	0.01	0.02	0.03	0.06	0.01	0.13	0.14
	1.02	0.06	0.01	0.02	0.07	0.05	0.15	0.20
	1.49	0.03	0.03	0.05	0.1	0.02	0.21	0.24
	2.03	0.07	0	0.01	0.02	0	0.04	0.15

Table A.2 Uncertainty Analysis on DR over Pt/Pd-CNT/zeolite at Various Flow

T/K	Flow Rate (sccm)	Feed CH_4/CO_2	$\sigma_{y_{CH_4 0}}$ (%)	$\sigma_{y_{CO_2 0}}$ (%)	$\sigma_{y_{CH_4}}$ (%)	$\sigma_{y_{CO_2}}$ (%)	$\sigma_{y_{CO}}$ (%)	$\sigma_{y_{H_2O}}$ (%)	$\sigma_{y_{H_2}}$ (%)
923	**46.7**	0.98	0.03	0.04	0	0.03	0.02	0.10	0.12
	66.7	1.01	0.07	0.04	0.13	0.06	0.28	0.31	0.43
	100.0	1.02	0.03	0.07	0	0.01	0.01	0.14	0.15
	133.3	1.01	0.04	0.03	0.01	0.01	0.06	0.09	0.12
873	**46.7**	0.98	0.01	0.03	0	0.01	0.01	0.06	0.07
	66.7	1.01	0	0	0	0	0	0.00	0.00
	100.0	1.02	0.05	0	0.01	0.01	0.01	0.02	0.10
	133.3	1.01	0.04	0.05	0.03	0.05	0.07	0.16	0.19

Table A.3 Uncertainty Analysis on DR over Ru/CNT-zeolite at Various Flow

T/K	Flow Rate (sccm)	Feed CH_4/CO_2	$\sigma_{y_{CH_4 0}}$ (%)	$\sigma_{y_{CO_2 0}}$ (%)	$\sigma_{y_{CH_4}}$ (%)	$\sigma_{y_{CO_2}}$ (%)	$\sigma_{y_{CO}}$ (%)	$\sigma_{y_{H_2O}}$ (%)	$\sigma_{y_{H_2}}$ (%)
973	**46.7**	0.98	0.02	0.02	0.03	0.03	0.09	0.12	0.14
	66.7	1.01	0.04	0.02	0.07	0.07	0.15	0.21	0.26
	100.0	1.02	0.01	0	0.04	0.04	0.05	0.09	0.13
	133.3	1.01	0.05	0.02	0.01	0.02	0	0.06	0.12
	166.7	1.03	0.01	0.02	0.05	0.05	0.09	0.14	0.17
923	**46.7**	0.98	0.01	0.01	0.02	0.01	0.02	0.03	0.06
	66.7	1.00	0.05	0.03	0.06	0.02	0	0.07	0.17
	100.0	1.00	0.01	0.02	0	0	0	0.04	0.04
	133.3	1.00	0.03	0	0	0	0	0.00	0.06
	166.7	1.01	0.01	0	0.03	0	0.01	0.01	0.06
873	**46.7**	1.02	0	0.02	0.02	0.01	0.04	0.06	0.07
	66.7	1.03	0.07	0.03	0.01	0.01	0.04	0.07	0.16
	100.0	1.03	0.05	0.01	0.05	0.02	0.01	0.05	0.15
	133.3	1.05	0.08	0.09	0.03	0.04	0.05	0.20	0.27
	166.7	1.04	0	0	0.04	0.02	0.02	0.04	0.09

Table A.4 Uncertainty Analysis on DR overRu/CNT-zeolite at Constant Flow

T/K	Feed CH_4/CO_2	$\sigma_{y_{CH_4\,0}}$ (%)	$\sigma_{y_{CO_2\,0}}$ (%)	$\sigma_{y_{CH_4}}$ (%)	$\sigma_{y_{CO_2}}$ (%)	$\sigma_{y_{CO}}$ (%)	$\sigma_{y_{H_2O}}$ (%)	$\sigma_{y_{H_2}}$ (%)
973	0.51	0.08	0.02	0.02	0.01	0	0.04	0.17
	0.77	0.05	0.01	0.01	0.04	0.10	0.13	0.16
	1.01	0.04	0.02	0.07	0.07	0.15	0.21	0.26
	1.53	0.01	0.04	0	0	0	0.08	0.08
	2.08	0.01	0	0.33	0.13	0.38	0.46	0.80
923	0.51	0.01	0.01	0.03	0.01	0.02	0.03	0.07
	0.77	0.55	0.06	0.01	0	0.03	0.12	1.11
	1	0.05	0.03	0.06	0.02	0	0.07	0.17
	1.5	0.03	0.05	0.03	0.01	0.06	0.12	0.15
	2.03	0.03	0.01	0.01	0	0.04	0.04	0.08
873	0.51	0.02	0.01	0.04	0.07	0.04	0.15	0.17
	0.74	0.02	0.01	0.04	0.02	0.07	0.08	0.12
	1.03	0.07	0.03	0.01	0.01	0.06	0.09	0.17
	1.48	0.02	0.01	0.03	0.06	0.10	0.16	0.17
	2.05	0.01	0.02	0.01	0.03	0.06	0.09	0.10
823	0.51	0.02	0.01	0.03	0	0.03	0.04	0.08
	0.78	0.03	0.02	0	0.03	0.03	0.08	0.10
	1.04	0.01	0	0.01	0.02	0	0.04	0.05
	1.51	0.05	0	0.04	0	0.01	0.01	0.13
	2.04	0	0	0.03	0.01	0	0.02	0.06
773	0.52	0.01	0.01	0.02	0.03	0	0.06	0.08
	0.76	0.01	0.03	0.06	0.07	0.05	0.16	0.20
	1.02	0.03	0	0.02	0.01	0.02	0.03	0.08
	1.48	0.01	0.01	0.04	0	0.02	0.03	0.09
	2.03	0.04	0.02	0.03	0.02	0.02	0.06	0.12

Table A.5 Uncertainty Analysis on RWGS over Pt/Pd-CNT/zeolite at Constant Flow

T/K	Feed CO_2/H_2	$\sigma_{y_{CO_2 0}}$ (%)	$\sigma_{y_{H_2 0}}$ (%)	$\sigma_{y_{CO_2}}$ (%)	$\sigma_{y_{CH_4}}$ (%)	$\sigma_{y_{CO}}$ (%)	$\sigma_{y_{H_2O}}$ (%)	$\sigma_{y_{H_2}}$ (%)
923	0.49	0.01	0.25	0.05	0.01	0.01	0.10	0.27
	0.76	0	0.36	0.01	0.01	0	0.02	0.36
	1.02	0.03	0.16	0.03	0	0.01	0.09	0.18
	1.51	0.01	0.09	0.01	0	0.04	0.05	0.10
	1.99	0.03	0.1	0	0	0.03	0.07	0.12
873	0.52	0.07	0.26	0.03	0.01	0.01	0.15	0.30
	0.75	0.01	0.13	0.01	0	0.01	0.03	0.13
	1.00	0.03	0.24	0.02	0	0.01	0.07	0.25
	1.50	0.05	0.14	0.01	0	0.01	0.10	0.17
	2.00	0.06	0.24	0	0.01	0.01	0.12	0.27
823	0.50	0.02	0.06	0	0	0.02	0.04	0.07
	0.75	0.02	0.31	0.01	0	0	0.04	0.31
	1.00	0.04	0.06	0.03	0.01	0.02	0.10	0.12
	1.50	0.02	0.14	0	0	0.02	0.04	0.15
	2.00	0.17	0.24	0	0.01	0.06	0.35	0.42
773	0.50	0.05	0.33	0.03	0	0.03	0.12	0.35
	0.75	0.03	0.1	0.03	0.02	0.01	0.09	0.13
	1.00	0.04	1.06	0.02	0.01	0.02	0.09	1.06
	1.50	0.12	0.67	0.03	0	0.03	0.25	0.71
	2.00	0.06	0.21	0.05	0.01	0.02	0.16	0.26

APPENDIX B

DATA OF METHANE DEHYDROAROMATIZATION

Table B.1 and B.2 show MDA data in Chapter 5.

Table B.1 Reactants and Products results from Chemkin Simulation

T/K	Flow Rate (sccm)	Feed Mole Fractions (%)		Outlet Mole Fractions (%)					
		CH_4	He	CH_4	H_2	C_2H_4	C_6H_6	$C_{10}H_{10}$	He
923	12.3	95	5	72.76	20.61	0.14	1.41	0.44	4.52
	24.7	95	5	75.16	18.30	0.19	1.34	0.33	4.60
	36.9	95	5	76.45	17.04	0.23	1.30	0.27	4.62
	49.3	95	5	77.35	16.16	0.26	1.26	0.23	4.64
873	12.3	95	5	76.78	16.86	0.13	1.18	0.34	4.63
	24.7	95	5	78.84	14.87	0.17	1.11	0.25	4.67
	36.9	95	5	79.95	13.80	0.20	1.07	0.20	4.70
	49.3	95	5	80.72	13.05	0.23	1.03	0.18	4.71
823	12.3	95	5	80.36	13.52	0.11	0.97	0.26	4.70
	24.7	95	5	82.07	11.88	0.15	0.90	0.19	4.74
	36.9	95	5	83.01	10.97	0.18	0.86	0.15	4.76
	49.3	95	5	83.66	10.34	0.20	0.83	0.13	4.77
773	12.3	95	5	83.47	10.64	0.09	0.77	0.19	4.77
	24.7	95	5	84.88	9.28	0.13	0.72	0.14	4.80
	36.9	95	5	85.64	8.55	0.15	0.68	0.11	4.81
	49.3	95	5	86.16	8.04	0.17	0.66	0.09	4.82

Table B.2 Reactants and Products Results from 3-Reaction Model Simulation

T/K	Flow Rate (sccm)	Feed Mole Fractions (%)		Outlet Mole Fractions (%)					
		CH_4	He	CH_4	H_2	C_2H_4	C_6H_6	$C_{10}H_{10}$	He
923	12.3	95	5	71.30	22.01	0.12	1.60	0.46	4.51
	24.7	95	5	74.12	19.28	0.17	1.54	0.32	4.57
	36.9	95	5	76.44	17.06	0.23	1.40	0.25	4.62
	49.3	95	5	78.10	15.46	0.29	1.29	0.20	4.66
873	12.3	95	5	74.92	18.63	0.10	1.38	0.37	4.59
	24.7	95	5	77.99	15.69	0.15	1.26	0.25	4.65
	36.9	95	5	80.03	13.73	0.21	1.13	0.20	4.69
	49.3	95	5	81.42	12.39	0.27	1.03	0.16	4.72
823	12.3	95	5	78.27	15.50	0.08	1.20	0.28	4.66
	24.7	95	5	81.18	12.73	0.13	1.05	0.19	4.72
	36.9	95	5	82.91	11.08	0.18	0.94	0.14	4.75
	49.3	95	5	84.06	9.97	0.23	0.85	0.12	4.78
773	12.3	95	5	81.59	12.42	0.07	0.98	0.21	4.72
	24.7	95	5	84.20	9.93	0.12	0.83	0.14	4.78
	36.9	95	5	85.60	8.59	0.16	0.73	0.10	4.81
	49.3	95	5	86.51	7.71	0.21	0.66	0.08	4.83

APPENDIX C

CHEMKIN CODE FOR METHANE DEHYROAROMATIZATION

Appendix C shows the Chemkin code for MDA simulation in Chapter 5.

```
!%%%%%%%%%%%%%%%%%%%%%%%%%%%%%%%%%%%%%%%%%%%%%%%%%%%%%%%%%%%%%%%%%%%%%%%%%%%!
!%%%%%%%%   Thermodynamically consistent MDA reaction mechanism      %%%%%%%%!
!%%%%%%%%   Catalyst is 6 wt.% Mo/HZSM-5                             %%%%%%%%!
!%%%%%%%%   C. Karakaya, S.H.Morejudo, H. Zhu and R.J. Kee           %%%%%%%%!
!%%%%%%%%   Journal:Industrial and Engineering Chemistru Research    %%%%%%%%!
!%%%%%%%%   Surface thermo is based on the reversibility,            %%%%%%%%!
!%%%%%%%%   adjustment procedure. Gas-phase thermo is from  Burcat data  %%%%!
!%%%%%%%%   ADDED "FAKE" SPECIES FOR H2 MEMBRANE BY R.BARAT - 4/12/17 %%%%%%%!
SITE/Mo_surface/    SDEN/1.26E-10/
    CH4(s)
    CH2(s)
    C2H6(s)
    Mo2C(s)
END
SITE/H-ZSM_surface/    SDEN/1.5604E-9/
    CH3(s)
    C2H5(s)
    C4H7(s)
    C4H9(s)
    C6H7(s)
    C6H9(s)
    C7H9(s)
    C6H11(s)
    CYC(s)
    C6H13(s)
    C10H9(s)
    C10H11(s)
    C10H13(s)
    H-ZSM(s)
END
MATERIAL MEMBRANE
SITE/MEM_SURFACE/     SDEN/1.0E-9/
H2(S)     (S)
END
BULK/MEM_DIFFUSE/
H2(B)
END
THERMO
```

```
0300.00  1000.00  5000.00
H2                J 3/77H   2    0    0    0G   300.000  5000.000
 0.30667095E+01 0.57473755E-03 0.13938319E-07-0.25483518E-10 0.29098574E-14
-0.86547412E+03-0.17798424E+01 0.33553514E+01 0.50136144E-03-0.23006908E-06
-0.47905324E-09 0.48522585E-12-0.10191626E+04-0.35477228E+01
CH4       RRHO SSNL121296C   1H   4    0    0G   300.000  5000.000
 1.68347883E 00 1.02372356E-02-3.87512864E-06 6.78558487E-10-4.50342312E-14
-1.00807871E 04 9.62339497E 00 7.78741479E-01 1.74766835E-02-2.78340904E-05
 3.04970804E-08-1.22393068E-11-9.82522852E 03 1.37221947E 01
C2H4           SNLL121286C   2H   4    0    0G   300.000  5000.000
 3.52841878E 00 1.14851845E-02-4.41838529E-06 7.84460053E-10-5.26684849E-14
 4.42828857E 03 2.23038912E 00-8.61487985E-01 2.79616285E-02-3.38867721E-05
 2.78515220E-08-9.73787891E-12 5.57304590E 03 2.42114868E 01
C2H6              T12/78C   2H   6    0    0G   300.000  4000.000
 0.48259382E 01 0.13840429E-01-0.45572588E-05 0.67249672E-09-0.35981614E-13
-0.12717793E 05-0.52395067E 01 0.14625387E 01 0.15494667E-01 0.57805073E-05
-0.12578319E-07 0.45862671E-11-0.11239176E 05 0.14432295E 02
C4H8              T05/09C  4.H  8.    0.    0.G   200.000  6000.000 1000.
 7.86795262E+00 2.24448843E-02-8.07705438E-06 1.30179988E-09-7.77958472E-14
-4.23853340E+03-1.65662549E+01 5.13226136E+00 5.33862838E-03 6.02928960E-05
-7.60364685E-08 2.87324693E-11-2.16718358E+03 3.82936810E+00-3.72842176E+00
C10H8                    C  10H   8    0    0G   200.000  6000.000 1000.
 1.86129884E+01 3.04494175E-02-1.11224825E-05 1.81615474E-09-1.09601281E-13
 8.91578988E+03-8.00230396E+01-1.04919475E+00 4.62970781E-02 7.07591636E-05
-1.38408111E-07 6.20475407E-11 1.59848987E+04 3.02121626E+01 1.81107678E+04
C6H10             U 5/78C   6H  10    0    0G   300.000  5000.000
 0.15927771E+02 0.23744129E-01-0.69086718E-05 0.81097773E-09-0.26831226E-13
-0.86426562E+04-0.65251862E+02-0.13942280E+01 0.47206931E-01 0.11960419E-04
-0.41628958E-07 0.17403357E-10-0.22177900E+04 0.31296036E+02
C6H12 1-Hexene    T10/10C  6.H 12.    0.    0.G   200.000  6000.000 1000.
 1.22080929E+01 3.32790650E-02-1.19875911E-05 1.92939941E-09-1.15062647E-13
-1.12223522E+04-3.43171769E+01 6.59375238E+00 5.81209593E-03 1.17056541E-04
-1.57671202E-07 6.35227163E-11-7.71664325E+03 4.70097229E+00-4.73979778E+03
C6H6                     C   6H   6    0    0G   200.000  6000.000 1000.
 1.10809576E+01 2.07176746E-02-7.52145991E-06 1.22320984E-09-7.36091279E-14
 4.30641035E+03-4.00413310E+01 5.04818632E-01 1.85020642E-02 7.38345881E-05
-1.18135741E-07 5.07210429E-11 8.55247913E+03 2.16412893E+01 9.96811598E+03
C7H8              T 9/81C   7H   8    0    0G   300.000  5000.000
 0.13957725E+02 0.24616607E-01-0.83795358E-05 0.12537165E-08-0.67675520E-13
-0.10295066E+04-0.52245728E+02-0.25368824E+01 0.52898869E-01 0.14038515E-05
-0.40762323E-07 0.20377519E-10 0.44778477E+04 0.37415115E+02
4
C10H10            T 7/98C  10H  10O   0    0G   200.000  6000.000
1
 1.92211178E+01 3.51247274E-02-1.27719042E-05 2.07903232E-09-1.25191968E-13
```

```
2
 4.39595221E+03-8.19390283E+01-1.92135165E-01 4.50394780E-02 8.64482370E-05
-1.56640588E-07 6.88727900E-11 1.16587583E+04 2.82951960E+01 1.40900666E+04
C10H12                  C  10H  12          0G   300.000  5000.000 1000.00
 1.40212742E+01 4.90185301E-02-1.98576311E-05 3.67394634E-09-2.54888278E-13
-4.53781982E+03-5.35246467E+01-2.62027066E+00 6.33205124E-02 3.70856910E-05
-8.65524655E-08 3.53677639E-11 1.40369900E+03 3.98272366E+01
HE                120186HE  1               G  0300.00   5000.00  1000.00
 0.02500000E+02 0.00000000E+00 0.00000000E+00 0.00000000E+00 0.00000000E+00
-0.07453750E+04 0.09153489E+01 0.02500000E+02 0.00000000E+00 0.00000000E+00
 0.00000000E+00 0.00000000E+00-0.07453750E+04 0.09153488E+01
AR REF ELEMENT    g 5/97AR 1.    0.    0.    0.G   200.000  6000.000 1000.
 2.50000000E+00 0.00000000E+00 0.00000000E+00 0.00000000E+00 0.00000000E+00
-7.45375000E+02 4.37967491E+00 2.50000000E+00 0.00000000E+00 0.00000000E+00
 0.00000000E+00 0.00000000E+00-7.45375000E+02 4.37967491E+00 0.00000000E+00
H-ZSM(s)                Al  1H   1          I  0298.00   3000.00  1500.00
 0.00000000E+00 0.00000000E+00-0.00000000E+00 0.00000000E+00-0.00000000E+00
 0.00000000E+00 0.00000000E+00-0.00000000E+00 0.00000000E+00-0.00000000E+00
 0.00000000E+00 0.00000000E+00-0.00000000E+00 0.00000000E+00
CH3(s)                  C   1H   3Al  1     I  0298.00   3000.00  1500.00
 2.04869372e+00-2.82345981e-02 3.82378069e-05-1.53491564e-08 1.99108083e-12
-0.00000000E+00 1.96475499e+00-1.67008999e+01-3.70784321e-02 2.08102819e-04
-2.12219778e-07 6.46289158e-11 0.00000000E+00 1.02827713e+02
C2H5(s)                 C   2H   5Al  1     I  0298.00   3000.00  1500.00
 1.59019185e+00 5.38267690e-03 7.71346434e-06-5.21090084e-09 8.63459918e-13
-0.00000000E+00 1.21943743e+01-3.40691508e+00 6.85890188e-03 4.75028848e-05
-5.64068643e-08 1.78879785e-11 0.00000000E+00 3.77937811e+01
C4H7(s)                 C   4H   7Al  1     I  0298.00   3000.00  1500.00
 1.03530807e+00 2.01793840e-02-8.06341767e-07-2.44214972e-09 4.88497454e-13
-0.00000000E+00 1.44535867e+01-3.47355790e+00 9.31599107e-03 6.91101307e-05
-7.77814254e-08 2.38544380e-11 0.00000000E+00 4.01265110e+01
C4H9(s)                 C   4H   9Al  1     I  0298.00   3000.00  1500.00
 5.51368198e+00-3.43794519e-02 6.05836997e-05-2.57920346e-08 3.44218409e-12
-0.00000000E+00 2.11329628e+01-3.01607205e+01-4.84119029e-02 3.80547427e-04
-4.01116484e-07 1.23645382e-10 0.00000000E+00 2.12099520e+02
C6H7(s)                 C   6H   7Al  1     I  0298.00   3000.00  1500.00
-1.44704451e+00 4.62687881e-02-2.27546132e-05 4.94638016e-09-3.81640383e-13
-0.00000000E+00 9.36014902e+00 4.26161950e+00 2.99381539e-02-1.52750751e-05
 1.04480689e-08-3.83653430e-12 0.00000000E+00-1.79296337e+01
C6H9(s)                 C   6H   9Al  1     I  0298.00   3000.00  1500.00
-1.92758423e+00 5.54404212e-02-2.97246011e-05 7.15216905e-09-6.26300708e-13
-0.00000000E+00 9.98234485e+00 4.65190246e+00 4.22867610e-02-3.58131835e-05
 2.50560975e-08-7.50314046e-12 0.00000000E+00-2.27292346e+01
C7H9(s)                 C   7H   9Al  1     I  0298.00   3000.00  1500.00
-1.88323990e+00 6.21518315e-02-3.64351232e-05 9.61651435e-09-9.32980580e-13
```

-0.00000000E+00 1.28060547e+01 6.18773977e+00 5.32682196e-02-6.54036201e-05
 5.06477856e-08-1.46905811e-11 0.00000000E+00-2.87132710e+01
C6H13(s)   C   6H 13Al 1   I 0298.00   3000.00 1500.00
 6.35536713e+00-1.54669475e-02 4.85611635e-05-2.15822064e-08 2.85785017e-12
-0.00000000E+00 3.34284459e+01-3.12808336e+01-3.56193170e-02 3.99924756e-04
-4.29040753e-07 1.32856648e-10 0.00000000E+00 2.36173277e+02
C6H11(s)   C   6H 11Al 1   I 0298.00   3000.00 1500.00
 4.13450310e+00-1.13514907e-02 4.95199012e-05-2.36006051e-08 3.30408721e-12
-0.00000000E+00 2.18134322e+01-2.80444994e+01-4.17261157e-02 3.91488601e-04
-4.09991347e-07 1.25177929e-10 0.00000000E+00 1.97398250e+02
CYC(s)   C   6H 11Al 1   I 0298.00   3000.00 1500.00
 4.75642235e+00-2.43600378e-02 6.32792728e-05-2.85623070e-08 3.89698094e-12
-0.00000000E+00 2.06248017e+01-3.49311969e+01-5.66213317e-02 4.67243964e-04
-4.87764210e-07 1.49041679e-10 0.00000000E+00 2.36389796e+02
C10H13(s)   C 10H 13Al 1   I 0298.00   3000.00 1500.00
-1.61803020e+00 9.00232557e-02-5.21079142e-05 1.35825017e-08-1.30175831e-12
-0.00000000E+00 2.53346198e+01 8.62894384e+00 7.74648636e-02-8.32172247e-05
 5.93383823e-08-1.67124972e-11 0.00000000E+00-2.72864421e+01
C10H9(s)   C 10H   9Al 1   I 0298.00   3000.00 1500.00
-6.47296006e+00 1.29702390e-01-1.01588854e-04 3.29125788e-08-3.77076657e-12
-0.00000000E+00 1.06442806e+01 2.77530018e+01 1.24415398e-01-3.37354488e-04
 3.18805260e-07-9.59212525e-11 0.00000000E+00-1.70240271e+02
C10H11(s)   C 10H 11Al 1   I 0298.00   3000.00 1500.00
-4.17186831e+00 1.06924594e-01-7.18740033e-05 2.10281836e-08-2.22429669e-12
-0.00000000E+00 1.61764066e+01 1.63451707e+01 9.57959026e-02-1.84959696e-04
 1.63881194e-07-4.86850043e-11 0.00000000E+00-9.10854726e+01
Mo2C(s)   C   0H   0Mo 2   I 0298.00   3000.00 1500.00
 0.00000000E+00 0.00000000E+00-0.00000000E+00 0.00000000E+00-0.00000000E+00
 0.00000000E+00 0.00000000E+00-0.00000000E+00 0.00000000E+00-0.00000000E+00
 0.00000000E+00 0.00000000E+00-0.00000000E+00 0.00000000E+00
CH4(s)   C   1H   4Mo 2   I 0298.00   3000.00 1500.00
 1.70340796e+00-4.92917054e-03 1.09764549e-05-4.03084260e-09 4.22774698e-13
-0.00000000E+00 8.43877813e+00-8.30185098e+00-1.53671476e-02 1.14959320e-04
-1.19086612e-07 3.63793862e-11 0.00000000E+00 6.37400925e+01
CH2(s)   C   1H   2Mo 2   I 0298.00   3000.00 1500.00
 8.89624304e-01 7.31327960e-04 4.48490304e-06-2.07888615e-09 2.59429518e-13
-0.00000000E+00 5.75007971e+00-2.01029027e+00-6.43826983e-03 4.57869472e-05
-4.45320654e-08 1.30441624e-11 0.00000000E+00 2.26653455e+01
C2H6(s)   C   2H   6Mo 2   I 0298.00   3000.00 1500.00
 4.59349718e+00-2.81188736e-02 4.49820478e-05-1.86410663e-08 2.44662608e-12
-0.00000000E+00 1.76537048e+01-1.75202238e+01-4.14168404e-02 2.53153560e-04
-2.57297594e-07 7.80186353e-11 0.00000000E+00 1.37218284e+02
(S)   H   0   S   300.0   3000.0 1000.0
 0.00000000E+00 0.00000000E+00 0.00000000E+00 0.00000000E+00 0.00000000E+00
 0.00000000E+00 0.00000000E+00 0.00000000E+00 0.00000000E+00 0.00000000E+00

```
 0.00000000E+00 0.00000000E+00 0.00000000E+00 0.00000000E+00
H2(S)                     H    2                 S     300.0     3000.0   1000.0
 0.00000000E+00 0.00000000E+00 0.00000000E+00 0.00000000E+00 0.00000000E+00
 0.00000000E+00 0.00000000E+00 0.00000000E+00 0.00000000E+00 0.00000000E+00
 0.00000000E+00 0.00000000E+00 0.00000000E+00 0.00000000E+00
H2(B)                     H    2                 S     300.0     3000.0   1000.0
 0.00000000E+00 0.00000000E+00 0.00000000E+00 0.00000000E+00 0.00000000E+00
 0.00000000E+00 0.00000000E+00 0.00000000E+00 0.00000000E+00 0.00000000E+00
 0.00000000E+00 0.00000000E+00 0.00000000E+00 0.00000000E+00
END
!****************************************************************************
REACTIONS       MWOFF    KJOULES/MOLE
Mo2C(s) +CH4 =>CH4(s)                              2.939E+13    0.172        94.841
CH4(s) =>Mo2C(s) +CH4                              2.905E+14   -0.172        54.487
CH4(s) =>CH2(s) +H2                                1.359E+13    0.172       126.541
CH2(s) +H2 =>CH4(s)                                6.628E+12   -0.172       102.987
CH2(s) +CH4 =>C2H6(s)                              4.211E+12    0.172       110.641
C2H6(s) =>CH2(s) +CH4                              1.231E+12   -0.172       102.987
C2H6(s) =>Mo2C(s) +C2H4 +H2                        1.236E+12    0.172       146.341
Mo2C(s) +C2H4 +H2 =>C2H6(s)                        6.628E+14   -0.172        19.487
H-ZSM(s) +C2H4 =>C2H5(s)                           9.688E+10    1.439        73.974
    COV/C2H5(s)                                 0.000E+00   0.000       110.000/
       FORD/C2H4 0.75/
C2H5(s) =>H-ZSM(s) +C2H4                           1.355E+15   -0.400       139.878
    COV/C2H5(s)                                 0.000E+00   0.000        60.000/
C2H5(s) +C2H4 =>C4H9(s)                            1.001E+11    0.278        30.751
    COV/C2H5(s)                                 0.000E+00   0.000       -50.000/
C4H9(s) =>C2H5(s) +C2H4                            6.097E+15    0.349       195.495
C4H9(s) +C2H4 =>C6H13(s)                           2.412E+11    0.947        10.288
C6H13(s) =>C4H9(s) +C2H4                           2.668E+14   -0.951        66.124
C6H13(s) =>H-ZSM(s) +C6H12                         6.652E+10    0.306        94.784
H-ZSM(s) +C6H12 =>C6H13(s)                         3.791E+14    0.218        13.108
H-ZSM(s) +C6H12 =>C6H11(s) +H2                     6.557E+13    0.491       104.359
C6H11(s) +H2 =>H-ZSM(s) +C6H12                     5.128E+13   -0.289        93.388
C2H5(s) +C6H12 =>C6H11(s) +C2H6                    1.389E+13   -0.485        62.912
    COV/C2H5(s)                                 0.000E+00   0.000       -50.000/
C6H11(s) +C2H6 =>C2H5(s) +C6H12                    8.000E+10    0.485       121.963
C6H11(s) =>CYC(s)                                  5.164E+13   -0.161         3.351
CYC(s) =>C6H11(s)                                  7.794E+14    0.200        31.702
CYC(s) =>H-ZSM(s) +C6H10                           1.159E+12   -0.200       152.450
H-ZSM(s) +C6H10 =>CYC(s)                           8.204E+12    0.200       100.850
C4H9(s) =>H-ZSM(s) +C4H8                           9.091E+13    0.000       122.361
H-ZSM(s) +C4H8 =>C4H9(s)                           1.990E+12    0.000       0.000
C2H5(s) +C4H8 =>C6H13(s)                           1.405E+13    1.409        47.579
    COV/C2H5(s)                                 0.000E+00   0.000       -50.000/
```

```
C6H13(s) =>C2H5(s) +C4H8                          5.156E+13    1.347       159.883
H-ZSM(s) +C4H8 =>C4H7(s) +H2                      1.095E+13   -0.175       109.744
    COV/C4H7(s)                                0.000E+00   0.000        42.000/
C4H7(s) +H2 =>H-ZSM(s) +C4H8                      4.711E+14   -1.083       121.025
H-ZSM(s) +C6H10 =>C6H9(s) +H2                     4.851E+13   -0.265       105.273
C6H9(s) +H2 =>H-ZSM(s) +C6H10                     5.538E+13    0.265        64.427
C6H9(s) =>C6H7(s) +H2                             5.213E+13   -0.265        98.273
C6H7(s) +H2 =>C6H9(s)                             1.856E+10    0.265       103.427
C6H7(s) =>H-ZSM(s) +C6H6                          6.076E+13    0.100       147.072
H-ZSM(s) +C6H6 =>C6H7(s)                          1.856E+11    0.265        93.327
C4H7(s) +C6H6 =>C10H13(s)                         5.297E+11    1.083        76.143
    COV/C4H7(s)                                0.000E+00   0.000       -42.000/
C10H13(s) =>C4H7(s) +C6H6                         5.985E+13    0.204        91.219
C10H13(s) =>H-ZSM(s) +C10H12                      7.718E+09   -0.204         2.437
H-ZSM(s) +C10H12 =>C10H13(s)                      1.558E+14    0.204        32.397
H-ZSM(s) +C10H12 =>C10H11(s) +H2                  4.799E+12    0.316       110.896
C10H11(s) +H2 =>H-ZSM(s) +C10H12                  1.023E+12    0.000        46.022
C10H11(s) =>H-ZSM(s) +C10H10                      1.381E+13    0.000        21.646
H-ZSM(s) +C10H10 =>C10H11(s)                      1.023E+13    0.000         0.000
H-ZSM(s) +C10H10 =>C10H9(s) +H2                   6.190E+12   -0.141       115.197
C10H9(s) +H2 =>H-ZSM(s) +C10H10                   1.333E+12    0.141        86.503
C10H9(s) =>H-ZSM(s) +C10H8                        1.069E+13   -0.141         7.384
H-ZSM(s) +C10H8 =>C10H9(s)                        1.333E+11    0.141         1.616
H-ZSM(s) +CH4 =>CH3(s) +H2                        4.273E+06    0.341       108.644
CH3(s) +H2 =>H-ZSM(s) +CH4                        1.495E+13   -0.305       107.156
CH3(s) +C6H6 =>C7H9(s)                            9.226E+12    0.188       136.254
C7H9(s) =>CH3(s) +C6H6                            2.820E+11   -0.188       103.846
C7H9(s) =>H-ZSM(s) +C7H8                          1.064E+13    0.188       108.554
H-ZSM(s) +C7H8 =>C7H9(s)                          1.627E+12   -0.188       103.146
! specify probability that H2 will get caught by membrane surface after
collision
H2 + (S) => H2(S)                                 0.700E+00    0.0           0.0
STICK
! diffusion rate of H2 thru membrane wall (bulk) to vacuum
H2(S) => H2(B) + (S)                              1.000E-06    0.0           0.0
END
```

APPENDIX D

MATLAB CODE FOR METHANE DEHYROAROMATIZATION

Appendix D shows the Matlab code for MDA simulation in Chapter 5.

```
clear all
clc
close all

format compact

 kp1 = 1.139E-04;
 kp2 = 1.042E+05;
 kp3 = 8.954E+03;

 P=0.99;

FHE=[ 0.001506122 0.00302449 0.004518367 0.006036735];

FM_test=[2.19E-02 4.55E-02 6.91E-02 9.34E-02];
FB_test=[4.24E-04 8.13E-04 1.17E-03 1.52E-03];
FE_test=[4.33E-05 1.17E-04 2.09E-04 3.17E-04];
FH_test=[6.21E-03 1.11E-02 1.54E-02 1.95E-02];
FN_test=[1.34E-04 1.97E-04 2.44E-04 2.83E-04];

 FM1=[0.028616327 0.057465306 0.08584898 0.114697959];
 FH1=[0.0000001 0.0000001 0.0000001 0.0000001];
 FB1=[0.0000001 0.0000001 0.0000001 0.0000001];
 FE1=[0.0000001 0.0000001 0.0000001 0.0000001];
 FN1=[0.0000001 0.0000001 0.0000001 0.0000001];

 stepsize=0.001;
 v=[0:stepsize:2.453];


k1 = [0.11:0.001:0.13];
k2 = [0.09:0.001:0.11];
k3 = [2.1:0.01:2.3];

L1= length(k1);
L2= length(k2);
L3= length(k3);

for jj=1:length(FM1)
    jj

final_FM =[];
final_FH=[];
final_FE=[];
final_FN =[];
```

```
final_FB=[];
FM=[];
FH=[];
FB=[];
FE=[];
FN=[];
FT=[];

 for i1=1:L1;
     i1
 for i2=1:L2;
 for i3=1:L3;

 FM=[ FM1(jj) zeros(1,length(v)-1)];
 FH=[FH1(jj)  zeros(1,length(v)-1)];
 FB=[FB1(jj) zeros(1,length(v)-1)];
 FE=[FE1(jj) zeros(1,length(v)-1)];
 FN=[FN1(jj) zeros(1,length(v)-1)];
 FT=zeros(1,length(v)-1);

 eta1=zeros(1,length(v)-1);
 eta2=zeros(1,length(v)-1);
 eta3=zeros(1,length(v)-1);

for j=2:length(v)
j;
FT(j-1)=FM(j-1)+FH(j-1)+FB(j-1)+FE(j-1)+FN(j-1)+FHE(jj);

eta1(j-1)=((P/FT(j-1))^1)*((FE(j-1))^1)*((FH(j-1))^2)/((FM(j-1)^2)*kp1);
eta2(j-1)=((P/FT(j-1))^1)*((FB(j-1))^1)*((FH(j-1))^3)/((FE(j-1)^3)*kp2);
eta3(j-1)=((P/FT(j-1))^1)*((FN(j-1))^1)*((FH(j-1))^3)/(FB(j-1)*(FE(j-
1))^2*kp3);

FM(j)=FM(j-1)-(2*k1(i1)*FM(j-1)*((P/FT(j-1))^1)*(1-eta1(j-1)))*stepsize;

FH(j)=FH(j-1)+(2*k1(i1)*FM(j-1)*((P/FT(j-1))^1)*(1-eta1(j-
1))+3*k2(i2)*FE(j-1)*((P/FT(j-1))^1)*(1-eta2(j-1))+3*k3(i3)*FE(j-
1)*FB(j-1)*((P/FT(j-1))^2)*(1-eta3(j-1)))*stepsize;

FE(j)=FE(j-1)+(1*k1(i1)*FM(j-1)*((P/FT(j-1))^1)*(1-eta1(j-1))-
3*k2(i2)*FE(j-1)*((P/FT(j-1))^1)*(1-eta2(j-1))-2*k3(i3)*FE(j-1)*FB(j-
1)*((P/FT(j-1))^2)*(1-eta3(j-1)))*stepsize;

FB(j)=FB(j-1)+(k2(i2)*FE(j-1)*((P/FT(j-1))^1)*(1-eta2(j-1))-
k3(i3)*FE(j-1)*FB(j-1)*((P/FT(j-1))^2)*(1-eta3(j-1)))*stepsize;

FN(j)=FN(j-1)+(k3(i3)*FE(j-1)*FB(j-1)*((P/FT(j-1))^2)*(1-eta3(j-
1)))*stepsize;

end

final_FM=[final_FM FM(end-1)];
final_FE=[final_FE FE(end-1)];
final_FH=[final_FH FH(end-1)];
```

```
final_FB=[final_FB FB(end-1)];
final_FN=[final_FN FN(end-1)];

end
end
 end

 FINAL_FM(jj,:)=final_FM;
FINAL_FE(jj,:)=final_FE;
 FINAL_FH(jj,:)=final_FH;
FINAL_FN(jj,:)=final_FN;
 FINAL_FB(jj,:)=final_FB;
end

MMSE_temp=0;
for ii=1:length(FM_test)
MMSE_temp=MMSE_temp+((FINAL_FM(ii,:)-FM_test(ii))/FM_test(ii)).^2
+((FINAL_FN(ii,:)-FN_test(ii))/FN_test(ii)).^2+((FINAL_FE(ii,:)-
FE_test(ii))/FE_test(ii)).^2+((FINAL_FH(ii,:)-
FH_test(ii))/FH_test(ii)).^2+((FINAL_FB(ii,:)-
FB_test(ii))/FB_test(ii)).^2;
end
MMSE=MMSE_temp/(5*length(FM_test));
sizeMMSE=size(MMSE)
min_MMSE=min(MMSE)
position=find(MMSE==min_MMSE)-1;

 remain1=rem(position,L2*L3);
 factor1=(position-remain1)/(L2*L3);

remain2=rem(remain1,L3);
factor2=(remain1-remain2)/(L3);

Final_k1=factor1
Final_k2=factor2
Final_k3=remain2
```

APPENDIX E

POLYMATH CODE FOR METHANE DEHYROAROMATIZATION

Appendix E shows the Polymath code for MDA simulation in Chapter 5.

```
# PBR - MDA test

d(FM)/d(V) = -2 * k1 * FM * (P / FT) * (1 - eta1)
FM(0) = 0.028616327
FMo = 0.028616327 # CH4 feed rate (mole/hr)

d(FH)/d(V) = 2 * k1 * FM * (P / FT) * (1 - eta1) + 3 * k2 * FE * (P / FT) * (1 - eta2) + 3 * k3 * FE *
FB * (P / FT) ^ 2 * (1 - eta3)
FH(0) = 0.0000001 # non-zero for eta calc at V = 0

d(FE)/d(V) = k1 * FM * (P / FT) * (1 - eta1) - 3 * k2 * FE * (P / FT) * (1 - eta2) - 2 * k3 * FE * FB *
(P / FT) ^ 2 * (1 - eta3)
FE(0) = 0.0000001 # non-zero for eta calc at V = 0

d(FB)/d(V) = k2 * FE * (P / FT) * (1 - eta2) - k3 * FE * FB * (P / FT) ^ 2 * (1 - eta3)
FB(0) = 0.0000001 # non-zero for eta calc

d(FN)/d(V) = k3 * FE * FB * (P / FT) ^ 2 * (1 - eta3)
FN(0) = 0.0000001 # non-zero for eta calc

V(0) = 0
V(f) = 4.9 # catalyst volume in cm3

eta1 = FE * FH ^ 2 * (P / FT) / FM ^ 2 / Kp1
eta2 = FB * FH ^ 3 * (P / FT) / FE ^ 3 / Kp2
eta3 = FN * FH ^ 3 * (P / FT) / FB / FE ^ 2 / Kp3

k1 = 0.064
k2 = 0.08
k3 = 2.61

Kp1 = 1.630E-05
Kp2 = 1.790E+05
Kp3 = 1.063E+04

P = 0.99 # pressure in atm
FT = FM + FE + FH + FB + FN + FHE # mole/hr
FHE = 0.001506122
T = 948 # temp in K
X_M = (FMo - FM) / FMo

yH = FH / FT
yM = FM / FT
yE = FE / FT
yB = FB / FT
yN = FN / FT
yHE = FHE / FT
```

APPENDIX F

DATA OF DRY REFORMING OVER PT/PD-CNT/ZEOLITE

Table F.1 to F.18 show all DR over Pt/Pd-CNT/zeolite data in Chapter 6.

Table F.1 Reactants and Products Mole Fractions from Experiments at 66.7 sccm

T/K	Feed CH_4/CO_2	Reactants Mole Fractions (%)		Products Mole Fractions (%)				
		CH_4	CO_2	CH_4	CO_2	H_2	CO	H_2O
923	0.49	4.72	9.65	1.73	5.22	3.10	5.98	2.88
	0.76	6.27	8.27	2.92	4.60	4.77	5.41	1.93
	1.01	7.06	7.01	3.68	3.35	5.34	5.90	1.42
	1.48	8.61	5.80	5.00	2.43	5.82	5.34	1.40
	1.99	9.60	4.83	5.95	1.87	6.19	4.81	1.11
873	0.47	4.71	10.04	3.37	7.84	1.68	3.40	1.00
	0.72	6.31	8.72	4.67	6.42	1.93	3.25	1.35
	0.99	7.52	7.61	5.8	5.35	2.26	3.34	1.18
	1.46	8.89	6.07	7.03	3.99	2.67	3.11	1.05
	1.96	10.06	5.14	8.19	2.90	2.22	2.96	1.52
823	0.52	4.80	9.29	4.14	8.16	0.71	1.65	0.61
	0.78	6.09	7.83	5.30	6.66	1.03	1.79	0.55
	1.02	6.96	6.81	6.17	5.61	0.94	1.76	0.64
	1.52	8.34	5.50	7.58	4.41	1.02	1.68	0.50
	2.03	9.59	4.73	8.78	3.72	1.25	1.65	0.37
773	0.49	4.62	9.45	4.31	8.83	0.19	0.81	0.43
	0.78	6.26	8.04	5.95	7.48	0.29	0.79	0.33
	1.02	7.57	7.40	7.14	6.76	0.37	0.79	0.49
	1.49	8.40	5.63	8.14	5.13	0.32	0.80	0.20
	2.03	9.62	4.75	9.32	4.27	0.42	0.78	0.18

Table F.2 Reactants and Products Mole Fractions from Various Flow Rate Experiments

T/K	Flow Rate (sccm)	Feed CH_4/CO_2	Reactants Mole Fractions (%)		Products Mole Fractions (%)				
			CH_4	CO_2	CH_4	CO_2	H_2	CO	H_2O
923	**44.6**	0.98	7.07	7.2	3.71	3.75	4.97	5.15	1.75
	66.6	1.01	7.06	7.01	3.68	3.35	5.34	5.9	1.42
	100	1.02	7.34	7.2	4.13	4.14	4.8	4.5	1.62
	133.3	1.01	6.5	6.41	3.64	3.8	4.15	3.65	1.57
873	**44.6**	0.98	6.64	6.76	4.51	4.13	3.12	4.14	1.12
	66.6	1.02	6.98	6.85	4.69	4.47	3.69	3.87	0.89
	100	1.02	6.8	6.66	4.77	4.2	2.97	3.83	1.09
	133.3	1.03	6.03	5.88	4.34	3.93	2.5	3.02	0.88

Table F.3 CH_4 and CO_2 Conversions from Experiments at 66.7 sccm

T/K	Feed CH_4/CO_2	Conversions (%)		T/K	Feed CH_4/CO_2	Conversions (%)	
		CH_4	CO_2			CH_4	CO_2
923	0.49	63.36	38.04	**873**	0.47	28.56	21.98
	0.76	53.42	44.4		0.72	25.98	26.41
	1.01	47.82	52.3		0.99	22.89	29.67
	1.48	41.98	58.15		1.46	20.89	34.35
	1.99	38.08	61.11		1.96	18.62	43.51
823	0.52	13.84	12.18	**773**	0.49	6.7	6.44
	0.78	12.91	14.99		0.78	5.02	7
	1.02	11.38	17.58		1.02	5.73	8.7
	1.52	9.19	19.82		1.49	3.04	8.76
	2.03	8.43	21.4		2.03	3.2	10.07

Table F.4 CH_4 and CO_2 Conversions from Various Flow Rate Experiments

T/K	Flow Rate (sccm)	Feed CH_4/CO_2	Conversions (%)		T/K	Flow Rate (sccm)	Feed CH_4/CO_2	Conversions (%)	
			CH_4	CO_2				CH_4	CO_2
923	**44.6**	0.98	47.54	48.01	**873**	**44.6**	0.98	32.05	38.94
	66.6	1.01	47.82	52.30		**66.6**	1.02	32.89	34.79
	100	1.02	43.65	42.57		**100**	1.02	30.28	36.98
	133.3	1.01	30.56	40.79		**133.3**	1.03	28.04	33.19

Table F.5 Reactants and Products Mole Fractions from Equilibrium Calculation

T/K	Feed CH_4/CO_2	Reactants Mole Fractions (%)		Products Mole Fractions (%)				
		CH_4	CO_2	CH_4	CO_2	H_2	CO	H_2O
923	0.49	4.72	9.65	0.02	5.26	4.60	2.88	4.12
	0.76	6.27	8.27	0.06	3.77	6.50	2.74	4.39
	1.01	7.06	7.01	0.10	2.84	8.02	2.53	4.40
	1.48	8.61	5.80	0.18	1.78	10.27	2.15	4.15
	1.99	9.60	4.83	0.26	1.84	11.85	1.84	3.82
873	0.47	4.71	10.04	0.04	5.53	3.91	1.69	4.78
	0.72	6.31	8.72	0.09	3.94	5.60	1.58	5.22
	0.99	7.52	7.61	0.16	2.93	6.99	1.45	5.32
	1.46	8.89	6.07	0.30	1.79	9.11	1.20	5.11
	1.96	10.06	5.14	0.44	1.19	10.63	1.00	4.74
823	0.52	4.80	9.29	0.06	5.57	3.15	0.88	5.51
	0.78	6.09	7.83	0.14	3.88	4.60	0.81	6.13
	1.02	6.96	6.81	0.25	2.81	5.84	0.72	6.30
	1.52	8.34	5.50	0.49	1.62	7.79	0.57	6.10
	2.03	9.59	4.73	0.72	1.03	9.24	0.46	5.65
773	0.49	4.62	9.45	0.08	5.44	2.36	0.40	6.25
	0.78	6.26	8.04	0.21	3.65	3.56	0.36	7.05
	1.02	7.57	7.40	0.38	2.54	4.62	0.31	7.30
	1.49	8.40	5.63	0.77	1.34	6.35	0.24	7.06
	2.03	9.62	4.75	1.15	0.78	7.69	0.18	6.49

Table F.6 CH_4 and CO_2 Conversions from Equilibrium Calculation

T/K	Feed CH_4/CO_2	Conversions (%)		T/K	Feed CH_4/CO_2	Conversions (%)	
		CH_4	CO_2			CH_4	CO_2
923	0.49	99.54	45.17	**873**	0.47	99.24	42.42
	0.76	99.10	54.15		0.72	98.52	52.15
	1.01	98.66	60.57		0.99	97.78	59.27
	1.48	97.90	69.15		1.46	96.49	68.94
	1.99	97.30	61.60		1.96	95.45	75.19
823	0.52	98.85	41.95	**773**	0.49	98.40	43.29
	0.78	97.69	52.84		0.78	96.62	55.64
	1.02	96.47	60.91		1.02	94.67	64.77
	1.52	94.27	71.81		1.49	91.04	76.71
	2.03	92.49	78.63		2.03	88.00	83.66

Table F.7 CH_4 and CO_2 Conversions from Power Law Model at 66.7 sccm

T/K	Feed CH_4/CO_2	Conversions (%)		T/K	Feed CH_4/CO_2	Conversions (%)	
		CH_4	CO_2			CH_4	CO_2
923	0.49	63.36	45.91	**873**	0.47	33.54	25.83
	0.76	57.36	47.64		0.72	29.25	29.68
	1.01	49.52	54.00		0.99	25.54	33.17
	1.48	42.02	58.23		1.46	20.87	34.17
	1.99	36.49	58.81		1.96	17.24	40.43
823	0.52	15.35	12.18	**773**	0.49	6.69	6.54
	0.78	13.01	14.99		0.78	5.68	7.99
	1.02	11.26	17.58		1.02	5.24	7.98
	1.52	9.08	19.82		1.49	3.94	11.31
	2.03	7.86	21.4		2.03	3.35	10.84

Table F.8 CH_4 and CO_2 Conversions from Power Law Model for Various Flow Rate

T/K	Flow Rate (sccm)	Feed CH_4/CO_2	Conversions (%)		T/K	Flow Rate (sccm)	Feed CH_4/CO_2	Conversions (%)	
			CH_4	CO_2				CH_4	CO_2
923	**44.6**	0.98	59.97	60.46	**873**	**44.6**	0.98	30.44	36.91
	66.6	1.01	49.39	54.36		**66.6**	1.02	24.40	25.84
	100	1.02	41.54	40.37		**100**	1.02	17.08	21.13
	133.3	1.01	32.34	29.93		**133.3**	1.03	12.13	14.35

Table F.9 Reactants and Products Mole Fractions from 3-Reaction Model at 66.7 sccm

T/K	Feed CH_4/CO_2	Reactants Mole Fractions (%)		Products Mole Fractions (%)				
		CH_4	CO_2	CH_4	CO_2	H_2	CO	H_2O
923	0.49	4.72	9.65	2.04	5.90	3.68	5.43	1.81
	0.76	6.27	8.27	2.90	4.47	4.65	5.57	1.68
	1.01	7.06	7.01	3.65	3.59	5.27	5.44	1.56
	1.48	8.61	5.80	4.80	2.49	6.02	4.97	1.33
	1.99	9.60	4.83	5.67	1.85	6.36	4.51	1.21
873	0.47	4.71	10.04	3.33	7.38	1.79	3.57	1.19
	0.72	6.31	8.72	4.51	5.88	2.26	3.68	1.13
	0.99	7.52	7.61	5.45	4.92	2.55	3.62	1.07
	1.46	8.89	6.07	6.88	3.68	2.79	3.38	0.89
	1.96	10.06	5.14	7.89	2.91	2.85	3.03	0.83
823	0.52	4.80	9.29	4.29	8.70	0.72	1.75	0.60
	0.78	6.09	7.83	5.61	7.23	0.90	1.87	0.60
	1.02	6.96	6.81	6.63	6.21	1.02	1.81	0.54
	1.52	8.34	5.50	8.08	4.83	1.09	1.69	0.48
	2.03	9.59	4.73	9.11	3.98	1.09	1.51	0.42
773	0.49	4.62	9.45	4.69	9.37	0.22	0.79	0.31
	0.78	6.26	8.04	6.08	7.97	0.29	0.85	0.30
	1.02	7.57	7.40	7.12	6.87	0.33	0.85	0.28
	1.49	8.40	5.63	8.64	5.48	0.36	0.73	0.24
	2.03	9.62	4.75	9.68	4.50	0.36	0.67	0.21

Table F.10 Mole Fractions from 3-Reaction Model for Various Flow Rate

T/K	Flow Rate (sccm)	Feed CH_4/CO_2	Reactants Mole Fractions (%)		Products Mole Fractions (%)				
			CH_4	CO_2	CH_4	CO_2	H_2	CO	H_2O
923	44.6	0.98	7.07	7.2	2.87	3.20	6.64	6.15	1.64
	66.6	1.01	7.06	7.01	3.65	3.59	5.27	5.44	1.56
	100	1.02	7.34	7.2	4.46	4.14	3.95	4.65	1.49
	133.3	1.01	6.5	6.41	4.99	4.54	3.10	4.01	1.36
873	44.6	0.98	6.64	6.76	4.88	4.46	3.45	4.38	1.18
	66.6	1.02	6.98	6.85	5.45	4.92	2.55	3.62	1.07
	100	1.02	6.8	6.66	5.99	5.47	1.76	2.83	0.92
	133.3	1.03	6.03	5.88	6.31	5.80	1.29	2.34	0.78

Table F.11 Mole Fractions from Chemkin with High Density for Various Flow Rate

T/K	Flow Rate (sccm)	Feed CH_4/CO_2	Reactants Mole Fractions (%)		Products Mole Fractions (%)				
			CH_4	CO_2	CH_4	CO_2	H_2	CO	H_2O
923	44.6	0.98	7.07	7.2	2.31	1.73	7.63	9.04	0.7
	66.6	1.01	7.06	7.01	2.35	1.63	7.58	8.92	0.67
	100	1.02	7.34	7.2	2.5	1.68	7.75	9.13	0.69
	133.3	1.01	6.5	6.41	2.11	1.43	7.18	8.36	0.59
873	44.6	0.98	6.64	6.76	3.16	2.53	5.42	6.89	0.74
	66.6	1.02	6.98	6.85	3.41	2.54	5.53	7.01	0.74
	100	1.02	6.8	6.66	3.3	2.45	5.45	6.88	0.72
	133.3	1.03	6.03	5.88	2.84	2.08	5.08	6.31	0.62

Table F.12 Conversions from Chemkin with High Density for Various Flow Rate

T/K	Flow Rate (sccm)	Feed CH_4/CO_2	Conversions (%)		T/K	Flow Rate (sccm)	Feed CH_4/CO_2	Conversions (%)	
			CH_4	CO_2				CH_4	CO_2
923	**44.6**	0.98	67.33	75.97	**873**	**44.6**	0.98	52.41	62.57
	66.6	1.01	66.71	76.75		**66.6**	1.02	51.15	62.92
	100	1.02	65.94	76.67		**100**	1.02	51.47	63.21
	133.3	1.01	67.54	77.69		**133.3**	1.03	52.90	64.63

Table F.13 Mole Fractions from Chemkin with High Density at 66.7 sccm

T/K	Feed CH_4/CO_2	Reactants Mole Fractions (%)		Products Mole Fractions (%)				
		CH_4	CO_2	CH_4	CO_2	H_2	CO	H_2O
923	0.49	4.72	9.65	0.63	3.88	6.16	8.78	1.31
	0.76	6.27	8.27	1.59	2.47	7.38	9.27	0.95
	1.01	7.06	7.01	2.35	1.63	7.58	8.92	0.67
	1.48	8.61	5.80	3.89	0.91	7.66	8.46	0.4
	1.99	9.60	4.83	5.15	0.51	7.24	7.7	0.23
873	0.47	4.71	10.04	1.39	5.15	4.82	7.32	1.25
	0.72	6.31	8.72	2.62	3.84	5.52	7.58	1.03
	0.99	7.52	7.61	3.7	2.94	5.81	7.49	0.84
	1.46	8.89	6.07	5.11	1.89	5.84	7.01	0.58
	1.96	10.06	5.14	6.35	1.31	5.76	6.6	0.42
823	0.52	4.80	9.29	2.47	5.79	3.26	5.23	0.98
	0.78	6.09	7.83	3.65	4.48	3.52	5.18	0.83
	1.02	6.96	6.81	4.49	3.64	3.62	5.04	0.71
	1.52	8.34	5.50	5.87	2.6	3.69	4.78	0.55
	2.03	9.59	4.73	7.11	2.01	3.71	4.6	0.44
773	0.49	4.62	9.45	3.18	7.12	1.88	3.4	0.76
	0.78	6.26	8.04	4.72	5.78	2.06	3.41	0.67
	1.02	7.57	7.40	5.96	5.16	2.18	3.43	0.63
	1.49	8.40	5.63	6.86	3.67	2.16	3.13	0.49
	2.03	9.62	4.75	8.08	2.92	2.18	3.00	0.41

Table F.14 CH_4 and CO_2 Conversions from Chemkin with High Density at 66.7 sccm

T/K	Feed CH_4/CO_2	Conversions (%)		T/K	Feed CH_4/CO_2	Conversions (%)	
		CH_4	CO_2			CH_4	CO_2
923	0.49	86.65	59.79	**873**	0.47	70.49	48.71
	0.76	74.64	70.13		0.72	58.48	55.96
	1.01	66.71	76.75		0.99	50.80	61.37
	1.48	54.82	84.31		1.46	42.52	68.86
	1.99	46.35	89.44		1.96	36.88	74.51
823	0.52	48.54	37.67	**773**	0.49	31.17	24.66
	0.78	40.07	42.78		0.78	24.60	28.11
	1.02	35.49	46.55		1.02	21.27	30.27
	1.52	29.62	52.73		1.49	18.33	34.81
	2.03	25.86	57.51		2.03	16.01	38.53

Table F.15 Mole Fractions from Chemkin with Low Density for Various Flow Rate

T/K	Flow Rate (sccm)	Feed CH_4/CO_2	Reactants Mole Fractions (%)		Products Mole Fractions (%)				
			CH_4	CO_2	CH_4	CO_2	H_2	CO	H_2O
923	**44.6**	0.98	7.07	7.2	6.25	4.99	0.0465	2.82	1.39
	66.6	1.01	7.06	7.01	6.27	4.89	0.0436	2.71	1.33
	100	1.02	7.34	7.2	6.57	5.12	0.0402	2.66	1.31
	133.3	1.01	6.5	6.41	5.82	4.55	0.0365	2.39	1.18
873	**44.6**	0.98	6.64	6.76	6.1	5.29	0.0256	1.89	0.93
	66.6	1.02	6.98	6.85	6.45	5.41	0.0241	1.85	0.91
	100	1.02	6.8	6.66	6.3	5.31	0.0216	1.73	0.86
	133.3	1.03	6.03	5.88	5.59	4.68	0.0195	1.55	0.76

Table F.16 Conversions from Chemkin with Low Density for Various Flow Rate

T/K	Flow Rate (sccm)	Feed CH_4/CO_2	Conversions (%)		T/K	Flow Rate (sccm)	Feed CH_4/CO_2	Conversions (%)	
			CH_4	CO_2				CH_4	CO_2
923	**44.6**	0.98	11.60	30.69	**873**	**44.6**	0.98	8.13	21.75
	66.6	1.01	11.19	30.24		**66.6**	1.02	7.59	21.02
	100	1.02	10.49	28.89		**100**	1.02	7.35	20.27
	133.3	1.01	10.46	29.02		**133.3**	1.03	7.30	20.41

Table F.17 Mole Fractions from Chemkin with Low Density at 66.7 sccm

T/K	Feed CH_4/CO_2	Reactants Mole Fractions (%)		Products Mole Fractions (%)				
		CH_4	CO_2	CH_4	CO_2	H_2	CO	H_2O
923	0.49	4.72	9.65	3.9	7.28	0.0355	2.98	1.47
	0.76	6.27	8.27	5.44	5.99	0.0407	2.89	1.43
	1.01	7.06	7.01	6.27	4.89	0.0436	2.71	1.33
	1.48	8.61	5.80	7.86	3.84	0.048	2.52	1.24
	1.99	9.60	4.83	8.89	3.05	0.051	2.32	1.13
873	0.47	4.71	10.04	4.14	8.4	0.0193	2.06	1.02
	0.72	6.31	8.72	5.73	7.11	0.0222	2.03	1.01
	0.99	7.52	7.61	6.95	6.07	0.0243	1.97	0.97
	1.46	8.89	6.07	8.35	4.66	0.0267	1.81	0.89
	1.96	10.06	5.14	9.54	3.83	0.0285	1.7	0.83
823	0.52	4.80	9.29	4.46	8.3	0.0097	1.25	0.62
	0.78	6.09	7.83	5.75	6.87	0.0111	1.21	0.6
	1.02	6.96	6.81	6.62	5.89	0.0121	1.17	0.58
	1.52	8.34	5.50	8.02	4.65	0.0134	1.1	0.54
	2.03	9.59	4.73	9.27	3.92	0.0145	1.05	0.52
773	0.49	4.62	9.45	4.43	8.89	0.004	0.7	0.35
	0.78	6.26	8.04	6.06	7.49	0.0048	0.7	0.35
	1.02	7.57	7.40	7.37	6.85	0.0053	0.7	0.35
	1.49	8.40	5.63	8.21	5.13	0.0059	0.64	0.32
	2.03	9.62	4.75	9.43	4.28	0.0065	0.62	0.3

Table F.18 CH_4 and CO_2 Conversions from Chemkin with Low Density at 66.7 sccm

T/K	Feed CH_4/CO_2	Conversions (%)		T/K	Feed CH_4/CO_2	Conversions (%)	
		CH_4	CO_2			CH_4	CO_2
923	0.49	17.37	24.56	**873**	0.47	12.10	16.33
	0.76	13.24	27.57		0.72	9.19	18.46
	1.01	11.19	30.24		0.99	7.58	20.24
	1.48	8.71	33.79		1.46	6.07	23.23
	1.99	7.40	36.85		1.96	5.17	25.49
823	0.52	7.08	10.66	**773**	0.49	4.11	5.93
	0.78	5.58	12.26		0.78	3.19	6.84
	1.02	4.89	13.51		1.02	2.64	7.43
	1.52	3.84	15.45		1.49	2.26	8.88
	2.03	3.34	17.12		2.03	1.98	9.89

APPENDIX G

POLYMATH CODE FOR POWER LAW MODEL OF DRY REFORMING OVER PT/PD-CNT/ZEOLITE

Appendix G shows the Polymath code for DR over Pt/Pd-CNT/zeolite simulation in Chapter 6.

```
# PFR Power Law- Dry Reforming test-Pt/Pd

d(yA)/d(W) = -k / FTo * (P / R / T) ^ (alpha + beta) * (yA ^ alpha) * (b ^ beta) * (yo + yA) ^ beta # PBR species balance for CH4 (using mole fraction)
yA(0) = 0.0706 # feed mole fraction of CH4 -- MUST be same as yAo value below

d(XA)/d(W) = k / FAo * (P / R / T * yAo) ^ (alpha + beta) * (1 - XA) ^ alpha * (yBo / b / yAo - XA) ^ beta * (b ^ beta) # PBR species balance for CH4 (using conversion)
XA(0) = 0 # inlet conversion

W(0) = 0 # initial catalyst mass (grams)
W(f) = 2.0 # final catalyst mass (grams)

yo = yBo / b - yAo # simplifying term
b = 1.0828 # converted CO2/converted CH4 (experiemental value)
yBo = 0.0701 # feed mole fraction of CO2
FTo = 66.67 / 82.1 * 1 / 298 # total molar rate at inlet (moles/min)
yAo = 0.0706 # feed mole fraction of CH4

P = (30 + 14.7) / 14.7 # reactor pressure (atm)
R = 82.1 # gas constant (cm^3-atm/mole-K)
T = 650 + 273 # reactor temperature (K)

alpha = 1 # kinetic parameter (order on CH4)
beta = 1 # kinetic parameter (order on CO2)
k = 1.24E7 # rate constant

FAo = yAo * FTo # Feed molar rate of CH4 (moles/min)
FBo = yBo * FTo # Feed molar rate of O2 (moles/min)
FA = yA * FTo # molar rate of CH4 in reactor (moles/min) assuming FT ~ FTo
FB = yB * FTo # molar rate of CO2 in reactor (moles/min) assuming FT ~ FTo
yB = b * (yo + yA) # mole fraction of CO2 in reactor
XB = 1 - FB / FBo
```

APPENDIX H

MATLAB CODE FOR DRY REFORMING OVER PT/PD-CNT/ZEOLITE

Appendix H shows the Matlab code for DR over Pt/Pd-CNT/zeolite simulation in Chapter 6.

```
clear all
clc
close all

format compact

T=273+650;
kp1 = exp(-1 / T * 31247 + 34.105);
kp2 = exp(-1 / T * 4386.6 + 4.0251);
kp3 = exp(-1 / T * 21136 + 25.766);

 P=3.04;

Fhe=[0.139 0.139 0.139 0.139 0.139 0.097 0.208 0.278];

FM_test=[0.002824631 0.004767585 0.006008464 0.008163673 0.009714771
0.004240303 0.010114286 0.011886309 ];
FCD_test=[0.008522875 0.007510580 0.005469661 0.003967545 0.003053214
0.004286020 0.010138776 0.012408784 ];
FH_test=[0.005061478 0.007788144 0.008718803 0.009502516 0.010106628
0.005680406 0.011755102 0.013551698 ];
FCo_test=[0.009763753 0.008833095 0.009633135 0.008718803 0.007853454
0.005886135 0.011020408 0.011918963 ];
Fw_test=[0.004702276 0.003151178 0.002318483 0.002285829 0.001812336
0.002000143 0.003967347 0.005126787 ];

FM1=[0.008163673 0.010498484 0.012245510 0.014694612 0.016327347
0.008572041 0.018367347 0.024491020 ];
FCD1=[0.016327347 0.013992536 0.012245510 0.009796408 0.008163673
0.008572041 0.018367347 0.024491020 ];
FH1=[0.0000001 0.0000001 0.0000001 0.0000001  0.0000001 0.0000001
0.0000001 0.0000001 0.0000001];
FCo1=[0.0000001 0.0000001 0.0000001 0.0000001 0.0000001 0.0000001
0.0000001 0.0000001 0.0000001];
Fw1=[0.0000001 0.0000001 0.0000001 0.0000001 0.0000001 0.0000001
0.0000001 0.0000001 0.0000001];

stepsize=0.001;
w=[0:stepsize:2];

k1 = [0:0.01:0.1];
k2 = [0.025:0.001:0.035];
k3 = [0.008:0.0001:0.009];

L1= length(k1);
L2= length(k2);
```

```
L3= length(k3);

for jj=1:length(FM1)
    jj

final_FM =[];
final_FH=[];
final_FCD=[];
final_FW =[];
final_FCo=[];
FM=[];
FH=[];
FCD=[];
FCo=[];
Fw=[];
FT=[];

for i1=1:L1;
    i1
for i2=1:L2;
for i3=1:L3;

 FM=[FM1(jj) zeros(1,length(w)-1)];
 FH=[FH1(jj)  zeros(1,length(w)-1)];
 FCD=[FCD1(jj) zeros(1,length(w)-1)];
 FCo=[FCo1(jj) zeros(1,length(w)-1)];
 Fw=[Fw1(jj) zeros(1,length(w)-1)];
 FT=zeros(1,length(w)-1);

eta1=zeros(1,length(w)-1);
eta2=zeros(1,length(w)-1);
eta3=zeros(1,length(w)-1);

for j=2:length(w)
j;
FT(j-1)=FM(j-1)+FH(j-1)+FCD(j-1)+FCo(j-1)+Fw(j-1)+Fhe(jj);

eta1(j-1)=((P/FT(j-1))^2)*((FCo(j-1))^2)*((FH(j-1))^2)/(FM(j-1)*FCD(j-
1)*kp1);
eta2(j-1)=((FCo(j-1))^1)*((Fw(j-1))^1)/(FH(j-1)*FCD(j-1)*kp2);
eta3(j-1)=((P/FT(j-1))^1)*((FCo(j-1))^1)*((FH(j-1))^2)/(FM(j-1)*kp3);

FM(j)=FM(j-1)-(k1(i1)*FM(j-1)*FCD(j-1)*((P/FT(j-1))^2)*(1-eta1(j-
1))+k3(i3)*FM(j-1)*(P/FT(j-1))*(1-eta3(j-1)))*stepsize;
FH(j)=FH(j-1)+(2*k1(i1)*FM(j-1)*FCD(j-1)*((P/FT(j-1))^2)*(1-eta1(j-1))-
k2(i2)*FCD(j-1)*((P/FT(j-1))^1)*(1-eta2(j-1))+2*k3(i3)*FM(j-1)*(P/FT(j-
1))*(1-eta3(j-1)))*stepsize;
FCD(j)=FCD(j-1)-(k1(i1)*FM(j-1)*FCD(j-1)*((P/FT(j-1))^2)*(1-eta1(j-
1))+k2(i2)*FCD(j-1)*((P/FT(j-1))^1)*(1-eta2(j-1)))*stepsize;

FCo(j)=FCo(j-1)+(2*k1(i1)*FM(j-1)*FCD(j-1)*((P/FT(j-1))^2)*(1-eta1(j-
1))+k2(i2)*FCD(j-1)*((P/FT(j-1))^1)*(1-eta2(j-1)))*stepsize;

Fw(j)=Fw(j-1)+(k2(i2)*FCD(j-1)*((P/FT(j-1))^1)*(1-eta2(j-1)))*stepsize;
```

```
end

final_FM=[final_FM FM(end-1)];
final_FCD=[final_FCD FCD(end-1)];
final_FH=[final_FH FH(end-1)];
final_FCo=[final_FCo FCo(end-1)];
final_FW=[final_FW Fw(end-1)];

end
end
end

FINAL_FM(jj,:)=final_FM
FINAL_CD(jj,:)=final_FCD
FINAL_FH(jj,:)=final_FH
FINAL_FW(jj,:)=final_FW
FINAL_Co(jj,:)=final_FCo
end

MMSE_temp=0;
for ii=1:length(FM_test)
MMSE_temp=MMSE_temp+((FINAL_FM(ii,:)-FM_test(ii))/FM_test(ii)).^2
+((FINAL_CD(ii,:)-FCD_test(ii))/FCD_test(ii)).^2+((FINAL_Co(ii,:)-
FCo_test(ii))/FCo_test(ii)).^2+((FINAL_FH(ii,:)-
FH_test(ii))/FH_test(ii)).^2+((FINAL_FW(ii,:)-
Fw_test(ii))/Fw_test(ii)).^2;
end
MMSE=MMSE_temp/(5*length(FM_test));
sizeMMSE=size(MMSE)
min_MMSE=min(MMSE)
position=find(MMSE==min_MMSE)-1;

 remain1=rem(position,L2*L3);
 factor1=(position-remain1)/(L2*L3);

remain2=rem(remain1,L3);
factor2=(remain1-remain2)/(L3);

Final_k1=factor1
Final_k2=factor2
Final_k3=remain2
```

APPENDIX I

POLYMATH CODE FOR 3-REACTION MODEL OF DRY REFORMING OVER PT/PD-CNT/ZEOLITE

Appendix I shows the Polymath code for 3-reaction model simulation in Chapter 6.

```
# PFR 3-Reaction Model - Dry Reforming test-Pt/Pd

d(FM)/d(W) = -k1 * FM * FCD * (P / FT) ^ 2 * (1 - eta1) - k3 * FM * (P / FT) * (1 - eta3)

FM(0) = 0.011527107
FMo = 0.011527107 # CH4 feed rate (mole/hr)

d(FH)/d(W) = 2 * k1 * FM * FCD * (P / FT) ^ 2 * (1 - eta1) - k2 * FCD * (P / FT) ^ 1 * (1 - eta2) + 2
* k3 * FM * (P / FT) * (1 - eta3)

FH(0) = 0.0000001 # non-zero for eta calc at W = 0

d(FCD)/d(W) = -k1 * FM * FCD * (P / FT) ^ 2 * (1 - eta1) - k2 * FCD * (P / FT) ^ 1 * (1 - eta2)
FCD(0) = 0.011445470
FCDo = 0.011445470 # CO2 feed rate (mole/hr)

d(FCO)/d(W) = 2 * k1 * FM * FCD * (P / FT) ^ 2 * (1 - eta1) + k2 * FCD * (P / FT) ^ 1 * (1 - eta2)
FCO(0) = 0.0000001 # non-zero for eta calc

d(FW)/d(W) = k2 * FCD * (P / FT) ^ 1 * (1 - eta2)
FW(0) = 0.0000001 # non-zero for eta calc

W(0) = 0
W(f) = 2. # catalyst mass

eta1 = FCO ^ 2 * FH ^ 2 * (P / FT) ^ 2 / FM / FCD / Kp1
eta2 = FW * FCO / FCD / FH / Kp2
eta3 = FH ^ 2 * (P / FT) / FM / Kp3

k1 = 0.07
k2 = 0.029
k3 = 0.0082

Kp1 = exp(-1 / T * 31247 + 34.105)
Kp2 = exp(-1 / T * 4386.6 + 4.0251)
Kp3 = exp(-1 / T * 21136 + 25.766)
P = 3.04 # pressure in atm
FT = FM + FW + FH + FCO + FCD + FHE # mole/hr
FHE = 0.139
T = 273 + 650 # temp in K
X_M = (FMo - FM) / FMo
X_CD = (FCDo - FCD) / FCDo

H_CO_ratio = FH / FCO
```

APPENDIX J

EQUILIBRIUM CALCULATION FOR DRY REFORMING OVER PT/PD-CNT/ZEOLITE

Figure J.1 to J.4 show the equilibrium calculation procedures for a typical sample.

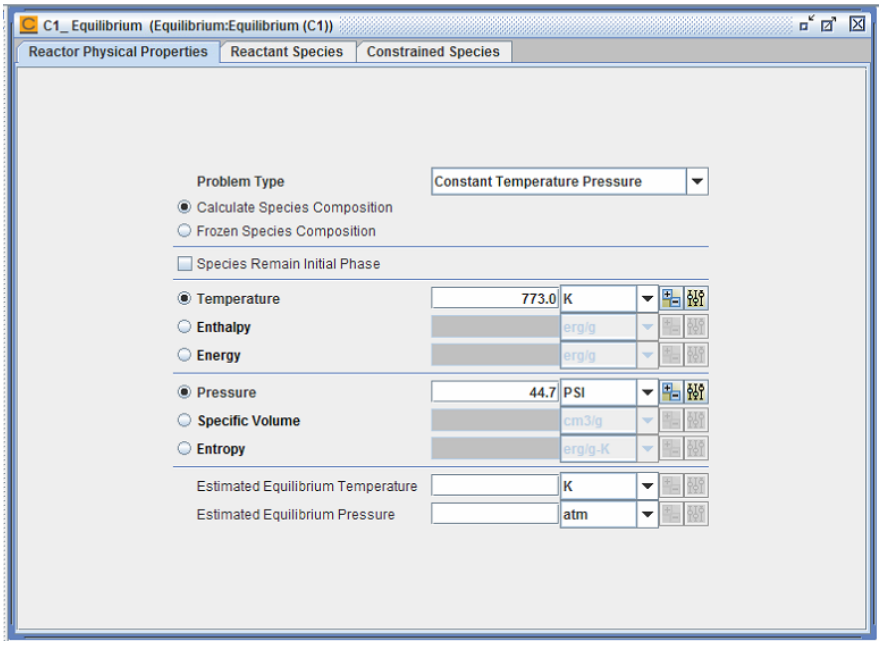

Figure J.1 Equilibrium Calculation Procedures for a Typical Sample (a).

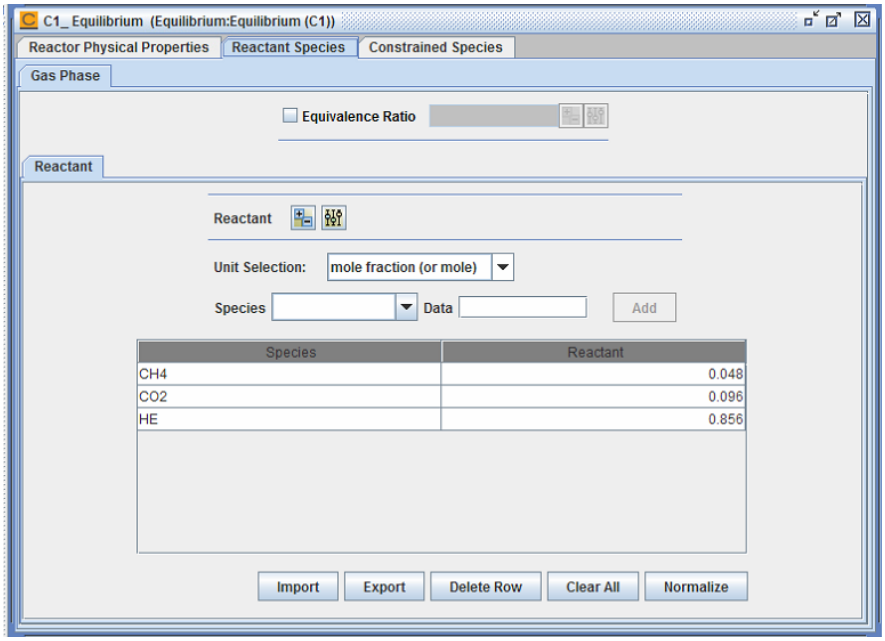

Figure J.2 Equilibrium Calculation Procedures for a Typical Sample (b).

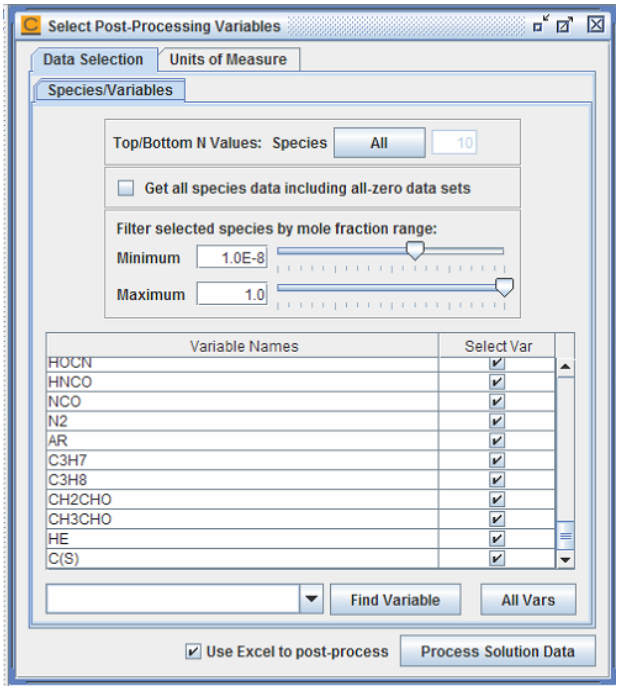

Figure J.3 Equilibrium Calculation Procedures for a Typical Sample (c).

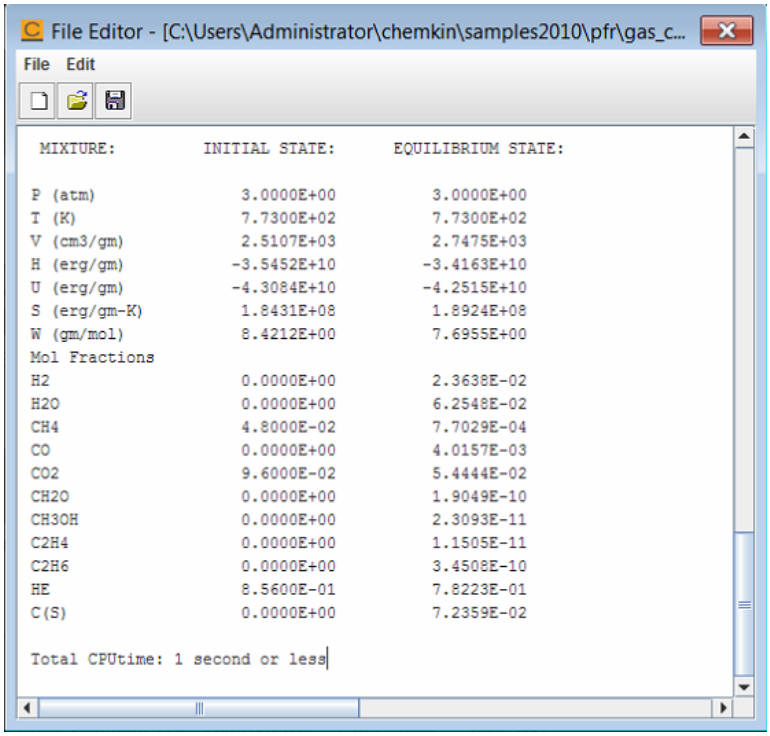

Figure J.4 Equilibrium Calculation Procedures for a Typical Sample (d).

APPENDIX K

CHEMKIN CODE FOR DRY REFORMING OVER PT/PD-CNT/ZEOLITE

Appendix K shows the Chemkin code for DR over Pt/Pd-CNT/zeolite simulation in Chapter 6.

```
!SURFACE MECHANISM OF CH4 REFORMING AND OXIDATION OVER NI
!************************************************************************
!****
!****     CH4 ON Ni - SURFACE MECHANISM
*
!****
!****     Version 1.2  (March 2006)
!****
!****     L. Maier, V. Janardhanan, B. Schaedel, O. Deutschmann
!****     ITCP, University of Karlsruhe, Germany
!****     Contact: mail@detchem.com (O. Deutschmann)
!****
!****     NOTE: That is a first version that needs further
!****           improvements,
!****           e.g. NiO formation, coking,
!****                temp. range 500-2000
!****
!****     References:
!****     L. Maier, B. Schaedel, S. Tischer, O. Deutschmann,
!****         submitted to Catal. Lett.
!****     V.M. Janardhanan, O. Deutschmann.
!****         Journal of Power Sources 162 (2006), 1192-1202
!****         Zeitschrift f. Phys. Chem. 221 (2007) 443-479
!****     www.detchem.com/mechanisms
!****
!****     Kinetic data:
!****      k = A * T**b * exp (-Ea/RT)          A          b        Ea
!****                                        (cm,mol,s)    -       J/mol
!****
!****
!****     Surface site density: 2.66E-9 mol/cm**2 (original)
!****     Site Density:  7.57E-11 (based on CO adsorp of Pt/Pd/CNT)
!****                    5.42E-11 (based on CO adsorp of Ru/CNT)
!****     (SURFACE CHEMKIN format)
!****
!************************************************************************
SITE   /NI_surface/   SDEN /2.66E-9/
```

```
     NI(s)              /1/
     H2O(s)             /1/
     H(s)               /1/
     OH(s)              /1/
     CO(s)              /1/
     C(s)               /1/
     CH3(s)             /1/
     CH2(s)             /1/
     CH(s)              /1/
     CH4(s)             /1/
     O(s)               /1/
     CO2(s)             /1/
     HCO(s)             /1/
END
THERMO ALL
   300.0   1000.0   5000.0
CH4             (adjust)  C   1H   4    0    0     300.00   5000.00 1000.00
 1.68347883E+00 1.02372356E-02-3.87512864E-06 6.78558487E-10-4.50342312E-14
-1.00807871E+04 9.62339497E+00 7.78741479E-01 1.74766835E-02-2.78340904E-05
 3.04970804E-08-1.22393068E-11-9.82522852E+03 1.37221947E+01
H2              (adjust)  H   2    0    0    0     300.00   5000.00 1000.00
 3.06670950E+00 5.74737550E-04 1.39383190E-08-2.54835180E-11 2.90985740E-15
-8.65474120E+02-1.77984240E+00 3.35535140E+00 5.01361440E-04-2.30069080E-07
-4.79053240E-10 4.85225850E-13-1.01916260E+03-3.54772280E+00
H2O             (adjust)  H   2O   1    0    0     300.00   5000.00 1000.00
 2.61104720E+00 3.15631300E-03-9.29854380E-07 1.33315380E-10-7.46893510E-15
-2.98681670E+04 7.20912680E+00 4.16772340E+00-1.81149700E-03 5.94712880E-06
-4.86920210E-09 1.52919910E-12-3.02899690E+04-7.31354740E-01
CO              (adjust)  C   1O   1    0    0     300.00   5000.00 1000.00
 3.02507806E+00 1.44268852E-03-5.63082779E-07 1.01858133E-10-6.91095156E-15
-1.42683496E+04 6.10821772E+00 3.26245165E+00 1.51194085E-03-3.88175522E-06
 5.58194424E-09-2.47495123E-12-1.43105391E+04 4.84889698E+00
CO2             (adjust)  C   1O   2    0    0     300.00   5000.00 1000.00
 4.45362282E+00 3.14016873E-03-1.27841054E-06 2.39399667E-10-1.66903319E-14
-4.89669609E+04-9.55395877E-01 2.27572465E+00 9.92207229E-03-1.04091132E-05
 6.86668678E-09-2.11728009E-12-4.83731406E+04 1.01884880E+01
O2              (adjust)  O   2    0    0    0     300.00   5000.00 1000.00
 3.61221390E+00 7.48531660E-04-1.98206470E-07 3.37490080E-11-2.39073740E-15
-1.19781510E+03 3.67033070E+00 3.78371350E+00-3.02336340E-03 9.94927510E-06
-9.81891010E-09 3.30318250E-12-1.06381070E+03 3.64163450E+00
AR              (adjust)  AR  1    0    0    0     300.00   5000.00 1000.00
 2.50000000E+00 0.00000000E+00 0.00000000E+00 0.00000000E+00 0.00000000E+00
-7.45375020E+02 4.36600060E+00 2.50000000E+00 0.00000000E+00 0.00000000E+00
 0.00000000E+00 0.00000000E+00-7.45374980E+02 4.36600060E+00
N2              (adjust)  N   2    0    0    0     300.00   5000.00 1000.00
```

2.85328990E+00 1.60221280E-03-6.29368930E-07 1.14410220E-10-7.80574650E-15
-8.90080930E+02 6.39648970E+00 3.70441770E+00-1.42187530E-03 2.86703920E-06
-1.20288850E-09-1.39546770E-14-1.06407950E+03 2.23362850E+00
NI(s)   (adjust) NI   1   0   0   0   300.00   3000.00 1000.00
0.00000000E+00 0.00000000E+00 0.00000000E+00 0.00000000E+00 0.00000000E+00
0.00000000E+00 0.00000000E+00 0.00000000E+00 0.00000000E+00 0.00000000E+00
0.00000000E+00 0.00000000E+00 0.00000000E+00 0.00000000E+00
H2O(s)   (adjust) H   2O   1NI 1   0   500.00   2000.00 2000.00
3.50421382E+00 6.68594839E-04 1.76268743E-06-1.17030152E-09 2.26185355E-13
-3.79129166E+04-1.05582534E+01 3.50421382E+00 6.68594839E-04 1.76268743E-06
-1.17030152E-09 2.26185355E-13-3.79129166E+04-1.05582534E+01
H(s)   (adjust) H   1NI 1   0   0   500.00   2000.00 2000.00
1.38522354E+00-3.60291509E-05 1.01482878E-06-6.39234047E-10 1.26064639E-13
-5.45886573E+03-5.04262898E+00 1.38522354E+00-3.60291509E-05 1.01482878E-06
-6.39234047E-10 1.26064639E-13-5.45886573E+03-5.04262898E+00
OH(s)   (adjust) H   1O   1NI 1   0   500.00   2000.00 2000.00
2.08905501E+00 1.71443903E-03-4.27838552E-07 9.11211411E-12 1.13760370E-14
-2.67334298E+04-3.86138841E+00 2.08905501E+00 1.71443903E-03-4.27838552E-07
9.11211411E-12 1.13760370E-14-2.67334298E+04-3.86138841E+00
CO(s)   (adjust) C   1O   1NI 1   0   500.00   2000.00 2000.00
1.04958397E+00 5.37825549E-03-3.51895909E-06 1.06323431E-09-1.12689240E-13
-2.73744388E+04 7.60559022E+00 1.04958397E+00 5.37825549E-03-3.51895909E-06
1.06323431E-09-1.12689240E-13-2.73744388E+04 7.60559022E+00
C(s)   (adjust) C   1NI 1   0   0   500.00   2000.00 2000.00
-3.49330914E+00 5.23524687E-03-3.03308918E-06 6.55611035E-10-1.40966550E-14
-2.23124726E+03 7.68421239E+00-3.49330914E+00 5.23524687E-03-3.03308918E-06
6.55611035E-10-1.40966550E-14-2.23124726E+03 7.68421239E+00
CH3(s)   (adjust) C   1H   3NI 1   0   500.00   2000.00 2000.00
-6.10760599E-01 8.61612510E-03-2.17714930E-06-6.63815294E-10 3.13819319E-13
-8.89792082E+03-2.00828704E+00-6.10760599E-01 8.61612510E-03-2.17714930E-06
-6.63815294E-10 3.13819319E-13-8.89792082E+03-2.00828704E+00
CH2(s)   (adjust) C   1H   2NI 1   0   500.00   2000.00 2000.00
-1.56917589E+00 7.30948876E-03-2.33683999E-06-2.63575385E-10 2.08877321E-13
1.94307500E+03 4.44265982E+00-1.56917589E+00 7.30948876E-03-2.33683999E-06
-2.63575385E-10 2.08877321E-13 1.94307500E+03 4.44265982E+00
CH(s)   (adjust) C   1H   1NI 1   0   500.00   2000.00 2000.00
-2.52762352E+00 6.00297402E-03-2.49669461E-06 1.36758705E-10 1.03915796E-13
9.56681068E+03 7.44010148E+00-2.52762352E+00 6.00297402E-03-2.49669461E-06
1.36758705E-10 1.03915796E-13 9.56681068E+03 7.44010148E+00
CH4(s)   (adjust) C   1H   4NI 1   0   500.00   2000.00 2000.00
3.47651462E-01 9.92277358E-03-2.01747493E-06-1.06404583E-09 4.18759375E-13
-1.38997273E+04-4.61646253E+00 3.47651462E-01 9.92277358E-03-2.01747493E-06
-1.06404583E-09 4.18759375E-13-1.38997273E+04-4.61646253E+00
O(s)   (adjust) O   1NI 1   0   0   500.00   2000.00 2000.00
9.33885773E-01 1.49287485E-03-1.51153811E-06 7.60133452E-10-1.42499395E-13

```
-2.88011883E+04-3.47247502E+00 9.33885773E-01 1.49287485E-03-1.51153811E-06
 7.60133452E-10-1.42499395E-13-2.88011883E+04-3.47247502E+00
CO2(s)          (adjust)  C    1O    2NI   1     0      500.00    2000.00 2000.00
 2.15782085E+00 8.85798101E-03-7.33295570E-06 3.01455469E-09-4.83617407E-13
-5.17211366E+04-3.96778204E-01 2.15782085E+00 8.85798101E-03-7.33295570E-06
 3.01455469E-09-4.83617407E-13-5.17211366E+04-3.96778204E-01
HCO(s)          (adjust)  C    1H    1O    1NI   1      500.00    2000.00 2000.00
 1.42054865E+00 6.41898600E-03-3.25611216E-06 6.60406470E-10-1.25958802E-14
-1.72299589E+04-1.34060408E+00 1.42054865E+00 6.41898600E-03-3.25611216E-06
 6.60406470E-10-1.25958802E-14-1.72299589E+04-1.34060408E+00
END
REACTIONS   KJOULES/MOLE
   H2      +   2NI(s)    =>   2H(s)                  1.000E-002  0.00      0.0
           STICK
  2H(s)                  =>    H2      +   2NI(s)   2.545E+019  0.00     81.2
   O2      +   2NI(s)    =>   2O(s)                  1.000E-002  0.00      0.0
           STICK
  2O(s)                  =>    O2      +   2NI(s)   4.283E+023  0.00    474.9
   CH4     +    NI(s)    =>    CH4(s)               8.000E-003  0.00      0.0
           STICK
   CH4(s)                =>    CH4     +    NI(s)   8.705E+015  0.00     37.5
   H2O     +    NI(s)    =>    H2O(s)               1.000E-001  0.00      0.0
           STICK
   H2O(s)                =>    H2O     +    NI(s)   3.732E+012  0.00     60.8
   CO2     +    NI(s)    =>    CO2(s)               1.000E-005  0.00      0.0
           STICK
   CO2(s)                =>    CO2     +    NI(s)   6.447E+007  0.00     26.0
   CO      +    NI(s)    =>    CO(s)                5.000E-001  0.00      0.0
           STICK
   CO(s)                 =>    CO      +    NI(s)   3.563E+011  0.00    111.3
           COV         /CO(s)                       0.000E+000  0.00    -50.0/
   H(s)    +    O(s)     =>    NI(s)   +    OH(s)   5.000E+022  0.00     97.9
   NI(s)   +    OH(s)    =>    H(s)    +    O(s)    1.781E+021  0.00     36.1
   H(s)    +    OH(s)    =>    NI(s)   +    H2O(s)  3.000E+020  0.00     42.7
   NI(s)   +    H2O(s)   =>    H(s)    +    OH(s)   2.271E+021  0.00     91.8
  2OH(s)                 =>    H2O(s)  +    O(s)    3.000E+021  0.00    100.0
   H2O(s)  +    O(s)     =>   2OH(s)                 6.373E+023  0.00    210.9
   C(s)    +    O(s)     =>    NI(s)   +    CO(s)   5.200E+023  0.00    148.1
   NI(s)   +    CO(s)    =>    C(s)    +    O(s)    1.354E+022 -3.00    116.1
           COV         /CO(s)                       0.000E+000  0.00    -50.0/
   CO(s)   +    O(s)     =>    NI(s)   +    CO2(s)  2.000E+019  0.00    123.6
           COV         /CO(s)                       0.000E+000  0.00    -50.0/
   NI(s)   +    CO2(s)   =>    CO(s)   +    O(s)    4.653E+023 -1.00     89.3
   NI(s)   +    HCO(s)   =>    H(s)    +    CO(s)   3.700E+021  0.00      0.0
           COV         /CO(s)                       0.000E+000  0.00     50.0/
```

```
    H(s)    +     CO(s)    =>     NI(s)    +     HCO(s)  4.019E+020 -1.00    132.2
    NI(s)   +     HCO(s)   =>     CH(s)    +     O(s)    3.700E+024 -3.00     95.8
    CH(s)   +     O(s)     =>     NI(s)    +     HCO(s)  4.604E+020  0.00    110.0
    NI(s)   +     CH4(s)   =>     H(s)     +     CH3(s)  3.700E+021  0.00     57.7
    H(s)    +     CH3(s)   =>     NI(s)    +     CH4(s)  6.034E+021  0.00     61.6
    NI(s)   +     CH3(s)   =>     H(s)     +     CH2(s)  3.700E+024  0.00    100.0
    H(s)    +     CH2(s)   =>     NI(s)    +     CH3(s)  1.293E+023  0.00     55.3
    NI(s)   +     CH2(s)   =>     H(s)     +     CH(s)   3.700E+024  0.00     97.1
    H(s)    +     CH(s)    =>     NI(s)    +     CH2(s)  4.089E+024  0.00     79.2
    NI(s)   +     CH(s)    =>     H(s)     +     C(s)    3.700E+021  0.00     18.8
    H(s)    +     C(s)     =>     NI(s)    +     CH(s)   4.562E+022  0.00    161.1
    CH4(s)  +     O(s)     =>     OH(s)    +     CH3(s)  1.700E+024  0.00     88.3
    OH(s)   +     CH3(s)   =>     CH4(s)   +     O(s)    9.876E+022  0.00     30.4
    CH3(s)  +     O(s)     =>     OH(s)    +     CH2(s)  3.700E+024  0.00    130.1
    OH(s)   +     CH2(s)   =>     CH3(s)   +     O(s)    4.607E+021  0.00     23.6
    CH2(s)  +     O(s)     =>     OH(s)    +     CH(s)   3.700E+024  0.00    126.8
    OH(s)   +     CH(s)    =>     CH2(s)   +     O(s)    1.457E+023  0.00     47.1
    CH(s)   +     O(s)     =>     OH(s)    +     C(s)    3.700E+021  0.00     48.1
    OH(s)   +     C(s)     =>     CH(s)    +     O(s)    1.625E+021  0.00    128.6
END
```

APPENDIX L

CHEMKIN SIMULATION FOR DRY REFORMING OVER PT/PD-CNT/ZEOLITE

Figure L.1 to L.4 show the Chemkin simulation procedures for a typical sample.

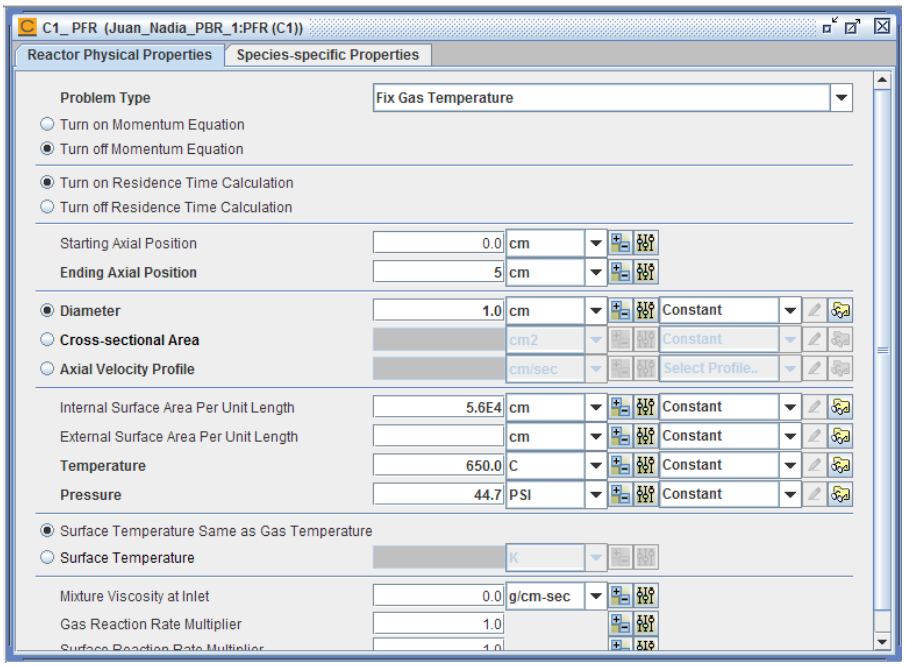

Figure L.1 Chemkin Simulation Procedures for a Typical Sample (a).

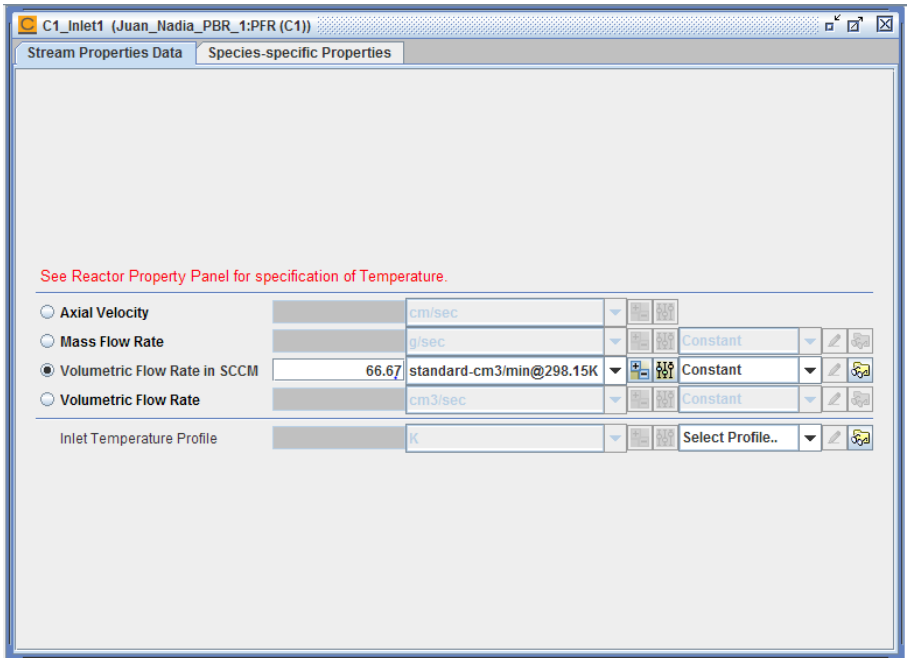

Figure L.2 Chemkin Simulation Procedures for a Typical Sample (b).

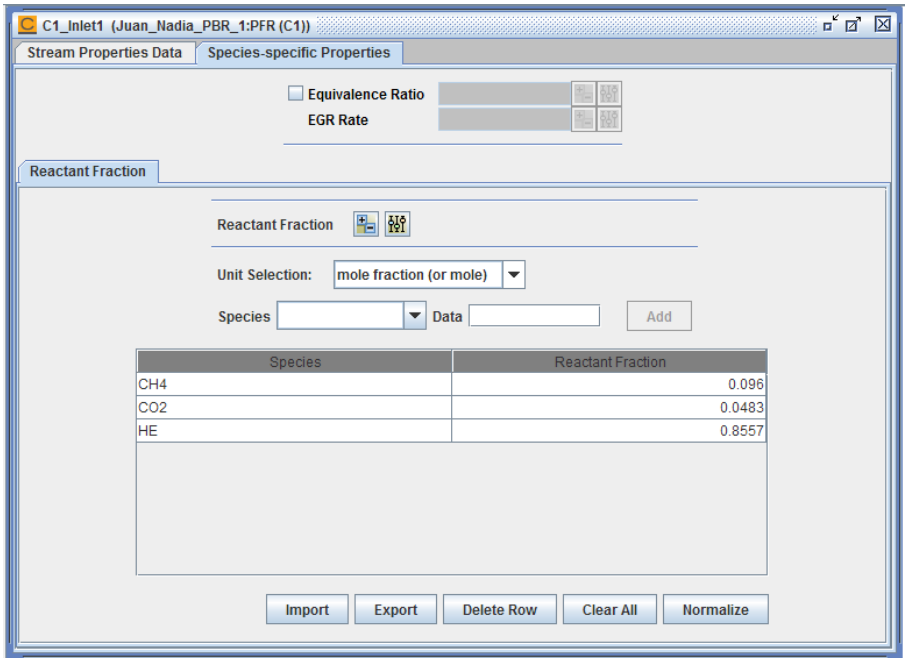

Figure L.3 Chemkin Simulation Procedures for a Typical Sample (c).

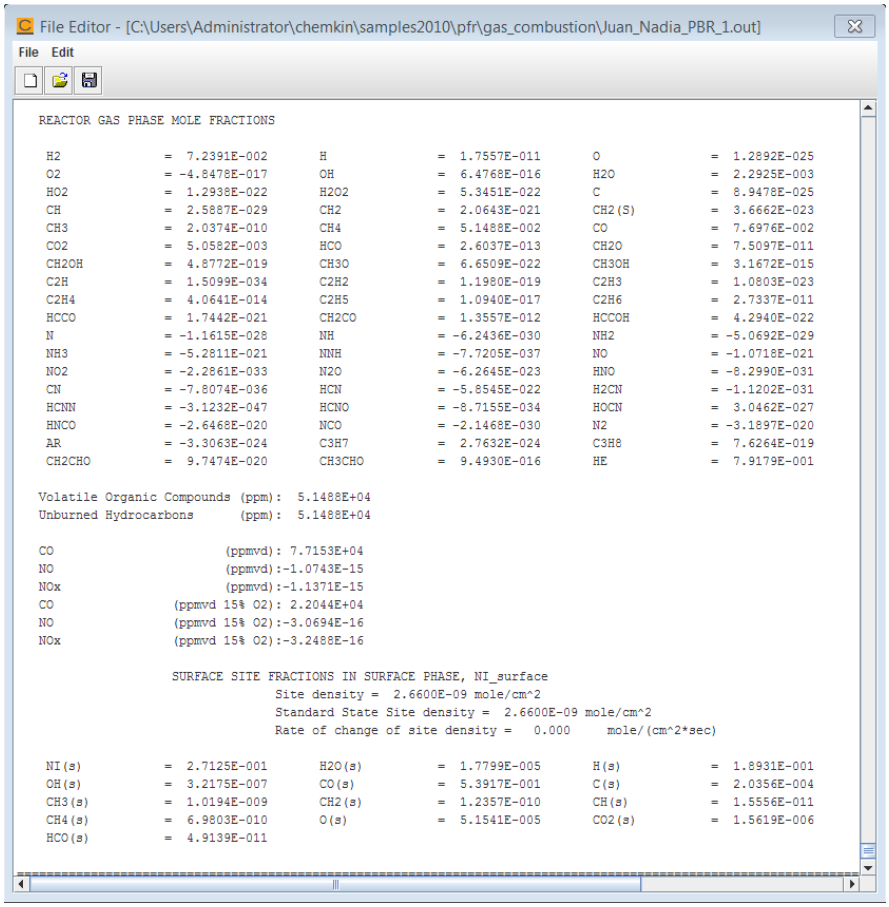

Figure L.4 Chemkin Simulation Procedures for a Typical Sample (d).

APPENDIX M

DATA OF DRY REFORMING OVER RU/CNT-ZEOLITE

Table M.1 to M.18 show the data of DR over Pt/Pd-CNT/zeolite in Chapter 7.

Table M.1 Reactants and Products Mole Fractions from Experiments at 66.7 sccm

T/K	Feed CH_4/CO_2	Reactants Mole Fractions (%)		Products Mole Fractions (%)				
		CH_4	CO_2	CH_4	CO_2	H_2	CO	H_2O
973	0.51	4.88	9.6	4.06	2.34	5.18	7.80	1.64
	0.77	6.17	8.02	4.95	1.65	4.64	7.92	1.22
	1.01	7.31	7.24	2.39	5.81	5.23	3.09	1.65
	1.53	8.78	5.75	3.57	4.62	5.34	3.72	1.42
	2.08	9.52	4.58	4.63	4.10	5.05	3.95	1.41
923	0.51	4.76	9.25	5.73	2.85	4.69	4.67	1.17
	0.77	6.14	8.00	6.75	2.24	4.11	4.97	1.01
	1.00	7.31	7.33	3.51	7.54	3.41	1.91	1.05
	1.50	8.65	5.78	4.67	6.16	3.45	2.11	1.07
	2.03	9.74	4.8	5.8	4.96	3.78	2.52	1.00
873	0.51	4.99	9.77	7.21	3.93	3.41	2.67	0.75
	0.74	6.26	8.42	8.37	2.98	3.30	2.90	0.64
	1.03	7.56	7.35	3.74	7.81	2.55	1.27	0.93
	1.48	8.92	6.01	5.23	6.43	2.53	1.45	0.79
	2.05	10.14	4.95	6.44	5.70	2.54	1.60	0.74
823	0.51	4.84	9.55	7.77	4.40	2.47	1.75	0.51
	0.78	6.35	8.09	8.52	3.43	2.21	1.85	0.41
	1.04	7.61	7.34	4.37	8.53	1.27	0.61	0.37
	1.51	8.9	5.89	5.52	7.18	1.26	0.74	0.52
	2.04	9.65	4.74	6.52	6.14	1.26	0.76	0.40
773	0.52	4.86	9.35	7.95	5.03	1.21	0.87	0.21
	0.76	6.15	8.07	9.49	4.26	1.06	0.64	0.16
	1.02	7.1	6.97	4.06	2.34	5.18	7.80	1.64
	1.48	8.49	5.74	4.95	1.65	4.64	7.92	1.22
	2.03	9.89	4.87	2.39	5.81	5.23	3.09	1.65

Table M.2 Reactants and Products Mole Fractions from Various Flow Rate Experiments

T/K	Flow Rate (sccm)	Feed CH_4/CO_2	Reactants Mole Fractions (%)		Products Mole Fractions (%)				
			CH_4	CO_2	CH_4	CO_2	H_2	CO	H_2O
973	**46.7**	0.98	6.81	6.92	2.76	2.92	6.41	6.31	1.69
	66.7	1.01	7.31	7.24	3.19	3.19	6.55	6.41	1.69
	100. 0	1.02	7.24	7.08	3.43	2.95	5.90	6.54	1.72
	133.3	1.01	6.32	6.23	2.80	2.44	5.77	6.31	1.27
	166. 7	1.03	7.32	7.14	3.43	2.80	6.00	6.90	1.78
923	**46.7**	0.98	7.14	7.29	4.42	4.17	3.93	4.73	1.51
	66.7	1.00	7.31	7.33	4.63	4.10	3.95	5.05	1.41
	100. 0	1.00	7.51	7.48	4.82	4.15	3.84	5.12	1.54
	133.3	1.00	6.66	6.67	4.16	3.61	3.69	4.81	1.31
	166. 7	1.01	7.71	7.65	4.88	4.13	4.05	5.43	1.61
873	**46.7**	1.02	7.45	7.28	5.47	4.76	2.96	4.04	1.00
	66.7	1.03	7.56	7.35	5.80	4.96	2.52	3.78	1.00
	100. 0	1.03	7.44	7.19	5.72	4.93	2.57	3.65	0.87
	133.3	1.05	6.47	6.18	5.00	4.25	2.47	3.39	0.47
	166. 7	1.04	7.32	7.03	5.46	4.67	2.79	3.79	0.93

Table M.3 CH_4 and CO_2 Conversions from Experiments at 66.7 sccm

T/K	Feed CH_4/CO_2	Conversions (%)		T/K	Feed CH_4/CO_2	Conversions (%)	
		CH_4	CO_2			CH_4	CO_2
973	0.51	66.00	45.91	**923**	0.51	49.89	37.18
	0.77	62.35	50.46		0.77	41.87	42.29
	1.01	56.41	56.07		1.00	36.65	44.04
	1.53	53.74	59.29		1.50	33.78	50.78
	2.08	48.02	64.04		2.03	30.73	53.28
873	0.51	29.72	22.82	**823**	0.51	22.81	18.25
	0.74	25.39	26.84		0.78	17.62	20.62
	1.03	23.25	32.53		1.04	15.38	22.39
	1.48	19.23	34.37		1.51	12.64	25.29
	2.05	17.41	39.89		2.04	11.74	27.77
773	0.52	10.02	8.78				
	0.76	10.08	11.09				
	1.02	8.07	11.95				
	1.48	6.28	12.38				
	2.03	4.08	12.51				

Table M.4 CH_4 and CO_2 Conversions from Various Flow Rate Experiments

T/K	Flow Rate (sccm)	Feed CH_4/CO_2	Conversions (%)		T/K	Flow Rate (sccm)	Feed CH_4/CO_2	Conversions (%)	
			CH_4	CO_2				CH_4	CO_2
973	**46.7**	0.98	59.55	57.94	**923**	**46.7**	0.98	38.09	42.90
	66.7	1.01	56.41	56.07		**66.7**	1.00	36.65	44.04
	100.0	1.02	52.64	58.29		**100.0**	1.00	35.75	44.54
	133.3	1.01	55.76	60.85		**133.3**	1.00	37.42	45.84
	166.7	1.03	53.18	60.82		**166.7**	1.01	36.86	46.04
873	**46.7**	1.02	26.59	34.60					
	66.7	1.03	23.25	32.53					
	100.0	1.03	23.14	31.35					
	133.3	1.05	22.82	31.17					
	166.7	1.04	25.17	33.51					

Table M.5 Reactants and Products Mole Fractions from Equilibrium Calculation

T/K	Feed CH_4/CO_2	Reactants Mole Fractions (%)		Products Mole Fractions (%)				
		CH_4	CO_2	CH_4	CO_2	H_2	CO	H_2O
973	0.51	4.88	9.6	0.01	4.84	5.22	4.39	3.57
	0.77	6.17	8.02	0.03	3.43	7.31	4.22	3.68
	1.01	7.31	7.24	0.06	2.56	8.96	3.95	3.60
	1.53	8.78	5.75	0.11	1.60	11.34	3.40	3.30
	2.08	9.52	4.58	0.16	1.09	12.97	2.95	2.98
923	0.51	4.76	9.25	0.02	5.30	4.63	2.90	4.14
	0.77	6.14	8.00	0.06	2.75	6.54	2.75	4.41
	1.00	7.31	7.33	0.10	2.86	8.07	2.55	4.43
	1.50	8.65	5.78	0.18	1.79	10.33	2.16	4.18
	2.03	9.74	4.8	0.26	1.22	11.92	1.85	3.84
873	0.51	4.99	9.77	0.04	5.57	3.93	1.70	4.81
	0.74	6.26	8.42	0.09	3.97	5.63	1.59	5.25
	1.03	7.56	7.35	0.16	2.95	7.03	1.45	5.35
	1.48	8.92	6.01	0.31	1.80	9.16	1.20	5.14
	2.05	10.14	4.95	0.44	1.20	10.70	1.01	4.77
823	0.51	4.84	9.55	0.06	5.61	3.16	0.88	5.54
	0.78	6.35	8.09	0.15	3.91	4.63	0.81	6.16
	1.04	7.61	7.34	0.26	2.83	5.87	0.73	6.34
	1.51	8.9	5.89	0.50	1.63	7.83	0.58	6.13
	2.04	9.65	4.74	0.73	1.03	9.29	0.47	5.68
773	0.52	4.86	9.35	0.08	5.48	2.38	0.40	6.29
	0.76	6.15	8.07	0.21	3.68	3.58	0.36	7.09
	1.02	7.1	6.97	0.39	2.55	4.64	0.32	7.34
	1.48	8.49	5.74	0.79	1.35	6.38	0.24	7.10
	2.03	9.89	4.87	1.17	0.79	7.72	0.18	6.52

Table M.6 CH_4 and CO_2 Conversions from Equilibrium Calculation

T/K	Feed CH_4/CO_2	Conversions (%)		T/K	Feed CH_4/CO_2	Conversions (%)	
		CH_4	CO_2			CH_4	CO_2
973	0.51	99.74	49.91	**923**	0.51	99.54	45.16
	0.77	99.48	58.63		0.77	99.09	66.76
	1.01	99.22	64.66		1.00	98.65	60.60
	1.53	98.76	72.44		1.50	97.88	69.18
	2.08	98.39	77.36		2.03	97.27	74.75
873	0.51	99.18	42.41	**723**	0.51	98.84	41.93
	0.74	98.50	52.14		0.78	97.67	52.83
	1.03	97.76	59.29		1.04	96.44	60.93
	1.48	96.45	68.96		1.51	94.22	71.81
	2.05	95.41	75.24		2.04	92.42	78.66
773	0.52	98.38	43.26				
	0.76	96.59	55.62				
	1.02	94.62	64.78				
	1.48	90.93	76.70				
	2.03	87.90	83.67				

Table M.7 CH_4 and CO_2 Conversions from Power Law Model at 66.7 sccm

T/K	Feed CH_4/CO_2	Conversions (%)		T/K	Feed CH_4/CO_2	Conversions (%)	
		CH_4	CO_2			CH_4	CO_2
973	0.51	71.87	49.92	**923**	0.51	46.17	34.48
	0.77	64.76	52.55		0.77	40.09	40.47
	1.01	58.88	58.44		1.00	36.64	44.04
	1.53	51.64	56.98		1.50	30.09	45.19
	2.08	43.78	58.34		2.03	25.84	44.9
873	0.51	31.26	24.05	**723**	0.51	20.3	16.27
	0.74	26.94	28.47		0.78	17.14	19.94
	1.03	23.38	32.66		1.04	15.46	22.47
	1.48	19.32	34.88		1.51	12.45	24.8
	2.05	16.04	36.57		2.04	10.2	24.06
773	0.52	10.9	9.48				
	0.76	9.44	10.17				
	1.02	8.14	11.86				
	1.48	6.71	13.05				
	2.03	5.59	17.3				

Table M.8 CH_4 and CO_2 Conversions from Power Law Model for Various Flow Rate

T/K	Flow Rate (sccm)	Feed CH4/CO2	Conversions (%)		T/K	Flow Rate (sccm)	Feed CH4/CO2	Conversions (%)	
			CH_4	CO_2				CH_4	CO_2
973	**46.7**	0.98	61.64	59.91	**923**	**46.7**	0.98	45.31	50.9
	66.7	1.01	58.88	58.44		**66.7**	1.00	36.64	44.04
	100.0	1.02	41.89	46.43		**100.0**	1.00	28.46	35.38
	133.3	1.01	32.62	35.63		**133.3**	1.00	21.34	26.08
	166.7	1.03	30.54	34.93		**166.7**	1.01	19.91	24.96
873	**46.7**	1.02	30.05	39.14					
	66.7	1.03	23.38	32.66					
	100.0	1.03	16.96	23.06					
	133.3	1.05	11.76	16.17					
	166.7	1.04	10.87	14.37					

Table M.9 Reactants and Products Mole Fractions from 3-Reaction Model at 66.7 sccm

T/K	Feed CH_4/CO_2	Reactants Mole Fractions (%)		Products Mole Fractions (%)				
		CH_4	CO_2	CH_4	CO_2	H_2	CO	H_2O
973	0.51	4.88	9.6	1.33	4.96	4.73	6.86	2.08
	0.77	6.17	8.02	2.06	3.55	6.07	7.04	1.83
	1.01	7.31	7.24	2.74	2.74	6.85	6.85	1.65
	1.53	8.78	5.75	3.82	1.77	7.75	6.21	1.37
	2.08	9.52	4.58	4.62	1.26	8.16	5.54	1.20
923	0.51	4.76	9.25	2.40	6.10	3.11	5.34	1.64
	0.77	6.14	8.00	3.44	4.67	3.91	5.48	1.52
	1.00	7.31	7.33	4.26	3.73	4.32	5.36	1.40
	1.50	8.65	5.78	5.59	2.68	4.72	4.95	1.17
	2.03	9.74	4.8	6.59	2.04	4.90	4.49	0.99
873	0.51	4.99	9.77	3.45	7.44	1.85	3.51	1.01
	0.74	6.26	8.42	4.63	6.00	2.26	3.62	0.95
	1.03	7.56	7.35	5.58	5.04	2.49	3.62	0.83
	1.48	8.92	6.01	7.06	3.80	2.61	3.32	0.71
	2.05	10.14	4.95	8.09	3.03	2.62	3.03	0.59
823	0.51	4.84	9.55	3.90	8.16	1.20	2.52	0.78
	0.78	6.35	8.09	5.21	6.71	1.50	2.58	0.72
	1.04	7.61	7.34	6.17	5.75	1.62	2.57	0.66
	1.51	8.9	5.89	7.66	4.43	1.74	2.40	0.54
	2.04	9.65	4.74	8.69	3.60	1.74	2.16	0.48
773	0.52	4.86	9.35	4.49	9.10	0.55	1.21	0.36
	0.76	6.15	8.07	5.87	7.69	0.73	1.27	0.32
	1.02	7.1	6.97	6.90	6.66	0.79	1.27	0.29
	1.48	8.49	5.74	8.36	5.21	0.79	1.15	0.23
	2.03	9.89	4.87	9.39	4.30	0.79	1.09	0.20

Table M.10 Mole Fractions from 3-Reaction Model for Various Flow Rate

T/K	Flow Rate (sccm)	Feed CH_4/CO_2	Reactants Mole Fractions (%)		Products Mole Fractions (%)				
			CH_4	CO_2	CH_4	CO_2	H_2	CO	H_2O
973	**46.7**	0.98	6.81	6.92	2.02	2.42	8.22	7.42	1.61
	66.7	1.01	7.31	7.24	2.74	2.74	6.85	6.85	1.65
	100. 0	1.02	7.24	7.08	3.54	3.20	5.35	6.08	1.66
	133.3	1.01	6.32	6.23	4.14	3.58	4.37	5.48	1.60
	166. 7	1.03	7.32	7.14	4.57	3.91	3.68	4.97	1.55
923	**46.7**	0.98	7.14	7.29	3.62	3.29	5.52	6.18	1.40
	66.7	1.00	7.31	7.33	4.26	3.73	4.32	5.36	1.40
	100. 0	1.00	7.51	7.48	4.99	4.32	3.18	4.48	1.30
	133.3	1.00	6.66	6.67	5.46	4.75	2.46	3.83	1.19
	166. 7	1.01	7.71	7.65	5.75	5.08	2.00	3.36	1.10
873	**46.7**	1.02	7.45	7.28	5.13	4.55	3.28	4.46	0.93
	66.7	1.03	7.56	7.35	5.58	5.04	2.49	3.62	0.83
	100. 0	1.03	7.44	7.19	5.32	4.81	3.00	4.10	0.79
	133.3	1.05	6.47	6.18	5.93	5.45	2.09	3.04	0.66
	166. 7	1.04	7.32	7.03	6.27	5.86	1.59	2.40	0.55

Table M.11 Mole Fractions from Chemkin with High Density for Various Flow Rate

T/K	Flow Rate (sccm)	Feed CH_4/CO_2	Reactants Mole Fractions (%)		Products Mole Fractions (%)				
			CH_4	CO_2	CH_4	CO_2	H_2	CO	H_2O
973	**46.7**	0.98	6.81	6.92	1.35	0.93	9.10	10.13	0.51
	66.7	1.01	7.31	7.24	1.55	0.96	9.51	10.57	0.53
	100. 0	1.02	7.24	7.08	1.56	0.91	9.42	10.43	0.50
	133.3	1.01	6.32	6.23	1.26	0.76	8.56	9.40	0.42
	166. 7	1.03	7.32	7.14	1.59	0.92	9.48	10.50	0.51
923	**46.7**	0.98	7.14	7.29	2.34	1.76	7.69	9.12	0.72
	66.7	1.00	7.31	7.33	2.45	1.75	7.77	9.2	0.71
	100. 0	1.00	7.51	7.48	2.55	1.79	7.89	9.35	0.73
	133.3	1.00	6.66	6.67	2.16	1.53	7.32	8.58	0.63
	166. 7	1.01	7.71	7.65	2.65	1.85	8.02	9.52	0.75
873	**46.7**	1.02	7.45	7.28	3.70	2.75	5.74	7.32	0.79
	66.7	1.03	7.56	7.35	3.77	2.77	5.78	7.38	0.8
	100. 0	1.03	7.44	7.19	3.71	2.69	5.72	7.28	0.78
	133.3	1.05	6.47	6.18	3.13	2.20	5.27	6.57	0.65
	166. 7	1.04	7.32	7.03	3.64	2.61	5.66	7.18	0.76

Table M.12 Conversions from Chemkin with High Density for Various Flow Rate

T/K	Flow Rate (sccm)	Feed CH4/CO2	Conversions (%)		T/K	Flow Rate (sccm)	Feed CH4/CO2	Conversions (%)	
			CH_4	CO_2				CH_4	CO_2
973	**46.7**	0.98	80.18	86.56	923	**46.7**	0.98	67.23	75.86
	66.7	1.01	78.80	86.74		**66.7**	1.00	66.48	76.13
	100.0	1.02	78.45	87.15		**100.0**	1.00	66.05	76.07
	133.3	1.01	80.06	87.80		**133.3**	1.00	67.57	77.06
	166.7	1.03	78.28	87.11		**166.7**	1.01	65.63	75.82
873	**46.7**	1.02	50.34	62.23					
	66.7	1.03	50.13	62.31					
	100.0	1.03	50.13	62.59					
	133.3	1.05	51.62	64.40					
	166.7	1.04	50.27	62.87					

Table M.13 Mole Fractions from Chemkin with High Density at 66.7 sccm

T/K	Feed CH_4/CO_2	Reactants Mole Fractions (%)		Products Mole Fractions (%)				
		CH_4	CO_2	CH_4	CO_2	H_2	CO	H_2O
973	0.51	4.88	9.6	0.23	3.16	7.09	9.86	1.39
	0.77	6.17	8.02	0.77	1.61	8.78	10.44	0.83
	1.01	7.31	7.24	1.55	0.96	9.51	10.57	0.53
	1.53	8.78	5.75	3.29	0.34	9.14	9.54	0.2
	2.08	9.52	4.58	4.75	0.13	7.94	8.09	0.08
923	0.51	4.76	9.25	0.68	3.6	6.21	8.69	1.24
	0.77	6.14	8.00	1.55	2.35	7.27	9.08	0.91
	1.00	7.31	7.33	2.45	1.75	7.77	9.2	0.71
	1.50	8.65	5.78	3.93	0.9	7.66	8.45	0.39
	2.03	9.74	4.8	5.28	0.49	7.24	7.68	0.22
873	0.51	4.99	9.77	1.59	4.87	4.97	7.39	1.21
	0.74	6.26	8.42	2.62	3.65	5.48	7.46	0.99
	1.03	7.56	7.35	3.77	2.77	5.78	7.38	0.8
	1.48	8.92	6.01	5.15	1.85	5.83	6.98	0.57
	2.05	10.14	4.95	6.48	1.21	5.7	6.48	0.39
823	0.51	4.84	9.55	2.49	5.99	3.28	5.3	1.01
	0.78	6.35	8.09	3.84	4.65	3.59	5.3	0.86
	1.04	7.61	7.34	4.99	3.97	3.78	5.31	0.77
	1.51	8.9	5.89	6.31	2.84	3.82	5	0.59
	2.04	9.65	4.74	7.17	2.02	3.72	4.61	0.44
773	0.52	4.86	9.35	3.39	7.01	1.92	3.43	0.76
	0.76	6.15	8.07	4.62	5.81	2.05	3.4	0.68
	1.02	7.1	6.97	5.55	4.83	2.11	3.3	0.6
	1.48	8.49	5.74	6.93	3.76	2.17	3.17	0.5
	2.03	9.89	4.87	8.32	3.01	2.21	3.05	0.42

Table M.14 CH_4 and CO_2 Conversions from Chemkin with High Density at 66.7 sccm

T/K	Feed CH_4/CO_2	Conversions (%)		T/K	Feed CH_4/CO_2	Conversions (%)	
		CH_4	CO_2			CH_4	CO_2
973	0.51	66	45.91	**923**	0.51	49.89	37.18
	0.77	62.35	50.46		0.77	41.87	42.29
	1.01	56.41	56.07		1.00	36.65	44.04
	1.53	53.74	59.29		1.50	33.78	50.78
	2.08	48.02	64.04		2.03	30.73	53.28
873	0.51	29.72	22.82	**723**	0.51	22.81	18.25
	0.74	25.39	26.84		0.78	17.62	20.62
	1.03	23.25	32.53		1.04	15.38	22.39
	1.48	19.23	34.37		1.51	12.64	25.29
	2.05	17.41	39.89		2.04	11.74	27.77
773	0.52	10.02	8.78				
	0.76	10.08	11.09				
	1.02	8.07	11.95				
	1.48	6.28	12.38				
	2.03	4.08	12.51				

Table M.15 Mole Fractions from Chemkin with Low Density for Various Flow Rate

T/K	Flow Rate (sccm)	Feed CH_4/CO_2	Reactants Mole Fractions (%)		Products Mole Fractions (%)				
			CH_4	CO_2	CH_4	CO_2	H_2	CO	H_2O
973	**46.7**	0.98	6.81	6.92	5.84	4.27	0.04	3.38	1.67
	66.7	1.01	7.31	7.24	6.32	4.56	0.04	3.43	1.69
	100. 0	1.02	7.24	7.08	6.29	4.52	0.04	3.27	1.62
	133.3	1.01	6.32	6.23	5.49	3.96	0.04	2.92	1.44
	166. 7	1.03	7.32	7.14	6.41	4.69	0.03	3.13	1.55
923	**46.7**	0.98	7.14	7.29	6.39	5.26	0.03	2.59	1.28
	66.7	1.00	7.31	7.33	6.58	5.35	0.03	2.53	1.25
	100. 0	1.00	7.51	7.48	6.8	5.55	0.02	2.46	1.22
	133.3	1.00	6.66	6.67	6.03	4.94	0.02	2.21	1.1
	166. 7	1.01	7.71	7.65	7.03	5.8	0.02	2.35	1.17
873	**46.7**	1.02	7.45	7.28	6.93	5.87	0.02	1.79	0.89
	66.7	1.03	7.56	7.35	7.05	5.98	0.01	1.74	0.86
	100. 0	1.03	7.44	7.19	6.97	5.90	0.01	1.64	0.81
	133.3	1.05	6.47	6.18	6.06	5.06	0.01	1.44	0.72
	166. 7	1.04	7.32	7.03	6.88	5.85	0.01	1.51	0.75

Table M.16 Conversions from Chemkin with Low Density for Various Flow Rate

T/K	Flow Rate (sccm)	Feed CH4/CO2	Conversions (%)		T/K	Flow Rate (sccm)	Feed CH4/CO2	Conversions (%)	
			CH_4	CO_2				CH_4	CO_2
973	**46.7**	0.98	14.24	38.29	923	**46.7**	0.98	10.50	27.85
	66.7	1.01	13.54	37.02		**66.7**	1.00	9.99	27.01
	100.0	1.02	13.12	36.16		**100.0**	1.00	9.45	25.80
	133.3	1.01	13.13	36.44		**133.3**	1.00	9.46	25.94
	166.7	1.03	12.43	34.31		**166.7**	1.01	8.82	24.18
873	**46.7**	1.02	6.98	19.37					
	66.7	1.03	6.75	18.64					
	100.0	1.03	6.32	17.94					
	133.3	1.05	6.34	18.12					
	166.7	1.04	6.01	16.79					

Table M.17 Mole Fractions from Chemkin with Low Density at 66.7 sccm

T/K	Feed CH_4/CO_2	Reactants Mole Fractions (%)		Products Mole Fractions (%)				
		CH_4	CO_2	CH_4	CO_2	H_2	CO	H_2O
973	0.51	4.88	9.6	3.84	6.63	0.03	3.73	1.85
	0.77	6.17	8.02	5.17	5.24	0.04	3.53	1.75
	1.01	7.31	7.24	6.32	4.56	0.04	3.43	1.69
	1.53	8.78	5.75	7.86	3.35	0.05	3.09	1.52
	2.08	9.52	4.58	8.69	2.48	0.05	2.73	1.34
923	0.51	4.76	9.25	4.03	7.15	0.02	2.64	1.31
	0.77	6.14	8.00	5.41	5.97	0.02	2.57	1.27
	1.00	7.31	7.33	6.58	5.35	0.03	2.53	1.25
	1.50	8.65	5.78	7.97	4	0.03	2.29	1.13
	2.03	9.74	4.8	9.1	3.17	0.03	2.11	1.04
873	0.51	4.99	9.77	4.48	8.3	0.01	1.85	0.92
	0.74	6.26	8.42	5.75	7	0.01	1.8	0.89
	1.03	7.56	7.35	7.05	5.98	0.01	1.74	0.86
	1.48	8.92	6.01	8.46	4.75	0.02	1.63	0.81
	2.05	10.14	4.95	9.68	3.79	0.02	1.51	0.75
823	0.51	4.84	9.55	4.53	8.65	0.01	1.13	0.56
	0.78	6.35	8.09	6.04	7.21	0.01	1.11	0.55
	1.04	7.61	7.34	7.29	6.48	0.01	1.1	0.55
	1.51	8.9	5.89	8.6	5.09	0.01	1.03	0.51
	2.04	9.65	4.74	9.37	4.01	0.01	0.94	0.47
773	0.52	4.86	9.35	4.69	8.85	0	0.63	0.31
	0.76	6.15	8.07	5.97	7.58	0	0.62	0.31
	1.02	7.1	6.97	6.93	6.49	0	0.61	0.3
	1.48	8.49	5.74	8.32	5.29	0	0.58	0.29
	2.03	9.89	4.87	9.72	4.44	0	0.56	0.28

Table M.18 CH_4 and CO_2 Conversions from Chemkin with Low Density at 66.7 sccm

T/K	Feed CH_4/CO_2	Conversions (%)		T/K	Feed CH_4/CO_2	Conversions (%)	
		CH_4	CO_2			CH_4	CO_2
973	0.51	21.31	30.94	**923**	0.51	15.34	22.70
	0.77	16.21	34.66		0.77	11.89	25.38
	1.01	13.54	37.02		1.00	9.99	27.01
	1.53	10.48	41.74		1.50	7.86	30.80
	2.08	8.72	45.85		2.03	6.57	33.96
873	0.51	10.22	15.05	**723**	0.51	6.40	9.42
	0.74	8.15	16.86		0.78	4.88	10.88
	1.03	6.75	18.64		1.04	4.20	11.72
	1.48	5.16	20.97		1.51	3.37	13.58
	2.05	4.54	23.43		2.04	2.90	15.40
773	0.52	3.50	5.35				
	0.76	2.93	6.07				
	1.02	2.39	6.89				
	1.48	2.00	7.84				
	2.03	1.72	8.83				

APPENDIX N

POLYMATH CODE FOR POWER LAW MODEL OF DRY REFORMING OVER RU/CNT-ZEOLITE

Appendix N shows the Polymath code for DR over Ru/CNT-zeolite simulation in Chapter 7.

```
# PFR Power Law- Dry Reforming test-Ru

d(yA)/d(W) = -k / FTo * (P / R / T) ^ (alpha + beta) * (yA ^ alpha) * (b ^ beta) * (yo + yA) ^ beta # PBR species balance for CH4 (using mole fraction)
yA(0) = 0.0731 # feed mole fraction of CH4 -- MUST be same as yAo value below

d(XA)/d(W) = k / FAo * (P / R / T * yAo) ^ (alpha + beta) * (1 - XA) ^ alpha * (yBo / b / yAo - XA) ^ beta * (b ^ beta) # PBR species balance for CH4 (using conversion)
XA(0) = 0 # inlet conversion

W(0) = 0 # initial catalyst mass (grams)
W(f) = 2.0 # final catalyst mass (grams)

yo = yBo / b - yAo # simplifying term
b = 0.9830 # converted CO2/converted CH4 (experiemental value)
yBo = 0.0624 # feed mole fraction of CO2
FTo = 66.67 / 82.1 * 1 / 298 # total molar rate at inlet (moles/min)
yAo = 0.0731 # feed mole fraction of CH4

P = (30 + 14.7) / 14.7 # reactor pressure (atm)
R = 82.1 # gas constant (cm^3-atm/mole-K)
T = 700 + 273 # reactor temperature (K)

alpha = 1 # kinetic parameter (order on CH4)
beta = 1 # kinetic parameter (order on CO2)
k = 1.495E7 # rate constant

FAo = yAo * FTo # Feed molar rate of CH4 (moles/min)
FBo = yBo * FTo # Feed molar rate of CO2 (moles/min)
FA = yA * FTo # molar rate of CH4 in reactor (moles/min) assuming FT ~ FTo
FB = yB * FTo # molar rate of CO2 in reactor (moles/min) assuming FT ~ FTo
yB = b * (yo + yA) # mole fraction of CO2 in reactor
XB = 1 - yB / yBo
```

APPENDIX O

MATLAB CODE FOR DRY REFORMING OVER RU/CNT-ZEOLITE

Appendix O shows the Matlab code for DR over Ru/CNT-zeolite simulation in Chapter 7.

```
clear all
clc
close all

format compact


T=273+700;
kp1 = exp(-1 / T * 31247 + 34.105);
kp2 = exp(-1 / T * 4386.6 + 4.0251);
kp3 = exp(-1 / T * 21136 + 25.766);

P=3.04;

Fhe=[0.139 0.139 0.139 0.139 0.139 0.097 0.208 0.278 0.347];

FM_test=[0.002710340 0.003804272 0.005208424 0.006628903 0.008082037
0.003154511 0.008400000 0.009143314 0.014000280 ];
FCD_test=[0.008490220 0.006481957 0.005208424 0.003820599 0.002694012
0.003337381 0.007224490 0.007967745 0.011428800 ];
FH_test=[0.007249342 0.009339242 0.010694412 0.012735331 0.012931259
0.007326238 0.014448980 0.018841758 0.024490286 ];
FCo_test=[0.011102596 0.010024991 0.010465829 0.008457566 0.007575889
0.007211944 0.016016327 0.020605112 0.028163829 ];
Fw_test=[0.003265469 0.003200160 0.002759322 0.002677685 0.001991936
0.001931567 0.004212245 0.004147146 0.007265451];

FM1=[0.008163673 0.010498484 0.012245510 0.014694612 0.016327347
0.008572041 0.018367347 0.024491020 0.030612857];
FCD1=[0.016327347 0.013992536 0.012245510 0.009796408 0.008163673
0.008572041 0.018367347 0.024491020 0.030612857 ];
FH1=[0.0000001 0.0000001 0.0000001 0.0000001  0.0000001 0.0000001
0.0000001  0.0000001 0.0000001];
FCo1=[0.0000001 0.0000001 0.0000001 0.0000001 0.0000001 0.0000001
0.0000001  0.0000001 0.0000001];
Fw1=[0.0000001 0.0000001 0.0000001 0.0000001 0.0000001 0.0000001
0.0000001  0.0000001 0.0000001];

 stepsize=0.001;
 w=[0:stepsize:2];

k1 = [0.129];
k2 = [0.050];
k3 = [0.0109];

L1= length(k1);
```

```
L2= length(k2);
L3= length(k3);

for jj=1:length(FM1)
    jj

final_FM =[];
final_FH=[];
final_FCD=[];
final_FW =[];
final_FCo=[];
FM=[];
FH=[];
FCD=[];
FCo=[];
Fw=[];
FT=[];

for i1=1:L1;
     i1
for i2=1:L2;
for i3=1:L3;

 FM=[ FM1(jj) zeros(1,length(w)-1)];
 FH=[FH1(jj)  zeros(1,length(w)-1)];
 FCD=[FCD1(jj) zeros(1,length(w)-1)];
 FCo=[FCo1(jj) zeros(1,length(w)-1)];
 Fw=[Fw1(jj) zeros(1,length(w)-1)];
 FT=zeros(1,length(w)-1);

eta1=zeros(1,length(w)-1);
eta2=zeros(1,length(w)-1);
eta3=zeros(1,length(w)-1);

for j=2:length(w)
j;
FT(j-1)=FM(j-1)+FH(j-1)+FCD(j-1)+FCo(j-1)+Fw(j-1)+Fhe(jj);

eta1(j-1)=((P/FT(j-1))^2)*((FCo(j-1))^2)*((FH(j-1))^2)/(FM(j-1)*FCD(j-
1)*kp1);
eta2(j-1)=((FCo(j-1))^1)*((Fw(j-1))^1)/(FH(j-1)*FCD(j-1)*kp2);
eta3(j-1)=((P/FT(j-1))^1)*((FCo(j-1))^1)*((FH(j-1))^2)/(FM(j-1)*kp3);

FM(j)=FM(j-1)-(k1(i1)*FM(j-1)*FCD(j-1)*((P/FT(j-1))^2)*(1-eta1(j-
1))+k3(i3)*FM(j-1)*(P/FT(j-1))*(1-eta3(j-1)))*stepsize;
FH(j)=FH(j-1)+(2*k1(i1)*FM(j-1)*FCD(j-1)*((P/FT(j-1))^2)*(1-eta1(j-1))-
k2(i2)*FCD(j-1)*((P/FT(j-1))^1)*(1-eta2(j-1))+2*k3(i3)*FM(j-1)*(P/FT(j-
1))*(1-eta3(j-1)))*stepsize;
FCD(j)=FCD(j-1)-(k1(i1)*FM(j-1)*FCD(j-1)*((P/FT(j-1))^2)*(1-eta1(j-
1))+k2(i2)*FCD(j-1)*((P/FT(j-1))^1)*(1-eta2(j-1)))*stepsize;

FCo(j)=FCo(j-1)+(2*k1(i1)*FM(j-1)*FCD(j-1)*((P/FT(j-1))^2)*(1-eta1(j-
1))+k2(i2)*FCD(j-1)*((P/FT(j-1))^1)*(1-eta2(j-1)))*stepsize;

Fw(j)=Fw(j-1)+(k2(i2)*FCD(j-1)*((P/FT(j-1))^1)*(1-eta2(j-1)))*stepsize;
```

```
end

final_FM=[final_FM FM(end-1)];
final_FCD=[final_FCD FCD(end-1)];
final_FH=[final_FH FH(end-1)];
final_FCo=[final_FCo FCo(end-1)];
final_FW=[final_FW Fw(end-1)];

end
end
end

FINAL_FM(jj,:)=final_FM
FINAL_CD(jj,:)=final_FCD
FINAL_FH(jj,:)=final_FH
FINAL_FW(jj,:)=final_FW
FINAL_Co(jj,:)=final_FCo
end

MMSE_temp=0;
for ii=1:length(FM_test)
MMSE_temp=MMSE_temp+((FINAL_FM(ii,:)-FM_test(ii))/FM_test(ii)).^2
+((FINAL_CD(ii,:)-FCD_test(ii))/FCD_test(ii)).^2+((FINAL_Co(ii,:)-
FCo_test(ii))/FCo_test(ii)).^2+((FINAL_FH(ii,:)-
FH_test(ii))/FH_test(ii)).^2+((FINAL_FW(ii,:)-
Fw_test(ii))/Fw_test(ii)).^2;
end
MMSE=MMSE_temp/(5*length(FM_test));
sizeMMSE=size(MMSE)
min_MMSE=min(MMSE)
position=find(MMSE==min_MMSE)-1;

 remain1=rem(position,L2*L3);
 factor1=(position-remain1)/(L2*L3);

remain2=rem(remain1,L3);
factor2=(remain1-remain2)/(L3);

Final_k1=factor1
Final_k2=factor2
Final_k3=remain2
```

APPENDIX P

POLYMATH CODE FOR 3-REACTION MODEL OF DRY REFORMING OVER RU/CNT-ZEOLITE

Appendix P shows the Polymath code for 3-reaction model simulation in Chapter 7.

```
# PFR-3 Reaction Model - Dry Reforming test-Ru

d(FM)/d(W) = -k1 * FM * FCD * (P / FT) ^ 2 * (1 - eta1) - k3 * FM * (P / FT) * (1 - eta3)

FM(0) = 0.010612776
FMo = 0.010612776 # CH4 feed rate (mole/hr)

d(FH)/d(W) = 2 * k1 * FM * FCD * (P / FT) ^ 2 * (1 - eta1) - k2 * FCD * (P / FT) ^ 1 * (1 - eta2) + 2
* k3 * FM * (P / FT) * (1 - eta3)

FH(0) = 0.0000001 # non-zero for eta calc at W = 0

d(FCD)/d(W) = -k1 * FM * FCD * (P / FT) ^ 2 * (1 - eta1) - k2 * FCD * (P / FT) ^ 1 * (1 - eta2)
FCD(0) = 0.010465829
FCDo = 0.010465829 # CO2 feed rate (mole/hr)

d(FCO)/d(W) = 2 * k1 * FM * FCD * (P / FT) ^ 2 * (1 - eta1) + k2 * FCD * (P / FT) ^ 1 * (1 - eta2)
FCO(0) = 0.0000001 # non-zero for eta calc

d(FW)/d(W) = k2 * FCD * (P / FT) ^ 1 * (1 - eta2)
FW(0) = 0.0000001 # non-zero for eta calc

W(0) = 0
W(f) = 2. # catalyst mass

eta1 = FCO ^ 2 * FH ^ 2 * (P / FT) ^ 2 / FM / FCD / Kp1
eta2 = FW * FCO / FCD / FH / Kp2
eta3 = FH ^ 2 * (P / FT) / FM / Kp3

k1 = 0.065
k2 = 0.0243
k3 = 0.0043

Kp1 = exp(-1 / T * 31247 + 34.105)
Kp2 = exp(-1 / T * 4386.6 + 4.0251)
Kp3 = exp(-1 / T * 21136 + 25.766)

P = 3.04 # pressure in atm
FT = FM + FW + FH + FCO + FCD + FHE # mole/hr
FHE = 0.139
T = 273 + 650 # temp in K
X_M = (FMo - FM) / FMo
X_CD = (FCDo - FCD) / FCDo
H_CO_ratio = FH / FCO
```

APPENDIX Q

DATA OF REVERSE WATER GAS SHIFT OVER PT/PD-CNT/ZEOLITE

Table Q.1 to Q.10 shows the data of RWGS over Pt/Pd-CNT/zeolite in Chapter 9.

Table Q.1 Reactants and Products Mole Fractions from Experiments at 66.7 sccm

T/K	Feed CO_2/H_2	Reactants Mole Fractions (%)		Products Mole Fractions (%)				
		CO_2	H_2	CO_2	H_2	CO	H_2O	CH_4
923	0.49	4.65	9.43	2.6	6.67	1.98	2.12	0.32
	0.76	5.94	7.83	3.75	5.22	2.25	2.13	0.24
	1.02	6.8	6.69	4.57	4.28	2.35	2.11	0.15
	1.51	8.19	5.44	6.07	3.43	2.39	1.85	0.08
	1.99	8.95	4.49	7.04	2.82	2.23	1.59	0.04
873	0.52	4.78	9.26	2.81	6.55	1.85	2.09	0.31
	0.75	6.25	8.33	4.13	5.77	2.14	2.1	0.23
	1.00	7.18	7.18	5.02	4.71	2.23	2.09	0.19
	1.50	8.76	5.84	6.66	3.64	2.24	1.96	0.12
	2.00	9.72	4.86	7.77	2.93	2.15	1.75	0.09
823	0.50	5.69	11.38	3.52	8.78	2.08	2.26	0.17
	0.75	7.33	9.78	5.04	7.18	2.26	2.32	0.14
	1.00	8.29	8.29	6.08	5.91	2.32	2.1	0.14
	1.50	9.98	6.65	7.88	4.53	2.22	1.98	0.07
	2.00	10.7	5.35	8.99	3.78	1.99	1.43	0.07
773	0.50	5.29	10.57	3.58	8.67	1.7	1.72	0.09
	0.75	6.72	8.96	4.93	7.08	1.84	1.74	0.07
	1.00	7.84	7.84	5.88	5.62	1.86	2.06	0.08
	1.50	9.42	6.3	7.68	4.55	1.83	1.65	0.05
	2.00	10.63	5.32	8.98	3.69	1.77	1.53	0.05

Table Q.2 H_2 and CO_2 Conversions from Experiments at 66.7 sccm

T/K	Feed CO_2/H_2	Conversions (%)		T/K	Feed CO_2/H_2	Conversions (%)	
		CO_2	H_2			CO_2	H_2
923	0.49	44.16	29.29	**873**	0.52	41.29	29.27
	0.76	36.91	33.33		0.75	33.97	30.73
	1.02	32.76	36.02		1.00	30.00	34.40
	1.51	25.89	36.95		1.50	23.95	37.67
	1.99	21.32	37.19		2.00	20.09	39.71
823	0.50	38.13	22.85	**773**	0.50	32.3	17.98
	0.75	31.31	26.58		0.75	26.66	20.98
	1.00	26.68	28.71		1.00	24.94	28.32
	1.50	21.03	31.88		1.50	18.51	27.78
	2.00	15.92	29.35		2.00	15.59	30.64

Table Q.3 Reactants and Products Mole Fractions from Equilibrium Calculation

T/K	Feed CO_2/H_2	Reactants Mole Fractions (%)		Products Mole Fractions (%)				
		CO_2	H_2	CO_2	H_2	CO	H_2O	CH_4
923	0.49	4.65	9.43	1.90	4.92	1.02	4.49	0.01
	0.76	5.94	7.83	3.15	3.49	1.24	4.34	0.00
	1.02	6.8	6.69	4.12	2.65	1.33	4.03	0.00
	1.51	8.19	5.44	5.68	1.83	1.41	3.61	0.00
	1.99	8.95	4.49	6.68	1.33	1.37	3.16	0.00
873	0.52	4.78	9.26	1.97	4.19	0.62	5.02	0.02
	0.75	6.25	8.33	3.32	3.23	0.79	5.08	0.01
	1.00	7.18	7.18	4.40	2.46	0.86	4.71	0.00
	1.50	8.76	5.84	6.21	1.68	0.94	4.16	0.00
	2.00	9.72	4.86	7.43	1.22	0.94	3.63	0.00
823	0.50	5.69	11.38	2.08	4.43	0.37	6.85	0.05
	0.75	7.33	9.78	3.78	3.11	0.49	6.63	0.02
	1.00	8.29	8.29	5.04	2.29	0.53	5.98	0.01
	1.50	9.98	6.65	7.13	1.51	0.58	5.13	0.00
	2.00	10.7	5.35	8.27	1.06	0.57	4.29	0.00
773	0.50	5.29	10.57	1.67	3.33	0.15	7.11	0.07
	0.75	6.72	8.96	3.26	2.19	0.21	6.72	0.03
	1.00	7.84	7.84	4.63	1.62	0.24	6.19	0.01
	1.50	9.42	6.3	6.67	1.05	0.26	5.24	0.01
	2.00	10.63	5.32	8.20	0.76	0.27	4.54	0.00

Table Q.4 CO_2 and H_2 Conversions from Equilibrium Calculation

T/K	Feed CO_2/H_2	Conversions (%)		T/K	Feed CO_2/CO_2	Conversions (%)	
		CO_2	H_2			CO_2	H_2
923	0.49	59.21	47.78	**873**	0.52	58.85	54.78
	0.76	46.93	55.46		0.75	46.96	61.21
	1.02	39.41	60.33		1.00	38.78	65.69
	1.51	30.64	66.40		1.50	29.09	71.29
	1.99	25.34	70.41		2.00	23.52	74.80
823	0.50	63.40	61.05	**773**	0.50	68.49	68.48
	0.75	48.49	68.21		0.75	51.46	75.56
	1.00	39.24	72.36		1.00	40.96	79.30
	1.50	28.60	77.25		1.50	29.19	83.35
	2.00	22.67	80.16		2.00	22.85	85.71

Table Q.5 CO_2 and H_2 Conversions from Power Law Model at 66.7 sccm

T/K	Feed CO_2/H_2	Conversions (%)		T/K	Feed CO_2/CO_2	Conversions (%)	
		H_2	CO_2			H_2	CO_2
923	0.49	31.82	39.37	**873**	0.52	29.46	39.27
	0.76	38.82	38.25		0.75	36.85	38.34
	1.02	43.25	35.49		1.00	40.68	33.03
	1.51	50.92	31.04		1.50	49.11	24.47
	1.99	56.66	20.72		2.00	52.04	21.67
823	0.50	26.3	38.17	**773**	0.50	22.99	33.43
	0.75	33.07	34.96		0.75	28.78	30
	1.00	37.69	29.12		1.00	33.83	23.68
	1.50	44.46	24.2		1.50	40.44	16.69
	2.00	48.07	18.27		2.00	44.09	17.42

Table Q.6 Reactants and Products Mole Fractions from 3-Reaction Model at 66.7 sccm

T/K	Feed CO_2/H_2	Reactants Mole Fractions (%)		Products Mole Fractions (%)				
		CO_2	H_2	CO_2	H_2	CO	H_2O	CH_4
923	0.49	4.65	9.43	2.60	6.81	2.04	2.23	0.24
	0.76	5.94	7.83	3.72	5.40	2.36	2.17	0.16
	1.02	6.8	6.69	4.59	4.47	2.48	2.11	0.10
	1.51	8.19	5.44	6.00	3.40	2.60	1.98	0.05
	1.99	8.95	4.49	6.87	2.72	2.54	1.80	0.03
873	0.52	4.78	9.26	2.85	6.70	1.86	2.11	0.27
	0.75	6.25	8.33	4.06	5.66	2.22	2.28	0.23
	1.00	7.18	7.18	4.99	4.68	2.28	2.22	0.18
	1.50	8.76	5.84	6.57	3.50	2.39	2.09	0.13
	2.00	9.72	4.86	7.60	2.82	2.33	1.90	0.10
823	0.50	5.69	11.38	3.43	8.54	1.98	2.29	0.17
	0.75	7.33	9.78	4.86	6.91	2.22	2.40	0.14
	1.00	8.29	8.29	5.85	5.61	2.29	2.29	0.12
	1.50	9.98	6.65	7.59	4.16	2.29	2.17	0.09
	2.00	10.7	5.35	8.53	3.21	2.18	1.94	0.07
773	0.50	5.29	10.57	3.59	8.45	1.46	1.88	0.10
	0.75	6.72	8.96	4.94	6.77	1.52	1.95	0.09
	1.00	7.84	7.84	6.03	5.67	1.58	1.95	0.07
	1.50	9.42	6.3	7.60	4.26	1.64	1.89	0.06
	2.00	10.63	5.32	8.86	3.46	1.58	1.76	0.05

Table Q.7 Mole Fractions from Chemkin with High Density at 66.7 sccm

T/K	Feed CO_2/H_2	Reactants Mole Fractions (%)		Products Mole Fractions (%)				
		CO_2	H_2	CO_2	H_2	CO	H_2O	CH_4
923	0.49	4.65	9.43	6.56	2.09	2.47	2.68	0.11
	0.76	5.94	7.83	4.94	3.19	2.71	2.8	0.047
	1.02	6.8	6.69	3.87	4.05	2.73	2.77	0.02
	1.51	8.19	5.44	2.73	5.5	2.68	2.7	0.01
	1.99	8.95	4.49	1.99	6.46	2.49	2.49	0
873	0.52	4.78	9.26	5.96	2.46	2.01	2.69	0.34
	0.75	6.25	8.33	5.06	3.66	2.39	2.85	0.23
	1.00	7.18	7.18	4.15	4.56	2.51	2.78	0.14
	1.50	8.76	5.84	3.05	6.14	2.57	2.69	0.06
	2.00	9.72	4.86	2.3	7.24	2.46	2.51	0.03
823	0.50	5.69	11.38	5.85	3.28	1.45	3.61	1.08
	0.75	7.33	9.78	4.85	4.8	1.83	3.46	0.81
	1.00	8.29	8.29	4.07	5.79	2.02	3.17	0.57
	1.50	9.98	6.65	3.16	7.49	2.23	2.88	0.33
	2.00	10.7	5.35	2.47	8.36	2.2	2.55	0.17
773	0.50	5.29	10.57	5.54	3.04	1.39	3.31	0.96
	0.75	6.72	8.96	4.55	4.38	1.73	3.13	0.7
	1.00	7.84	7.84	3.9	5.46	1.94	2.98	0.52
	1.50	9.42	6.3	3.03	7.05	2.14	2.72	0.29
	2.00	10.63	5.32	2.46	8.3	2.19	2.54	0.17

Table Q.8 CO_2 and H_2 Conversions from Chemkin with High Density at 66.7 sccm

T/K	Feed CO_2/H_2	Conversions (%)		T/K	Feed CO_2/CO_2	Conversions (%)	
		H_2	CO_2			H_2	CO_2
923	0.49	30.43	55.05	**873**	0.52	35.64	48.54
	0.76	36.91	46.30		0.75	39.26	41.44
	1.02	42.15	40.44		1.00	42.20	36.49
	1.51	49.82	32.84		1.50	47.77	29.91
	1.99	55.68	27.82		2.00	52.67	25.51
823	0.50	48.59	42.36	**773**	0.50	47.59	42.53
	0.75	50.41	34.52		0.75	49.22	34.82
	1.00	50.90	30.16		1.00	50.26	30.36
	1.50	52.48	24.95		1.50	51.90	25.16
	2.00	53.83	21.87		2.00	53.76	21.92

Table Q.9 Mole Fractions from Chemkin with Low Density at 66.7 sccm

T/K	Feed CO_2/H_2	Reactants Mole Fractions (%)		Products Mole Fractions (%)				
		CO_2	H_2	CO_2	H_2	CO	H_2O	CH_4
923	0.49	4.65	9.43	5.29	0.53	4.12	4.13	0.0056
	0.76	5.94	7.83	2.58	0.72	5.21	5.23	0.0102
	1.02	6.8	6.69	1.23	1.40	5.39	5.42	0.0184
	1.51	8.19	5.44	0.43	3.30	4.86	4.94	0.0381
	1.99	8.95	4.49	0.21	4.84	4.07	4.18	0.0548
873	0.52	4.78	9.26	6.49	2.02	2.76	2.76	0.0019
	0.75	6.25	8.33	4.60	2.53	3.72	3.73	0.0028
	1.00	7.18	7.18	2.54	2.55	4.63	4.63	0.0042
	1.50	8.76	5.84	0.59	3.55	5.20	5.23	0.0120
	2.00	9.72	4.86	0.30	5.23	4.48	4.52	0.0220
823	0.50	5.69	11.38	10.12	4.43	1.26	1.26	0.0004
	0.75	7.33	9.78	8.07	5.63	1.70	1.70	0.0006
	1.00	8.29	8.29	6.20	6.20	2.09	2.09	0.0008
	1.50	9.98	6.65	3.76	7.09	2.89	2.89	0.0001
	2.00	10.7	5.35	1.60	6.96	3.74	3.74	0.0023
773	0.50	5.29	10.57	10.14	4.86	0.43	0.43	0.0001
	0.75	6.72	8.96	8.38	6.14	0.58	0.58	0.0001
	1.00	7.84	7.84	7.12	7.12	0.72	0.72	0.0002
	1.50	9.42	6.3	5.33	8.45	0.96	0.97	0.0003
	2.00	10.63	5.32	4.12	9.43	1.20	1.20	0.0004

Table Q.10 CO_2 and H_2 Conversions from Chemkin with Low Density at 66.7 sccm

T/K	Feed CO_2/H_2	Conversions (%)		T/K	Feed CO_2/CO_2	Conversions (%)	
		H_2	CO_2			H_2	CO_2
923	0.49	43.90	88.60	**873**	0.52	29.86	57.74
	0.76	67.05	87.87		0.75	44.81	59.59
	1.02	81.59	79.46		1.00	64.65	64.47
	1.51	92.11	59.76		1.50	89.91	59.52
	1.99	95.39	45.97		2.00	93.87	46.24
823	0.50	11.06	22.11	**773**	0.50	4.06	8.11
	0.75	17.43	23.24		0.75	6.49	8.64
	1.00	25.19	25.16		1.00	9.18	9.17
	1.50	43.47	28.92		1.50	15.33	10.25
	2.00	70.04	34.95		2.00	22.55	11.27

APPENDIX R

POLYMATH CODE FOR POWER LAW MODEL OF REVERSE WATER GAS SHIFT OVER PT/PD-CNT/ZEOLITE

Appendix R shows the Polymath code for RWGS over Pt/Pd-CNT/zeolite simulation in Chapter 9.

```
# PFR Power Law- Reverse Water Gas Shift test

d(yA)/d(W) = -k / FTo * (P / R / T) ^ (alpha + beta) * (yA ^ alpha) * (b ^ beta) * (yo + yA) ^ beta # PBR species balance for H2 (using mole fraction)
yA(0) = 0.0833 # feed mole fraction of H2 -- MUST be same as yAo value below

d(XA)/d(W) = k / FAo * (P / R / T * yAo) ^ (alpha + beta) * (1 - XA) ^ alpha * (yBo / b / yAo - XA) ^ beta * (b ^ beta) # PBR species balance for H2 (using conversion)
XA(0) = 0 # inlet conversion

W(0) = 0 # initial catalyst mass (grams)
W(f) = 2.0 # final catalyst mass (grams)

yo = yBo / b - yAo # simplifying term
b = 0.812 # converted CO2/converted H2 (experiemental value)
yBo = 0.0625 # feed mole fraction of CO2
FTo = 66.67 / 82.1 * 1 / 298 # total molar rate at inlet (moles/min)
yAo = 0.0833 # feed mole fraction of H2

P = (30 + 14.7) / 14.7 # reactor pressure (atm)
R = 82.1 # gas constant (cm^3-atm/mole-K)
T = 600 + 273 # reactor temperature (K)

alpha = 1 # kinetic parameter (order on H2)
beta = 1 # kinetic parameter (order on CO2)
k = 6.8E6 # rate constant

FAo = yAo * FTo # Feed molar rate of H2 (moles/min)
FBo = yBo * FTo # Feed molar rate of CO2 (moles/min)
FA = yA * FTo # molar rate of H2 in reactor (moles/min) assuming FT ~ FTo
FB = yB * FTo # molar rate of CO2 in reactor (moles/min) assuming FT ~ FTo
yB = b * (yo + yA) # mole fraction of CO2 in reactor
XB = 1 - yB / yBo
```

APPENDIX S

MATLAB CODE FOR REVERSE WATER GAS SHIFT OVER PT/PD-CNT/ZEOLITE

Appendix S shows the Matlab code for RWGS over Pt/Pd-CNT/zeolite simulation in Chapter 9.

```
clear all
clc
close all

format compact

T=273+650;
kp1 = 0.4825;
kp2 = 0.3071;
kp3 = 0.1822;

 P=3.04;

Fhe=[0.139 0.139 0.139 0.139 0.139 ];

FM_test=[0.000522475 0.000391856 0.000244910 0.000130619 0.000065309];
FCD_test=[0.004245110 0.006122755 0.007461598 0.009910700 0.011494452];
FH_test=[0.009910700 0.008000400 0.006351338 0.005110460 0.003053214];
FCo_test=[0.003232815 0.003673653 0.003836927 0.003902236 0.003640998];
Fw_test=[0.003461398 0.003477725 0.003445070 0.003020559 0.002596048];



FM1=[0.0000001 0.0000001 0.0000001 0.0000001 0.0000001];
FCD1=[0.007592216 0.009698444 0.011102596 0.013372097 0.014612976];
FH1=[0.015396688 0.012784313 0.010922995 0.008882077 0.007330979];
FCo1=[0.0000001 0.0000001 0.0000001 0.0000001 0.0000001];
Fw1=[0.0000001 0.0000001 0.0000001 0.0000001 0.0000001];

 stepsize=0.001;
 w=[0:stepsize:2];

k1 = [0.065:0.001:0.075];
k2 = [0.001:0.0001:0.002];
k3 = [0.0015:0.0001:0.0025];

L1= length(k1);
L2= length(k2);
L3= length(k3);

for jj=1:length(FM1)
    jj

final_FM =[];
```

```
final_FH=[];
final_FCD=[];
final_FW =[];
final_FCo=[];
 FM=[];
 FH=[];
FCD=[];
FCo=[];
Fw=[];
FT=[];

for i1=1:L1;
     i1
for i2=1:L2;
for i3=1:L3;

 FM=[ FM1(jj) zeros(1,length(w)-1)];
 FH=[FH1(jj)  zeros(1,length(w)-1)];
 FCD=[FCD1(jj) zeros(1,length(w)-1)];
 FCo=[FCo1(jj) zeros(1,length(w)-1)];
 Fw=[Fw1(jj) zeros(1,length(w)-1)];
 FT=zeros(1,length(w)-1);

eta1=zeros(1,length(w)-1);
eta2=zeros(1,length(w)-1);
eta3=zeros(1,length(w)-1);

for j=2:length(w)
j;
FT(j-1)=FM(j-1)+FH(j-1)+FCD(j-1)+FCo(j-1)+Fw(j-1)+Fhe(jj);

eta1(j-1)=((FCo(j-1))^1)*((Fw(j-1))^1)/(FH(j-1)*FCD(j-1)*kp1);
eta2(j-1)=((FCo(j-1))^2*(P/FT(j-1)))/(FCD(j-1)*kp2);
eta3(j-1)=((FM(j-1))^1)*((Fw(j-1))^2)/(((FH(j-1)^4)*FCD(j-1)*(P/FT(j-
1))^2)*kp3);

FH(j)=FH(j-1)-(k1(i1)*FH(j-1)*FCD(j-1)*((P/FT(j-1))^2)*(1-eta1(j-
1))+4*k3(i3)*(FH(j-1))^1*(P/FT(j-1))^1*(1-eta3(j-1)))*stepsize;
FCD(j)=FCD(j-1)-(k1(i1)*FH(j-1)*FCD(j-1)*((P/FT(j-1))^2)*(1-eta1(j-
1))+k2(i2)*FCD(j-1)*((P/FT(j-1))^1)*(1-eta2(j-1))+k3(i3)*(FH(j-
1))^1*(P/FT(j-1))^1*(1-eta3(j-1)))*stepsize;
FCo(j)=FCo(j-1)+(k1(i1)*FH(j-1)*FCD(j-1)*((P/FT(j-1))^2)*(1-eta1(j-
1))+2*k2(i2)*FCD(j-1)*((P/FT(j-1))^1)*(1-eta2(j-1)))*stepsize;
Fw(j)=Fw(j-1)+(k1(i1)*FH(j-1)*FCD(j-1)*((P/FT(j-1))^2)*(1-eta1(j-
1))+2*k3(i3)*(FH(j-1))^1*(P/FT(j-1))^1*(1-eta3(j-1)))*stepsize;
FM(j)=FM(j-1)+(k3(i3)*(FH(j-1))^1*(P/FT(j-1))^1*(1-eta3(j-1)))*stepsize;
end

final_FM=[final_FM FM(end-1)];
final_FCD=[final_FCD FCD(end-1)];
final_FH=[final_FH FH(end-1)];
final_FCo=[final_FCo FCo(end-1)];
final_FW=[final_FW Fw(end-1)];

end
```

```
end
end

FINAL_FM(jj,:)=final_FM
FINAL_CD(jj,:)=final_FCD
FINAL_FH(jj,:)=final_FH
FINAL_FW(jj,:)=final_FW
FINAL_Co(jj,:)=final_FCo
end

MMSE_temp=0;
for ii=1:length(FM_test)
MMSE_temp=MMSE_temp+((FINAL_FM(ii,:)-FM_test(ii))/FM_test(ii)).^2
+((FINAL_CD(ii,:)-FCD_test(ii))/FCD_test(ii)).^2+((FINAL_Co(ii,:)-
FCo_test(ii))/FCo_test(ii)).^2+((FINAL_FH(ii,:)-
FH_test(ii))/FH_test(ii)).^2+((FINAL_FW(ii,:)-
Fw_test(ii))/Fw_test(ii)).^2;
end
MMSE=MMSE_temp/(5*length(FM_test));
sizeMMSE=size(MMSE)
min_MMSE=min(MMSE)
position=find(MMSE==min_MMSE)-1;

 remain1=rem(position,L2*L3);
 factor1=(position-remain1)/(L2*L3);

remain2=rem(remain1,L3);
factor2=(remain1-remain2)/(L3);

Final_k1=factor1
Final_k2=factor2
Final_k3=remain2
```

APPENDIX T

POLYMATH CODE FOR 3-REACTION MODEL OF REVERSE WATER GAS SHIFT OVER PT/PD-CNT/ZEOLITE

Appendix G shows the Polymath code for 3-reaction model simulation in Chapter 9.

```
# PFR-3 Reaction Model - RWGS test

d(FH)/d(W) = -k1 * FH * FCD * (P / FT) ^ 2 * (1 - eta1) - 4 * k3 * FH * (P / FT) * (1 - eta3)

FH(0) = 0.010922995
FHo = 0.010922995 # CH4 feed rate (mole/hr)

d(FCD)/d(W) = -k1 * FH * FCD * (P / FT) ^ 2 * (1 - eta1) - k2 * FCD * (P / FT) * (1 - eta2) - k3 * FH
* (P / FT) * (1 - eta3)
FCD(0) = 0.011102596
FCDo = 0.011102596 # CO2 feed rate (mole/hr)

d(FCO)/d(W) = k1 * FH * FCD * (P / FT) ^ 2 * (1 - eta1) + 2 * k2 * FCD * (P / FT) * (1 - eta2)
FCO(0) = 0.0000001 # non-zero for eta calc at W = 0

d(FW)/d(W) = k1 * FH * FCD * (P / FT) ^ 2 * (1 - eta1) + 2 * k3 * FH * (P / FT) * (1 - eta3)
FW(0) = 0.0000001 # non-zero for eta calc

d(FM)/d(W) = k3 * FH * (P / FT) * (1 - eta3)
FM(0) = 0.0000001 # non-zero for eta calc


W(0) = 0
W(f) = 2. # catalyst mass

eta1 = FW * FCO / FH / FCD / Kp1
eta2 = FCO ^ 2 * (P / FT) / FCD / Kp2
eta3 = FM * FW ^ 2 / FCD / FH ^ 4 / (P / FT) ^ 2 / Kp3

k1 = 0.071
k2 = 0.0015
k3 = 0.0019


Kp1 = 0.4825
Kp2 = 0.3071
Kp3 = 0.1822

P = 3.04 # pressure in atm
FT = FM + FW + FH + FCO + FCD + FHE # mole/hr
FHE = 0.139
T = 273 + 650 # temp in K
X_H = (FHo - FH) / FHo
X_CD = (FCDo - FCD) / FCDo
```

REFERENCES

Daza, Y.A., & Kuhn, J. N. (2016). CO_2 Conversion by Reverse Water Gas Shift Catalysis: Comparison of Catalysts, Mechanisms and Their Consequences for CO_2 Conversion to Liquid Fuels. *RCS Advances.* 6, 49675-49691.

Alaba, P. A., Abbas, A., & Daud. W.M.W. (2017). Insight into Catalytic Reduction of CO_2: Catalysis and Reactor Design. *Journal of Cleaner Production*. 140, 1298-1312.

Hauri, C., Friedrich, T., & Timmermann, A. (2016). Abrupt Onset and Prolongation of Aragonite Undersaturation Events in the Southern Ocean. *Nature Climate Change.* 6, 172-176.

Usman, M., Daud, W.M.A.W., & Abbas, H.F. (2015). Dry Reforming of Methane: Influence of Process Parameters—A Review. *Renewable and Sustainable Energy Reviews.* 45, 710-744.

Qu, Y., Sutherland, A.M. & Guo, T. (2008). Carbon Dioxide Reforming of Methane by Ni/Co Nanoparticle Catalysts Immobilized on Single-Walled Carbon Nanotubes. *Energy & Fuels.* 22, 2183–2187.

Alvarez-Galvan, M.C., Mota, N., Ojeda, M., Rojas, S., Navarro, R.M., & Fierro, J.L.G. (2011). Direct Methane Conversion Routes to Chemicals and Fuels. *Catalysis Today.* 171, 15-23.

Ma, Q., Wang, D., Wu, M., Zhao, T., Yoneyama, Y., & Tsubaki, N. (2013). Effect of Catalytic Site Position: Nickel Nanocatalyst Selectively Loaded Inside or Outside Carbon Nanotubes for Methane Dry Reforming. *Fuel*. 108, 430-438.

Wu, T., Zhang, Q., Cai, W., Zhang, P., Song, X., Sun, Z., & Gao, L. (2015). Phyllosilicate Evolved Hierarchical Ni- and Cu–Ni/SiO_2 Nanocomposites for Methane Dry Reforming Catalysis. *Applied Catalysis A: General*. 503, 94–102.

Drif, A., Bion, N., Brahmi, R., Ojala, S., Pirault-Roy, L., Turpeinen, E., Seelam, P.K., Keiski, R.L., & Epron, F. (2015). Study of the Dry Reforming of Methane and Ethanol using Rh Catalysts Supported on Doped Alumina. *Applied Catalysis A: General*. 504, 576–584.

Zhang, J. & Li, F. (2015). Coke-Resistant Ni@SiO_2 Catalyst for Dry Reforming of Methane. *Applied Catalysis B: Environmental*. 176–177, 513–521.

Yamagishi,T., Furikado,I., Ito, S., Miyao,T., Naito,S., Tomishige,K. & Kunimori, K. (2006). Catalytic Performance and Characterization of $RhVO_4/SiO_2$ for Hydroformylation and CO Hydrogenation. *Journal of Molecular Catalysis A: Chemical.* 244, 201-212.

Tomishige, K., Asadullah, M., & Kunimori, K. (2004). Syngas Production by Biomass Gasification Using $Rh/CeO_2/SiO_2$ Catalysts and Fluidized Bed Reactor. *Catalysis Today,* 89, 389-403.

Khajenoori, M., Rezaei, M., & Meshkani, F. (2015). Dry Reforming over CeO_2-Promoted Ni/MgO Nano-Catalyst: Effect of Ni Loading and CH_4/CO_2 Molar ratio. *Journal of Industrial and Engineering Chemistry*. 21, 717–722.

Ay, H., & Uner, D. (2015). Dry Reforming of Methane over CeO2 Supported Ni, Co and Ni–Co Catalysts. *Applied Catalysis B: Environmental*. 179, 128–138.

Garc á-Di éguez, M., Pieta, I.S., Herrera, M.C., Larrubia, M.A., & Alemany, L.J. (2010). Nanostructured Pt- and Ni-based Catalysts for CO_2-Reforming of Methane. *Journal of Catalysis.* 270, 136–145.

Whang, H.S., Choi, M.S., Lim, J., Kim, C., Heo, I., Chang, T.S., & Lee, H. (2017). Enhanced Activity and Durability of Ru Catalyst Dispersed on Zirconia for Dry Reforming of Methane. *Catalysis Today.* 293-294, 122-128.

Abdullah, B., Azeanni, N., Ghani, A., & Vo, D.V.N. (2017). Recent Advances in Dry Reforming of Methane over Ni-based Catalysts. *Journal of Cleaner Production.* 162, 170-185.

Oshima, K., Shinagawa, T., Nogami, Y., Manabe, R., Ogo, S., & Sekine, Y. (2014). Low Temperature Catalytic Reverse Water Gas Shift Reaction Assisted by an Electric Field. *Catalysis Today.* 232, 27-32.

Galv án, C.A., Schumann, J., Behrens, M., Fierro, J.L.G., Schl ögl, R., & Frei, E. (2016). Reverse Water-Gas Shift Reaction at the Cu/ZnO Interface: Influence of The Cu/Zn Ratio on Structure-Activity Correlations. *Applied Catalysis B: Environmental.* 195, 104-111.

Yang, X., Su, X., Chen, X., Duan, H., Liang, B., Liu, Q., Liu, X., Ren, Y., Huang, Y., & Zhang, T. (2017). Promotion Effects of Potassium on the Activity and Selectivity of Pt/zeolite Catalysts for Reverse Water Gas Shift Reaction. *Applied Catalysis B: Environmental.* 216, 95-105.

Nobuhiro, I., Kenji, H., Kiyotaka, N., & Atsushi, F. (2016). Selective Synthesis of Carbon Monoxide via Formates in Reverse Water-Gas Shift Reaction over Alumina-Supported Gold Catalyst. *Journal of Energy Chemistry*. 25, 306-310.

Saeidi, S., Amin, N.A.S., & Rahimpour, M.R. (2014). Hydrogenation of CO_2 to Value-Added Products—A Review and Potential Future Developments. *Journal of CO_2 Utilization.* 5, 66-81.

Chen, X., Su, X., Duan, H., Liang, B., Huang, Y., & Zhang, T. (2017). Catalytic Performance of the Pt/TiO_2 Catalysts in Reverse Water Gas Shift Reaction: Controlled Product Selectivity and a Mechanism Study. *Catalysis Today.* 281, 312-318.

Rodriguez, J.A., Evans, J., Feria, L., Vidal, A.B., Liu, P., Nakamura, K., & Illas, F. (2013). CO_2 Hydrogenation on Au/TiC, Cu/TiC, and Ni/TiC Catalysts: Production of CO, Methanol, and Methane. *Journal of Catalysis.* 307, 162-169.

Chen, C.S., Cheng, W.H., & Lin, S.S. (2003). Study of Reverse Water Gas Shift Reaction by TPD, TPR and CO_2 Hydrogenation over Potassium-Promoted Cu/SiO_2 Catalyst. *Applied Catalysis A: General.* 238, 55-67.

Taheri, A., Thompson, E.J., Fettinger, J.C., & Berben, L.A. (2015). An Iron Electrocatalyst for Selective Reduction of CO_2 to Formate in Water: Including Thermochemical Insights. *ACS Catalysis.* 5, 7140-7151.

Liu, C., Cundari, T.R., & Wilson, A.K. (2012). CO_2 Reduction on Transition Metal (Fe, Co, Ni, and Cu) Surfaces: In Comparison with Homogeneous Catalysis. *Journal of Physical Chemistry C.* 116, 5681-5688.

Chen, C.S., Wu, J.H. & Lai, T.W. (2010). Carbon Dioxide Hydrogenation on Cu Nanoparticles. *Journal of Physical Chemistry C.* 114, 15021-15028.

Ginés, M.J.L., Marchi, A.J., & Apesteguía, C.R. (1997). Kinetic Study of the Reverse Water-Gas Shift Reaction over $CuO/ZnO/Al_2O_3$ Catalysts. *Applied Catalysis A: General.* 154, 155-171.

Jin, T., Zhou, Y., Mains, G.J., & White, J.M. (1987). Infrared and X-Ray Photoelectron Spectroscopy Study of Carbon Monoxide and Carbon Dioxide on Platinum/Ceria. *Journal of Physical Chemistry.* 91, 5931-5937.

Tibiletti, D., Goguet, A., Meunier, F.C., Breena, J.P. & Burch, R. (2004). On the Importance of Steady-State Isotopic Techniques for the Investigation of the Mechanism of the Reverse Water-Gas-Shift Reaction. *Chemical Communications.* 0, 1636-1637.

Jacobs, G., Crawford, A.C., & Davis, B.H. (2005). Water-Gas Shift: Steady State Isotope Switching Study of the Water-Gas Shift Reaction over Pt/Ceria Using in-situ DRIFTS. *Catalysis Letters.* 100, 147-152.

Chen C.S., Lin J.H., You J.H., & Chen C.R. (2006). Properties of Cu(thd)2 as a Precursor to Prepare Cu/SiO_2 Catalyst Using the Atomic Layer Epitaxy Technique. *Journal of the American Chemical Society.* 128, 15950-15951.

Goguet, A., Meunier, F., Breen, J.P., Burch, R., Petch, M.I., & Ghenciu, A.F. (2004). Study of the Origin of the Deactivation of a Pt/CeO_2 Catalyst during Reverse Water Gas Shift (RWGS) Reaction. *Journal of Catalysis.* 226, 382-392.

Jessop, P.G., Joó, F., & Tai, C.C. (2004). Recent Advances in the Homogeneous Hydrogenation of Carbon Dioxide. *Coordination Chemistry Reviews.* 248, 2425-2442.

Inoue, T., Iizuka, T., & Tanabe, K. (1989). Hydrogenation of Carbon Dioxide and Carbon Monoxide over Supported Rhodium Catalysts under 10 bar Pressure. *Applied Catalysis.* 46, 1-9.

Matsubu, J.C., Yang, V.N., & Christopher, P. (2015). Isolated Metal Active Site Concentration and Stability Control Catalytic CO_2 Reduction Selectivity. *Journal of the American Chemical Society.* 137, 3076-3084.

Bandoa, K.K., Sogab, K., Kunimorib, K., & Arakawac, H. (1998). Effect of Li Additive on CO_2 Hydrogenation Reactivity of Zeolite Supported Rh Catalysts. *Applied Catalysis A: General.* 175, 67-81.

Iijima, S. (1991). Helical Cicrotubules of Graphitic Carbon. *Nature*. 354, 56-58.

Fu, X., Yu, H., Peng, F., Wang, H., and Qian, Y. (2007). Facile Preparation of RuO_2 /CNT Catalyst by a Homogeneous Oxidation Precipitation Method and Its Catalytic Performance. *Applied Catalysis A: General.* 321, 190-197.

Donphai, W., Faungnawakij, K., & Chareonpanich, M. (2014). Effect of Ni-CNTs/mesocellular Silica Composite Catalysts on Carbon Dioxide Reforming of Methane. *Applied Catalysis A: General.* 475, 16-26.

Khavarian, M., Chai, S.P., & Mohamed, A.R. (2015). The Effects of Process Parameters on Carbon Dioxide Reforming of Methane over Co–Mo–MgO/MWCNTs Nanocomposite Catalysts. *Fuel*. 158,129–138.

Chen, Y. & Mitra, S. (2008). Fast Microwave-Assisted Purification, Functionalization and Dispersion of Multi-Walled Carbon Nanotubes. *Journal of nanoscience and nanotechnology.* 11, 5770-5775.

Cheng, X., Yan, P., Zhang, X., Yang, F., Dai, C., Li, D., & Ma, X.X. (2017). Enhanced Methane Dehydroaromatization in the Presence of CO_2 over Fe- and Mg-Modified Mo/ZSM-5. *Molecular Catalysis.* 437, 114-120.

Kosinov, N., Coumans, F.J.A.G., Li, G., Uslamin, E., Mezari, B., Wijpkema, A.S.G., Pidko, E.A., & Hensen, E.J.M. (2017). Stable Mo/HZSM-5 Methane Dehydroaromatization Catalysts Optimized for High-Temperature Calcination-Regeneration. *Journal of Catalysis.* 346, 125-133.

Ma, S., Guo, X., Zhao, L., Scott, S., & Bao, X. (2013). Recent Progress in Methane Dehydroaromatization: From Laboratory Curiosities to Promising Technology. *Journal of Energy Chemistry.* 22, 1-20.

Karakaya, C., Zhu, H., & Kee, R.J. (2015). Kinetic Modeling of Methane Dehydroaromatization Chemistry on Mo/Zeolite Catalysts in Packed-Bed Reactors. *Chemical Engineering Science.* 123, 474-486.

Li, L., Borry, R.W., & Iglesia, E. (2002). Design and optimization of Catalysts and Membrane Reactors for the Non-Oxidative Conversion of Methane. *Chemical Engineering Science.* 57, 4595-4604.

Karakaya, C., Morejudo, S.H., Zhu, H., & Kee, R.J. (2016). Catalytic Chemistry for Methane Dehydroaromatization (MDA) on a Bifunctional Mo/HZM-5 Catalyst in a Packed Bed. *Industrial & Engineering Chemistry Research.* 55, 9895-9906.

Chemkin-Pro, 2013. Version 15131. Reaction Design, San Diego, from http://www.ansys.com/products/fluids/ansys-chemkin-pro.

Goodwin, D., Moffat, H., & Speth, R. (2016). Cantera: An Object- Oriented Software Toolkit for Chemical Kinetics, Thermodynamics, and Transport Processes. Retrieved January 26, 2016, from http://www.cantera.org.

Hla, S.S., Sun, Y., Duffy, G.J., Morpeth, L.D., Ilyushechkin, A., Cousins, A., Roberts, D.G., & Edwards, J.H. (2011). Kinetics of the Water-Gas Shift Reaction over a $La_{0.7}Ce_{0.2}FeO_3$ Perovskite-Like Catalyst Using Simulated Coal-Derived Syngas at High Temperature. *International Journal of Hydrogen Energy.* 36, 518-527.